

The Pennsylvania State University  
The Graduate School

**THE GENETIC ARCHITECTURE AND EVOLUTIONARY FUNCTION  
OF HUMAN SCALP HAIR MORPHOLOGY**

A Dissertation in  
Anthropology  
by  
Tina Lasisi

© 2021 Tina Lasisi

Submitted in Partial Fulfillment  
of the Requirements  
for the Degree of

Doctor of Philosophy

August 2021

The dissertation of Tina Lasisi was reviewed and approved by the following:

Nina G. Jablonski  
Evan Pugh Professor of Anthropology  
Dissertation Co-Advisor  
Co-Chair of Committee

Mark D. Shriver  
Professor of Anthropology  
Dissertation Co-Advisor  
Co-Chair of Committee

George H. Perry  
Associate Professor of Anthropology and Biology  
Chair of Intercollege Graduate Degree Program in Bioinformatics and Genomics

Timothy H. Ryan  
Professor of Anthropology  
Head of the Department of Anthropology

W. Lawrence Kenney  
Professor and Marie Underhill Noll Chair in Human Performance

George Havenith  
Professor of Environmental Physiology and Ergonomics  
Director of the Environmental Ergonomics Research Centre  
Loughborough University  
Special Member

# Abstract

Most hair follicles on the human body have evolved to be miniaturized, rendering us practically ‘naked’. Despite sparse body hair, we retain thick hair on our scalps that varies significantly among populations. Yet little is known of the evolutionary history of our scalp hair and its variation. It has been suggested that scalp hair, and tightly curled hair in particular, evolved to moderate thermal load in humans. However, this functional hypothesis has never been directly tested. Existing research on human hair variation has relied on subjective and qualitative descriptors of hair morphology and samples have been historically had a strong Eurocentric bias.

Despite its relevance to several evolutionary hypotheses, scalp hair has yet to be studied in a comprehensive evolutionary, functional, and genetic framework. The functional work described in this dissertation revisits the recurrent question of the role of thermoregulation in shaping early human evolution. This work is the first to extensively investigate the potential role of scalp hair and variation in its morphology in modulating heat balance in humans. More broadly, the methods, samples, and hypotheses tested in this dissertation serve to replace racialized terminology and conceptions of human scalp hair variation.

Current public discussions of human biological variation demonstrate that anthropologists must continue to oppose tendencies to perceive human variation in racial terms, and focusing on hair—one of the most visible and variable human traits—will provide anthropologists with evidence of how and why variation evolved. This dissertation synthesizes methods and knowledge from various disciplines with new data, generating an innovative perspective on both human origins and modern variation and laying the foundation for future work.

# Table of Contents

List of Figures	ix
List of Tables	xxv
Acknowledgments	xxvi
<b>Chapter 1</b>	
<b>Introduction and background</b>	<b>1</b>
1.1 What is missing in our methods: a racialized lens and limited lexicon . . .	1
1.2 Phenotype-genotype associations: how much do we know about hair morphology? . . . . .	3
1.3 How does heat factor into the evolutionary history of human head hair? .	5
1.4 Motivation for the work . . . . .	6
1.5 Outline of chapters . . . . .	8
<b>Chapter 2</b>	
<b>The constraints of racialization:         how classification and valuation hinder scientific research         on         human variation</b>	<b>11</b>
2.1 Classification and Distortion . . . . .	11
2.1.1 The perceived variability of European traits . . . . .	12
2.1.2 Objective variation and subjective salience . . . . .	14
2.2 Thinly veiled value judgements . . . . .	16
2.2.1 Valuation as sexual selection . . . . .	16
2.2.2 Devaluation as pathologization . . . . .	19
2.3 The constraints of racialization . . . . .	21
2.3.1 Biased perceptions lead to misguided questions . . . . .	22
2.3.2 Reckoning with the remnants of race . . . . .	23
2.3.3 Transforming knowledge and practice in human biological sciences	24

## Chapter 3

### High-throughput phenotyping methods for quantifying hair fiber morphology

	<b>26</b>
3.1	Introduction . . . . . 26
3.2	Results . . . . . 28
3.2.1	Cutting hair fibers into fragments as a scalable method for washing and imaging hair fibers for curvature analysis . . . . . 28
3.2.2	Automated image analysis for unsupervised high-throughput processing . . . . . 30
3.2.3	Measurement error in hair fiber curvature estimation . . . . . 31
3.2.4	Measurement error in cross-sectional parameter estimation . . . . . 32
3.2.5	Self-reported hair texture and “objective” classification fail to capture quantitative variation in curvature . . . . . 34
3.2.6	Quantitative hair fiber morphology elucidates the relationship between curvature and cross-sectional shape and genetic architecture . . . . . 35
3.3	Discussion . . . . . 37
3.4	Methods . . . . . 39
3.4.1	Hair samples and genotype data . . . . . 39
3.4.2	Hair embedding, sectioning and imaging protocol . . . . . 39
3.4.3	Hair sample preparation and imaging protocol for curvature . . . . . 40
3.4.4	Image analysis protocol for curvature . . . . . 42
3.4.5	Data simulation for curvature and cross-sectional image analysis validation . . . . . 43
3.4.6	Analyses with simulated data and real data . . . . . 43

## Chapter 4

### The genetic architecture of human scalp hair morphology

	<b>45</b>
4.1	Introduction . . . . . 45
4.2	Results . . . . . 48
4.2.1	Sample ancestry description . . . . . 48
4.3	Genetic variation underlies hair morphology differences between European and African populations . . . . . 49
4.3.1	Correlation between curvature and cross-sectional eccentricity are primarily driven by ancestry stratification . . . . . 54
4.3.2	Associations of genetic variants with quantitative scalp hair morphology . . . . . 55
4.3.2.1	Replication of known loci . . . . . 55
4.3.2.2	Genetic architecture of traits . . . . . 56
4.4	Discussion . . . . . 62
4.4.1	Hair morphology . . . . . 62
4.4.2	Genetic architecture of skin and hair loci . . . . . 63
4.4.3	Future directions and conclusions . . . . . 64

4.5	Methods . . . . .	65
4.5.1	Participant recruitment, hair samples, and genotype data . . . . .	65
4.5.2	Phenotyping methods . . . . .	65
4.5.3	Estimation of admixture . . . . .	66
4.5.4	Genotype-phenotype associations . . . . .	66

## Chapter 5

	<b>Experimental evidence from thermal manikin for the role of human scalp hair as an evolutionary adaptation</b>	<b>67</b>
5.1	Introduction . . . . .	67
5.1.1	Thermoregulatory constraints in human evolution . . . . .	67
5.1.2	Hair plays an important role in mammalian thermoregulation . . . . .	68
5.1.3	Considering a thermal role for human scalp hair . . . . .	69
5.2	Results . . . . .	70
5.2.1	Brief Methods . . . . .	70
5.2.2	Solar influx and evaporative cooling create distinct heat loss patterns . . . . .	71
5.2.3	Sweating potential vs. sweating requirements result in different optimal scenarios . . . . .	74
5.2.4	Thermocouple data interpretation issues on thermal manikins . . . . .	76
5.3	Discussion . . . . .	80
5.4	Methods . . . . .	84
5.4.1	Materials & equipment . . . . .	84
5.4.1.1	Wigs . . . . .	84
5.4.1.2	Equipment . . . . .	85
5.4.1.3	Analyses . . . . .	87

## Chapter 6

	<b>Conclusion: Lessons learned and Future directions</b>	<b>90</b>
6.1	Deconstructing and reconstructing knowledge across disciplinary boundaries . . . . .	90
6.2	Thermoregulation and the function of hair . . . . .	91
6.3	Genomic insights into human scalp hair morphology . . . . .	93
6.4	Measuring hair to understand its biology . . . . .	96
6.5	Future directions in the study of hair and other racialized traits . . . . .	98

## Appendix A

	<b>Chapter 3 Supplementary: Background information on hair morphology quantification</b>	<b>99</b>
A.1	Previous work on cross-sectional geometry . . . . .	99
A.2	Methods for embedding & sectioning hairs are laborious . . . . .	100

A.3	Previous work on curvature . . . . .	102
A.4	Methods to quantify curvature have issues with replicability . . . . .	103

## Appendix B

### Chapter 3 Supplementary:

	<b>Image analysis validation</b>	<b>107</b>
B.1	Curvature . . . . .	107
B.1.1	Simulated vs. estimated curvature & length . . . . .	107
B.1.2	Measurement error in curvature and length . . . . .	109
B.1.2.1	Error statistics . . . . .	110
B.1.2.2	Root mean square error . . . . .	110
B.1.2.3	Percent error . . . . .	111
B.2	Cross-section . . . . .	113
B.2.1	Correlation between simulated and estimated section parameters . . . . .	114
B.2.2	Measurement error for cross-sectional parameters . . . . .	115
B.2.2.1	Root mean square error . . . . .	115
B.2.2.2	Percent error . . . . .	117

## Appendix C

### Chapter 3 Supplementary:

	<b>Biological significance of new methods</b>	<b>119</b>
C.1	Self-reported hair texture vs. quantitative hair curvature . . . . .	119
C.2	Objective hair texture classification vs. quantitative curvature . . . . .	121
C.3	Ancestry vs. hair morphology . . . . .	122
C.3.1	Admixture components . . . . .	122
C.3.2	Ancestry vs. curvature . . . . .	123
C.3.3	Curvature vs. eccentricity . . . . .	125
C.3.3.1	Uncorrected . . . . .	125
C.3.3.2	Corrected . . . . .	126
C.3.4	Curvature vs. skin pigmentation . . . . .	127
C.3.4.1	Uncorrected . . . . .	127
C.3.4.2	Corrected . . . . .	129

## Appendix D

### Chapter 4 Supplementary:

	<b>Admixture &amp; phenotype correlations</b>	<b>131</b>
D.1	Admixture components . . . . .	131
D.2	Phenotypic distributions . . . . .	133
D.3	Sex differences . . . . .	139
D.4	Ancestry vs. hair morphology . . . . .	142
D.4.1	Uncorrected . . . . .	142
D.4.2	Corrected . . . . .	145
D.5	Comparison with categorical . . . . .	150

## Appendix E

### Chapter 4 Supplementary:

#### Admixture & phenotype correlations for > 15% AFR ancestry

	<b>151</b>
E.1 Phenotypic distributions . . . . .	151
E.2 Sex differences . . . . .	156
E.3 Ancestry vs. hair morphology . . . . .	159
E.3.1 Uncorrected . . . . .	159
E.3.2 Corrected . . . . .	163
E.4 Comparison with categorical . . . . .	167

## Appendix F

### Chapter 4 Supplementary:

#### Genome-wide association results

	<b>168</b>
F.1 QQ plots . . . . .	169
F.2 Overlap with previously reported SNPs . . . . .	171
F.2.1 Hair replicated SNPs . . . . .	171
F.2.2 Skin replicated SNPs . . . . .	171
F.3 Admixture mapping . . . . .	183
F.3.1 Hair novel SNPs . . . . .	195

## Appendix G

### Chapter 5 Supplementary:

#### Thermal manikin experiment results

	<b>202</b>
G.1 Heat loss (4°C) . . . . .	202
G.1.1 Linear model . . . . .	203
G.2 Solar influx (4°C) . . . . .	206
G.2.1 Linear model . . . . .	207
G.3 Heat loss (30°C) . . . . .	209
G.3.1 Linear model . . . . .	210
G.4 Solar influx (30°C) . . . . .	213
G.4.1 Linear model . . . . .	214
G.5 Effect of radiation and evaporation (30°C) . . . . .	216
G.5.1 Linear model . . . . .	218
G.5.1.1 Separate wet and dry lm . . . . .	218
G.6 Inferred effect of heat loss through sweating at 30°C . . . . .	221
G.6.1 Linear model . . . . .	222
G.6.1.1 Combined wet and dry lm . . . . .	222
G.6.1.2 Separate max and zero gain . . . . .	224

## References

References . . . . .	<b>227</b>
----------------------	------------

# List of Figures

3.1	<b>Quantifiable aspects of hair morphology.</b> <b>a</b> , Diagram of cross-sectional eccentricity and area. <b>b</b> , Curvature is calculated as the inverse of the radius in mm ( $radius^{-1}$ ), ergo an increase in curvature corresponds with a decrease in the radius of the circle fitting the curve. . . . .	27
3.2	<b>Flowcharts of laboratory protocols used.</b> <b>a</b> , Embedding protocol for cross-sectional imaging. <b>b</b> , Sample preparation protocol for curvature imaging. . . . .	29
3.3	<b><i>fibermorph</i> image analysis workflow.</b> <b>a</b> , Cross-sectional image processing and analysis. <b>b</b> , Curvature image processing and analysis. . . . .	31
3.4	<b>Performance of <i>fibermorph</i> on simulated data.</b> <b>a</b> , Correlation between estimated and true (simulated) curvature. The red line represents $y = x$ and the blue line represents the line of best fit. <b>b</b> , Distribution of hair fragment length estimates. The dashed red line shows the true simulated length of each fragment. <b>c</b> , Correlation between estimated and true cross-sectional area. <b>d</b> , Correlation between estimated and true eccentricity. . . . .	33
3.5	<b>Comparison of quantitative and qualitative hair morphology.</b> <b>a</b> , Self-reported hair form shows inconsistency among individuals with regards to the level of curvature encompassed by each category. <b>b</b> , Classifying hair based on objective curvature Loussouarn et al. 2007, obscures the wide range of variation that exists in the “Very Curly” category. . . . .	34
3.6	<b>The effect of population structure on trait-trait correlations.</b> <b>a</b> , The correlation between hair curvature and melanin index without controlling for ancestry. <b>b</b> , The correlation between hair curvature and melanin index controlling for African ancestry. <b>c</b> , The correlation between hair curvature and cross-sectional eccentricity without controlling for ancestry. <b>d</b> , The correlation between hair curvature and cross-sectional eccentricity controlling for African ancestry. . . . .	36

4.1	<b>Proportion of various ancestry components for our sample.</b> ADMIXTURE for our sample of 192 admixed individuals shows predominantly African and European ancestries. . . . .	49
4.2	<b>Violin plots of phenotypic trait values across samples of different ancestries.</b> <b>a</b> , Melanin Index, <b>b</b> , Hair fiber curvature ( $1/radius_{(mm)}$ ), <b>c</b> , cross-sectional area of hair fiber ( $\mu m^2$ ), <b>d</b> , eccentricity of cross-section, <b>e</b> , minimum diameter of hair fiber ( $\mu m$ ), <b>f</b> , maximum diameter of hair fiber ( $\mu m$ ). Only significant comparisons are shown. . . . .	51
4.3	<b>PCA results for quantitative hair traits.</b> <b>a</b> , Scree plot showing the percentage of variance explained for each PC <b>b</b> , Contributing variables for first two PC dimensions <b>c</b> , Individual points colored according to proportion of AFR ancestry <b>d</b> , Individual points colored according to median hair fiber curvature . . . . .	53
4.4	<b>Scatter plot of proportion of African ancestry (x-axis) against phenotypic trait values (y-axis).</b> <b>a</b> , Melanin Index, <b>b</b> , Hair fiber curvature ( $1/radius_{(mm)}$ ) <b>c</b> , cross-sectional area of hair fiber ( $\mu m^2$ ), <b>d</b> , eccentricity of cross-section, <b>e</b> , minimum diameter of hair fiber ( $\mu m$ ), <b>f</b> , maximum diameter of hair fiber ( $\mu m$ ). . . . .	54
4.5	<b>Correlation matrices for the various traits</b> <b>a</b> , without ancestry correction and <b>b</b> with ancestry correction. . . . .	55
4.6	<b>Manhattan plot of admixture mapping for various traits.</b> <b>a</b> , skin pigmentation. Highlighted SNP represents <i>SLC24A5</i> . <b>b</b> , hair curvature . . . . .	57
4.7	<b>Allele frequency map of rs310644.</b> Derived C allele shows high frequencies in African and Melanesian populations, while ancestral T allele is at high frequencies across Eurasian populations. . . . .	58
4.8	<b>QQ plots for various ancestry corrections and phenotypes.</b> Columns represent different ancestry corrections and rows are different phenotypes. Shown here are (from top to bottom): Melanin Index, curvature, cross-sectional area, cross-sectional eccentricity, minimum diameter, and maximum diameter . . . . .	60
4.9	<b>QQ plots for various ancestry corrections and phenotypes.</b> Columns represent different ancestry corrections and rows are different phenotypes. Shown here are (from top to bottom): PC1 for hair traits, PC2 for hair traits, PC1 for residualized hair traits, PC2 for residualized hair traits, objectively classified hair texture. . . . .	61

5.1	<b>Solar influx as a function of wind speed at 30° C.</b> Wind speed shown on the x-axis with solar influx on the y-axis. Dry experiments shown on the left and wet experiment results on the right. . . . .	72
5.2	<b>Heat loss vs. radiation across experimental conditions.</b> Heat loss with radiation off/on (top to bottom) and in dry and wet conditions (left to right) calculated for ambient temperature of 30C. Dashed line represents $y=0$ . . . . .	73
5.3	<b>Results for linear regression on heat loss.</b> Dot-and-whisker plot of linear models for heat loss at 30°C for (a) dry and (b) wet conditions . . .	74
5.4	<b>Plot showing evaporative potential/requirement under different conditions.</b> The quantity of sweat that can be maximally evaporated (left) and that is required for zero heat gain (right) with various head coverings under three wind speeds. . . . .	75
5.5	<b>Linear regression results for evaporative potential and requirements for heat loss.</b> Dot-and-whisker plots for linear regression of (a) maximum sweat potential and (b) sweat required for zero heat gain. . . .	76
5.6	<b>Dot-and-whisker plot for linear regression on solar influx.</b> Regression coefficient on x-axis with terms on the y-axis. Only significant terms are shown. . . . .	78
5.7	<b>Scatter plot of solar influx for different experimental conditions.</b> Line represents zero influx. Negative numbers represent negative solar influx (i.e. a higher temperature was found with no radiation than with radiation). Wigs are indicated by color and thermocouple ID is indicated by shape. . . . .	79
5.8	<b>Thermocouple readings for across experiments for wind speed of 1 m/s.</b> The green line represents the cut off for burns sustained at that temperature after 100 minutes. The dashed and dotted orange lines represent that same limit but for burns sustained after only 10 and 1 minute respectively. . . . .	80

5.9	<b>Wigs used in experiments.</b> The wigs used in the experiment are made of human hair and were purchased from a purveyor who fashions different hair styles out of “Chinese virgin hair”. Reflectance measures were taken to ensure they were similar between the wigs and cross-sectional measures were checked from various points in the wig as an indicator of similarity across the wigs. The wigs are all made with hair fibers that are 8” long - the only difference is the tightness of the curl that was set in the wigs. . . . .	84
5.10	<b>Diagram of experimental setup.</b> The thermal manikin was sitting with its back towards the source of radiation. . . . .	85
5.11	<b>Image of experimental setup.</b> The set-up inside the climate-controlled chamber at Loughborough University. . . . .	86
5.12	<b>Manikin with thermocouple placement.</b> Thermocouples were spaced evenly along the midline to capture temperature from multiple points on the head during the experiments. . . . .	87
A.1	<b>Example of hairs moving during resin drying process.</b> This is an image taken of a hair embedded using an older protocol that involved hooking the hairs along small strips of transparencies. Even with this precaution, hairs could move while the resin dried. . . . .	100
A.2	<b>Example of discrepancy in number of measurements taken in high vs. low curvature hair with previous methods.</b> This image is from a previous publication (Lasisi et al., 2016) where circles were fitted to a hair’s curvature using ImageJ. This image shows the discrepancy in the number of data points gathered for tightly curled vs. straighter hair. . . . .	103
B.1	<b>Error in estimated curvature and length a,</b> Scatter plot of correlation between simulated and estimated hair curvature (using <i>fibermorph</i> ) and <b>b,</b> Histogram of distribution of estimated lengths with the red line showing the true simulated length. . . . .	108
B.2	<b>Simulated curvature vs estimated length</b> Simulated curvature on the x-axis and estimated length on the y-axis with a scatter plot showing a small negative correlation between the two, but a larger error in estimating length given a lower curvature. . . . .	109

B.3	<b>Root mean square error for curvature and length a</b> , Error in curvature estimation with simulated curvature on the x-axis and root mean square error (RMSE) on the y-axis and <b>b</b> , Histogram plot of distribution of RMSE for length estimation. . . . .	110
B.4	<b>Correlation between curvature and RMSE for length</b> Simulated curvature on the x-axis and root mean square error (RMSE) on the y-axis. The scatter plot shows a positive correlation between the two suggesting that the tighter the curl, the more error there is in accurate estimation of the hair fiber length. . . . .	111
B.5	<b>Percent error for curvature and length a</b> , Scatter plot of simulated curvature (x-axis) and percent error in curvature estimation (y-axis), and <b>b</b> , Histogram plot of distribution of percent error for length estimation .	112
B.6	<b>Correlation between curvature and percent error for estimated length</b> Simulated curvature on the x-axis is compared with the percent error in estimated length on the y-axis. . . . .	113
B.7	<b>Correlation between simulated and estimated cross-sectional parameters a</b> , Correlation between simulated area (x-axis) and estimated area (y-axis), <b>b</b> , Correlation between simulated eccentricity (x-axis) and estimated eccentricity (y-axis), <b>c</b> , Correlation between simulated minimum diameter (x-axis) and estimated minimum diameter (y-axis), <b>c</b> , Correlation between simulated maximum diameter (x-axis) and estimated maximum diameter (y-axis) . . . . .	114
B.8	<b>Correlation between simulated and RMSE for cross-sectional parameters, a</b> , Correlation between simulated area (x-axis) and RMSE of area (y-axis), <b>b</b> , Correlation between simulated eccentricity (x-axis) and RMSE of eccentricity (y-axis), <b>c</b> , Correlation between simulated minimum diameter (x-axis) and RMSE of minimum diameter (y-axis), <b>c</b> , Correlation between RMSE of maximum diameter (x-axis) and estimated maximum diameter (y-axis) . . . . .	116
B.9	<b>Correlation between simulated and percent error cross-sectional parameters, a</b> , Correlation between simulated area (x-axis) and percent error for area (y-axis), <b>b</b> , Correlation between simulated eccentricity (x-axis) and percent error for eccentricity (y-axis), <b>c</b> , Correlation between simulated minimum diameter (x-axis) and percent error for minimum diameter (y-axis), <b>c</b> , Correlation between percent error for maximum diameter (x-axis) and estimated maximum diameter (y-axis) . . . . .	118

C.1	<b>Self-reported hair texture vs. quantitative hair curvature</b> <b>a</b> , Mean hair fiber curvature (x-axis) and self-reported hair texture on (y-axis), <b>b</b> , Median hair fiber curvature (x-axis) and self-reported hair texture on (y-axis) . . . . .	120
C.2	<b>Image of hair sample with artefact biasing the measurement</b> Image of hair fibers used for curvature quantification with a red arrow pointing towards a stray fiber that appears to be contaminating the sample and biasing the curvature measurement. . . . .	121
C.3	<b>Objective hair classification vs. quantitative curvature</b> <b>a</b> , Mean hair fiber curvature (x-axis) and objectively categorized hair texture on (y-axis), <b>b</b> , Median hair fiber curvature (x-axis) and objectively categorized hair texture on (y-axis) . . . . .	122
C.4	<b>Admixture components for sample</b> Plot for K=5 ADMIXTURE of sample (n=192) with predominantly AFR and EUR ancestry. The colors represent ancestries that correspond to the following 1000 Genomes populations: - SAS = South Asian - AMR = American - AFR = African - EUR = European - EAS = East Asian. Each of these are meta-populations based on the grouping of multiple (sub)continental population groups in the 1000 Genomes repository. . . . .	123
C.5	<b>Percentage of African ancestry vs. M-index, curvature and eccentricity</b> <b>a</b> , African ancestry (x-axis) vs. Melanin Index (y-axis), <b>b</b> , African ancestry (x-axis) vs. median hair fiber curvature (y-axis), <b>c</b> , African ancestry (x-axis) vs. cross-sectional eccentricity (y-axis) . . . . .	124
C.6	<b>Curvature vs. eccentricity (without correction for ancestry)</b> Median eccentricity on the x-axis vs. median curvature on the y-axis show a positive correlation when they are plotted without correction for ancestry.	126
C.7	<b>Curvature vs. eccentricity (with correction for ancestry)</b> Median eccentricity on the x-axis vs. median curvature on the y-axis show no correlation when they are plotted with correction for ancestry. . . . .	127
C.8	<b>Curvature vs. M-index (without correction for ancestry)</b> Melanin Index on the x-axis vs. median curvature on the y-axis show a positive correlation when they are plotted without correction for ancestry. . . . .	128
C.9	<b>Curvature vs. M-index (with correction for ancestry)</b> Melanin Index on the x-axis vs. median curvature on the y-axis show no correlation when they are plotted with correction for ancestry. . . . .	130

D.1	<b>Admixture components for sample</b> Plot for K=5 ADMIXTURE of sample (n=192) with predominantly AFR and EUR ancestry. The colors represent ancestries that correspond to the following 1000 Genomes populations: - SAS = South Asian - AMR = American - AFR = African - EUR = European - EAS = East Asian. Each of these are meta-populations based on the grouping of multiple (sub)continental population groups in the 1000 Genomes repository. . . . .	132
D.2	<b>Correlation between different AFR calculations for the sample.</b> On the x-axis we have the proportion of AFR ancestry calculated with K=5 and on the y-axis we have the proportion of AFR ancestry calculated with K=2. The two estimates are highly correlated with most of the variance being in the individuals with low AFR ancestry. . . . .	133
D.3	<b>Grouped scatter plots showing phenotypic distributions for each phenotype with regional details for the reference samples.</b> <b>a</b> , Melanin Index <b>b</b> , median hair fiber curvature <b>c</b> , cross-sectional area <b>d</b> , cross-sectional eccentricity <b>e</b> , minimum diameter of cross-section <b>f</b> , maximum diameter of cross-section. . . . .	135
D.4	<b>Density plots showing phenotypic distributions for each phenotype for the reference samples and the current sample marked as Admixed (US).</b> <b>a</b> , Melanin Index <b>b</b> , median hair fiber curvature <b>c</b> , cross-sectional area <b>d</b> , cross-sectional eccentricity <b>e</b> , minimum diameter of cross-section <b>f</b> , maximum diameter of cross-section. . . . .	136
D.5	<b>Violin plots showing phenotypic distributions for each phenotype for the reference samples and the current sample marked as Admixed (US).</b> <b>a</b> , Melanin Index <b>b</b> , median hair fiber curvature <b>c</b> , cross-sectional area <b>d</b> , cross-sectional eccentricity <b>e</b> , minimum diameter of cross-section <b>f</b> , maximum diameter of cross-section. . . . .	137
D.6	<b>Grouped scatter plots showing phenotypic distributions for each phenotype for the reference samples with regional details and the current sample marked as Admixed (US).</b> <b>a</b> , Melanin Index <b>b</b> , median hair fiber curvature <b>c</b> , cross-sectional area <b>d</b> , cross-sectional eccentricity <b>e</b> , minimum diameter of cross-section <b>f</b> , maximum diameter of cross-section. . . . .	138
D.7	<b>Density plots showing phenotypic distributions for each phenotype per self-reported sex.</b> <b>a</b> , Melanin Index <b>b</b> , median hair fiber curvature <b>c</b> , cross-sectional area <b>d</b> , cross-sectional eccentricity <b>e</b> , minimum diameter of cross-section <b>f</b> , maximum diameter of cross-section. . . . .	140

D.8	<b>Violin plots showing phenotypic distributions for each phenotype per self-reported sex.</b> <b>a</b> , Melanin Index <b>b</b> , median hair fiber curvature <b>c</b> , cross-sectional area <b>d</b> , cross-sectional eccentricity <b>e</b> , minimum diameter of cross-section <b>f</b> , maximum diameter of cross-section. . . . .	141
D.9	<b>PCA results for quantitative hair phenotypes (without ancestry correction).</b> <b>a</b> , Scree plot showing the percentage of variance explained for each PC <b>b</b> , Contributing variables for first two PC dimensions. . . . .	142
D.10	<b>Scatter plot of individual PC scores along first two dimensions</b> <b>a</b> , Individual points colored according to proportion of AFR ancestry <b>b</b> , Individual points colored according to median hair fiber curvature . . . . .	143
D.11	<b>Scatter plots of all phenotypes against AFR ancestry</b> <b>a</b> , Melanin Index <b>b</b> , median hair curvature <b>c</b> , objectively classified hair texture <b>d</b> , cross-sectional area <b>e</b> , cross-sectional eccentricity <b>f</b> , minimum cross-sectional diameter <b>g</b> , maximum cross-sectional diameter <b>h</b> , PC1 for quantitative hair variables <b>i</b> , PC2 for quantitative hair variables. . . . .	144
D.12	<b>Correlation matrix of quantitative hair variables and Melanin Index.</b> This correlation matrix shows the correlation between each of the phenotypes without correction for ancestry. . . . .	145
D.13	<b>PCA results for quantitative hair phenotypes (with correction, using residualized phenotypic values).</b> <b>a</b> , Scree plot showing the percentage of variance explained for each PC <b>b</b> , Contributing variables for first two PC dimensions. . . . .	146
D.14	<b>Scatter plot of individual PC scores along first two dimensions</b> <b>a</b> , Individual points colored according to proportion of AFR ancestry <b>b</b> , Individual points colored according to median hair fiber curvature . . . . .	146
D.15	<b>Scatter plots of all phenotypes (residualized) against AFR ancestry</b> <b>a</b> , Melanin Index <b>b</b> , median hair curvature <b>c</b> , objectively classified hair texture <b>d</b> , cross-sectional area <b>e</b> , cross-sectional eccentricity <b>f</b> , minimum cross-sectional diameter <b>g</b> , maximum cross-sectional diameter <b>h</b> , PC1 for quantitative hair variables <b>i</b> , PC2 for quantitative hair variables. . . . .	147
D.16	<b>Correlation matrix of quantitative hair variables and Melanin Index.</b> This correlation matrix shows the correlation between each of the phenotypes with correction for ancestry. . . . .	148

D.17	<b>Scatter plots of raw phenotypes of interest (left) against their residualized comparison (right)</b> <b>a</b> , Cross-sectional area vs. minimum cross-sectional diameter <b>b</b> , Cross-sectional area vs. minimum cross-sectional diameter (residualized) <b>c</b> , Cross-sectional area vs. maximum cross-sectional diameter <b>d</b> , Cross-sectional area vs. maximum cross-sectional diameter (residualized) <b>e</b> , Maximum cross-sectional diameter vs. minimum cross-sectional diameter <b>f</b> , Maximum cross-sectional diameter vs. minimum cross-sectional diameter (residualized) <b>g</b> , Maximum cross-sectional diameter vs. cross-sectional eccentricity <b>h</b> Maximum cross-sectional diameter vs. cross-sectional eccentricity (residualized) . . . . .	149
D.18	<b>Categorical hair texture compared to quantitative hair curvature and proportion of AFR ancestry</b> <b>a</b> , Hair texture here is classified objectively according to cut offs suggested by Loussouarn et al. (2007) and <b>b</b> , shows hair texture according to participant self-report. . . . .	150
E.1	<b>Violin plots showing phenotypic distributions for each phenotype for the reference samples.</b> <b>a</b> , Melanin Index <b>b</b> , median hair fiber curvature <b>c</b> , cross-sectional area <b>d</b> , cross-sectional eccentricity <b>e</b> , minimum diameter of cross-section <b>f</b> , maximum diameter of cross-section. . . . .	152
E.2	<b>Density plots showing phenotypic distributions for each phenotype for the reference samples and the current sample marked as Admixed (US).</b> <b>a</b> , Melanin Index <b>b</b> , median hair fiber curvature <b>c</b> , cross-sectional area <b>d</b> , cross-sectional eccentricity <b>e</b> , minimum diameter of cross-section <b>f</b> , maximum diameter of cross-section. . . . .	153
E.3	<b>Violin plots showing phenotypic distributions for each phenotype for the reference samples and the current sample marked as Admixed (US).</b> <b>a</b> , Melanin Index <b>b</b> , median hair fiber curvature <b>c</b> , cross-sectional area <b>d</b> , cross-sectional eccentricity <b>e</b> , minimum diameter of cross-section <b>f</b> , maximum diameter of cross-section. . . . .	154
E.4	<b>Grouped scatter plots showing phenotypic distributions for each phenotype for the reference samples with regional details and the current sample marked as Admixed (US).</b> <b>a</b> , Melanin Index <b>b</b> , median hair fiber curvature <b>c</b> , cross-sectional area <b>d</b> , cross-sectional eccentricity <b>e</b> , minimum diameter of cross-section <b>f</b> , maximum diameter of cross-section. . . . .	155

E.5	<b>Density plots showing phenotypic distributions for each phenotype per self-reported sex.</b> <b>a</b> , Melanin Index <b>b</b> , median hair fiber curvature <b>c</b> , cross-sectional area <b>d</b> , cross-sectional eccentricity <b>e</b> , minimum diameter of cross-section <b>f</b> , maximum diameter of cross-section. . . . .	157
E.6	<b>Violin plots showing phenotypic distributions for each phenotype per self-reported sex.</b> <b>a</b> , Melanin Index <b>b</b> , median hair fiber curvature <b>c</b> , cross-sectional area <b>d</b> , cross-sectional eccentricity <b>e</b> , minimum diameter of cross-section <b>f</b> , maximum diameter of cross-section. . . . .	158
E.7	<b>PCA results for quantitative hair phenotypes (without ancestry correction).</b> <b>a</b> , Scree plot showing the percentage of variance explained for each PC <b>b</b> , Contributing variables for first two PC dimensions. . . . .	159
E.8	<b>Scatter plot of individual PC scores along first two dimensions</b> <b>a</b> , Individual points colored according to proportion of AFR ancestry <b>b</b> , Individual points colored according to median hair fiber curvature . . . . .	160
E.9	<b>Scatter plots of all phenotypes against AFR ancestry</b> <b>a</b> , Melanin Index <b>b</b> , median hair curvature <b>c</b> , objectively classified hair texture <b>d</b> , cross-sectional area <b>e</b> , cross-sectional eccentricity <b>f</b> , minimum cross-sectional diameter <b>g</b> , maximum cross-sectional diameter <b>h</b> , PC1 for quantitative hair variables <b>i</b> , PC2 for quantitative hair variables. . . . .	161
E.10	<b>Correlation matrix of quantitative hair variables and Melanin Index.</b> This correlation matrix shows the correlation between each of the phenotypes without correction for ancestry. . . . .	162
E.11	<b>PCA results for quantitative hair phenotypes (with correction, using residualized phenotypic values).</b> <b>a</b> , Scree plot showing the percentage of variance explained for each PC <b>b</b> , Contributing variables for first two PC dimensions. . . . .	163
E.12	<b>Scatter plot of individual PC scores along first two dimensions</b> <b>a</b> , Individual points colored according to proportion of AFR ancestry <b>b</b> , Individual points colored according to median hair fiber curvature . . . . .	163
E.13	<b>Scatter plots of all phenotypes (residualized) against AFR ancestry</b> <b>a</b> , Melanin Index <b>b</b> , median hair curvature <b>c</b> , objectively classified hair texture <b>d</b> , cross-sectional area <b>e</b> , cross-sectional eccentricity <b>f</b> , minimum cross-sectional diameter <b>g</b> , maximum cross-sectional diameter <b>h</b> , PC1 for quantitative hair variables <b>i</b> , PC2 for quantitative hair variables. . . . .	164

E.14	<b>Correlation matrix of quantitative hair variables and Melanin Index.</b> This correlation matrix shows the correlation between each of the phenotypes with correction for ancestry. . . . .	165
E.15	<b>Scatter plots of raw phenotypes of interest (left) against their residualized comparison (right)</b> <b>a</b> , Cross-sectional area vs. minimum cross-sectional diameter <b>b</b> , Cross-sectional area vs. minimum cross-sectional diameter (residualized) <b>c</b> , Cross-sectional area vs. maximum cross-sectional diameter <b>d</b> , Cross-sectional area vs. maximum cross-sectional diameter (residualized) <b>e</b> , Maximum cross-sectional diameter vs. minimum cross-sectional diameter <b>f</b> , Maximum cross-sectional diameter vs. minimum cross-sectional diameter (residualized) <b>g</b> , Maximum cross-sectional diameter vs. cross-sectional eccentricity <b>h</b> Maximum cross-sectional diameter vs. cross-sectional eccentricity (residualized) . . . . .	166
E.16	<b>Categorical hair texture compared to quantitative hair curvature and proportion of AFR ancestry</b> <b>a</b> , Hair texture here is classified objectively according to cut offs suggested by Loussouarn et al. (2007) and <b>b</b> , shows hair texture according to participant self-report. . . . .	167
F.1	<b>QQ plots for various ancestry corrections and phenotypes.</b> Columns represent different ancestry corrections and rows are different phenotypes.	169
F.2	<b>QQ plots for various ancestry corrections and phenotypes.</b> Columns represent different ancestry corrections and rows are different phenotypes.	170
F.3	<b>Manhattan plot for Melanin Index.</b> First row with correction for ancestry using AFR (K=2), second row using first 2 PCs to correct for ancestry, and last row shows plot without correction for ancestry. Highlighted are previously associated loci. Here we see <i>SLC24A5</i> on Chromosome 15. . . . .	172
F.4	<b>Manhattan plot for median hair curvature.</b> First row with correction for ancestry using AFR (K=2), second row using first 2 PCs to correct for ancestry, and last row shows plot without correction for ancestry. Highlighted are previously associated loci. . . . .	173
F.5	<b>Manhattan plot for cross-sectional area.</b> First row with correction for ancestry using AFR (K=2), second row using first 2 PCs to correct for ancestry, and last row shows plot without correction for ancestry. Highlighted are previously associated loci. . . . .	174

F.6	<b>Manhattan plot for cross-sectional eccentricity.</b> First row with correction for ancestry using AFR ( $K=2$ ), second row using first 2 PCs to correct for ancestry, and last row shows plot without correction for ancestry. Highlighted are previously associated loci. . . . .	175
F.7	<b>Manhattan plot for minimum cross-sectional diameter.</b> First row with correction for ancestry using AFR ( $K=2$ ), second row using first 2 PCs to correct for ancestry, and last row shows plot without correction for ancestry. Highlighted are previously associated loci. . . . .	176
F.8	<b>Manhattan plot for maximum cross-sectional diameter.</b> First row with correction for ancestry using AFR ( $K=2$ ), second row using first 2 PCs to correct for ancestry, and last row shows plot without correction for ancestry. Highlighted are previously associated loci. . . . .	177
F.9	<b>Manhattan plot for PC1 on quantitative hair traits.</b> First row with correction for ancestry using AFR ( $K=2$ ), second row using first 2 PCs to correct for ancestry, and last row shows plot without correction for ancestry. Highlighted are previously associated loci. . . . .	178
F.10	<b>Manhattan plot for PC2 on quantitative hair traits.</b> First row with correction for ancestry using AFR ( $K=2$ ), second row using first 2 PCs to correct for ancestry, and last row shows plot without correction for ancestry. Highlighted are previously associated loci. . . . .	179
F.11	<b>Manhattan plot for PC1 on residualized quantitative hair traits.</b> First row with correction for ancestry using AFR ( $K=2$ ), second row using first 2 PCs to correct for ancestry, and last row shows plot without correction for ancestry. Highlighted are previously associated loci. . . .	180
F.12	<b>Manhattan plot for PC2 on residualized quantitative hair traits.</b> First row with correction for ancestry using AFR ( $K=2$ ), second row using first 2 PCs to correct for ancestry, and last row shows plot without correction for ancestry. Highlighted are previously associated loci. . . .	181
F.13	<b>Manhattan plot for objectively classified hair texture.</b> First row with correction for ancestry using AFR ( $K=2$ ), second row using first 2 PCs to correct for ancestry, and last row shows plot without correction for ancestry. Highlighted are previously associated loci. . . . .	182

F.14	<b>Manhattan plot for Melanin Index on subset of alleles with high frequency difference between YRI-CEU.</b> First row with correction for ancestry using AFR (K=2), second row using first 2 PCs to correct for ancestry, and last row shows plot without correction for ancestry. Highlighted are previously associated loci. The strongest highlighted signal is <i>SLC24A5</i> . . . . .	184
F.15	<b>Manhattan plot for median hair curvature on subset of alleles with high frequency difference between YRI-CEU.</b> First row with correction for ancestry using AFR (K=2), second row using first 2 PCs to correct for ancestry, and last row shows plot without correction for ancestry. Highlighted are previously associated loci. . . . .	185
F.16	<b>Manhattan plot for cross-sectional area on subset of alleles with high frequency difference between YRI-CEU.</b> First row with correction for ancestry using AFR (K=2), second row using first 2 PCs to correct for ancestry, and last row shows plot without correction for ancestry. Highlighted are previously associated loci. . . . .	186
F.17	<b>Manhattan plot for cross-sectional eccentricity on subset of alleles with high frequency difference between YRI-CEU.</b> First row with correction for ancestry using AFR (K=2), second row using first 2 PCs to correct for ancestry, and last row shows plot without correction for ancestry. Highlighted are previously associated loci. . . . .	187
F.18	<b>Manhattan plot for minimum cross-sectional diameter on subset of alleles with high frequency difference between YRI-CEU.</b> First row with correction for ancestry using AFR (K=2), second row using first 2 PCs to correct for ancestry, and last row shows plot without correction for ancestry. Highlighted are previously associated loci. . . . .	188
F.19	<b>Manhattan plot for maximum cross-sectional diameter on subset of alleles with high frequency difference between YRI-CEU.</b> First row with correction for ancestry using AFR (K=2), second row using first 2 PCs to correct for ancestry, and last row shows plot without correction for ancestry. Highlighted are previously associated loci. . . .	189
F.20	<b>Manhattan plot for PC1 for quantitative hair traits on subset of alleles with high frequency difference between YRI-CEU.</b> First row with correction for ancestry using AFR (K=2), second row using first 2 PCs to correct for ancestry, and last row shows plot without correction for ancestry. Highlighted are previously associated loci. . . . .	190

F.21	<b>Manhattan plot for PC2 for quantitative hair traits on subset of alleles with high frequency difference between YRI-CEU.</b> First row with correction for ancestry using AFR (K=2), second row using first 2 PCs to correct for ancestry, and last row shows plot without correction for ancestry. Highlighted are previously associated loci. . . . .	191
F.22	<b>Manhattan plot for PC1 for residualized quantitative hair traits on subset of alleles with high frequency difference between YRI-CEU.</b> First row with correction for ancestry using AFR (K=2), second row using first 2 PCs to correct for ancestry, and last row shows plot without correction for ancestry. Highlighted are previously associated loci.	192
F.23	<b>Manhattan plot for PC2 for residualized quantitative hair traits on subset of alleles with high frequency difference between YRI-CEU.</b> First row with correction for ancestry using AFR (K=2), second row using first 2 PCs to correct for ancestry, and last row shows plot without correction for ancestry. Highlighted are previously associated loci.	193
F.24	<b>Manhattan plot for objectively classified hair texture on subset of alleles with high frequency difference between YRI-CEU.</b> First row with correction for ancestry using AFR (K=2), second row using first 2 PCs to correct for ancestry, and last row shows plot without correction for ancestry. Highlighted are previously associated loci. . . . .	194
G.1	<b>Comparison of dry heat loss and wet heat loss (dry + evaporative) for various head coverings at three wind speeds with radiation on and off at 4C.</b> Heat loss with radiation off (x-axis) vs. heat loss with radiation on (y-axis) for dry (left) and wet (right) experiments. Wigs are indicated by color and wind speed is indicated by shape. . . . .	203
G.2	<b>Dot-and-whisker plot for regression analysis of heat loss</b> Regression coefficient on the x-axis with different terms on the y-axis. Only significant results shown. . . . .	205
G.3	<b>Scatter plot of solar flux across experiments.</b> This plot shows the solar influx as a function of heat loss in the radiation off state. The horizontal line is at zero showing that all values are positive. . . . .	206
G.4	<b>Solar influx as a function of wind speed</b> Wind speed is shown on the x-axis with solar influx on the y-axis. Wigs are indicated by different colors. . . . .	207

G.5	<b>Dot-and-whisker plot of linear regression on solar influx.</b> Regression coefficient shown on the x-axis with terms on the y-axis. Only significant terms are shown . . . . .	209
G.6	<b>Comparison of dry heat loss and wet heat loss (dry + evaporative) for various head coverings.</b> Shown for three wind speeds with radiation on and off at 30°C. Solid line represents x=y and dashed lines represent 0 intercept for each axis. . . . .	210
G.7	<b>Dot-and-whisker plot for regression analysis of heat loss</b> Regression coefficient on the x-axis and terms on the y-axis. Only significant results shown. . . . .	212
G.8	<b>Scatter plot of heat loss and solar influx across experiments.</b> This plot shows the solar influx as a function of heat loss in the radiation off state. The horizontal line is at zero showing that all values are positive.	213
G.9	<b>Solar influx as a function of wind speed.</b> Wind speed is shown on the x-axis with solar influx on the y-axis. Wigs are indicated by color. . .	214
G.10	<b>Dot-and-whisker plot of linear regression on solar influx.</b> Regression coefficient is shown on the x-axis with terms on the y-axis. Only significant results are shown. . . . .	216
G.11	<b>Plot of wind speed and heat loss in different experimental conditions.</b> Heat loss with radiation off/on (top to bottom) and in dry and wet conditions (left to right) calculated for ambient temperature of 30°C. Dashed line represents y=0. . . . .	217
G.12	<b>Dot-and-whisker plot of linear models for heat loss at 30°C.</b> Regression coefficients shown on the x-axis with terms on the y-axis and separate plots for for (a) dry and (b) wet conditions . . . . .	220
G.13	<b>Plot of maximum sweat potential and required sweat in various experimental conditions</b> The quantity of sweat that can be maximally evaporated (left) and that is required for zero heat gain (right) with various head coverings under three wind speeds . . . . .	221
G.14	<b>Dot-and-whisker plot of linear model for quantity of sweat with wind, wig and sweat type as independent predictors.</b> Regression coefficient on the x-axis and terms on the y-axis. Only significant values shown . . . . .	223

G.15 **Dot-and-whisker plots for linear regression of sweat evaporation potential and requirement.** Only significant terms are plotted and separate plots show regression for (a) maximum sweat potential and (b) sweat required for zero heat gain . . . . . 226

# List of Tables

4.1	Table of significant replicated loci from GWAS meta-analysis on hair morphology (Liu et al., 2018) . . . . .	58
B.1	RMSE and Percent Error per variable . . . . .	110
B.2	RMSE and Percent Error per variable . . . . .	115
B.3	RMSE and Percent Error per variable . . . . .	115
F.1	Hair replicated SNPs . . . . .	171
F.2	Skin replicated SNPs . . . . .	172
F.3	Hair novel SNPs . . . . .	195
F.4	Complete table of significant SNPs . . . . .	196

# Acknowledgments

My greatest fortune has always been crossing paths with the right people at the right time. To each and every person who has given me opportunities, had faith in me, supported me in my academic achievements and my personal life: this milestone is yours as much as it is mine.

First and foremost, I would like to thank both my advisors, Nina Jablonski and Mark Shriver. When I first arrived, Nina had to deal with someone who was the epitome of bright-eyed and bushy-tailed. And without ever dousing that flame of excitement, Nina consistently and compassionately pointed me in the right direction, reminding me that I had a whole future ahead of me to explore my treasure chest of projects. I have had the immeasurable pleasure of sitting down for long conversations with Nina where she did not only impart her wisdom upon me, but she also listened carefully, always encouraging my curiosity and praising my musings. Mark Shriver is nothing if not an exceptionally patient man. From our first interaction, I felt comfortable enough to bombard him with toddler-like questions about everything: “What’s this? What’s that? How? Why?” Luckily, Mark is very good with toddlers. I am often reminded of how lucky I am to know Mark as, not only as the brilliant scientist that he is, but also as the advisor who was never too busy to sit on the lab floor with me as we devised new janky (albeit useful) “lab equipment”, or to visit me in the hospital and even to drive me home when I was released. Both Nina and Mark have always treated me as a colleague and had faith in me and my abilities, even when I did not have faith in myself. Thanks to both of you, my voice does not waver when I speak. Because of your support, I can confidently go into the world, share what I have learned, and pay forward the kindness you have shown me. Thank you.

I am often told I have too many people on my committee. That thought has certainly crossed my mind when I needed to schedule meetings, but I am truly indebted to each person on my committee. I like to think that Tim Ryan is indirectly responsible for my going to Penn State. If it had not been for his postdoc, Colin Shaw, going to Cambridge and mentoring me, I genuinely might not even have studied biological anthropology. I could not have learned Python without Tim putting me in touch with his other postdoc, Nick Stephens. Clearly, Tim Ryan has impeccable judgement when it comes to hiring postdocs, and for that I thank him. PJ Perry has, on more than one occasion, gone above and beyond to advocate for me, which has served as a reminder that there are people who will do what is right, even when it is uncomfortable. I was also lucky enough

to be in the cohort that had PJ teach our grant writing class. I have no doubt that this class was directly responsible for my successful application for the NSF DDRIG on the first attempt.

Larry Kenney and George Havenith are the two special (non-anthropologist) members of my committee responsible for broadening my horizons. We met almost four years ago in what felt like a chaotic series of events. I first met them in early October 2017 and by the end of that month, I was putting together a poster and figuring out the logistics of joining both of them at a conference in Japan. This experience laid the foundations for my dedication to interdisciplinary research. Larry, thank you for being patient and flexible with me, and letting me come to my own conclusions when I was clearly wrong. George, thank you for welcoming me into your lab and your home (heel gezellig), and for making your students and postdocs available to me. None of this could have happened without your efforts.

A number of people who contributed directly to my dissertation work deserve special mention. James Smallcombe held my hand through figuring out thermal manikins, climate-controlled chambers, and thermocouples. He even carried out additional experiments with the wigs after I had left! I am so grateful to both you and George for investing so much of your time in making sure this project went well. The experiments (and the interpretation of the raw data) would have been impossible without the both of you! I look forward to working with you in the future and answering more interesting questions at the intersection of both our disciplines.

Nick Stephens is the reason I know how to code in Python. I appreciate you helping me build something from scratch that I can truly call my own. Thank you for helping me find my footing. Of course, this program never would have gotten finished without Tim Webster! Tim, you have been an incredible mentor. You have helped me with genomics and bioinformatics questions, you were even one of my main sources of emotional support when I was going through a rough time. Thank you for making me an honorary member of your lab along with the other stray grad students you picked up. Liz Tapanes and Colin Brand would be the aforementioned stray grad students (although Dr. Tapanes is no longer a student!). I consider you both close friends and incredible colleagues. I didn't really have a cohort at Penn State, so I feel like you both ended up being the lab siblings I always wanted. I love being in meetings with you and hearing about your work and I appreciate you both for your brilliance and your friendship.

Jinguo Huang and Arslan Zaidi have both contributed immensely to the dissertation chapter on hair genetics (and to my mental health). Jinguo, I am so glad you joined the Shriver Lab! You are a genius and you are hilarious. I am really grateful to you for QCing the ADAPT data and running a gazillion phenotypes through Plink for me. Though I would never try to steal cat-Tina's place in your life, I do hope that we can keep being friends and working together so I can secure my spot as the top human-Tina in your life. Arslan, you've helped me learn so much and I adore all the conversations that we have (and the memes we share). You have been such an incredible friend over these years and I have come to see you as the older brother I've always wanted. Thank you for everything.

Sarita Greer came back into my life a few years ago as the Shriver Lab manager and she has done the incredible job of keeping the lab running, while somehow (seemingly by magic) keeping on top of the logistics of our running studies and even making sure I was fed and supported when I lost almost everything. I have learned so much from you and am constantly in awe of how much time and effort you manage to give to others when anyone else in your shoes would have crawled into bed unwilling to deal with the world. Thank you so much for your friendship and your help. You and Chris have been incredibly kind to me (and I don't just say this because you've given me food multiple times, but that definitely does contribute significantly to my gratitude).

Over the years, I have had the pleasure of working with a number of undergraduate research assistants. It has been a source of joy to watch so many of them grow and I am grateful that I could have been a part of that. Our RAs have helped me in numerous ways, but I am especially grateful for the time they have put in to help us recruit participants over the years, and for their patience in helping me develop and apply new lab methods. As an undergraduate, you generally look to graduate students for some degree of certainty and direction. For my RAs, there may have been some of that, but there was also a lot of "I have no idea; let's try stuff and see what happens!" Fei Rodell and Ben Davisson especially had to deal with the brunt of inefficient painstaking attempts at embedding hair. By the time Kendall Rouch took over, she played a huge role in all the trial-and-error that goes into testing out new methods. Yesenia Hill, Sam Muller, and Duneshka Cruz, all made sure these methods were recorded as the protocols that I present in this dissertation. Thank you all so much for your help and for letting me be a part of your research experience. I am proud of each and every one of you.

Tess Wilson, Audrey Chambers, and Robin Kephart have all helped me in numerous ways. In between all their other obligations, they've always found the time to answer my questions, or help me when I need something. Tess, thank you for checking in on me and listening to me (and for your kolaches recipe). Robin, I don't know what I would do without you (I'm sure you get that from everyone in the department), but you manage to navigate the deep, dark maze that is Penn State administration, and always come back with a solution, or at least an answer. Thank you for all your help. Audrey, I will never forget those 48 hours where I thought I was going to get deported and you managed to help me email around and get things sorted out. You are always a ray of sunshine, whether it is in person or in my inbox. Thank you all.

A few other people I would like to thank include: my mentors, Janina Jeff, Brandon Ogbunu, and Colin Shaw (the mentor who set me on this path!). Maria Nieves-Colón who helped me when I first submitted my NSF DDRIG. Kevin Flaherty, for our lovely chats, his superlative sense of humor, and his choice to help me with LaTeX instead of mocking me for trying to use something I'd never used before to format my dissertation a week before it was due. Thank you to Erin Marie Williams-Hatala and Kevin Hatala for hosting me on multiple occasions and giving me my first American Thanksgiving experience. I am so thankful to Connie Mulligan and Jenny Raff for inviting me to take part in a special issue of AJPA—it means a lot that you had faith in my abilities. I am grateful to all the members of the Black in Bio Anth Collective, who have provided

me with community and a vision for the kind of future I want to build with them. I'm indebted to the Black Graduate Student Association at Penn State, and especially Latisha Franklin, who has done so much to make me and others feel at home in State College.

I'm grateful to all the old friends I was able to reconnect with during the pandemic: Julianne Joswiak, Sian Ditchfield, Justin Wells, Jaap Saers, Jerome Singh, Laura Neumann, and Cheyenne Ritfeld. You have all supported me back since before this project was even an undergraduate dissertation! I also picked up a lot of new friends along the way: Kimberleigh Tommy, Bobbie Benavidez, Izzy Starr, Edelio Bazan, Antal Martinecz, Yesmar Oyarzun, Ampson Hagan, Chrystel Oloukoï, Delande Justinvil, Chelsey Carter, Sarah Bruno, Ashley Ngozi Agbasoga, Brendane Tynes, Kelly Chege. Each of you helped me in your own way when my life got turned upside down. I am especially grateful to Jerika Heinze for advocating for me when I reached out in need of help. I am also deeply thankful for having met Emily, Sarah, Geoff, and so many people at Centre Safe, who helped me through one of the most difficult periods of my life. I would like to thank all those who have provided me with the challenges I needed to overcome in order to realize my full potential.

To my mother and father, Aneta and Adisa: thank you for your faith that I would always succeed in life no matter what I chose to do. To my little brother, George: if you hadn't broken my Pokémon Crystal, I may have been a gamer instead of a scholar, so I guess you deserve some credit here (I love you, though). And finally, to my Winston: you are the best decision I have ever made in my life. You may never know it, but you gave me the strength to do what I needed to do, because I knew I would be fine, as long as I was with you.

## **Acknowledgement of funding support**

This material is based upon work supported by the National Science Foundation under Grant No. 1847845, The Wenner-Gren Foundation (Gr. 9911), The Pennsylvania State University Department of Anthropology Hill Fellowship Post-Comprehensive Examination Award, and The Pennsylvania State University Africana Research Center.

Any opinions, findings, and conclusions or recommendations expressed in this material are those of the author(s) and do not necessarily reflect the views of the National Science Foundation, The Wenner-Gren Foundation, or The Pennsylvania State University.

# Chapter 1 |

## Introduction and background

Humans have famously been dubbed “The Naked Ape” in honor of our seemingly hairless bodies (Morris, 1967). Human bodies have a few truly hairless (glabrous) body parts, including the palms of the hands and the soles of the feet, but the majority of our epidermis is covered in vellus hairs produced from miniaturized hair follicles (Jablonski, 2006). The most conspicuous exception to this mostly naked body is the tuft of terminal hair that graces the human scalp. The evolutionary function of this specifically human trait is not well understood. Similarly, the remarkable range of variation in scalp hair morphology among populations remains an evolutionary mystery.

### **1.1 What is missing in our methods: a racialized lens and limited lexicon**

The evolutionary function of scalp hair is unclear, but the variability of scalp hair morphology has been widely considered a fundamental trait distinguishing human groups. In fact, scalp hair morphology (alternatively hair form, texture, type, or shape) is part of a suite of traits that have historically been used to classify humans into discrete groups (Pruner-Bey, 1877; Garn, 1950, 1951; Linnaeus, 1758; Jablonski, 2020; Seta, Sato, & Miyake, 1988). Hair has been used alongside skin color and a number of other physical attributes to construct a racialized framework of human biological variation as neatly divisible into mutually exclusive categories. The taxonomic approach to continuous human variation developed by European scholars during the Enlightenment has affected all subsequent thinking and hindered our ability to understand these traits outside of a racial paradigm.

The study of racialized traits, such as hair morphology, necessitates objective (quan-

titative) methods to remove (or, at least, reduce) observer bias. The development and improvement of reflectance spectrophotometry for skin pigmentation has drastically altered the scientific study of this phenotype (Jablonski, 2012). These methods have allowed scientists to describe the clinal nature of skin pigmentation variation (Relethford, 2000; Jablonski & Chaplin, 2000), test hypotheses about its evolutionary function (Jablonski & Chaplin, 2000; Madrigal & Kelly, 2007), and uncover the genetic architecture that underlies it (Crawford et al., 2017; Martin et al., 2017; Beleza, Santos, et al., 2013). Similar advancements in cranial morphometrics and 3D facial image analysis have facilitated the complete departure from racial typologies and a sophisticated exploration of these complex traits (White et al., 2019; Zaidi et al., 2017; Relethford, 2002; Betti, Balloux, Hanihara, & Manica, 2009; Claes et al., 2014).

However, the absence of such methodological advancements has left the study of human variation in hair morphology relatively stagnant. The continued racialized framing of hair morphology was so strong that when anthropologists abandoned racial classifications in the second half of the 20th century, the study of human variation in hair morphology also fell out of favor. Indeed, we see that this object of study persisted most clearly in forensic science—a discipline where racial typologies were not only tolerated, but considered a central goal (Seta et al., 1988; Cole, 2020; Ogle & Fox, 1998). Dermatological and cosmetological interest in human hair variation has led to a significant body of research describing human hair morphology (De La Mettrie et al., 2007; Lindelöf, Forslind, & Hedblad, 1988; Franbourg, Hallegot, Baltenneck, Toutain, & Leroy, 2003). However, without a clear framework for understanding human biological variation, much of this literature has oscillated between using explicit racial paradigms (Khumalo, 2007) and presenting ethnicity as an essential and immutable biological category (Franbourg et al., 2003; He & Okoye, 2017; Cruz et al., 2013), or completely ignoring the potential effects of population structure by using distantly related populations as proxies for particular extremes of hair morphology, such as straight vs. curly (Thibaut, Gaillard, Bouhanna, Cannell, & Bernard, 2005; Wortmann, Wortmann, & Sripko, 2019).

Across disciplines, hair texture is described as “straight”, “wavy”, or “curly” giving the impression that every individual falls into a clear and mutually exclusive category. But the lines between hair texture categories are highly subjective. Additionally, when implicitly racialized categories such as “frizzy” are added, the apparent objectivity of these descriptors disappears as certain terms are exclusively used to describe particular populations, in much the same way that corresponding racial frameworks have done historically (Linnaeus, 1758). Moreover, the manner in which these terms are used, often

gives the erroneous impression that European populations have a wider range of variation than African or East Asian populations (against whom they are often compared).

The limitations of our lexicon suggest the need for methods that minimize subjective interpretations and, ideally, quantitatively reflect the continuous and multi-faceted nature of the phenotypic variation that is subsumed within the broad umbrella of human scalp hair morphology. There have been many attempts to solve this very problem, but the lack of universal (or even widespread) standards for the characterization of hair morphology ostensibly points to the complexity of the task. On the scale of the individual hair fiber, one can measure longitudinal curvature and cross-sectional properties. The cross-sectional morphology of hair fibers can be accurately assessed using a variety of established methods (Pruner-Bey, 1864; Kneberg, 1935; Hrdy, 1973; Lasisi, Ito, Wakamatsu, & Shaw, 2016), but curvature has proven much harder to characterize (Lasisi et al., 2020; Hrdy, 1973; Mkentane et al., 2017). These problems are compounded by the divergent needs of practitioners in different disciplines who want to measure hair, but who are limited by the materials, equipment, and skills available to them.

## **1.2 Phenotype-genotype associations: how much do we know about hair morphology?**

The laborious nature of existing methods for quantifying hair morphology have resulted in the propensity of large-scale genome-wide association studies (GWAS) to rely on simple subjective qualitative descriptions of hair, either by participant’s self-reporting or by the evaluation of the observer collecting participant samples and information (Liu et al., 2018). This qualitative approach coincides with the complete exclusion of African and African-descendant populations from these studies, who, in the straight/wavy/curly/frizzy framework, would be invariably described as having “frizzy” hair and thus, no variation to speak of that could be investigated in a GWAS<sup>1</sup>. Nevertheless, these qualitative approaches have yielded some significant associations with hair texture in some (mainly North European and East Asian) populations (Liu et al., 2018; Adhikari et al., 2016; Medland et al., 2009; Tan et al., 2013). The most notable exception to the qualitative approach is the landmark study associating a single nucleotide polymorphism (SNP)

---

<sup>1</sup>The one seeming exception to this would be the Adhikari et al. 2016 study as it featured a large sample of admixed Latin American populations. However, upon closer inspection, there is a surprising dearth of African ancestry in any of their samples, and, more problematically, their supplementary materials reveal that individuals describing their hair as “frizzy” were excluded from the analysis due to their small relative sample.

within the ectodysplasin A receptor (*EDAR*) in East Asian populations (Fujimoto et al., 2008a). This non-synonymous SNP, also referred to as the 1540C allele, was associated with an increase in hair thickness, which highlights the importance of the efforts the authors took to quantify the cross-sectional shape of each individual, as that variation would have been invisible otherwise. Other attempts to use quantitative approaches have relied on the application of methods used for sheep’s wool, without necessarily demonstrating the validity of those methods for the measurement of human hair (Ho et al., 2020, 2016).

Other avenues of research informing the genetic architecture of scalp hair morphology include Mendelian diseases and animal models. The inheritance patterns of a number of scalp hair disorders varies across various families around the world. Conditions described as “woolly hair syndrome” and “uncombable hair syndrome” have been used to medically categorize hair that is considered to be uncharacteristically coily, “frizzy”, “unmanageable” or “woolly” for the population (or racial category) that the diagnosed individual is considered to be (Pavone et al., 2017; Horev et al., 2009; Calderon, Otberg, & Shapiro, 2009). Though the medical diagnostic validity of these conditions may be questionable, research tracing so called “affected individuals” in pedigree studies are an important source of information for potential gene candidates for normal-range variation (non-Mendelian) GWAS. Such cross-validation of gene function is seen for *EDAR* for example, where certain variants in the locus (albeit different) cause both Mendelian disorders and affect normal-range variation (Fujimoto et al., 2008a; Stecksén-Blicks, Falk Kieri, Hägg, & Schmitt-Egenolf, 2015; Lee et al., 2014).

Lastly, a large body of literature exists in developmental biology with regards to gene expression associated with hair morphology in animal models. In mouse models, a number of genes have been found to be expressed in hair follicles, including *Prss53*, *Gata3*, and *Wnt10a* among many others (Adhikari et al., 2016; Vidal et al., 2005; Kimura et al., 2015; Peters et al., 2003). Though mouse models are traditionally used in many functional genomic studies, there is some question of the extent to which hair/fur results are transferable as mice, like many other mammals, have pelage that is different from human scalp hair in a number of ways, including the tendency to express crimped rather than curled hairs (Koch, Tridico, Bernard, Shriver, & Jablonski, 2020). Other non-model organisms used to explore the genetic architecture of hair morphology broadly include dogs and cats, where the wide variability of coat morphology across breeds has been leveraged to uncover a number of genes that play a role in this phenotype and may be of some relevance to human hair morphology (Cadieu et al., 2009; Gandolfi et al., 2010).

Overall, elucidating the genetic architecture of human scalp hair morphology is important on a number of levels for evolutionary anthropologists. Firstly, the remarkable variation among human populations begs the question of what selective pressures have shaped the evolution of human scalp hair diversity. Knowing the genetic underpinnings of this trait would allow us to investigate this question and test various hypotheses on the nature and timing of the selective events. Furthermore, investigating the evolutionary genomics of hair-related genes is the only window that allows us insight into the long-term evolutionary history of this trait in the hominin lineage. Hair leaves little to no trace in the fossil record, so interrogating the record left in the genomes of contemporary and available archaic genomes is the best chance we have at confidently inferring when, how and why scalp hair and its subsequent variation evolved.

### **1.3 How does heat factor into the evolutionary history of human head hair?**

In order to fully understand the evolution of human scalp hair, we must consider specific hypotheses that might explain the evolution of this phenotype and its subsequent morphological diversification. However, the anthropological literature on human evolution contains surprisingly little information on the topic, beyond surface-level speculation. Most commonly, sexual selection is invoked as the “functional” explanation for the presence and variation of human scalp hair. Darwin attributed much of human variation, including skin color, hair color and hair texture to sexual selection and different preferences of “races” (Darwin, 1871). Later discussions of the presence of scalp hair (particularly its relative length) has been attributed to social communication or sexual signalling (Neufeld & Conroy, 2004; Caldararo, 2005; Thierry, 2005). However, none of these has offered any explicitly testable hypotheses.

Among the few other discussions of human scalp hair evolution is the hypothesis that hairy scalps may have evolved as protective barriers against solar radiation in bipedal savannah dwellers (Wheeler, 1984). Managing thermal load would be particularly important in the context of a large thermogenic and thermosensitive brain. Furthermore, there exists a hypothesis that tightly curled hair may have been particularly adaptive under such intense solar regimes (Jablonski, 2006; Jablonski & Chaplin, 2014). If one considers the question of human scalp hair function in the broader context of mammalian fur, it is quite striking that thermoregulation has not been investigated more extensively.

For most mammals, hair plays an important role in thermoregulation, not only through insulating air warmed by body heat in cold environments, but also by reflecting much of the solar radiation before it reaches the skin. This protection from solar radiation does not merely protect from the effects of UV damage, but it also reduces the total heat load on an animal (Wheeler, 1985). In this context, variation in mammalian hair coats has been studied to understand how they may be adapting to different levels of solar radiation. Research on radiative heat gain in two species of squirrel (*Spermophilus lateralis* and *Spermophilus saturatus*) demonstrated using a heat flux plate that, while a lighter colored coat can avoid heat gain by reflecting most of the solar radiation, a similar reduction in radiative heat gain may be achieved by a deeper coat of fur (Wheeler, 1990). Additional studies in koalas, kangaroos, and polar bears confirmed the role of hair depth in thermal insulation (Dawson & Maloney, 2017; Dawson, Webster, & Maloney, 2014). In humans, hair depth can be created by the tight curling of hair, as well as thick fibers that create more volume, both of which maximize the distance between the surface of the hair and the surface of the scalp.

There are a few empirical studies in humans suggesting that, at the very least, scalp hair may have some effect on thermal balance. In particular, a number of studies have pointed to a significant effect of absence/presence of scalp hair in the context of heat loss. For example, Cabanac and Brinnet (1988) found that bald men evaporated sweat on their heads at a higher rate than men with scalp hair and this was corroborated by a recent study (Coelho et al., 2010). At face value, it appears that a bald head would be superior due to the increased sweat rate, however the Coelho et al. study suggests that this higher sweat rate may be offset by a higher heat load. Taken together with the mammalian fur research, there is certainly sufficient evidence to warrant a more thorough study of the potential effects of scalp hair, and variation in its morphology, on human heat load.

## 1.4 Motivation for the work

There are significant gaps in our knowledge of human scalp hair variation due to the culmination of a number of historical factors. First and foremost, the role of scalp hair as a trait for distinguishing human groups has led to the entanglement of scientific study of scalp hair with racial views of human biology. The interest anthropologist had historically shown in human scalp hair variation gave way to an avoidance of this phenotype due to its seemingly inextricable link to race. The inescapable link to a

history of scientific racism thus forms an obstacle to the study of this subject. This impediment is further exacerbated by the lack of practical methods for the study of hair morphology. For these reasons, it is likely that the topic of human scalp hair variation has appeared to many biological anthropologists to be a costly investment of time and effort with a considerable amount of uncertainty in the reception of this work among the larger scientific community. As a result of anthropological avoidance of human scalp hair variation, consideration of this phenotype is absent from crucial work on human evolution. A few scholars have called attention to the potential importance of scalp hair in the context of our species' evolution (Wheeler, 1985; Jablonski & Chaplin, 2014). Still, the relatively small surface area our scalp hair covers has misled many to assume that its effects could not possibly have significant consequences on our thermal biology (Hora, Pontzer, Wall-Scheffler, & Sládek, 2020). With such assumptions, this trait has been relegated to the status of superficially interesting, but superfluous in the grand scheme of evolutionary anthropological research.

The absence of biological anthropologists from the development of scientific knowledge on human scalp hair variation has been to the detriment to other disciplines as well as our own. The relatively abrupt pivot away from racial science within most of anthropology was achieved largely by the pursuit of research on human variation in traits relatively devoid of racial connotation (e.g. lactase persistence, disease resistance, high-altitude adaptation). The study of racialized traits in biological anthropology was largely guided by the availability of technologies that would allow for the almost complete detachment of subjective descriptions that risked alluding to race. For example, the reflectance spectrophotometer enabled biological anthropologists to describe variation around the world with numbers expressing skin reflectance, rather than perceived color categories. Similarly, the historically racist descriptions of stereotypical cranial and facial variation among populations had given way to geometric morphometric study of the head with unsupervised statistical approaches, such as Principal Components Analysis, that could be asserted as impervious to racial thinking.

The relative dearth of recent anthropological work on hair is in contrast to the considerable interest this trait has received from forensic scientists, dermatologists and the cosmetic industry. Unlike anthropology, the departure from racial approaches in these fields has been slower and, in some cases, faced active resistance due to the perceived usefulness of race as a biological concept. Rather than engaging with issues, disciplinary silos have led to an unspoken understanding that such critique is unfruitful and fields studying the same topic are separated by a seemingly insurmountable epistemic schism.

Yet, the many calls to interdisciplinary and transdisciplinary science suggest that, on some level, there is consensus that our status quo is undesirable (Leshner, 2004; Manlove et al., 2016; Luke et al., 2015; Croyle, 2008). The work I present in this dissertation is thus driven by the desire to address critical gaps in our own field by developing new methodologies and cross-disciplinary bridges that will promote the future study of a neglected facet of human variation.

## 1.5 Outline of chapters

In this dissertation, I preface my investigation into the evolution and genetic architecture of human scalp hair morphology by examining the racialized nature of this phenotype in Chapter 2: "The constraints of racialization: how classification and valuation hinder scientific research on human variation" and is based on a published article in the *American Journal of Physical Anthropology* (Lasisi, 2021). Here, I present the motivation for my focus on developing objective, quantitative methods that can be applied without reference to ancestry, ethnicity, or race. In this chapter, I set out a framework for examining the racialization of phenotypes based on two processes: classification and valuation. Using examples from the scientific literature on skin and hair color, I illustrate the ways in which classification facilitates the racialization of traits by distorting continuous variation in a manner that overemphasizes European variability and homogenizes other groups of people. Furthermore, I demonstrate how classification works synergistically with valuation to present certain subjective categories as superior to others. Specifically, I use examples of persistent, unsubstantiated claims of the universal preference for lighter skin presented as a legitimate sexual selection hypothesis, and the unjustified pathologization of hair that is typified as "African" when it is expressed in Eurasian populations.

In Chapter 3, I present the methodological contributions of this dissertation to the quantitative assessment of hair fiber curvature and cross-sectional morphology. This chapter is based on an article that has been submitted to *Scientific Reports* and can be found as a preprint manuscript on *bioRxiv* (Lasisi et al., 2020). As discussed above, hair morphology is of professional interest to dermatologists, cosmetologists, anthropologists, forensic scientists, and geneticists, but is poorly understood because hair itself is difficult to work with in the lab and continues to be studied with outdated methods and racialized typological frameworks. In light of this, I put my efforts towards developing a complete set of methods that include protocols for embedding hairs for sectioning, washing, and preparing hairs for curvature imaging, and an open-source Python package

(*fibermorph*) for the analysis of the image data. These methods are the culmination of seven years of work on the development of replicable high-throughput protocols, and they establish a much-needed baseline for future research on hair morphology. The *fibermorph* image analysis program is freely available through PyPi.org and on GitHub, where the source code can be found. The sample preparation protocols are publicly available on `Protocols.io` and include videos of the steps (Lasisi, 2020c, 2020b).

One of the primary motivations for the development of the hair quantification methods was to generate phenotypic data that better represented the complex continuous nature of the underlying biological structure. To test the usefulness of these methods, I applied the methods to a sample of admixed African-European individuals ( $n = 192$ ) for whom we had previously collected genotype data and hair samples. In Chapter 4, I describe the results from my investigation of the genetic architecture of quantitative scalp hair morphology. This chapter illustrates how previous literature has failed to take into account population structure when interpreting the co-occurrence of different aspects of hair morphology. Specifically, the persistent contrasting of what is categorized as (East) Asian hair with (West) African hair, has led to the erroneous conclusion that the round cross-sections considered archetypical of “Asian” hair are the cause of straight hair while the “flat” cross-sections associated with “African” hair are the cause of curled hair. This chapter demonstrates that, in our sample, the association between hair curvature and cross-sectional morphology is explained by population structure, pointing to the possibility of multiple independent factors contributing to the macromorphology of hair. Additionally, I report the successful replication of previously reported hair loci and the results of an exploratory admixture mapping analysis.

In Chapter 5, I present experimental results on the effect of scalp hair on thermal load. This work is based on a collaboration with the Environmental Ergonomics Research Centre (EERC) at Loughborough University in the United Kingdom. This chapter describes the findings of a series of thermal manikin experiments undertaken at the EERC under the supervision of Drs. George Havenith and James Smallcombe. The study takes a biophysical approach to the question, by using human hair wigs and a thermal manikin—a life-sized human model used to simulate heat transfer between the skin and the environment. Such an approach allows for the direct collection of data on the thermal properties of hair in isolation from physiological responses that humans may have to heat stress. Our results demonstrate that there is a distinct inverse relationship between hair curl and solar heat gain, where increasingly curled hair appears to reduce the heat gained from solar radiation on the scalp. Finally, in Chapter 6, I reflect on

lessons learned from the questions explored in each chapter and future directions for research on the evolution of human scalp hair.

## Chapter 2 |

# The constraints of racialization: how classification and valuation hinder scientific research on human variation

Racial thinking is deeply entrenched in the science of human biological variation. In much of the anthropological and biomedical work on human variation, we see the reproduction of race categories with new terminology due to an inability to surmount racialized frameworks (Bliss, 2012; Panofsky & Bliss, 2017; Benn Torres, 2019). As a consequence of this, scientific research has stagnated and reiterated thinly veiled race-based groupings (Saini, 2019).

Here, I illustrate how the use of classification systems and (implicit) valuing of certain trait variants over others entrenches the racialization of human variation. In light of this, I conclude with some thoughts on how we might move forward and overcome the issues that have led to our current state.

### 2.1 Classification and Distortion

A considerable number of classification systems used for human phenotypes are subjective and strongly influenced by racial ideas about human variation. This leads to the distortion of the biological variation they seek to represent and, frequently, the misdirection of scientific inquiry into those traits based on these biased perceptions. Examples of this can be found for every trait that has historically been used as a so-called “racial character” (Gates, 1925; Garn, 1951; Ogle & Fox, 1998). Many such typological approaches are still

used today. Most importantly, we can see a distinct Eurocentric bias in many of these examples.

### **2.1.1 The perceived variability of European traits**

Eurocentric bias in classification schemes often manifests as the illusion of a wider range of variability in European populations than all other populations. The Fitzpatrick scale is one such example. This scale was originally developed exclusively for the classification of “white skin” according to its response to solar radiation (Fitzpatrick, 1975). The original scale only consisted of four categories (Roman numerals I through IV) of “white skin” (though type IV is often described as “light brown” in color). Additional “brown” and “black” skin categories (V and VI, respectively) were, by Fitzpatrick’s own admission, an afterthought (Fitzpatrick, 1988).

This skin typing system classifies an individual according to skin color, sunburn, and tanning response. However, the scale only allows for particular combinations of these distinct epidermal traits. Only types I to III burn and the distinction between these three types is in their ability to tan (type I does not tan, type II tans minimally and type III tans). Types IV, V and VI do not burn and do tan—their only distinction is skin color. This information is collected through self-report.

Unsurprisingly perhaps, there has long been evidence that this system does not work for “non-white” populations (Gupta & Sharma, 2019; Kumar, Suliburk, Veeraraghavan, & Sabharwal, 2020; Pichon et al., 2010; Ware, Dawson, Shinohara, & Taylor, 2020; Park, Suh, & Youn, 1998; Willis & Earles, 2005). If we look at distributions of objective measures of skin reflectance around the world, the range of variation among European populations is the narrowest, while many populations that would be simply described as ‘brown’ or ‘black’ according to the Fitzpatrick scale, possess a range of skin color that is quantifiably more vast (Martin et al., 2017; Crawford et al., 2017).

Even among so-called “white-skinned” individuals the validity and value of this skin typing system is questionable. Rampen et al. attempt to apply this system to a sample of Dutch students and find that only 41% of these cases can be classified according to the original scale (Rampen, Fleuren, de Boo, & Lemmens, 1988). The authors explicitly criticize “the assumption that there is a reciprocal interdependence between the tendency to burn and the ability to tan”.

Despite these extensively discussed limitations, it continues to be used, even in such applications as DNA-based phenotyping (Chaitanya et al., 2018). Moreover, the literature contains many examples of studies that attempt to link other phenotypic traits (freckles,

hair color, eye color) to the Fitzpatrick skin types, demonstrating the strong appeal of the idea that humans can be classified into types with coherent and categorically exclusive phenotypic attributes (Azizi, Lusky, Kushelevsky, & Schewach-Millet, 1988; Guinot et al., 2005; Gupta & Sharma, 2019). While the limitations of classification of skin type is well known and there are quantitative alternatives, classification of other phenotypes remains relatively unchallenged.

There are many examples of the perceived uniqueness of European populations with regard to their hair and eye color, as well as their scalp hair texture (Biasutti, 1953; Adhikari et al., 2016; Morgan et al., 2018; Ogle & Fox, 1998). Even when privileging Eurocentric hair color typologies, the uniqueness of this European variability does not hold. For example, Melanesians are a well-known population in which blond hair is found (Kenny et al., 2012; Norton et al., 2006). This perception of unique European variability is heavily influenced by the range of variation that is encompassed by classificatory terminologies.

Categorical groupings of eye color, hair color and hair texture are inconsistent. Moreover, the categories that exist give a higher resolution to the variation associated with European populations. For example, eye color categories generally include blue and brown eyes, but may also distinguish grey, honey, hazel, brown, black, and various shades thereof.

Davenport and Davenport (Davenport & Davenport, 1907), for instance, claimed that “blue/grey and brown suffice”, the DNA phenotyping tool HIrisPlex-S claims to be able to predict eye color as being blue brown or “intermediate” (Chaitanya et al., 2018), and a recent genome-wide association study (GWAS) on admixed Latin Americans used the categories: blue/grey, honey, green, light brown, and dark brown/black (Adhikari et al., 2019). This inconsistency in the names and number of categories points to the subjectivity of these perceived phenotypes. The existence of these categories is asserted with little to no justification.

We see a similar pattern in hair color, where red, blond, brown and black are seen as distinct categories (Hysi et al., 2018; Branicki et al., 2011; Guenther, Tasic, Luo, Bedell, & Kingsley, 2014; Balanovska et al., 2020). Even more expansive hair color classification systems, such as the Fischer-Saller scale still present more categorical options for gradations of color seen across and within European populations (Fischer & Saller, 1928). With regards to hair texture, the most common classification is straight, wavy, curly, and sometimes the addition of a “frizzy” category or further subdivisions within these qualitative descriptors (Liu et al., 2018; Adhikari et al., 2016). These qualitative

descriptors are inconsistently interpreted and mask the range of variation that exists within tightly curled or “frizzy” hair (Lasisi et al., 2020).

In the cases where typologies are being proposed or justified, even a cursory examination of the populations informing these typologies reveals that Europeans are the main—if not, exclusive— pool of data (Fischer & Saller, 1928). Mostly, however, phenotypic typologies are invoked without any rationalization of their validity—they are simply asserted as self-evident truth. To some, it may be tempting to conclude that, while vague, existing qualitative categories of eye color, hair color, and hair texture are distinct and that there simply exists more biological variation in Europeans. However, a closer look at the known biology of each of these traits reveals that emphasis on the European range of variability is not only disproportionate to any objective quantitative measure of phenotypic variability, but that the categories themselves are unwarranted on the basis of the underlying biological processes.

### **2.1.2 Objective variation and subjective salience**

Our perception of hair color is mainly influenced by the type and quantity of melanin that hair fibers contain. The chemical analysis of degradation products associated with eumelanin (a brown melanin) and pheomelanin (a red melanin) can quantitatively describe the hair color in terms of the amount and relative proportion of these two fundamental components (Ito et al., 2011; Ozeki, Ito, Wakamatsu, & Thody, 1996).

These chemical analyses reveal that perceived hair categories differ on two main axes. The first is whether they have a significant amount of pheomelanin; such hair almost invariably appears red to some degree or another. The second axis of variation is a continuous increase in eumelanin that corresponds with our perception of light (blond) to dark brown and black hair (Ito & Wakamatsu, 2011).

However, existing data show a significant overlap in the eumelanin content between different perceived categories. Moreover, the range of variation seen black and dark brown hair, respectively, exceeds the collective range of variation seen in blond, light and medium brown hair combined (Ito & Wakamatsu, 2011; Lasisi et al., 2016). This suggests that while apparently less salient according to the literature, from a biological perspective, there may be more meaningful variation that is being subsumed within these darker categories, as has been suggested elsewhere (Norton et al., 2016).

Eye color is pigmented by the same two melanins, but unlike hair and skin, where the melanin is deposited by the dendritic melanocyte that produces it, melanin in the eye is contained within the cytoplasm of the melanocyte (Wakamatsu, Hu, McCormick, & Ito,

2008). Additionally, there are two divergent developmental lineages of melanocytes that contribute to pigmentation of the eyes: epithelial (of neural ectodermal origin) and uveal (of neural crest origin). Ocular pigment epithelium does not appear to contribute to any visible variation. Most variation in apparent eye color appears to come from the uveal melanocytes, located in the iris and the choroid (Wakamatsu et al., 2008).

Much like hair color, current evidence does not suggest qualitative differences, but rather a continuous spectrum of melanin production. But unlike hair, there is no equivalent pheomelanogenic outlier (like red hair) - all eye color appears to vary primarily in eumelanin content. The qualitative difference we perceive (blue vs. brown) is a result of structural coloration that occurs when light scatters on (relatively) depigmented layers of the iris (Sturm & Larsson, 2009).

Classification of hair texture goes even one step further than hair and eye color typologies: it presents a tautology where the classification of humans by race or ethnicity is eponymous for the classification of hair texture (e.g. “Caucasian hair” or “Oriental hair”). This is seen most frequently in dermatology, cosmetology and forensics (Ogle & Fox, 1998; Cruz, Costa, Gomes, Matamá, & Cavaco-Paulo, 2016; Franbourg et al., 2003; Lima, de Almeida, Velasco, & Matos, 2016). In the case of dermatology and cosmetology, this practice ironically stems from a relatively recent effort to cater to patients and consumers who, historically, have been excluded (Cruz et al., 2016; Franbourg et al., 2003; Lima et al., 2016). Forensic science, on the other hand, has a longer history of working with racialized hair categories, in part due to the overvaluation of racial profiling in criminal investigation (M’charek, Toom, & Jong, 2020; Ogle & Fox, 1998).

Yet, what we know about hair biology suggests that variation is more complex than the asserted racial classifications suggest (Khumalo, 2007; Lasisi et al., 2016, 2020; Loussouarn et al., 2007; Adeola, Khumalo, Arowolo, & Mehlala, 2020). Various studies of hair fiber curvature and cross-sectional geometry show continuous variation across populations (Lasisi et al., 2016; Loussouarn et al., 2007; Hrdy, 1973; Fujimoto et al., 2008a). Still, qualitative descriptors of hair morphology persist and are the main mode of phenotyping for large-scale GWAS (Liu et al., 2018; Medland et al., 2009; Eriksson et al., 2010; Adhikari et al., 2016) and other fields of research (Lima et al., 2016; Mieczkowski & Newel, 2020; Thibaut et al., 2005). The persistence (and continued justification) of all these classification systems demonstrates deep-rooted beliefs about whose variation actually matters.

## 2.2 Thinly veiled value judgements

Classification works synergistically with valuation to add a dimension of racial hierarchy. While explicit mention of certain populations being superior to others is generally rebuked, more subtle echoes of longstanding ideas of racial superiority permeate much of the literature. By framing value judgements in the language of selection, much the same effect is achieved by designating certain populations as (representative of) ancestral humans that give a window into the primitive history of more derived populations (Reardon & TallBear, 2012).

### 2.2.1 Valuation as sexual selection

This “ancestral vs. derived” dynamic that reproduces racial hierarchies is especially evident in narratives of sexual selection among human populations, which is corroborated by the recurrent (and widely cited) claim that sexual selection explains the evolution of depigmented populations (Aoki, 2002).

The issue with the particular example cited here is that it argues for the significant influence of mate choice (specifically selection exerted over female individuals) and the existence of a universal preference for lighter skin. Aoki supports his claim of universal preference for lighter skin with a series of literary anecdotes and with selective evidence from social psychology experiments.

The historical narratives he uses including descriptions of beauty standards in Ancient Rome and 8th to 20th century Japan. Quite disturbingly, Aoki interprets the sexual exploitation of enslaved (light skinned North European) women by ancient Romans as a “predisposition to find light-skinned females attractive even when they are members of a conquered group.” If sexual exploitation of enslaved women is evidence for their attractiveness, it is quite puzzling that Aoki does not mention the preponderance of evidence for Y-chromosomal contributions from (light-skinned) European males to (darker-skinned) Indigenous American, Pacific Islander and African women (Kayser et al., 2003; Brucato et al., 2010; Hurles et al., 1998). By his own reasoning, there appears to be far more evidence supporting the preference for darker skin.<sup>1</sup>

The selective evidence Aoki draws from social psychology are based on convoluted

---

<sup>1</sup>I make this argument to point out the lack of logic in Aoki’s reasoning (as well as other supporters of these ideas). However, it is important to note that the sexual violence should not be interpreted simplistically as a manifestation of attraction (a naturalistic fallacy) when there is extensive evidence that humans use this as a means of domination against individuals across the spectrum of gender and other identities (Armstrong, Gleckman-Krut, & Johnson, 2018).

(and misleading) interpretations of results based on “Caucasian” university students from the 1970s<sup>2</sup> and a misrepresentation of a flawed analysis of ethnographic data across 312 groups.<sup>3</sup> Furthermore, he fails to include mention of the lengths to which lightly pigmented individuals consciously risk skin cancer and cover themselves with tanning preparations (Fogel & Krausz, 2013; Cho, Hall, Kosmoski, Fox, & Mastin, 2010; Abdel-Malek et al., 1995; Garone, Howard, & Fabrikant, 2015). Despite these flaws and thorough critique (Madrigal & Kelly, 2007), the article continues to be cited as a scientifically valid and defensible hypothesis.

Selection (sexual or otherwise) is not inherently racist. But in its application, as far as the scientific literature is concerned, it has invariably depicted Europeans (and other populations with colonialist histories) as the culmination of evolutionary progress. These narratives of linear progress or racial superiority go against the very Darwinian theories they purport to apply. It is quite ironic that Aoki’s article has the subtitle “Darwin’s hypothesis revisited” when Darwin, himself, had the following to say on the matter:

*“It seems at first sight a monstrous supposition that the jet-blackness of the negro should have been gained through sexual selection; but this view supported by various analogies, and we know that negroes admire their own colour.”*  
(Darwin, 1871)

Among other similar passages,<sup>4</sup> it appears a strange omission for Aoki to focus solely on

---

<sup>2</sup>Aoki makes reference to a 1978 study of around 1000 undergraduates identified as Caucasian who were surveyed about their likes and dislikes (Feinman and Gill 1978). He summarizes the findings as follows “Most individuals regardless of sex preferred ‘medium white that tans to gold’, which is the fourth lightest (fifth darkest) category on the list. In other words, both sexes appear to prefer a slightly lighter-than-average—more precisely, a lighter-than-median—skin colour”.

Aoki also notes that “Many males dislike ‘black’, whereas the great majority of females dislike the two lightest shades.” Of the eight possible choices students were given, the most “liked” options were the darkest options that are associated with their own “Caucasian” group. Leaving aside that the category of “dark white” is an oxymoron and that the authors of the study acknowledge racial connotations likely played a part in the student’s choices, the data do not support Aoki’s statements. Even the emphasis on dislike for ‘black’ skin in males is incomprehensible considering that the absolute largest percentage of dislike in that category was ‘light skin which freckles’.

<sup>3</sup>The way Aoki summarizes the data from Van den Berghe & Frost (van den Berghe & Frost, 1986), one would assume that the majority of the data showed a preference for lighter skin (as concluded by the original authors themselves). However, the article describes that of the 312 societies for which ethnographic data was available on beauty ideals, only 51 included any mention of skin color as part of those. The authors then focused on the categories that did mention something about the matter to draw their conclusions, but this dismisses the more readily apparent conclusion that: the majority of societies give no importance to skin pigmentation.

<sup>4</sup>Chapter 19 from Darwin’s *Descent of Man* gives many more anecdotes on which he bases his conclusion that each “race” prefers their own group’s appearance. Another particularly interesting passage, cited from Mungo Park’s *Travels in Africa*: “With respect to colour, the negroes rallied Mungo

evidence of the preference of light skin. A non-biased application of (sexual) selection should focus more directly on testable hypotheses that make predictions related to fitness.

If Aoki could for example demonstrate evidence that (within a population) female individuals with less pigmented skin have more offspring, his claim would be more convincing. In absence of direct evidence, at the very least, a hypothesis arguing for the selection of a particular trait variant should articulate the mechanism by which it would affect fitness. But this absence of a clear link to fitness (and focus on value-laden proxies such as “beauty” and “preference”) is in line with the general tendency of research that implicitly naturalizes valuation using the language of selection.

This is not to say that it is impossible for mate choice to influence human phenotypic variation. A better example based on skin pigmentation data is seen in the complex and nuanced landscape of assortative mating seen in Indian populations (Iliescu et al., 2018). But even here, the effects of skin color preference did not drive Indian populations unidirectionally towards some uniform level of depigmentation, as Aoki would predict. If a case study with such clear social pressure for light skin does not result in a depigmented population, it is hardly imaginable that fickle individual “preference” could make a dent in the grand scheme of human evolution.

By contrast, strong, consistent, directional selection is very much plausible in a scenario where there is a selective pressure on biological factors (such as folate and vitamin D) directly affecting fetal development and numerous other aspects of human health (Jones, Lucock, Veysey, & Beckett, 2018; Clemens, Adams, Henderson, & Holick, 1982; Branda & Eaton, 1978; Jablonski & Chaplin, 2010; Walsh et al., 2020). It would be unfair to judge Aoki’s conclusions on the basis of the preponderance of evidence that has been uncovered in the 20 years since this publication. Still, considering the subjective nature of the anecdotal evidence he presents in favor of a universal preference for lighter skin, it is quite interesting that supporters of this hypothesis could more readily believe selection based on the power of “white skin” as the pinnacle of beauty, rather than selection based on the abundance of a vitamin known to affect human health.

---

Park on the whiteness of his skin and the prominence of his nose, both of which they considered as "unsightly and unnatural conformations." He in return praised the glossy jet of their skins and the lovely depression of their noses; this they said was "honeymoon," nevertheless they gave him food. The African Moors, also, "knitted their brows and seemed to shudder" at the whiteness of his skin. On the eastern coast, the negro boys when they saw Burton, cried out, "Look at the white man; does he not look like a white ape?" On the western coast, as Mr. Winwood Reade informs me, the negroes admire a very black skin more than one of a lighter tint. But their horror of whiteness may be attributed, according to this same traveller, partly to the belief held by most negroes that demons and spirits are white, and partly to their thinking it a sign of ill-health." (Darwin, 1871)

## 2.2.2 Devaluation as pathologization

In contrast to the unmistakable valuation of traits associated with beauty, we can consider the manifestation of devaluation as pathologization. Something that is pathological (in the medical sense), causes disease. But there is general recognition for the fact that disease is not self-evident or absolute (Scully, 2004). Defining what is “pathological” or “disease” requires a corresponding definition of what is “normal” or “healthy”. While some definitions of particular pathologies have changed as a result of advances in scientific knowledge, other “conditions” have moved in and out of the realm of pathology, not on the basis of self-reported patient suffering, but on the basis of political recognition for what is acceptable (or unacceptable) human variation (Bayer & Spitzer, 1982; Scully, 2004; McCrea, 1983; Scott, 1990). Thus, pathologization can be considered a special case of valuation.

Though many debates surrounding definitions of pathology pertain to mental, behavioral and cognitive variation, the definition of a physical pathology is not clear-cut either, as is especially evident in discussions of the pathologization of differences in sex development (Carpenter, 2018; Davis, Dewey, & Murphy, 2016; Davis, 2014). The medicalization of individuals threatening a rigidly essentialized biological sex binary finds some parallels with pathologies defined on the basis of comparably deep-rooted ideas about what is “appropriate” phenotypic variation for an individual within a population according to racial paradigms. In a framework where humans must exist in discrete types, relegating aberrant individuals to the category of “pathological” functions as a tourniquet for a scientific paradigm unable to account for their existence.

Extreme overt examples of racialized pathology include the antiquated diagnosis of “mongolism” stemming from a paper entitled “Observations on Ethnic Classifications of Idiots” (Down, 1867). In this diagnosis, “mental retardation” is associated with “certain characteristic oriental features” (Wagner, 1962). This description violently illustrates the successful dehumanization of both “races” perceived to be inferior, as well as individuals who do not live up to the narrow, ableist “racial standards” of their own group. The question is not whether any of the individuals described could justifiably be considered to suffer from a condition that benefits from medical treatment. The issue, rather, is the inclusion of certain racialized markers as diagnostic criteria.

The dermatological conditions of “woolly hair syndrome” and “uncombable hair syndrome” illustrate an inconsistent cluster of diagnostic criteria that center around the appearance of scalp hair in these individuals. Or, more specifically, the socially-determined unacceptability of their hair’s appearance. “Woolly Hair (WH) is an uncommon congenital

abnormality of the scalp hair consisting, by definition, of strongly coiled hair localized in a side or totally involving the scalp occurring in non-black people” (Pavone et al., 2017). Other descriptions give descriptions much to the same effect (Ramot & Zlotogorski, 2015; Shimomura et al., 2009; Horev et al., 2009; Chen, LeBoit, & Price, 2006) varying maybe only in the terminology they use to communicate what “race,” “ethnicity,” or population this condition is (not) associated with. Interestingly, these descriptions lack concomitant medical issues (heart or skin related) that might justify “woolly” hair as a proxy for an underlying disease. The emphasis in the clinical literature is strongly on the abnormality of the hair morphology for the “race” in question.<sup>5</sup>

Uncombable hair syndrome differs in that there is no emphasis on explicit racial context, but the language used to describe the hair aligns with pejorative racialized descriptions of what is commonly stereotyped as “African” hair. Additionally, there is sometimes an emphasis on the association with blond or lightly pigmented hair, which can be used as a racialized proxy for who this condition affects due to ideas about the racial associations of blond hair.

The justification for the medicalization of this “syndrome” revolves entirely around the “unruliness” of the hair. Indeed, the name itself describes the central fault with this phenotypic variant: it cannot be combed. But the combing of hair hardly seems like a criterion for determining health. If styling potential were indeed a medical concern, there is an apparent lack of an equivalent “unbraidable hair syndrome” for individuals whose hair is too limp to hold a braid. But holding hair’s ability to be “combed flat” in higher esteem than its ability to be braided can be explained by the regard for criteria of “whiteness” and associated beauty standards (Thompson, 2009).

Some of the descriptions speak to the absurdity of pathologizing this phenotype: “The family and the boy have psychologically accepted the scalp hair anomaly without particular problems”(Pavone et al., 2017). Though some parents did indeed appear distressed as evidenced by one case of “uncombable hair syndrome” describing “a healthy 6-year-old girl with blond hair who sought medical attention for the frizzy, unmanageable, and unusual appearance of her hair” (Calderon et al., 2009). Without minimizing the potential suffering that might be inflicted on individuals presenting “undesirable” traits associated with other “races”, one must ask where the medical reasoning is for treating this as a pathological medical condition.

---

<sup>5</sup>For example, in Chen et al. (Chen et al., 2006) : “We report woolly hair in an Asian family, a race in which we have not found woolly hair reported.” and in Horev et al. (Horev et al., 2009): “Woolly hair is a structural variant of scalp hair that, when found among Caucasians or Asians, is considered abnormal.

Dermatology and plastic surgery are both branches of medicine that straddle pathology and enhancement, so it is not necessarily inappropriate to see attempts to “improve” appearance in these particular medical settings. However, labeling certain racialized traits as pathological with no further justification than their inherent undesirability is not scientifically justifiable.

Both in the case of selection and pathology, we see clear cases where the valuation of certain phenotypic variants over others crosses the line into subjective, unjustified (and unjustifiable) value judgement. Entire branches of philosophy would allow those interested in generating knowledge about the value of traits and aesthetic superiority to engage in appropriate scholarly discourse on the matter.

However, scientific inquiry is bound by method, as well as subject matter (Hansson, 2009, 2017; Gieryn, 1983; Mahner, 2013). As regards the scientific study of human biological variation, the ascertainment of value is simply not appropriate as subject matter. The scientific method is not equipped to evaluate the kinds of knowledge encompassed in values and aesthetics. In examples where those boundaries are crossed, we enter into the realm of pseudoscience, which is precisely where scientific racism exists (Zuberi & Bonilla-Silva, 2008).

## **2.3 The constraints of racialization**

The overemphasis of European variability and the homogenization of other “races” is in line with expected cognitive biases of the people who have, for most of Western history, contributed to this body of knowledge (Saini, 2019). The overemphasis on (and overvaluation of) European variability, especially in combination with the homogenization of the Other reflects the biases of the people who have contributed most extensively to the canon of scientific literature on human biological variation. Science is not immune to subjectivity despite its objective ideals.

The formalization of these Eurocentric biases was facilitated by the use of subjective classification systems, as well as the inherent biases of the languages used to develop those systems. The various classification systems discussed in this paper illustrate that categories are based not on the objective range of biological variability, but on the range of variability that appears salient to the scientist in question. Moreover, there is extensive psychological literature on the existence and hypothesized basis of the subjective perception of one’s own (racial) group as more variable than others (Hughes et al., 2019; Wheeler & Fiske, 2005; Hugenberg, Young, Bernstein, & Sacco, 2010; Sporer, 2001).

But even in cases less controversial than racial profiling, we see subjectivity elevated to fact through classificatory language. This is especially evident in linguistic differences in the categorization of colors. For instance, English distinguishes between blue and green, while many languages around the world do not (Davies, Davies, & Corbett, 1994; Davies & Corbett, 1997; Goldstein, Davidoff, & Roberson, 2009; Raffaelli, Katunar, & Kerovec, 2019). Even other European languages have linguistic color nuances that differ from English categories. For example, Russian has a distinct word for lighter blue and darker blue, which has been demonstrated to allow Russian speakers to more readily discriminate between the two (Winawer et al., 2007).

These linguistic differences and related cognitive biases do not show a fundamentally altered capacity to perceive color, but rather a fine-tuned capacity to culturally (and linguistically) describe salient variation (Goldstein et al., 2009). This can explain why existing categories appear so distinct for both eye and hair color. But with the inclusion of eye color terms like “hazel” and “honey”, we delve into levels of nuances with cultural relevance, i.e. colors are named in reference to a naturally occurring object (Davies & Corbett, 1997; Gatschet, 1879). The linguistic limitations of classification are evident, but the effect of concomitant cognitive biases does not end there.

### **2.3.1 Biased perceptions lead to misguided questions**

The effect of language on our conceptualization of reality and subsequent scientific inquiry is significant. For example, a very palpable example of how misconceptions can misguide science is found in the scientific literature on skin color evolution.

In the mid-20th Century there was a distinct push against the idea that dark skin might confer some adaptive benefit in regions of high solar radiation. Despite the well-known geographical distribution of skin pigmentation and solar radiation, these scientists were perplexed at the seeming contradiction in “black” skin being advantageous over “white” skin in such conditions (Thomson, 1955). Their racialized idea of skin pigmentation as being comparable to the colors themselves set scientists up to formulate questions that were based on the complete absorption (black) and reflection (white) of light. Therefore, the inability of “Negro skin” to reflect as much light as “the white skinned race” was framed as a disadvantage causing Africans to absorb more solar radiation, which would (in the researchers’ view) obviously be negative (Thomson, 1955; Kuppenheim & Heer, 1952; Blum, 1945).

However, skin pigmentation is not described by the complete reflection or absorption of light (as the categories “black” and “white” would suggest). Rather, skin pigmentation

is a function of the quantity of melanin in the epidermis. As such, humans do not vary in color so much as they vary from translucent to opaque due to the melanin content in their skin.

Melanin has a fascinating photochemistry. It is absorbed over the entire visible light spectrum, which is why it is perceived as brown.<sup>6</sup> The broad absorbance spectrum of melanin contributes to its quality as a photoprotectant (Premi et al., 2015; Brenner & Hearing, 2008; Krol & Liebler, 1998; Kollias & Baqer, 1987; Chen et al., 2014). Therefore the perceived disadvantage of skin that contains these photoabsorbant chromophores is, in fact, the mechanism by which “black” skin stops UV-damage which can penetrate translucent, reflective “white” skin with little resistance. This misconception may appear silly in hindsight, but the way we currently classify hair and eye color is comparable in its level of misguidance considering the emphasis on perceived color and RGB spaces rather than measures of constitutive melanin content (Chaitanya et al., 2018; Adhikari et al., 2019).

### 2.3.2 Reckoning with the remnants of race

Confronting racial paradigms is crucial to an improved understanding of human biological variation. Advances we have made in the evolutionary genomics of human skin pigmentation were facilitated by the use of objective quantification methods and they have highlighted the extent to which we have underappreciated African and African-descendant variation (Martin et al., 2017; Crawford et al., 2017; Beleza, Johnson, et al., 2013).

Moreover, there is an increasing awareness of the ways in which racialized dermatology has failed all of us, but especially non-Europeans (Khumalo, 2007; Ware et al., 2020; Nelson, 2020). As a consequence, there is a push for the use of objective measures which will allow practitioners to evaluate their patients without relying on racial stereotypes (Granstein, Cornelius, & Shinkai, 2017; Pandya, Alexis, Berger, & Wintroub, 2016).

New methods will supplant old subjective classification systems. However, we must still actively evaluate whether these new methods are objectively informed by the biological processes underpinning traits of interest, or whether they simply provide a way to give subjectivity the appearance of objectivity. The reproduction of race under a new name is particularly of concern in DNA phenotyping and broader genomic science

---

<sup>6</sup>Brown does not exist as a distinct “color” in the sense of other colors that represent peaks in the range of visible wavelengths. However, reflection spectra that cover a broad range between red and green appear to us as brown (Andreae & Gelencsér, 2006; Sun, Biedermann, & Bond, 2007; Strutt, 1871). In RGB space, however, brown is achieved by creating an orange with low luminosity.

where classifications of populations and ancestries can border on essentialism (Panofsky & Bliss, 2017; M'charek, 2020; Bliss, 2011).

To stop reproducing racial paradigms of human variation, we must additionally do the work of critically evaluating existing work and halting the circulation of pseudoscience. An approach to our scholarship that relies on merely generating new and better data is, in effect, reliant on a flawed “marketplace of ideas” approach to manifest the “self-correcting” nature of science (Ball, 2017; Ingber, 1984).

As illustrated by the widely cited example arguing for the universal preference of light skin (van den Berghe & Frost, 1986), our current scientific process is not immune to poor scholarship permeating the literature. Moreover, as the work of human biology is extremely interdisciplinary, it is unlikely that we are able to fully evaluate the quality and validity of each citation we rely on. As such, it is our responsibility to do our part as reviewers and members of the scientific community to clearly articulate honest and constructive assessments of work we are qualified to speak on.

### **2.3.3 Transforming knowledge and practice in human biological sciences**

Transforming the way knowledge is created in human biological sciences requires changing the theoretical frameworks we use to interpret our data, but also changing the ways in which we “do” science. Knowledge is not created in a vacuum, but in intricate networks with actors and institutions whose influences are sometimes unnoticed and often unchallenged. Two ways of dealing with these influences are: centering marginalized scientists and scrutinizing institutionally imposed standards.

Certain parts of our scientific work are inherently subjective. The questions we have, the way we see the world, the variation we consider salient—all of this is affected by our positionality (Haraway, 1988; Wylie, 2003; Harding, 2004; Rose, 1983; Smith, 2011; Moreton-Robinson, 2013). The kind of bias embedded in scientific knowledge generated by a group with homogeneous lived experiences can be mitigated by the active inclusion of diverse perspectives - especially, ones that have historically been marginalized (Page, 2008; Hong & Page, 2004).

The key to propelling scientific paradigm shifts is the ability to live in multiple paradigms at once (Chen, 1997). Marginalized individuals are likely to have experienced this by force; living both in their own marginalized spheres and (trying to live) in the spheres of groups that oppress them (Nelson, 2019a; Athreya, 2019; Torres, 2019).

This experience is aptly described by Du Bois's concept of double consciousness: "this sense of always looking at one's self through the eyes of others" (Du Bois, 1903). Such experiences allow marginalized scientists to transcend certain limitations experienced by those who can only see the world from the perspective of dominant identities (Bolnick, Smith, & Fuentes, 2019; Moreton-Robinson, 2013; Collins, 2002, 2015; Tsosie, Begay, Fox, & Garrison, 2020; Claw et al., 2018; Smith & Bolnick, 2019; Watkins, 2020). Consequently, these individuals are able to hold both paradigms at once and elucidate the incommensurabilities that are solved by a new paradigm (Benn Torres, 2014; Nelson, 2020).

Regardless of the composition of the scientific community, little progress can be made if institutions constrain work that ventures outside existing paradigms. Institutional power is a key force promoting the use of outdated racialized frameworks (Ahmed, 2012). This power functions to promote science and scientists adhering to these ideas while hindering those who wish to unburden themselves of such limitations (McLean, 2019; Nelson, 2019a; Du Bois, 1939). Progress also critically calls for a change in the institutional structures that reinforce outdated racialized standards of scientific research (DiGangi & Bethard, 2021).

This work is by no means easy, nor does it have a clear and absolute end-goal. Dealing with racialized bias in science should be viewed as part of the perpetual process of self-reflexivity that should be inherent to scientific inquiry. Moving forward, scientists in human biology will need a more thorough understanding of and critical engagement with how racialization manifests in their research, including the terminologies, typologies, and citations they rely on (Nelson, 2019b; Wolf, Jablonski, & Kenney, 2020; Skinner, 2020). Most importantly, this endeavor cannot succeed without a dedicated commitment to challenging the broader institutional and societal structures that seek to reinforce the very racial hierarchies that hinder scientific progress.

# Chapter 3 |

## High-throughput phenotyping methods for quantifying hair fiber morphology

### 3.1 Introduction

Human scalp hair morphology is an important, but poorly understood phenotype that varies considerably within and among populations. Scalp hair morphology—alternatively described as hair texture, form, shape or type—refers to the structural appearance of the hair shaft protruding from the follicle. Hair morphology can be examined at multiple scales, from characterization of the cortical cells, medulla, and cuticle to descriptions of overall macroscopic "texture" perceived when considering a head of hair in its entirety. Variations in hair morphology have been linked to variation in DNA sequence, as well as in cellular, protein, and chemical structure (Koch et al., 2020). However, focus on investigating the underlying causes of the perceived macroscopic variation has come at the expense of developing language and methodology for the phenotype itself. This need is illustrated by the multitude of subjective and, at times, race-based classification systems used across disciplines interested in the variability of this trait (Adhikari et al., 2016; Khumalo, 2007; Trotter, 1938; Loussouarn et al., 2007).

The morphology of an individual hair shaft is the most immediate "macroscopic" scale after considering a head of hair as a whole. At hair-shaft scale, two objectively quantifiable aspects of hair morphology can be delineated: its longitudinal curvature and its cross-sectional geometry (see Fig. 3.1).

Work in this field has been plagued by a lack of standardization in methods and issues

of replicability, in part due to inadequate detailing of methods used and subjectivity in their application (Appendix A). In light of these challenges, we have developed sample preparation and image analysis methods that allow for the high-throughput phenotyping of hair fiber cross-sectional geometry and curvature. Our aim was to develop methods that would 1) be appropriate for the full range of human hair diversity, 2) minimize or eliminate subjective observer input, 3) require no specialized skills or equipment, and finally, 4) be efficient and scalable. Here, we present a comprehensive description of the protocols used for sample preparation and a novel computational tool for the analysis of images created with those protocols.

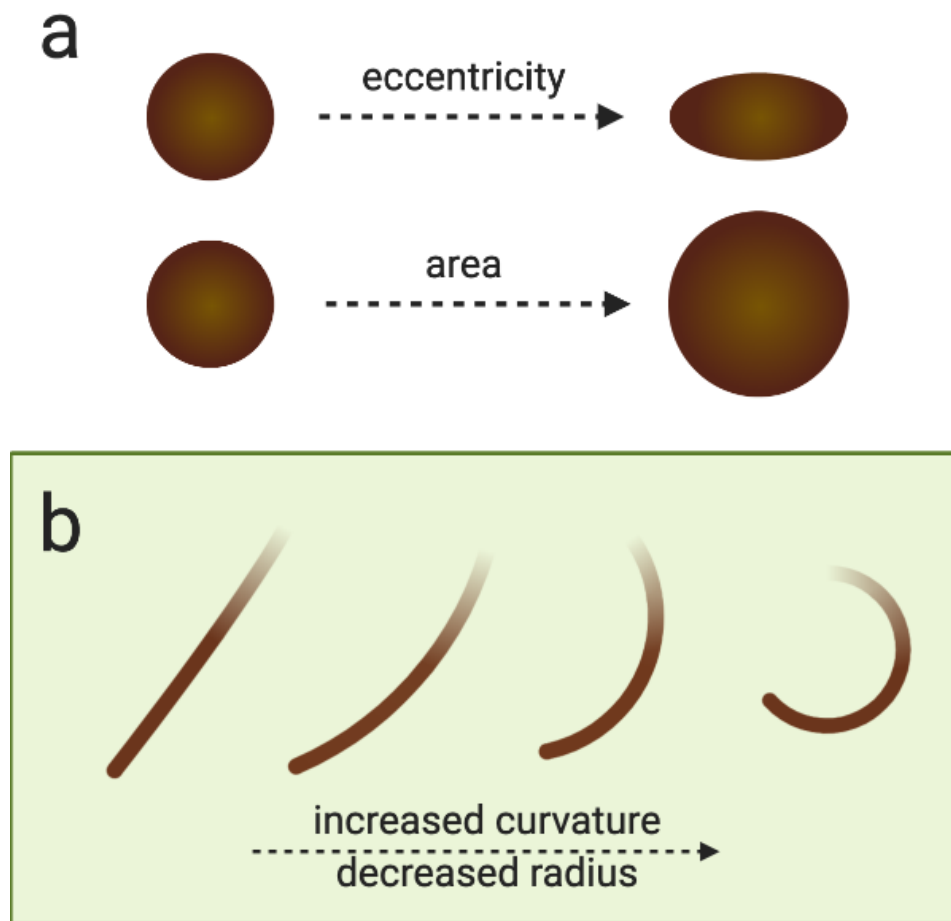


**Figure 3.1. Quantifiable aspects of hair morphology.** **a**, Diagram of cross-sectional eccentricity and area. **b**, Curvature is calculated as the inverse of the radius in mm ( $radius^{-1}$ ), ergo an increase in curvature corresponds with a decrease in the radius of the circle fitting the curve.

## 3.2 Results

Using a low melt point plastic for immediate embedding of multiple hairs. Cutting hairs at a perpendicular angle is crucial for the accurate visualization of a fiber’s cross-section. Traditional methods using resin or paraffin require long ( $\sim 24$ h) curing times and make it difficult to embed curled hairs for sectioning. We found that a low melt point plastic such as polycaprolactone allowed us to lay multiple hairs of any morphology in parallel lines. The material immediately encases curled hairs even when they are stretched straight. For our purposes, we embedded six hairs from each individual using polycaprolactone plastic sheets (Polly Plastics, Michigan, USA). We heated a strip of moldable plastic on a hot plate and stretched hair samples over this strip affixing them to the material. We then placed a second strip of plastic on top of the hairs and put a heated block on top to fuse both strips of plastic and embed the hairs completely. After storing the embedded samples in a 4C room for a minimum of two hours and we sectioned them with a PanaVise 507 Flat Ribbon Cable Cutter fitted to a PanaVise 502 Precision PanaPress. We found that a regular razor blade was equally capable of cutting through the samples, but the PanaVise set up allowed us to process samples at a higher rate. We then mounted the sectioned samples upright between two Plexiglas blocks for visualization and imaged with a Leica DMLS microscope (Leica, Wetzlar, Germany) at 10x with a Lumina GX8 camera (Panasonic, Osaka, Japan) attachment. Illumination was provided through the sides of the Plexiglas hair chip support using fiber optic dissecting scope lights. See Figure 3.2a and Methods for step-by-step protocol.

### 3.2.1 Cutting hair fibers into fragments as a scalable method for washing and imaging hair fibers for curvature analysis

Multiple factors associated with grooming can temporarily alter the curvature of a hair fiber (e.g. hair products, straightening irons, braiding). The first step of our sample preparation was developed to remove the effect of these extrinsic factors and to allow for the measurement of curvature in two dimensions. To achieve this, we cut hairs into small fragments and used a multi-step washing process to remove any residue and allow the hairs to revert to a shape representing the fiber’s intrinsic curvature. We used three to five hair fibers from the crown of each individual in order to capture a representative value of hair curvature for that individual. We placed hairs into a Petri dish containing 5mL of isopropyl alcohol (IPA) and cut them into fragments of 3mm with a curved-point

scalpel blade. We then transferred them to 2mL tubes using transfer pipettes. At this stage, lightly pigmented hairs were dyed black using a commercial hair dye kit to improve final imaging contrast. We washed hairs with a sodium dodecyl sulfate (SDS) mixture (1% SDS, 99% double distilled H<sub>2</sub>O) and rinsed them with H<sub>2</sub>O. Finally, we stored hairs in 1mL of IPA until imaged. For imaging, we decanted each sample into a petri dish containing 5mL of IPA and we used a Panasonic GH4 camera with Olympus f2.8 60mm macro lens to capture the images (see Fig. 3.2b,a and Methods for step-by-step protocol).

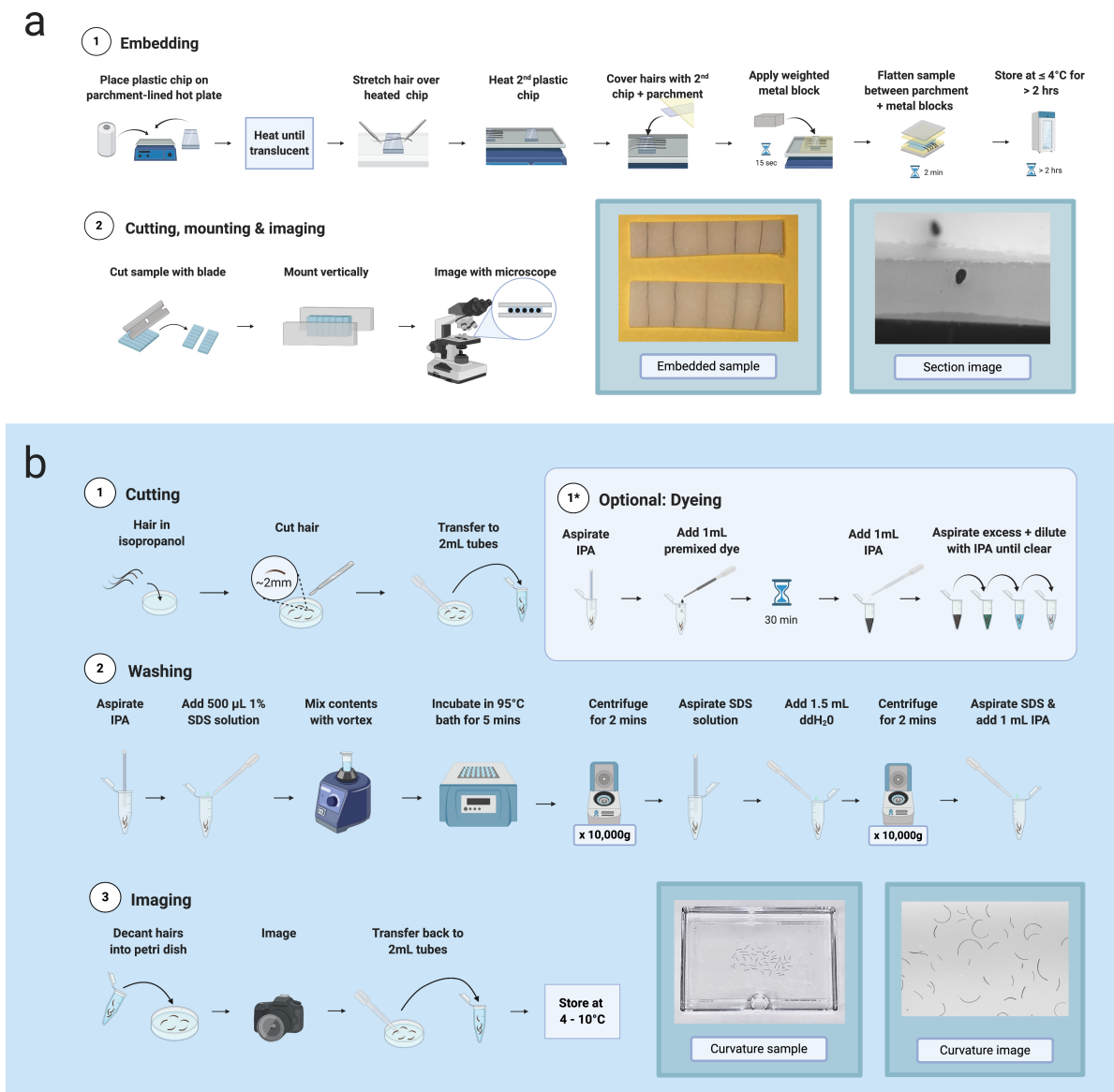


**Figure 3.2. Flowcharts of laboratory protocols used.** **a**, Embedding protocol for cross-sectional imaging. **b**, Sample preparation protocol for curvature imaging.

### **3.2.2 Automated image analysis for unsupervised high-throughput processing**

Our Python package, *fibermorph*, is a user-friendly, fully automated image analysis tool that provides a convenient way to estimate hair eccentricity and curvature from cross-sectional and longitudinal images (see Fig. 3.3). We designed this package to run on the command line and provide detailed guidance on its use so that any researchers who have images of hair sections or curvature can use it without programming experience. No comparable tools exist for these purposes, nor are there any computational tools that are consistently employed by researchers studying hair fiber curvature and cross-sectional morphology.

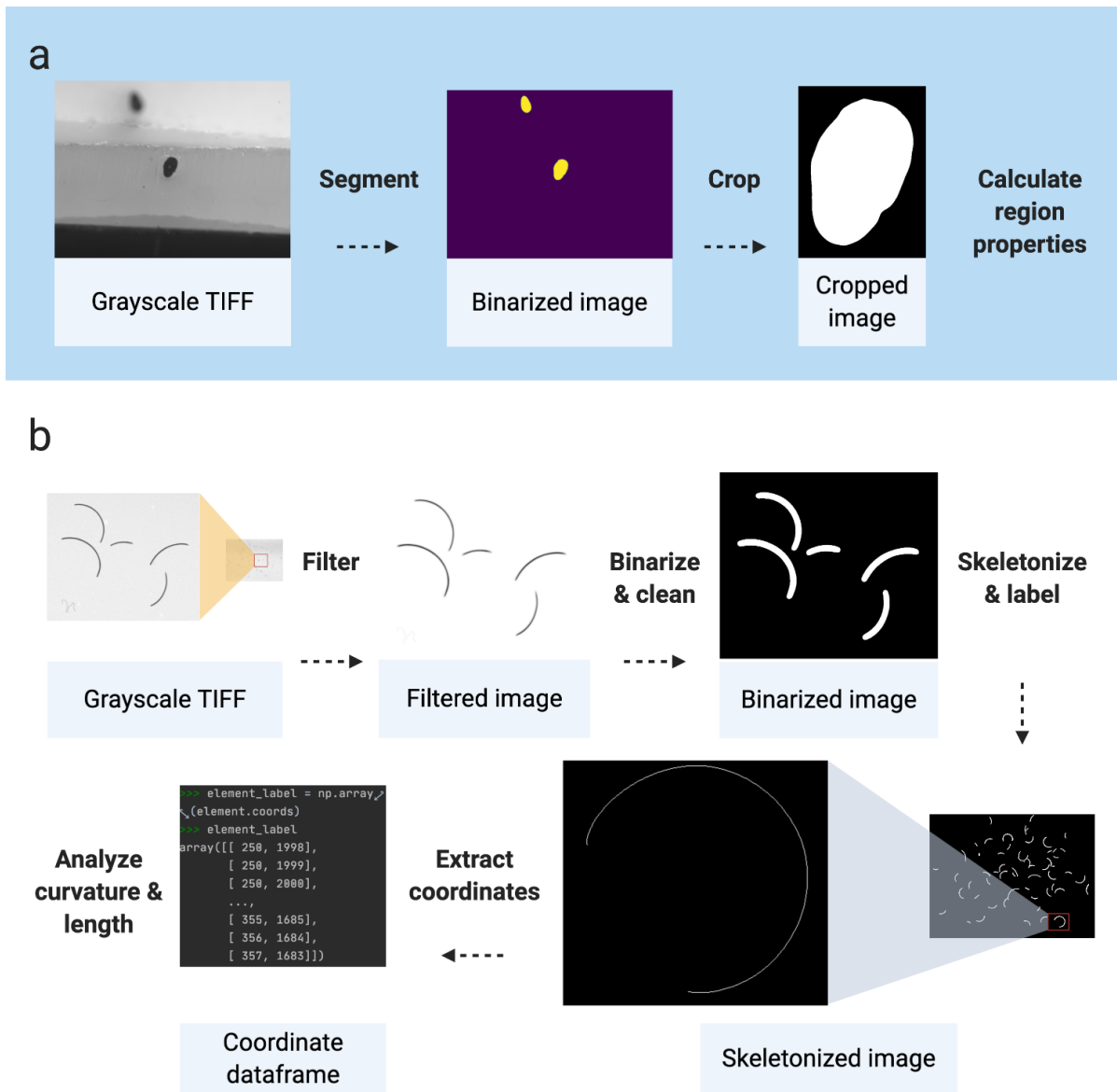


**Figure 3.3.** *fibermorph* image analysis workflow. **a**, Cross-sectional image processing and analysis. **b**, Curvature image processing and analysis.

### 3.2.3 Measurement error in hair fiber curvature estimation

*fibermorph*, is designed to simultaneously estimate curvature of multiple hair fragments in an image. The program first processes the image to extract hair fibers from the background and reduces each hair to 1 pixel width. The pixel coordinates are then used to estimate hair curvature using a circle fitting algorithm, returning the curvature for each fragment measured as the inverse of the (fitted) circle’s radius. The program returns a

spreadsheet for each image containing the image ID, mean and median curvature (across all hair fragments in the image), hair count, and mean and median length.

To test the accuracy of *fibermorph*'s curvature estimation, we simulated 20 images with a range of curvatures. Each image contained 25 hair fragments of the same length and curvature, but different orientations, representing a sample of hair collected from a single individual. The simulated curvature ranged from  $0.1mm^{-1}$  to  $2mm^{-1}$  representing the observed range of curvature in our sample of real hair. We used *fibermorph* to estimate the mean and median curvature and length of hair in each image and compared it to the known (simulated) length and curvature (see Fig. 3.4).

*fibermorph* accurately estimates hair curvature across a range of simulated curvature values ( $r^2 = 0.999$ ; Fig. 3.4a). The error in estimation was minimal overall with mean root mean squared error (RMSE) of  $2.21 \times 10^{-4}mm^{-1}$  (0.47%) The estimated length of each hair fragment was similarly accurate (Fig. 3.4b) with an RMSE of  $4.31 \times 10^{-4}mm$  (0.69%). See Appendix B for details on RMSE and percent error for curvature.

### 3.2.4 Measurement error in cross-sectional parameter estimation

*fibermorph* also processes micrographs of hair sections and measures a number of cross-sectional properties. The program first crops the images, then segments out the cross-section from the background using scikit-image's implementation of the Chan-Vese algorithm (Getreuer, 2012; van der Walt et al., 2014). The binarized image is then used to calculate area, minimum diameter, maximum diameter in microns ( $\mu m$ ), and eccentricity, which is a measure of how elliptical the cross-section is (see Methods for details).

To evaluate the measurement error in estimation of cross-sectional parameters, we simulated 100 ellipses with minimum and maximum diameters chosen at uniform intervals between 30 to 120  $\mu m$ . The range of minimum and maximum diameters is based on the range found in human scalp hairs. *fibermorph* accurately estimates the area and eccentricity of ellipses (Fig. 3.4c). The RMSE for area is  $0.51 \mu m^2$  (0.01%) and  $6.49 \times 10^{-4}$  (1%) for eccentricity. See Appendix B for details on RMSE and percent error for cross-sectional geometry.

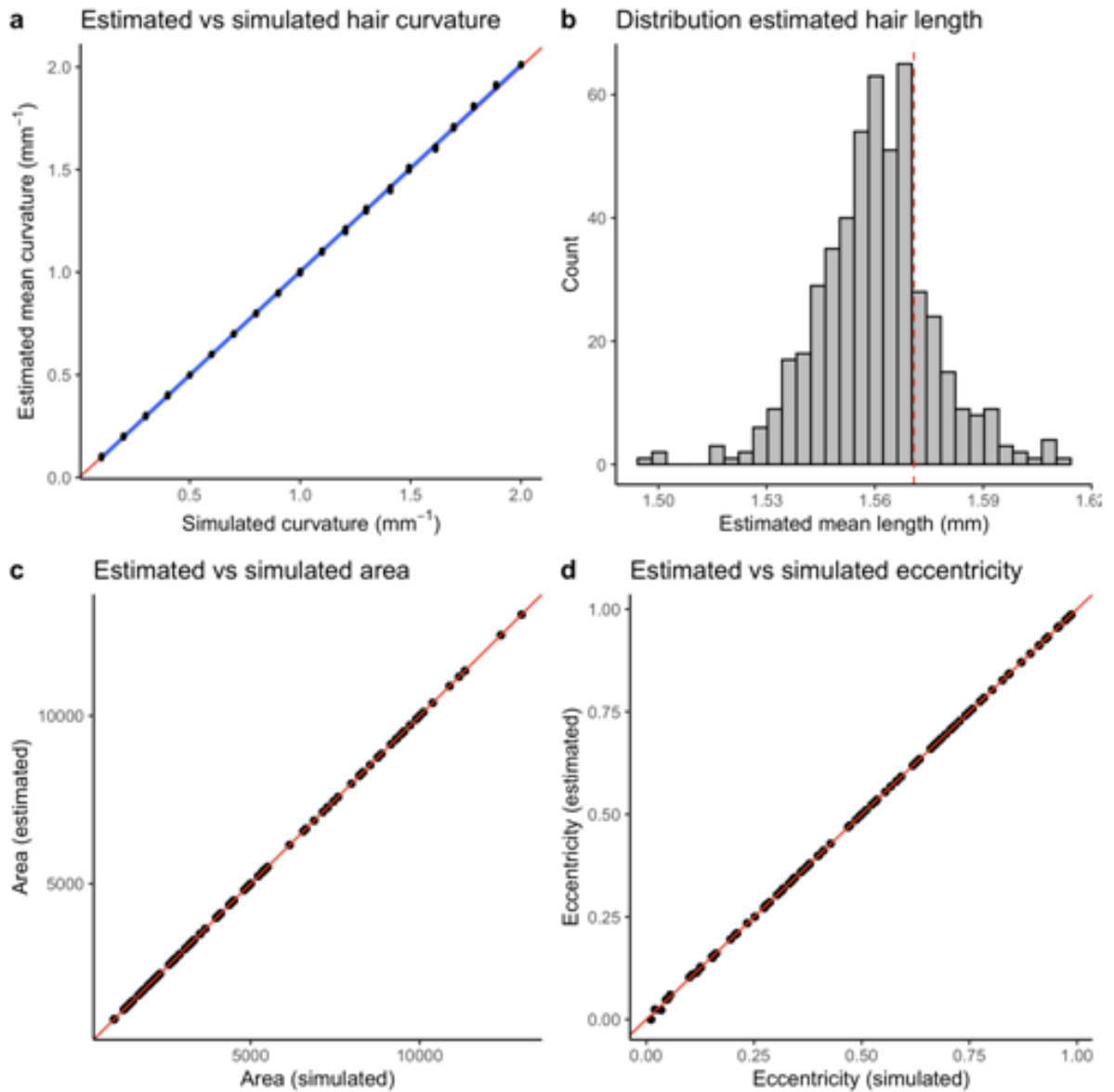


**Figure 3.4. Performance of *fibermorph* on simulated data.** **a**, Correlation between estimated and true (simulated) curvature. The red line represents  $y = x$  and the blue line represents the line of best fit. **b**, Distribution of hair fragment length estimates. The dashed red line shows the true simulated length of each fragment. **c**, Correlation between estimated and true cross-sectional area. **d**, Correlation between estimated and true eccentricity.

### 3.2.5 Self-reported hair texture and “objective” classification fail to capture quantitative variation in curvature

. We compared quantitative hair fiber curvature with self-reported hair texture in a sample of 140 individuals of admixed European and African ancestry. Self-reported hair texture or form is often used for phenotyping purposes in genome-wide association studies (GWAS) with ordinal categories such as “straight”, “wavy” and “curly”. However, we find that while there is a correlation between these ordinal categories, individuals are inconsistent in their perception of hair texture (see Fig. 3.5a). In other words, there seems to be variation in the level of perceived hair curl each of these categories encompass. An alternative to subjective hair form categorization is the classification of hair into ordinal categories based on their objective curvature (Loussouarn et al., 2007). We also analyzed the variation in hair curvature using the curvature thresholds described in the 2007 Loussouarn et al. paper (Loussouarn et al., 2007) (see Fig. 3.5b) and found that the continuous variation was binned in a manner that unequally represented variation across the categories.

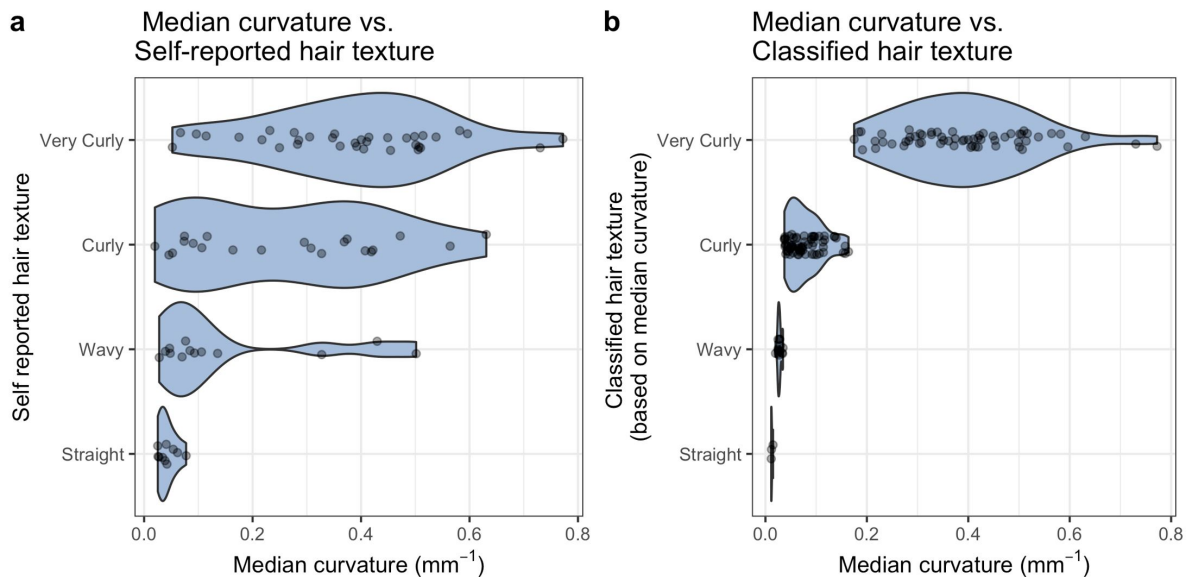


**Figure 3.5. Comparison of quantitative and qualitative hair morphology.** a, Self-reported hair form shows inconsistency among individuals with regards to the level of curvature encompassed by each category. b, Classifying hair based on objective curvature Loussouarn et al. 2007, obscures the wide range of variation that exists in the “Very Curly” category.

### 3.2.6 Quantitative hair fiber morphology elucidates the relationship between curvature and cross-sectional shape and genetic architecture

Many studies have reported a correlation between hair fiber curvature and cross-sectional shape, an observation which has been interpreted as a causal effect of eccentricity on hair curl. Specifically, the presence of elliptical cross-sections in populations with tightly curled hair (i.e. West African) and the presence of round cross-sections in populations with straight hair (i.e. East Asian) has been interpreted as evidence that cross-sectional shape of hair dictates its curvature (Wortmann et al., 2019; Fujimoto et al., 2008a). Whether these two traits are genetically and/or developmentally correlated is unknown because of population structure, which induces spurious correlations between traits (Parra, Kittles, & Shriver, 2004). For example, individuals with more West African ancestry tend to have more pigmented skin and curlier hair, on average, than individuals with more European ancestry. However, there is no reason to believe that these two traits are correlated because of a shared genetic architecture. We illustrate this in a sample of 140 individuals with mixed African and European ancestry. We show that the positive association between melanin index and hair curvature (slope t-statistic = 12.50, p-value  $< 2 \times 10^{-16}$ , Fig. 3.6c) is no longer significant when proportion of African ancestry is used as a covariate in the model to correct for ancestry stratification (slope t-statistic = 1.86, p-value = 0.065, Fig. 6d). Similarly, we show that the observed positive relationship between eccentricity and hair curvature (slope t-statistic = 6.08, p-value =  $1.96 \times 10^{-8}$ , Fig. 3.6a) is also not significant when corrected for proportion of African ancestry (slope t-statistic = 0.87, p-value = 0.386, Fig. 3.6b). This demonstrates that the correlation between hair curvature and cross-sectional shape in people of mixed African and European ancestry, as well as between Africans and Europeans, is driven by population structure, similar to the correlation between melanin index and curvature. More detailed analyses (e.g. estimation of genetic correlation and GWAS of both traits) in a larger sample will be needed to elucidate whether some component of the relationship between hair curvature and cross-sectional shape results from pleiotropy. See Appendix C for full set of analyses and admixture breakdown of the sample.

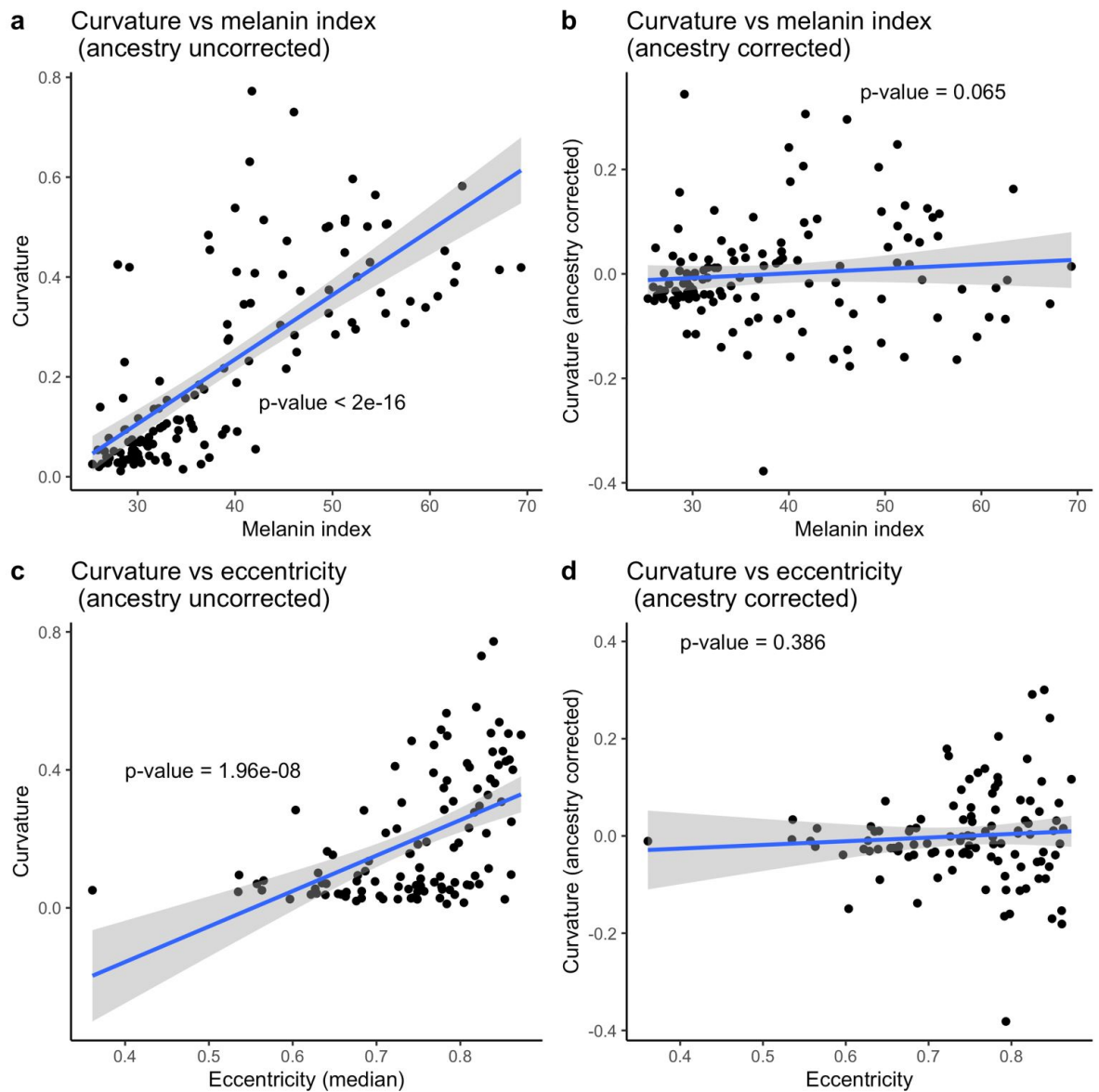


**Figure 3.6. The effect of population structure on trait-trait correlations.** **a**, The correlation between hair curvature and melanin index without controlling for ancestry. **b**, The correlation between hair curvature and melanin index controlling for African ancestry. **c**, The correlation between hair curvature and cross-sectional eccentricity without controlling for ancestry. **d**, The correlation between hair curvature and cross-sectional eccentricity controlling for African ancestry.

### 3.3 Discussion

Our results demonstrate that the methods we have developed can reliably quantify cross-sectional morphology and curvature in hair fibers. Moreover, we illustrate that the practice of categorizing hair either subjectively or by using arbitrary thresholds mischaracterizes the distribution of quantitative hair morphology, specifically, underestimating the variation that exists in more tightly curled hair.

Our sample preparation protocols and computational image analysis tool represent significant methodological advancements over previous attempts to quantify hair morphology. The sample preparation protocol for curvature imaging described here is considerably more scalable than methods used in other studies of hair curvature. Our protocol introduces a standardized method of washing hair samples that more closely resembles protocols used in sample preparation for trace element analysis in hair (Morton, Carolan, & Gardiner, 2002; Pozebon, Scheffler, & Dressler, 2017) and that is superior to previous methods that required handling of individual hairs with forceps (Lasisi et al., 2016; Bailey & Schliebe, 1986). Our method operationalizes the measurement of curvature by defining intrinsic curvature as the curvature that a hair fiber has when reduced to a short length ( $\sim 1 - 3\text{mm}$ ) which reduces the three dimensional curvature of certain hairs to a two dimensional curve that can be measured without the distortion that was needed in previous methods or the weight of the hair fiber itself.

Our embedding protocol using the low melt-point plastic (polycaprolactone) overcomes the problems of traditional embedding techniques that used resin or paraffin (Fujimoto et al., 2008a; Lasisi et al., 2016). These techniques are feasible for straight hairs, which can be easily manipulated to lie flat and parallel to each other, but are not practical for curly hairs because non-straight hairs cannot be reliably embedded in a manner that allows for a reproducible cross-sectional cut. Previous attempts to overcome this problem included using a heat-shrink tube and drawing the hair through the tube (Wagner, Heine, & Sachse, 2015), bundling hairs and slightly embedding them before embedding them fully (Reis, Brandão, Rodrigues, Coelho, & Machado, 2020), and stretching hairs over cardboard before embedding them in a large resin block (Lasisi et al., 2016). All of these methods are laborious and cannot be scaled to the study of large samples. Our method allows for the immediate embedding of hairs, regardless of shape, allowing researchers to prepare dozens of samples per hour.

Our novel computational tool streamlines the analysis of curvature and cross-sectional geometry of hair fibers. This tool requires no input from a user (other than the location

of the image files), and so removes inter-observer error and subjectivity in assessing curvature (Lasisi et al., 2016; Mkentane et al., 2017). It also saves time and improves accuracy and reproducibility because tasks that would have previously required hours of labor can now be executed unsupervised by an automated program that requires no additional cost or training to use. In the absence of comparable computational tools for hair fiber morphology, we demonstrated, in detail, the technical validity of these methods by testing fibermorph's performance on simulated geometric shapes of known parameters. Most importantly, the laboratory protocols are hosted in open-access repositories that allow for easy feedback and modification, and the code for the image analysis has been made open source to facilitate collaboration and further elaboration.

Our results show that both self-reported hair texture and "objective" classification obscure a considerable amount of variation (see Figure 5b). Moreover, our analysis of quantitative curvature compared to self-reported hair texture suggests that participant interpretations of subjective curl categories are inconsistent (see Fig. 3.5a). By applying "racial" categorization to hair, forensic scientists and dermatologists alike are bound in tautology that results from racial stereotyping, i.e. "African/Asian/European" individuals have "African/Asian/European" hair morphology and vice versa, the hair of a particular "racial" morphology is found only in those "races" (Ogle & Fox, 1998; Cruz et al., 2016; Wolfram, 2003). This presents a paradigm wherein individuals, and entire populations, who fall outside of those options cannot be considered or characterized. By applying our methods to an admixed African-European sample, we demonstrate the potential for uncovering the genetic architecture of hair morphology (see Figure 6b).

Researchers interested in understanding the biology underlying variation in hair fiber curvature are severely hindered by the oversimplification resulting from the use of qualitative hair types because these typologies preclude the analysis of the features that may independently contribute to macromorphology (e.g. the effect of cross-sectional eccentricity on curvature). In this sample, we were able to show that eccentricity does not predict hair curvature, which is in line with the findings of other studies (Wortmann et al., 2019; Lasisi et al., 2016; Hrdy, 1973). In fact, we explain this correlation as arising due to uncorrected population structure, which induces correlations between traits that are not necessarily genetically or physically linked. Nevertheless, the persistence of this idea demonstrates the importance of using quantitative methods to disentangle the factors contributing to hair morphology rather than relying on descriptive comparisons between racialized groups or ethnicities. Human scalp hair morphology is a complex phenotype that has remained poorly understood due to the high threshold of investment in time and

resources required to apply existing quantitative methods. With these high-throughput phenotyping methods, we provide researchers with a comprehensive starting point and the option to identify specific components to focus on befitting their specializations. Most importantly, due to the open access and open source infrastructure of this project, collaboration is facilitated and democratized, allowing anyone who is interested to work on this research. This work represents a much-needed baseline and standardization that is fundamental to the incremental improvements that were previously unfeasible in the study of this complex phenotype.

## **3.4 Methods**

### **3.4.1 Hair samples and genotype data**

The data consists of 140 hair samples and corresponding genotype data from individuals of admixed European and African ancestry (Lasisi, 2020a). These were collected as part of a larger study (Anthropometry, DNA, and Perception of Traits or ADAPT) with informed consent and ethical approval by the Pennsylvania State University Institutional Review Board (#44929 and #45727). To select these individuals, we merged the full genotype dataset (n=4257 individuals genotyped on the 23andMe V4 array) with the 1000 Genomes reference panel. (Consortium, The 1000 Genomes Project, 2010) We pruned SNPs for linkage disequilibrium (PLINK 1.9 “-indep-pairwise 100 10 0.” 1 yielding a set of 118x SNPs) and estimated genomic ancestry using an unsupervised clustering approach ( $k = 5$ ) with ADMIXTURE. (Chang et al., 2015; Alexander, Novembre, & Lange, 2009) We selected individuals with >80% combined African and European ancestry and <10% ancestry from any other group for whom hair samples (more than 4 hair fragments per person) and skin reflectance were available (n=140). The hair samples and genotype data for the admixed individuals were collected with informed consent and ethical approval by The Pennsylvania State University Institutional Review Board (#44929 and #45727).

### **3.4.2 Hair embedding, sectioning and imaging protocol**

In using polycaprolactone plastic sheets, we found that embedding hairs in this low melting point plastic offered considerable benefits compared to the use of resin. We were able to immediately encase hairs in the plastic, which solved the challenge of keeping curled hairs stretched in position for 24 hours when embedding in resin. For our purposes,

we used Polly Plastics (Michigan, USA) moldable plastic sheets which are readily available and affordable.

For the embedding process, we cut down the plastic sheets to  $\sim 15\text{mm}$  by  $\sim 30\text{mm}$  and heated them on a hot plate (lined with parchment paper) for 15 seconds until translucent and softened. For each hair sample, we embedded six hairs by stretching hairs in parallel lines over the heated plastic strip to encase them in the plastic. A second strip of heated plastic was then placed over the strip containing the embedded hairs. A heated steel block was then placed on top of the sample for 15 seconds to fuse both strips of plastic and completely embed the hairs. The sample was then removed and cooled for 5 minutes before cutting down excess plastic and hairs using a template. The sample was then stored in a  $4^\circ\text{C}$  refrigerated room for at least two hours to ensure the plastic was hardened (see Methods for details).

To section the hairs, we were able to use a flat-edged razor, but to facilitate the processing of a high volume of samples, we used a mechanical press with attached razor (PanaVise 502 Precision PanaPress with PanaVise 507 Flat Ribbon Cable Cutter). The low melting point of the plastic means that it will melt at body temperature, so it is important to handle the samples minimally and to section quickly, hence our decision to use this set up over manual sectioning with a razor. Sectioned samples were mounted upright between two clear blocks for visualization and imaged with a Leica DMLS microscope (Leica, Wetzlar, Germany) at 10x with a Lumina GX8 camera (Panasonic, Osaka, Japan) attachment. See step-by-step protocol on Protocols.io (Lasisi, 2020b).

### **3.4.3 Hair sample preparation and imaging protocol for curvature**

To obtain a representative sample for each individual we recommend that a minimum of five hair fibers ( $\leq 30\text{mm}$ ) are used per individual. For shorter hairs, a minimum of 10 hairs ( $\leq 10\text{mm}$ ) is recommended. Because hair samples were collected prior to the development of this protocol, we did not have enough hairs for each individual to adhere to this rule. As such, we demonstrate the results of our analyses (described below) with and without low hair count samples.

The first step of our protocol is to cut the hair sample into fragments in a Petri Dish containing 5mL of isopropyl alcohol (IPA). We found that hairs were easier to handle in this medium than in water, where hairs variably sunk to the bottom of the dish or stuck to the tools we used to handle and cut them. Hairs were placed into a Petri dish containing 5mL of isopropanol (IPA) and cut into fragments of 3mm with a new #10 scalpel blade for each sample (these blades were cleaned between the processing of

separate batches of samples). We found that scalpels with a curved point were easiest to use in the Petri dish, so other similar scalpel blades (e.g. #20, #21 or #22) could be used depending on preference and availability. Once cut, hairs were transferred into 2mL tubes using a fresh transfer pipette for each sample. Hair samples that appeared lightly pigmented at this stage were dyed using a commercial hair dye kit (L’Oreal Paris Feria 6.3fl oz in the color Bright Black) to ensure adequate contrast in the imaging stage. After cutting (and dyeing, if applicable) hairs were washed with a sodium dodecyl sulfate (SDS) mixture (1% SDS, 99% double distilled H<sub>2</sub>O) and rinsed with H<sub>2</sub>O. In this process, we attached tubing to a faucet to create an aspiration system where the flowing water created a vacuum. Using a pasteur pipette attached to the vacuum end of the tubing, we aspirated as much IPA from the samples in the 2mL tubes as we could without disturbing the hairs. We then filled the tubes with the SDS mixture until they reached the 2mL mark. Samples were then mixed using a Vortex mixer and placed in a warm water bath (99°C) for 5 minutes. We found that microcentrifuge tube caps were necessary to securely seal the tubes when in the water bath. The purpose of the warm water bath is to thoroughly clean the hair fibers and to ensure all hairs go through the same process of hydration and dehydration as variability in porosity may affect their morphology. Once removed from the water bath and cooled, the hairs were microcentrifuged to collect all hair fragments at the bottom of the tube. The SDS mixture was then aspirated from the tubes, and we refilled the tubes with H<sub>2</sub>O and microcentrifuged again to rinse the hairs. Finally, the H<sub>2</sub>O was aspirated and replaced with 1mL IPA. After this step, hairs were stored in these 2mL tubes until imaged.

To ensure the same resolution for each image, we mounted a camera to a stand and set the focus to the same standard for each sample. Immediately prior to imaging, samples were decanted from their 2mL tubes into a Petri dish containing 5mL of IPA. We found IPA to be a suitable medium as hairs invariably sunk to the bottom of the dish for each sample, ensuring consistency between images and removing the effect of shadows. Additionally, 5mL of IPA was enough to cover the hairs eliminating any glare from surface tension related to hairs protruding through the liquid. We imaged the samples using a Panasonic GH4 camera with Olympus f2.8 60mm macro lens producing images that were 5200 by 3900 pixels and at a resolution of 132 pixels per mm. A complete step-by-step protocol with images and video can be found on Protocols.io (Lasisi, 2020c).

Image analysis protocol for cross-section. The *fibermorph* section analysis program requires grayscale TIFF images as input. Where necessary, images are cropped as part of the preprocessing pipeline. Then, images are segmented using a Chan-Vese algorithm

(Getreuer, 2012) in scikit-image (van der Walt et al., 2014). This algorithm was chosen for its ability to segment images with poorly defined edges but significant differences in grayscale intensity between the region of interest and the rest of the image.

The parameters of the section identified are calculated using scikit-image’s regionprops function. We output the following: minimum diameter, maximum diameter, area and eccentricity. Eccentricity is defined as:

$$\varepsilon = \frac{\sqrt{a^2 - b^2}}{a}$$

where  $b$  is the minimum radius and  $a$  is the maximum radius of the ellipse. Diagrams for all the protocols were created using BioRender.com.

### 3.4.4 Image analysis protocol for curvature

The analysis of curvature begins with a grayscale TIFF image file as input. Our pipeline applies a ridge filter to extract the regions of interest (hairs), then binarizes and cleans the image before skeletonizing which reduces each hair fragment to 1 pixel width for the curvature analysis. The functions applied in this process are from the Python library scikit-image (van der Walt et al., 2014). The analysis of the processed image starts by labeling each element (hair) and calculating curvature for each of these elements using a Python function based on Taubin’s circle fitting algorithm (Taubin, 1991). The spreadsheet for each sample provides the length and curvature for each fragment and the summary spreadsheet provides the average length and curvature, as well as the number of hairs per image.

The spreadsheets containing the curvature and length measurement for each hair within an image are saved in the analysis folder. The default is to only produce this summary spreadsheet but a user can use a simple command to create a folder with the raw measurements per fragment should they so wish. The final summary spreadsheet contains the mean and medians for the curvatures calculated from those data frames, as well as mean and median length. Length for an element/hair is calculated from the total number of pixels in the thinned element. As the length of horizontal/vertical vs. diagonal pixels is a known issue in image analysis, we implement a correction by counting the number of diagonal pixels using a correction factor of  $(1 + \sqrt{2})$  as has been suggested elsewhere (Smit, Sprangers, Sablik, & Groenwold, 1994).

### 3.4.5 Data simulation for curvature and cross-sectional image analysis validation

To test the accuracy of *fibermorph*'s curvature estimation, we simulated 20 images, where each image contained 25 hair fragments of the same length and curvature, but different orientations, representing a sample of hair collected from a single individual. The curvature for each image was chosen with a range of 0.05 to 2 mm<sup>-1</sup> representing the observed range of curvature in our sample of real hair. To generate randomly oriented arcs, we sampled the start angle ( $\theta_{\text{start}}$ ) of each arc from a uniform distribution on the interval  $(0, \pi)$  and drew a line through 25 points with angles ( $\theta_i$ ) uniformly spaced between  $\theta_{\text{start}}$  and  $\theta_{\text{end}} = \theta_{\text{start}} + \frac{\pi}{2r}$  where  $r$  is the simulated radius. The  $x$  and  $y$  coordinates of these points were calculated as  $x = r \times \cos(\theta_i)$  and  $y = r \times \sin(\theta_i)$ .

Our Python script for ellipse simulation creates a canvas of 5200 × 3900 pixels, sets the resolution to 4.25 *pixels/μm*, and uses the chosen minimum and maximum diameters to draw the ellipse using scikit-image. The maximum diameter is chosen first (50 – 120 μm), then the eccentricity is chosen from a uniform distribution (0 – 1) and finally, the ellipse is set on an angle from a value chosen from a random distribution (0 – 360°). The parameters (minimum diameter, maximum diameter, area, eccentricity) are saved in a reference spreadsheet and the image is saved as a TIFF with the same name. We simulated 100 ellipses using these parameters for our analyses (Lasisi, 2020a).

### 3.4.6 Analyses with simulated data and real data

We estimated all curvature, length and cross-sectional parameters on both simulated and real data using our *fibermorph* Python package. In our analyses, we used the following R packages: workflowr (Blischak, Carbonetto, & Stephens, 2019), tidyverse (Wickham & Others, 2017), knitr (Xie, 2020), and cowplot (Wilke, 2016).

For simulated data, we estimated RMSE as  $\frac{\sum_i^n (\hat{x}_i - x_i)^2}{n}$  where  $x_i$  and  $\hat{x}_i$  are the true (simulated) and estimated values, respectively. To test whether the correlation between two traits was due to population structure, we fit the following linear model:  $y_i = \alpha + \beta_0 x_i + \beta_1 z_i$  where  $y_i$  is the value for one of the traits (e.g. hair curvature),  $x_i$  is the value for the other trait (e.g. eccentricity) and  $z_i$  is the proportion of African ancestry of the  $i_m^{\text{th}}$  individual. Because our sample is composed of admixed individuals of primarily African and European ancestry, the inclusion of African ancestry as a covariate should correct for the effects of ancestry stratification in our sample (Parra et al., 2004). To visualize the correlation between two traits after ancestry correction (e.g. in Fig.

3.6 ), we fitted a linear model between the first trait ( $y_i$ ) and African ancestry ( $z_i$ ) and plotted the residuals against the second the trait ( $x_i$ ).

# Chapter 4 |

## The genetic architecture of human scalp hair morphology

### 4.1 Introduction

Human scalp hair morphology is remarkably variable among populations. This variability is so considerable that it has historically been used as a marker of “race” (Pruner-Bey, 1877; Garn, 1951; Vernall, 1961) and the typological classification of hair by various racialized categories is still pervasive in the literature (Lindelöf et al., 1988; He & Okoye, 2017), despite frequent calls to end this practice (Khumalo, 2007). Unlike other traits that are comparably variable (e.g. eye and skin color), the adaptive function, genetic architecture, and evolutionary history of this phenotype have received relatively little attention.

The genetic architecture of human scalp hair morphological variation is not well known. A derived *EDAR* variant (V370A), has been associated with thicker and straighter hair in East Asian populations as well as straighter hair in South American populations with significant proportions of Native American ancestry (Fujimoto et al., 2008b; Adhikari et al., 2016). Genetic variation in the *FGFR2* gene has also been associated with hair thickness variation within East Asian populations (Fujimoto et al., 2009). In populations of exclusively or predominantly European ancestry, genome-wide association studies (GWASs) on variation in hair form have identified *TCHH*, *PRSS53*, and *GATA3* variants that are associated with straight hair (Medland et al., 2009; Adhikari et al., 2016; Liu et al., 2018). These GWAS have relied purely on gross phenotypic descriptions of hair morphological variation, as ‘straight’, ‘wavy’, or ‘curly’ (Medland et al., 2009), and, in the admixed sample, ‘frizzy’ (Adhikari et al., 2016). The literature on hair fiber morphology genetics reveals that there is no work on African populations or populations

with significant proportions of African ancestry.

Our limited knowledge of the genetic underpinnings of hair from large-scale genome wide association studies (GWAS) is further supplemented by many studies of Mendelian inheritance patterns in humans, as well as animal studies. Family pedigrees have yielded information on a number of genetic loci associated with conditions such as “woolly hair syndrome” and “uncombable hair syndrome” (Hayashi, Inoue, Suga, Aoki, & Shimomura, 2015; Ü Basmanav et al., 2016). A number of studies using mouse models have found evidence of differential gene expression in various strains of knockout mutants, resulting in a better general understanding of genes involved in the developmental biology of keratin, the hair follicle, and the epidermis, in addition to hair morphology, specifically (Adhikari et al., 2016; Kamberov et al., 2013). Studies of genetic variation among domestic breeds of cats and dogs have also revealed a number of genes of interest (Gandolfi et al., 2010; Parker, Chase, Cadieu, Lark, & Ostrander, 2010; Cadieu et al., 2009). An extensive list of previously associated genes can be found in Table 4.1.

The number of hair genes that have been implicated in hair related functions give the impression that the genetic underpinnings of human hair should be well known. However, as most of this knowledge comes from mouse studies and Mendelian conditions, there are limits to how informative this can be for our understanding of normal variation in human scalp hair morphology. Moreover, when we see that GWAS on hair have almost exclusively focused on European and East Asian populations, it becomes apparent that there is a considerable gap in the literature concerning global human hair variation. Furthermore, the focus on populations of relatively homogeneous recent ancestry means that GWAS have needed large numbers participants to have sufficient genetic and phenotypic variation to pick up a signal. Even with large sample sizes, such GWAS cannot detect alleles that are either at very low or very high frequencies even though these same alleles may contribute significantly to variation between populations.

Admixed populations are an excellent and underutilized resource for studies of scalp hair morphology. In admixed populations where a continuous trait has divergent distributions between the inferred ancestral populations. This is particularly beneficial in cases where genetic variants contributing to a phenotype are fixed in non-admixed populations. A classic example of the utility of such an endeavour is seen in the numerous studies that have discovered and replicated variants involved in skin pigmentation (Halder & Shriver, 2003; Bonilla et al., 2004; Quillen et al., 2019; Shriver et al., 2003; Norton et al., 2007). Admixture based approaches have been used to identify genetic variants contributing to variation across numerous populations and for normal-range, as well as

traits of clinical importance (Lopez et al., 2019; Perry et al., 2014; Tzur et al., 2010; Winkler, Nelson, & Smith, 2010).

The key to successful admixture mapping lies in the choice of phenotype. An admixture-based approach is most informative for phenotypes with a large mean difference between the ancestral populations. For example, a two way admixture between small-bodied Batwa rainforest hunter-gatherers and larger Bakiga agriculturalists has revealed a number of genetic loci associated with small adult body size (Perry et al., 2014). Likewise, skin pigmentation, as inferred from reflectance measurements of the inner arm, shows divergent distributions in Western Europeans and West Africans (Quillen et al., 2019). This divergence facilitates the discovery of significant associations between ancestry informative markers and variation in the phenotype.

However, the utility of admixture mapping is limited by our inability to adequately describe the continuous range of variation in scalp hair morphology exhibited in humans. This limitation is caused by the reliance on Eurocentric typologies that aim to qualitatively categorize hair by its macroscopic appearance as “straight”, “wavy”, “curly” or “frizzy” (Adhikari et al., 2016; Liu et al., 2018; Medland et al., 2009). The variation encompassed within these categories ignores much of the variation that is only apparent when various aspects of the individual hair fibers are quantified explicitly (Lasisi et al., 2016; Loussouarn et al., 2007; Hrdy, 1978). Even when the classification schemes are based on objective measurements, the binning of continuous variation considerably reduces statistical power. It is notable that one of the most frequently replicated hair-associated variants in *EDAR* was discovered by the use of quantitative methods to measure cross-sectional hair fiber area in East Asian populations. Therefore, it is reasonable to expect that using quantitative methods can yield a high resolution view of the considerable phenotypic variation in admixed populations. Given the large range of quantitative variation we can measure around the world and especially in African and African-derived populations (Loussouarn et al., 2007; Lasisi et al., 2016; Hrdy, 1973), quantitative phenotyping of hair could reveal more genes involved in scalp hair variation.

In this study, we attempt to elucidate the genetic architecture of scalp hair morphology in a sample of participants ( $n = 192$ ) with admixed African-European ancestry (see Methods for details). For our sample, we measured longitudinal curvature, cross-sectional geometry and used previously collected Melanin Index (M-index) with genotype data to investigate whether previously reported skin pigmentation and hair morphology loci would be significantly associated with ancestry informative markers (AIMs) in our sample.

## 4.2 Results

From a sample of 4257 individuals collected as part of a larger study, we selected individuals with primarily African and European ancestry with at least 10% African ancestry and available hair samples. From 192 individuals who fit these requirements, we measured hair fiber curvature for all samples and cross-sectional hair properties for all those who had sufficient hair ( $n=153$ ) as both curvature and cross-sectional methods required destructive sampling. We were able to find Melanin Index (or M-index) for most of the individuals ( $n=176$ ). A full description of the sample can be found in Appendix D.

### 4.2.1 Sample ancestry description

For the full sample ( $n=4257$ ), we estimated genomic ancestry using an unsupervised clustering approach ( $k=5$ ) with ADMIXTURE (Chang et al., 2015; Alexander et al., 2009). From this set, we selected individuals with primarily African and European ancestry ( $N = 192$ ). We then re-estimated ancestry for this subsample with  $k=2$  and used the inferred African ancestry from this analysis throughout our results (see Figure 4.1). Details on ancestry estimation and correlation between African ancestry for  $k = 5$  and  $k = 2$  can be found in Appendix D and a replication of our results with only individuals who have  $>15\%$  African Ancestry ( $K = 2$ ) can be found in Appendix E.

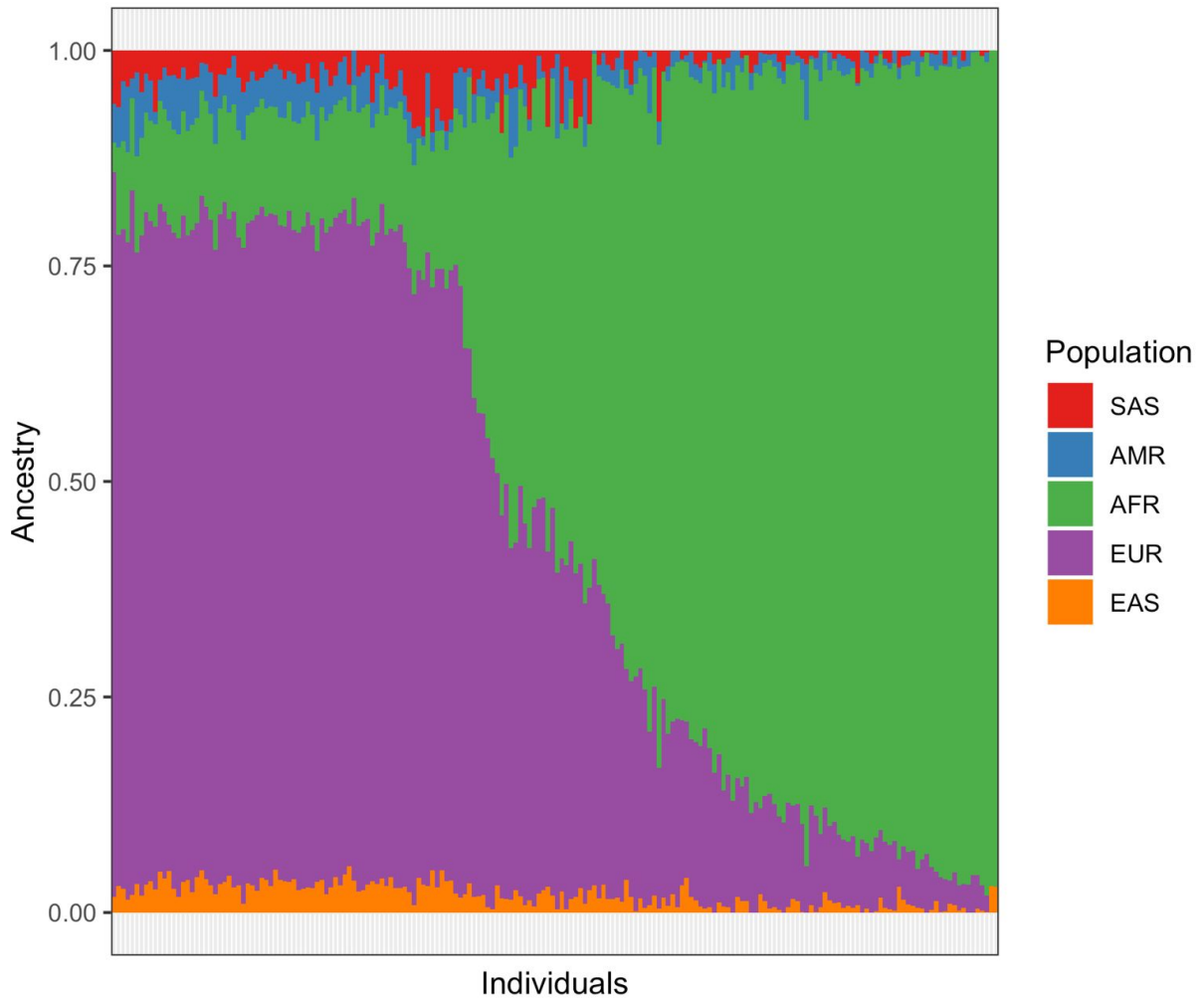


**Figure 4.1. Proportion of various ancestry components for our sample.** ADMIXTURE for our sample of 192 admixed individuals shows predominantly African and European ancestries.

### 4.3 Genetic variation underlies hair morphology differences between European and African populations

We plot the distribution of M-index and our quantitative hair morphology phenotypes for our sample and previously collected samples described elsewhere (Lasisi et al., 2016). Figure 4.2 shows the distributions of these previous samples (African, European and African Diaspora) and our current sample, labelled as Admixed (US). As expected, there is a mean difference in M-index and curvature between Africans and Europeans, with the African Diaspora and our Admixed (US) samples showing an intermediate

distribution that overlaps both these populations. Interestingly, despite the widespread use of eccentricity as a distinguishing feature between European and African individuals in forensic science, our results suggest that there is no clear divergence and significant overlap between these two populations (Ogle & Fox, 1998). While for most other phenotypes there is a statistically significant difference in the means between Europeans and Africans, the distributions overlap considerably (see Figure 4.2 and Appendix D and F for other visualizations of this distribution).

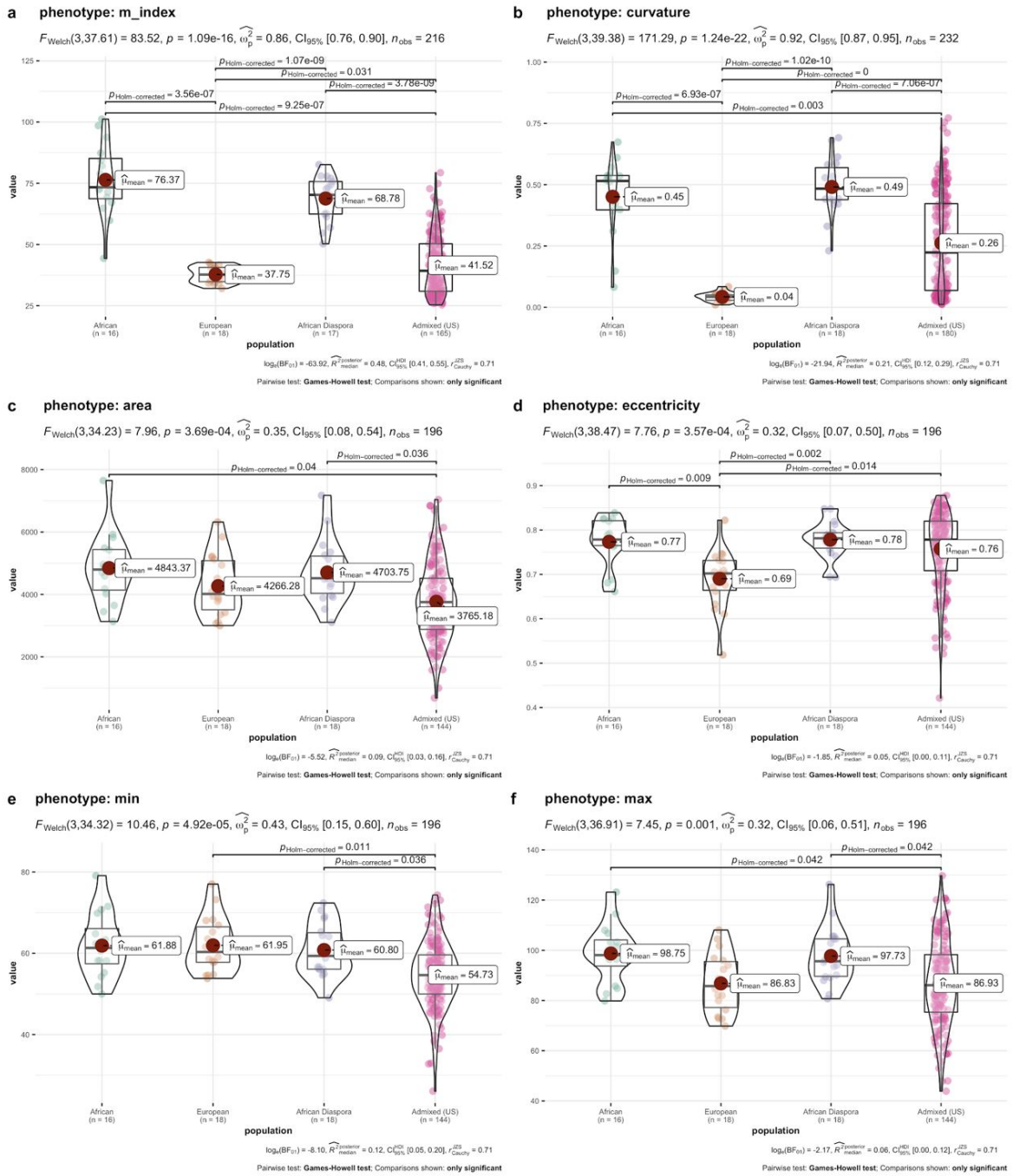


**Figure 4.2.** Violin plots of phenotypic trait values across samples of different ancestries. **a**, Melanin Index, **b**, Hair fiber curvature ( $1/\text{radius}_{(mm)}$ ), **c**, cross-sectional area of hair fiber ( $\mu\text{m}^2$ ), **d**, eccentricity of cross-section, **e**, minimum diameter of hair fiber ( $\mu\text{m}$ ), **f**, maximum diameter of hair fiber ( $\mu\text{m}$ ). Only significant comparisons are shown.

One way to test if genetic differences underlie mean phenotypic differences between

populations is to test for a correlation between the phenotype and ancestry in admixed populations. For example, Melanin Index, a trait that varies substantially between African and European populations is known to be strongly correlated with ancestry in people with mixed African and European ancestry (Beleza, Johnson, et al., 2013). We replicate this finding ( $r^2 = 0.83$ ,  $p = 2.72e - 42$ ) and show that median hair curvature is similarly positively correlated with African ancestry ( $r^2 = 0.85$ ,  $p = 5.17e - 51$ ) in our sample. This suggests, expectedly, that differences in hair curvature between Africans and Europeans are highly heritable. Another interesting finding is that there is a very wide distribution of cross-sectional eccentricity among the individuals with low African (and high European) ancestry proportions (see Figure 4.2).

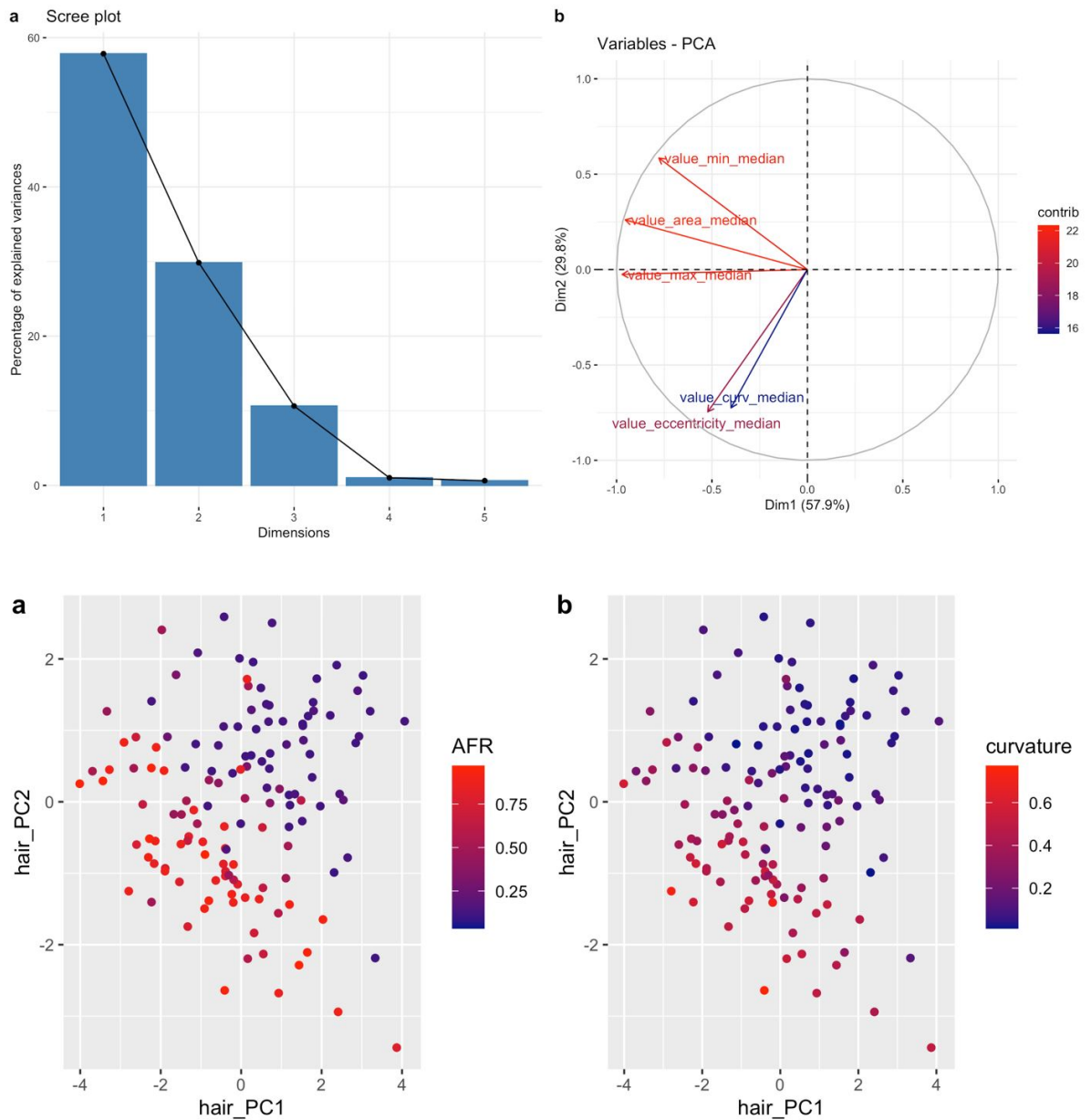


**Figure 4.3. PCA results for quantitative hair traits.** **a**, Scree plot showing the percentage of variance explained for each PC **b**, Contributing variables for first two PC dimensions **c**, Individual points colored according to proportion of AFR ancestry **d**, Individual points colored according to median hair fiber curvature

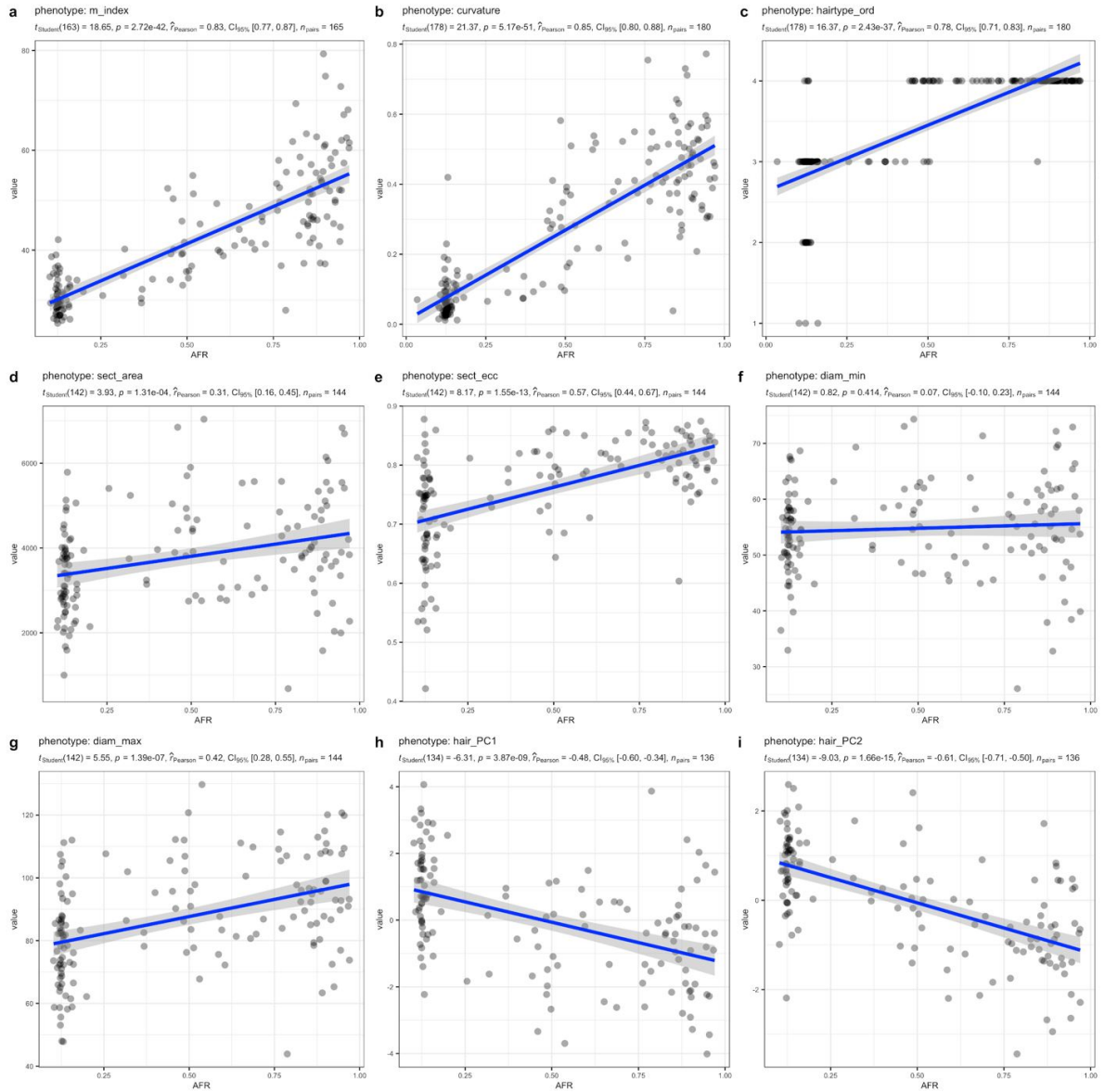


**Figure 4.4. Scatter plot of proportion of African ancestry (x-axis) against phenotypic trait values (y-axis).** a, Melanin Index, b, Hair fiber curvature ( $1/radius_{(mm)}$ ) c, cross-sectional area of hair fiber ( $\mu m^2$ ), d, eccentricity of cross-section, e, minimum diameter of hair fiber ( $\mu m$ ), f, maximum diameter of hair fiber ( $\mu m$ ).

### 4.3.1 Correlation between curvature and cross-sectional eccentricity are primarily driven by ancestry stratification

We find that the often described correlation between curvature and cross-sectional eccentricity appears to be primarily driven by ancestry stratification in our admixed

African-European sample. We plot a correlation matrix between all combinations of the phenotypes without correcting for ancestry (Figure 4.5a) and with a correction for ancestry, based on the phenotypic trait values residualized on ancestry (Figure 4.5b). The correlations we see between the various cross-sectional properties are predictable as they relate to increases in size (see Appendix D for more details on these correlations). However, none of the remaining traits are correlated with each other after ancestry correction, suggesting that these correlations are largely driven by ancestry stratification.

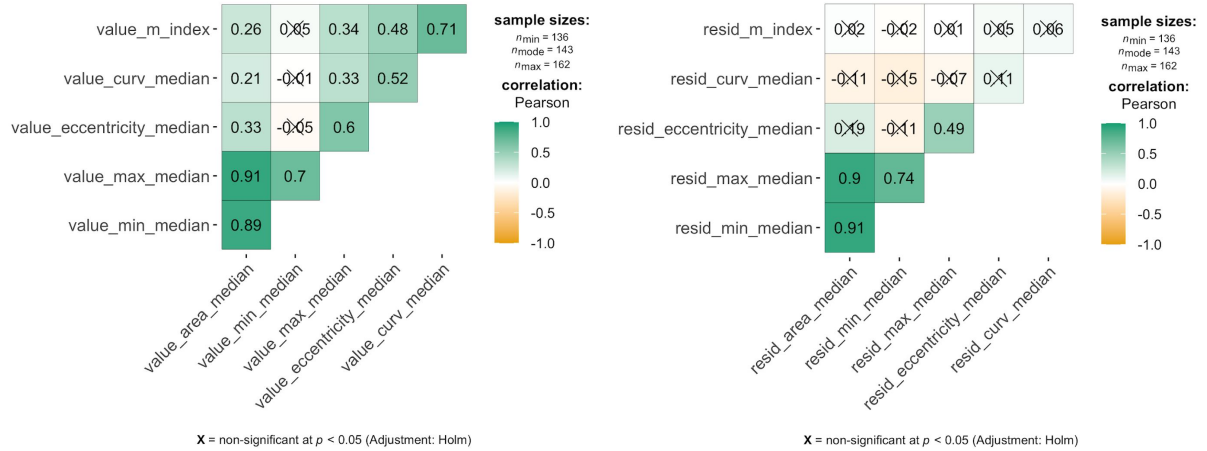


**Figure 4.5. Correlation matrices for the various traits a**, without ancestry correction and **b** with ancestry correction.

## 4.3.2 Associations of genetic variants with quantitative scalp hair morphology

### 4.3.2.1 Replication of known loci

First, we were interested in replicating loci that are already known to be associated with either skin pigmentation or hair morphology. We curated the literature and assembled a list of SNPs associated with skin pigmentation and for hair morphology. We highlight a number of SNPs replicated from a recent met-analysis on hair morphology below (see Table 4.1 and a full list of replicated SNPs can be found in Appendix F.

While the comparison between the effect size for both studies cannot be direct, due to differences in phenotyping (i.e. four categories vs. continuous curvature) and ancestry composition of the sample, the direction of the effect sizes was consistent across studies (Table 4.1). One of the SNPs associated with curvature for example is rs310644 ( $P = 0.004326$ ). The T allele is associated with an increase in curvature. Moreover, its

allele frequency distribution across the world shows that both African and Melanesian populations have higher frequencies of the effect allele (C) which was associated with higher hair fiber curvature in our sample (see Figure 4.7).

We replicated another previously reported locus with our quantitative measure of cross-sectional area (Table 4.1). The negative direction of the A allele suggests that this allele decreases the cross-sectional area (or thinner hair), with one exception having a positive value corresponding to a larger cross-sectional area. Comparing this to the reported effect sizes in Liu et al (2018), we see that for the same effect alleles, our study shows thinner hair and their study shows a higher curvature. Such a correlation between these traits has previously been reported for *EDAR* where a variant was associated with both thicker hair and straighter hair.

The results for the replicated loci with all other traits and levels of correction are available in Appendix D.

#### 4.3.2.2 Genetic architecture of traits

Next, we scanned the genome for any new loci. We are primarily interested in finding variants that contribute to differences in the mean phenotype between Africans and Europeans. Therefore, we restricted our analyses to SNPs with a high frequency difference ( $>0.5$ ) between Africans and Europeans. Such markers are often referred to as ancestry informative markers (AIMs). We did not find any variants above the genome-wide p-value threshold. However, we note that even the large effect variant in *SLC24A5* which is associated with skin pigmentation did not reach genome-wide significance in our sample due to a lack of adequate power. Nevertheless, the Manhattan plot for skin pigmentation shows clear peaks at known loci (Fig. 4.6) including the one at *SLC24A5*. In contrast, the peaks are not as clear in the Manhattan plot for hair curvature. Given that both skin pigmentation and hair curvature have similar correlations with ancestry, this might suggest a more complex genetic architecture for hair curvature though we would need to collect a larger sample size to show that.

## Melanin Index

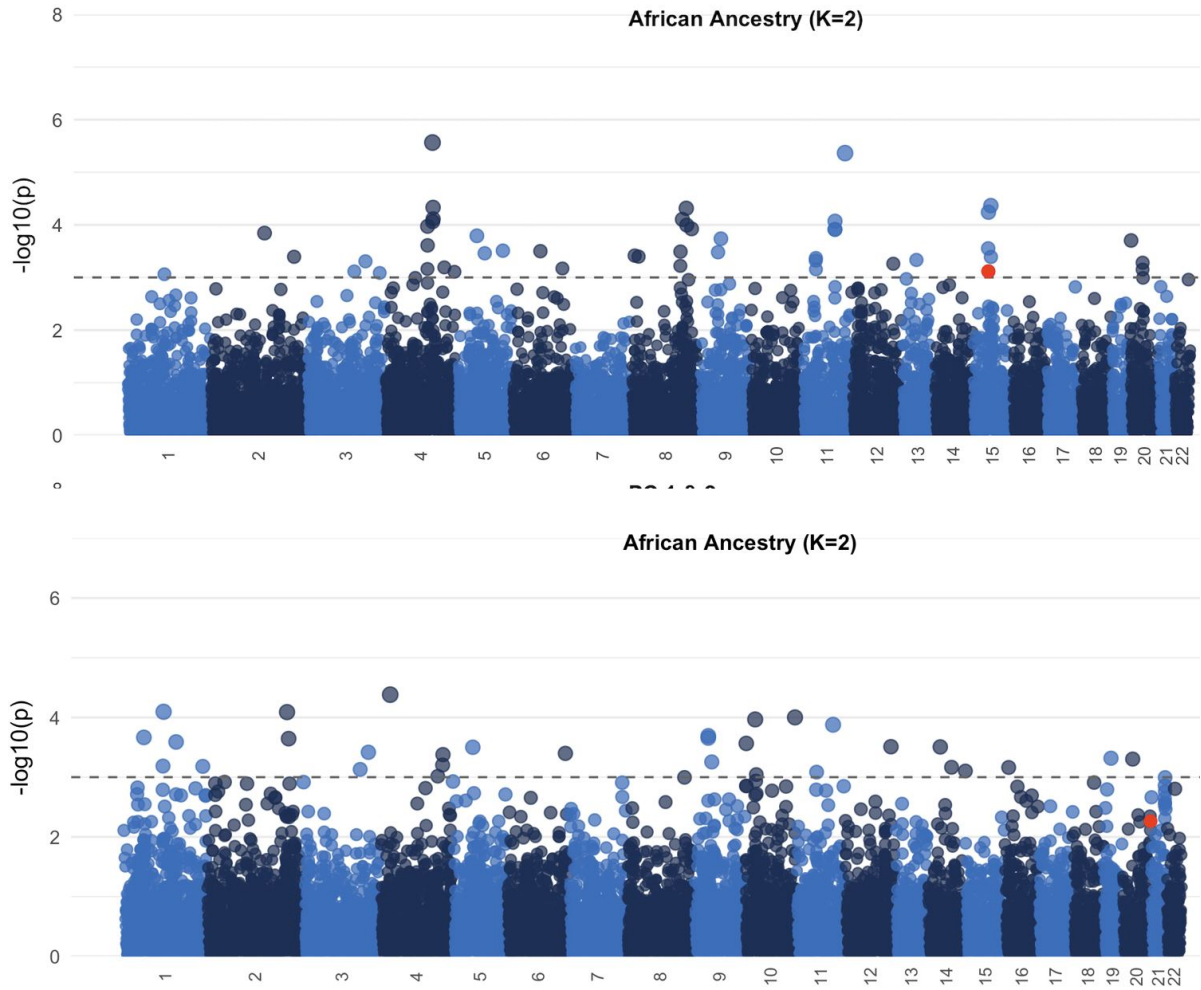


**Figure 4.6.** Manhattan plot of admixture mapping for various traits. **a**, skin pigmentation. Highlighted SNP represents *SLC24A5*. **b**, hair curvature

Curvature							
CHR	SNP	BP	EA	N	BETA	STAT	P
4	rs1385130	79293127	G	188	-0.02932	-2.192	0.0296
4	rs168283	79234317	G	186	0.02919	2.034	0.04339
4	rs6835769	79284694	T	188	-0.02835	-2.117	0.03561
20	rs310644	62159504	C	188	0.04405	2.889	0.004326
20	rs310654	62172269	A	186	0.05502	3.823	0.0001807
20	rs310655	62172281	T	183	0.04534	3.245	0.001401
Cross-sectional area							
CHR	SNP	BP	EA	N	BETA	STAT	P
1	rs499697	152493154	G	150	-419.6	-2.408	0.01729
1	rs6587673	152430152	A	149	352.5	2.866	0.004776
1	rs6661961	152442289	T	150	-290.1	-2.202	0.02922
1	rs6700998	152434009	T	150	-287.2	-2.17	0.03163

**Table 4.1.** Table of significant replicated loci from GWAS meta-analysis on hair morphology (Liu et al., 2018)

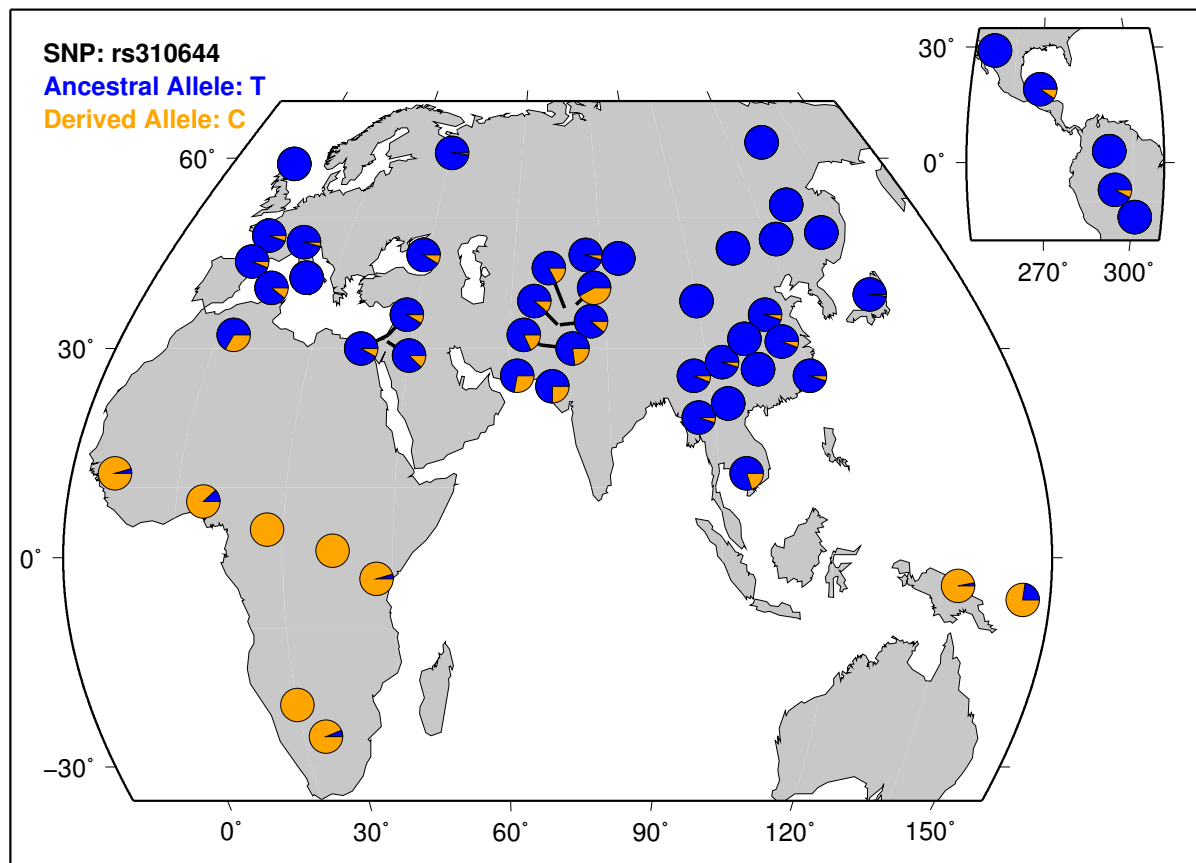


**Figure 4.7.** Allele frequency map of rs310644. Derived C allele shows high frequencies in African and Melanesian populations, while ancestral T allele is at high frequencies across Eurasian populations.

To ensure that our results were not driven by population structure, we examined the QQ plots for the association results (for all SNPs) (see Figure 4.8). We show that the observed distribution of test statistic follows the expected distribution showing that our correction for population structure (both with proportion of AFR ancestry in ADMIXTURE and using the first two PCs) is adequate.

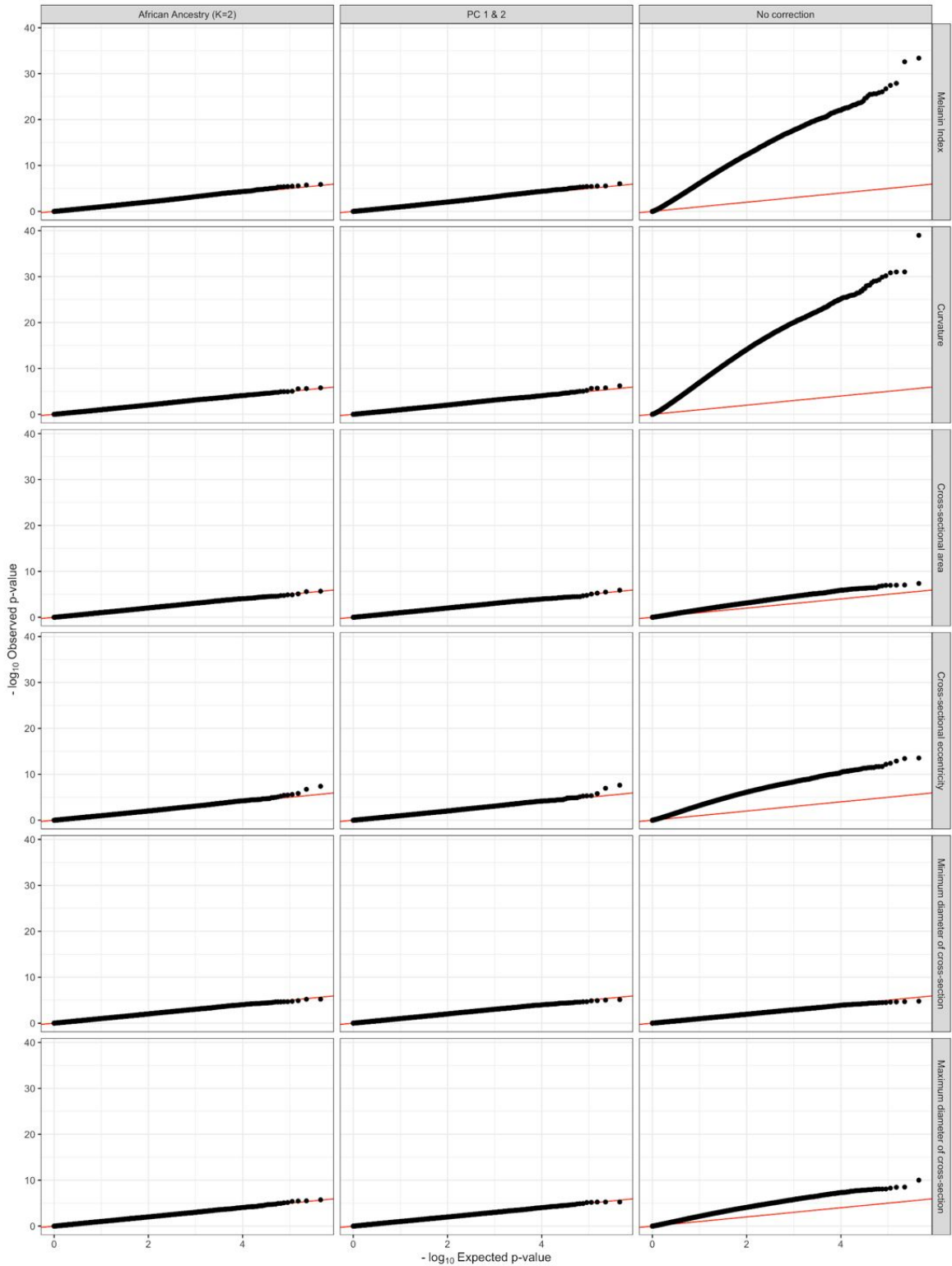


**Figure 4.8. QQ plots for various ancestry corrections and phenotypes.** Columns represent different ancestry corrections and rows are different phenotypes. Shown here are (from top to bottom): Melanin Index, curvature, cross-sectional area, cross-sectional eccentricity, minimum diameter, and maximum diameter 60

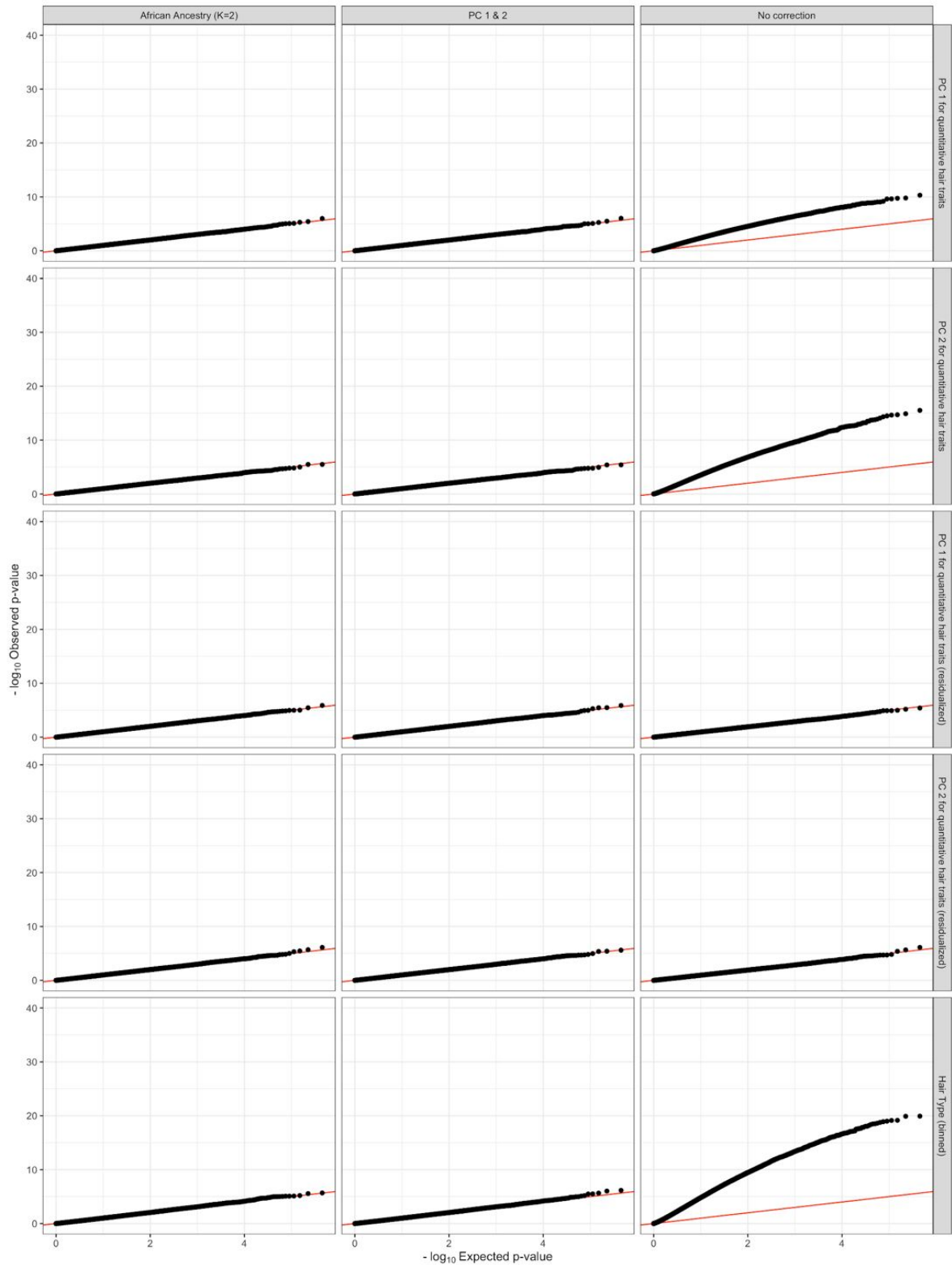


**Figure 4.9. QQ plots for various ancestry corrections and phenotypes.** Columns represent different ancestry corrections and rows are different phenotypes. Shown here are (from top to bottom): PC1 for hair traits, PC2 for hair traits, PC1 for residualized hair traits, PC2 for residualized hair traits, objectively classified hair texture.

## 4.4 Discussion

Hair morphology is a complex trait with considerable variation among human populations. Currently, our knowledge of its genetic architecture relies heavily on studies of European and East Asian populations with a palpable dearth of studies considering variation in African and African-descendant populations, despite their known genetic and phenotypic diversity. A major barrier to our understanding of the genetic underpinnings of human scalp hair morphology across populations is the overreliance on subjective typologies of hair that overemphasize certain types of hair variation, while ignoring others. The use of validated quantitative methods for measuring phenotypic variation in GWAS is promising and has previously proven useful in detecting genetic associations for variation in traits that cannot readily be discerned by typological approaches (Fujimoto et al., 2008b; Crawford et al., 2017; Martin et al., 2017).

In this study, we measured skin reflectance and multiple aspects of hair morphology using novel high-throughput methods in a sample of US-based participants of primarily African and European ancestry. With our analyses of the phenotypic and genotypic information on this sample, we were able to replicate a number of previously reported loci and we found further evidence supporting the complex and polygenic nature of human scalp hair morphology. Furthermore, we were able to elucidate the relationship among various aspects of hair morphology and the extent to which they might be affected by population structure in samples of similar ancestries.

### 4.4.1 Hair morphology

First, we examined the distribution of all collected phenotypic variation in our sample with comparable quantitative data from participants of self-reported African ancestry, European ancestry and individuals who described themselves as part of the African Diaspora. Our findings show that as expected, for skin pigmentation our admixed sample shows a distribution of M-index values that, similarly to the African Diaspora, spans the range from European and African values (Figures 4.2 a and b). Interestingly, hair curvature showed a similar pattern. Both these findings suggest that our terminology for describing skin color variation and hair curvature variation overemphasize the relatively small range of variation shown in European populations while minimizing the considerable range of variation shown in African and African-descendant populations. In contrast, other aspects of hair variation appear minor, including eccentricity, which is often described in forensic textbooks as a key morphological distinction between African and

European hair (Figures 4.2 c-f).

We use a Principal Components Analysis to explore the interrelation of the quantitative hair traits we have measured and their relationship to genomic ancestry (see Figure 4.4). The PCA for our sample does not show clear clusters according to ancestry or curvature. We repeat the PCA for the residualized hair traits (correcting for ancestry) and use both the unresidualized and residualized PC variables in our downstream analyses. We show the correlation between our phenotypic data with proportion of African Ancestry (see Figure 4.3) as well as the correlation among traits with and without ancestry correction (Figure 4.5). What emerges is that certain traits and relationships among traits are heavily driven by ancestry stratification in our sample. Most notably, the correlation between cross-sectional eccentricity and curvature, which is often seen as causal, appears to be primarily driven by stratification in our sample. Once we correct for ancestry, we find that the only correlations remaining are expectable covariation in relation to increased cross-sectional size and, interestingly, a significant correlation between eccentricity and maximum cross-sectional diameter, perhaps relating to a mechanism by which hair shafts are built. This finding may suggest that variation in cross-sectional shape is driven by the increase of the hair in its maximum dimension, rather than the decrease of its minimum diameter, but further work is needed to interpret this result.

#### 4.4.2 Genetic architecture of skin and hair loci

As a baseline, we first tested the association for skin pigmentation (as measured by skin reflectance) and found that we were able to successfully replicate *SLC24A5* in our sample. Even though *SLC24A5* was statistically significant, it would not have reached genome-wide significance if we were trying to find it in an agnostic scan. This suggests that our study is currently underpowered even to detect large effect loci. Nevertheless, we performed a GWAS and cross-referenced our significant SNPs with previously reported skin and hair loci, and we found a number of variants that were successfully replicated in our sample reaching a nominal significance level of at least  $P = 0.05$  (see Table 4.1 and Appendix F for full table of replicated loci). When we compare the direction of our effect size to those of the reference hair morphology GWAS (Liu et al., 2018), we see that it is the same for curvature, which adds confidence to the validity of our replication. Other replications are less straightforward to interpret, however the apparent correlation between decreased cross-sectional area (our study) and increased curvature (the meta-analysis) is a pattern that resembles the confounding association between the *EDAR* V370A allele, which is associated with increased cross-sectional area as well as

straighter hair in East Asian populations (Fujimoto et al., 2008b; Mou et al., 2008).

One of our strongest associations with hair curvature, which was not replicated for any other hair trait, is rs310644 on Chromosome 20. We examined allele frequency distribution around the world for this pattern and found that, in the case of this SNP, the derived allele (C) is present at a high frequency across African populations (it is even fixed in some of them) and the only other group with comparably high frequencies of the derived allele are Melanesian and Papuan populations who are also known to have tightly curled hair. Alongside our replication of higher curvature with the C-allele, this finding suggests that this locus warrants further investigation in the context of African and Austronesian populations.

For our admixture mapping, we took the results of our GWAS and filtered for SNPs that showed a high allele frequency difference ( $>0.5$ ) between YRI and CEU HapMap populations. Such SNPs would be the only variants that we could have the statistical power to detect in our small sample. However, no SNPs approached genome-wide significance. Using an adjusted P-value of 0.001, we were able to curate a list of candidates for further investigation (see Appendix F). Our failure to find SNPs reaching genome-wide significance in the context of our QQ plots suggest that hair curvature is likely highly polygenic. Additionally, we demonstrate the usefulness of using continuous quantitative phenotypic data over classification (even if based on objective data). The replication of one locus, in particular, on Chromosome 1 for our binned hair typing is likely a signal associated with *TCHH*, which has previously been associated with straighter hair in European populations (Medland et al., 2009; Liu et al., 2018). This demonstrates that certain signals are more readily apparent when categorical data is used, but others (e.g. the locus on Chromosome 20) are only apparent with the full resolution of the continuous data for variation on the end of the spectrum with higher curvature.

### 4.4.3 Future directions and conclusions

This study represents a step forward in the study of the genetics of human scalp hair morphology and suggests a number of promising future avenues of research. The most imminent next step would be to investigate more exhaustively the data at hand. One possibility is to calculate local ancestry for each region rather than relying solely on ancestry informative markers derived from high allele frequencies (Grinde, Brown, Reiner, Thornton, & Browning, 2019; Maples, Gravel, Kenny, & Bustamante, 2013). Additionally, selection-based approaches could yield candidate loci. Examining patterns of locus-specific

branch length across the genome in multiple populations would allow us to investigate whether hair and keratin-associated genes have longer branch lengths, on average, in African and Austronesian populations.

In summary, this study was able to replicate a number of previously reported loci and elucidate the genetic architecture of human scalp hair morphology using novel methods for phenotyping the continuous variation in this trait. By focusing on a sample with significant African admixture, this study was able to offer insight into variation in a population that has not received much attention from previous studies of hair genetics. Future steps for this work include expanding the sample in size and including other populations with high frequencies of tightly curled hair, such as South Africans and Melanesians.

## 4.5 Methods

### 4.5.1 Participant recruitment, hair samples, and genotype data

The hair samples and genotype data for the African-European admixed individuals were collected with informed consent and ethical approval by The Pennsylvania State University Institutional Review Board (#44929 and #45727). The hairs used as reference samples for the distribution of hair phenotypes (i.e., the African, European, and African Diaspora groups) were collected in London and Cambridge, UK, with informed consent and ethical approval by The University of Cambridge.

### 4.5.2 Phenotyping methods

A detailed description of the hair phenotyping methods can be found in Chapter 3. In brief, we used new methods for both sample preparation and image analysis of longitudinal curvature and cross-sectional morphology of hair. The sample preparation for curvature consisted of cutting hairs into fragments which were then washed and decanted into a Petri dish for imaging. Sample preparation of hairs for cross-sectional analysis involved embedding the hairs in a low melt point plastic (polycaprolactone), cutting the embedded sample and imaging it under a microscope. A Python image analysis program named *fibermorph* was developed for the processing and measuring of variables of interest in both images of curvature and cross-sections and can be downloaded from PyPi.org.

### 4.5.3 Estimation of admixture

We used unsupervised clustering with ADMIXTURE (K=5) on the full sample (n=4257) with 65218 LD pruned markers to estimate ancestry as described elsewhere (Zaidi et al., 2017). We selected a subset of 192 individuals of primary African and European ancestry. We redid the clustering for this sample at K = 2 and K = 3 and show that K = 2 provides the lowest cross-validation error. Therefore, we used the ancestry components from the K=2 run in downstream analyses. After removing related individuals and individuals with fewer than 2 hair fibers in their data sets, we had between 136 and 188 individuals in our analyses depending on the phenotypes involved in those particular comparisons.

### 4.5.4 Genotype-phenotype associations

We selected markers with a frequency difference of at least 0.5 between the YRI (Yoruba from Ibadan representing West African ancestry) and CEU (representing Western European ancestry) from the 1000 Genomes Project data. We tested their association with each phenotype using a simple linear model with ancestry (either African component or PCs 1-2) as covariates. We used the `-glm` function in plink 1.9 (Chang et al., 2015) for this. Code for the analyses presented in this dissertation can be found on GitHub at [https://github.com/tinalasisi/Afr\\_Admix\\_Assoc](https://github.com/tinalasisi/Afr_Admix_Assoc).

# Chapter 5 | Experimental evidence from thermal manikin for the role of human scalp hair as an evolutionary adaptation

## 5.1 Introduction

### 5.1.1 Thermoregulatory constraints in human evolution

Encephalization, bipedalism, and the loss of body hair are three traits of prime interest in the study of hominins and early *Homo* (Wheeler, 1985; Falk, 1990). The main interest has been in understanding what selective pressures may have acted to shape these quintessentially human traits, and whether (if at all) their appearance in the human lineage is linked. In each case, thermoregulation has been implicated as a potential contributing factor.

Thermoregulation is important for all living organisms, but some of the physical traits and behaviors that humans have evolved posed new challenges to their basic primate physiological mechanisms of temperature regulation. Principally, the emergence of prolonged bipedal striding and running occurred at the same time as the evolution of a larger brain size (Ruxton & Wilkinson, 2011; Ruff, Trinkaus, & Holliday, 1997). The possibility of overheating leading to cognitive deficit thus emerged as a significant threat because of the combined effects of metabolic heat production in a hot environment coupled with increased thermosensitivity of a large brain. These new thermoregulatory challenges required new solutions.

Sweating works in tandem with a seemingly hairless body to create a highly effective cooling system. But this physiological function is not without cost. Dehydration is a significant risk, even in modern humans. A negative water balance, in and of itself, can accelerate the development of hyperthermia and cause cognitive impairment. However, sweating also depletes electrolyte reserves, which in extreme situations can cause physiological dysfunction (e.g. cardiovascular disturbance) and, if left unchecked, can lead to death. In an environment where water may have been scarce and electrolytes difficult to replenish, it becomes apparent that sweating may have come at a considerable cost (Porter, 1993).

### **5.1.2 Hair plays an important role in mammalian thermoregulation**

Thermoregulatory systems are exceptionally conserved in vertebrate evolution. The extensive and fundamental interconnection between nervous and circulatory systems forms an integral constraint on the possibility of evolving non-deleterious modifications (Crawshaw, Moffitt, Lemons, & Downey, 1981; Siemens & Kamm, 2018). As such, the success of mammals in a wide range of thermal environments rests, in part, on the evolvability of hair - an adaptation that does not disturb the careful coordination of systems involved in internal temperature regulation (Guerrero & Rogers, 2019; Dawson et al., 2014; Wacker, McAllan, Körtner, & Geiser, 2016).

The multifaceted function and adaptability of hair explains why so few hairless mammals are found. Marine mammals aside, the list of terrestrial mammals that have evolved hairless skin, or more accurately miniaturized hair follicles, is very short. With the exception of special cases such as the naked mole-rat (that is poikilothermic rather than endothermic) and armored mammals, hairlessness is restricted to a few large-bodied species in extremely hot environments: elephants, rhinoceroses and hippopotamuses (Wheeler, 1984). The rarity of hairlessness among terrestrial mammals living in hot climates suggests that there may be several factors that outweigh the improved heat loss that comes with hairlessness.

The benefit of hair in cold environments is readily understood. But a mammalian coat is capable of more than simple heat retention. Protection from solar radiation is a key function of hair. This protection is not limited to UV damage, but is extended to an overall reduction of the total heat load on an animal. Experimental studies of the thermal conductance of various mammalian coats demonstrate that a reduction in heat gain can be achieved by a short and lightly pigmented reflective coat, but also by a sufficiently deep coat (Dawson et al., 2014; Dawson & Maloney, 2017; Walsberg, 1990).

This illustrates the versatility of mammalian hair, even in contexts where its reduction intuitively appears more beneficial.

### **5.1.3 Considering a thermal role for human scalp hair**

The function of human scalp hair has received relatively little attention from evolutionary anthropologists because, unlike bipedalism, encephalization, and hairlessness, the functional role of scalp hair is less apparent. A number of scholars have speculated about the evolutionary pressures that may have initiated the emergence (or retention) of scalp hair. Among these, the thermoprotective hypotheses stand out as the most readily testable. Yet, thermoregulatory models of early hominins have not explicitly examined the function of scalp hair.

By contrast, physiologists and environmental ergonomists have afforded the thermal effect of scalp hair some consideration. A few studies have looked at the effect of scalp hair on sweat rate and heat loss. Cabanac and Brinnet (Cabanac & Brinnet, 1988) found that bald men evaporated sweat on their heads at a rate two to three times higher than men with scalp hair. At first, this supports the intuitive expectation that a hairless head would be at an advantage in terms of heat loss, as it would have the fewest barriers to evaporation.

However, a more recent study by Coelho et al. (2010) suggests that this advantage may obscure the net disadvantage of a hairless head, as it would also be subject to a higher heat load. Coelho and colleagues compared sweat rate during exercise under the sun in a sample of 10 men before and after shaving their head hair. They found higher sweat rates in the "no hair" condition, suggesting that the head required more evaporative cooling when there was no hair to protect it. Therefore, these human trials challenge the common assumption that a bald head is best (Falk, 1990).

Nevertheless, the polar dichotomy of hair/no hair is not necessarily a realistic scenario. A study by Shin et al. (2015) examined the potential role of hair length and found a higher rate of heat loss in individuals who had trimmed hair (5mm) compared to those men when they had longer hair (100 -130mm) when exposed to a cooling hood with 10°C water. This begins to offer some insight into the vast spectrum of possibilities between a hirsute and hairless scalp. But one key question remains unexplored: how does scalp hair morphology affect thermal load?

Scalp hair morphology is one of the most variable traits among human populations (Lasisi et al., 2016; Koch, Shriver, & Jablonski, 2019; Hrdy, 1973). Moreover, tightly curled hair, as seen in many African populations, is a uniquely human feature among

mostly straight-haired mammals. This distinctive phenotype has been previously suggested to have a specific advantage in the reduction of heat gain from solar radiation (Jablonski & Chaplin, 2014). Additionally, the ubiquity of tightly curled hair in a continent with unmatched genetic diversity, suggests the role of scalp hair morphology deserves further attention.

In this paper, we re-examine the effect of scalp hair on thermal load and further explore the effect of morphology. By using a thermal manikin in combination with solar lamps and human hair wigs of various textures, we generate empirical data on how differences in human scalp hair morphology influence heat transfer. This biophysical approach to the question allows for the collection of data on the thermal properties of different hair without noise that may be introduced through variability in the physiological responses humans have when under heat stress. Finally, we interpret the results in light of the hypothesis that (tightly curled) scalp hair may have evolved as a result of selective pressures to reduce the heat load on an increasingly large human brain.

## 5.2 Results

### 5.2.1 Brief Methods

Experiments were conducted in a climate-controlled chamber using a full-body thermal manikin (model “Newton”, Thermetrics, Seattle, Washington, USA). Data presented in this paper are only from the head and face zone of the manikin (out of 20 independently controllable zones on the manikin). The wigs used in the experiment ranged from straight to tightly curled (see Appendix G) and were all naturally black human hair of Chinese origin made with 8<sup>#</sup> hair fibers. Solar radiation was simulated with two lamps reaching a net radiation of  $\sim 788$  W/m<sup>2</sup>.

The dry measurements were taken at two different temperatures - one with  $T_{manikin} = 34^{\circ}\text{C}$  and  $T_{ambient} = 10^{\circ}\text{C}$ , and another with  $T_{manikin} = 38^{\circ}\text{C}$  and  $T_{ambient} = 2^{\circ}\text{C}$ . The second set of temperature options was needed as certain conditions led to overheating of the manikin (See Appendix G for details). The wet measurements were taken with the temperature settings  $T_{manikin} = 34^{\circ}\text{C}$  and  $T_{ambient} = 34^{\circ}\text{C}$  or  $T_{manikin} = T_{ambient}$ . For the analyses below, we applied a correction to bring all the measurements to  $T_{ambient} = 30^{\circ}\text{C}$  with solar radiation (See Appendix G).

## 5.2.2 Solar influx and evaporative cooling create distinct heat loss patterns

When comparing the heat loss at  $T_{ambient} = 30^{\circ}\text{C}$  for dry vs. evaporative conditions and with/without solar radiation, we see distinct effects of solar influx and of evaporative cooling (see Figures 5.1 and 5.2). Our results show that in a dry heat loss with solar exposure setting, the absence of any barrier (nude/no wig) results in net heat gain. Curlier wigs are associated with higher heat loss. But in all other conditions, this pattern is reversed. Additionally, in the wet condition, the effect of wind speed is more pronounced than that of the different wigs.

Linear models model predicting heat loss for dry and wet conditions this particular pattern (see Figure 5.3) . In the dry condition, we see that radiation had the single strongest negative effect on heat loss, while the interaction between solar radiation and high curvature wig showed the highest positive effect on heat loss. All terms were found to be significant.

Conversely, for the wet conditions, none of the interactions between wig and solar radiation were significant with wind providing the single positive significant effect on heat loss and the wigs reducing heat loss with increased curvature (complete results in Appendix Thermoregulation Chapter).

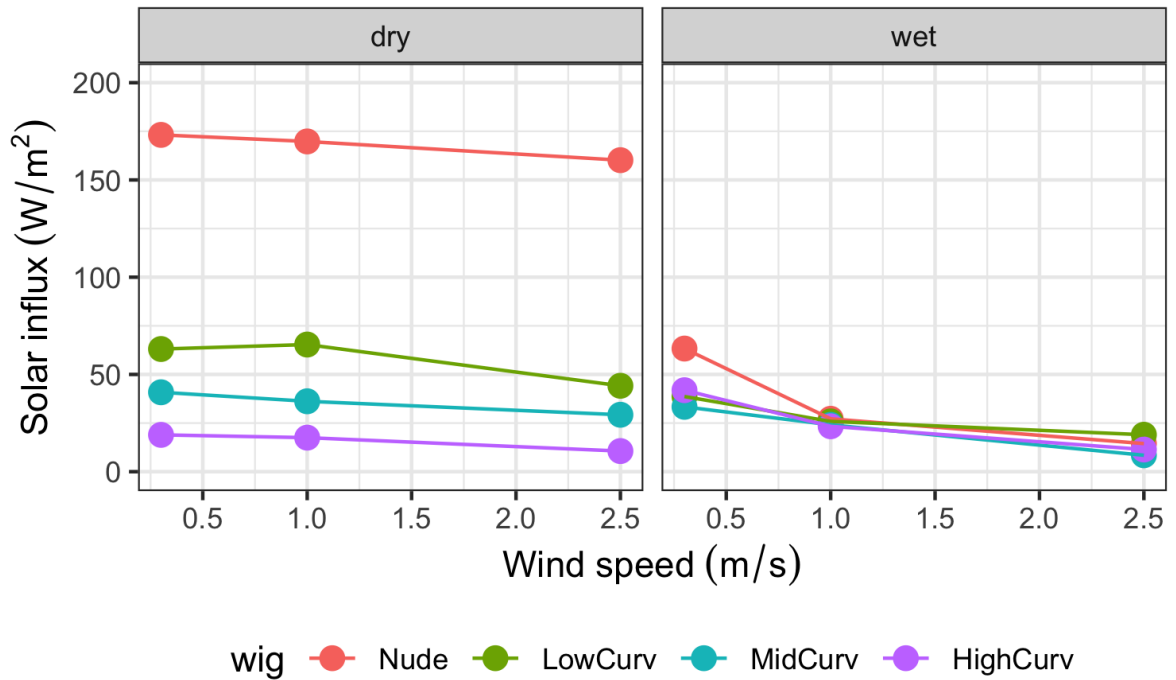


**Figure 5.1.** Solar influx as a function of wind speed at 30° C. Wind speed shown on the x-axis with solar influx on the y-axis. Dry experiments shown on the left and wet experiment results on the right.

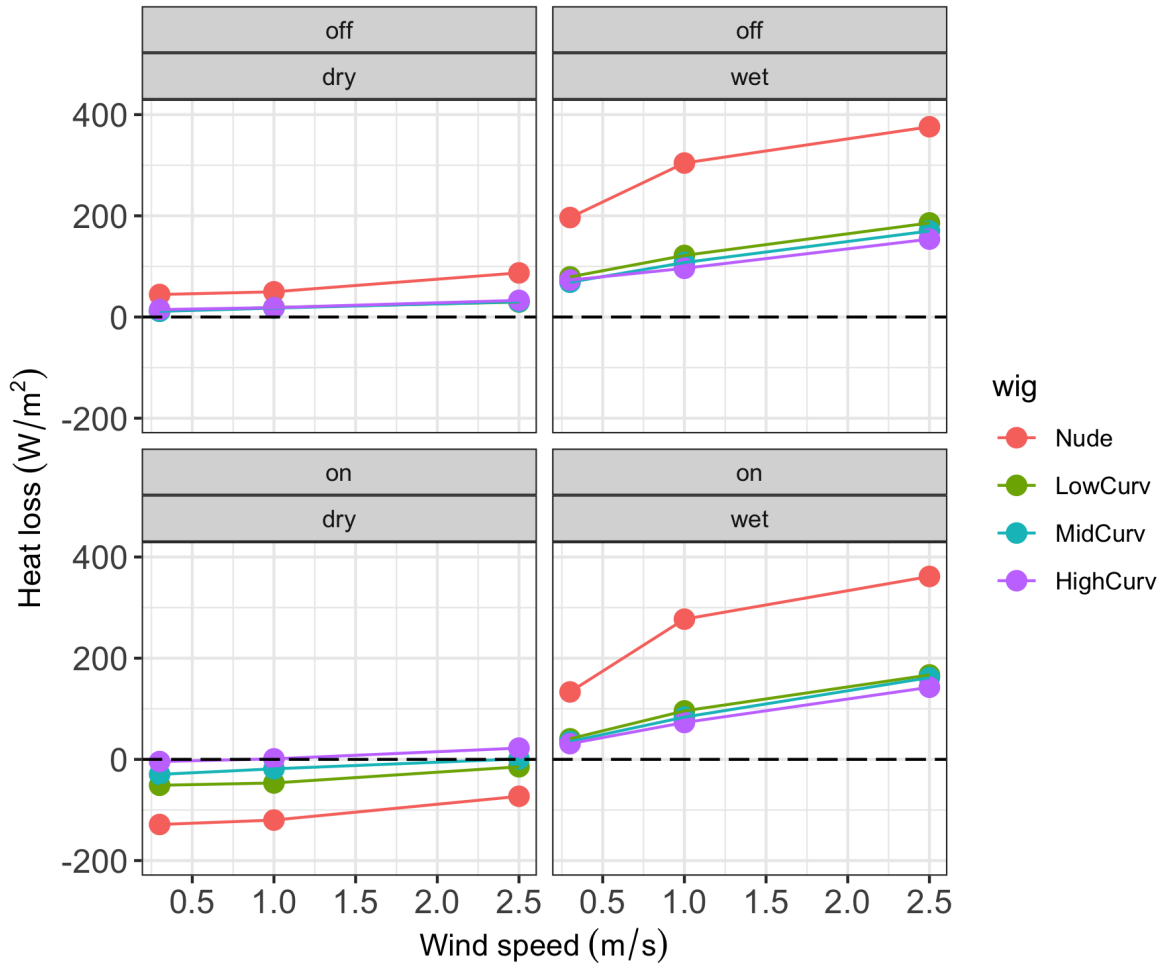


**Figure 5.2. Heat loss vs. radiation across experimental conditions.** Heat loss with radiation off/on (top to bottom) and in dry and wet conditions (left to right) calculated for ambient temperature of 30C. Dashed line represents  $y=0$ .

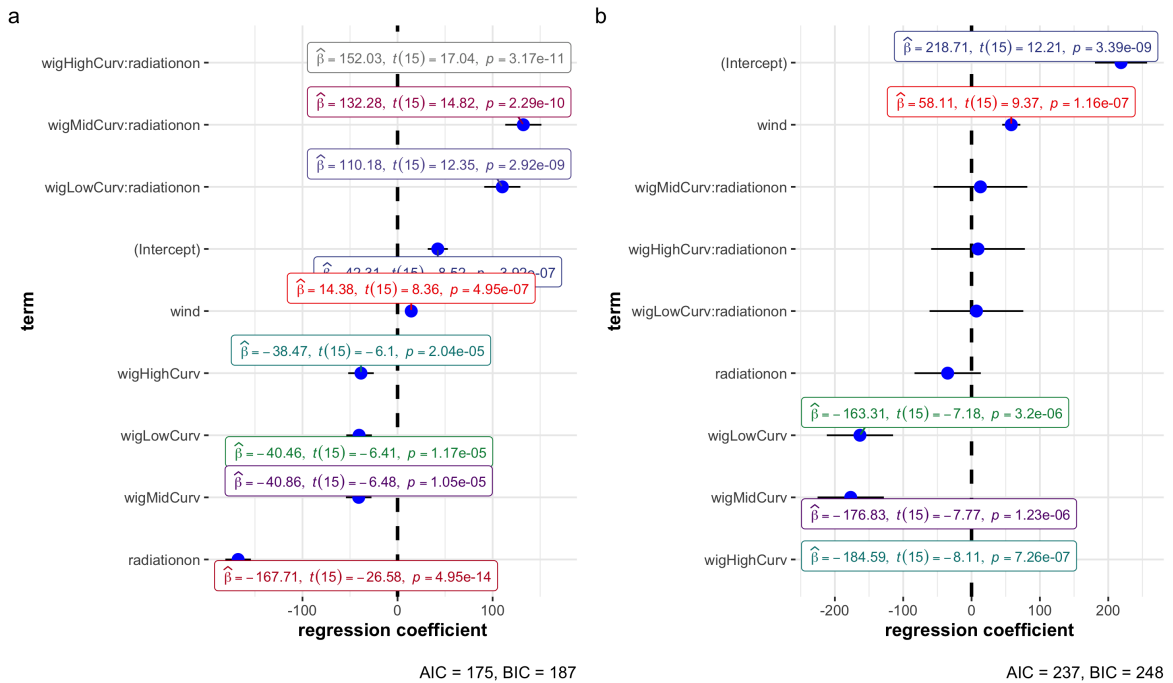


**Figure 5.3. Results for linear regression on heat loss.** Dot-and-whisker plot of linear models for heat loss at 30°C for (a) dry and (b) wet conditions

### 5.2.3 Sweating potential vs. sweating requirements result in different optimal scenarios

Based on our dry and wet data, we were able to calculate the amount of sweat evaporation that would be biophysically possible under the various conditions (maximum sweating potential) and the amount of sweating that would be required to achieve heat balance (i.e. zero heat gain).

Our results show that to maximize the evaporative potential, the most beneficial situation is one without any form of hair acting as a barrier. Interestingly, our results appear to suggest that hair curvature reduces the evaporative potential of the manikin’s scalp (Figure 5.4).

In the case of zero heat gain, we see that the benefit of increased evaporative potential is strongly reduced by the increased need for evaporative cooling. While the evaporative potential of a nude scalp is higher, this condition also requires more evaporative cooling to counteract the solar influx. Along the same lines, increasingly curled hair reduces the amount of evaporative cooling (i.e. sweating) required to cancel out heat gain in a scenario with considerable solar influx.

The linear models of sweat volume for both maximum sweating potential and sweating requirement (for zero heat gain) show that the effects of wig type and wind speed are significant (see Figure 5.5). In the case of maximum sweating potential, this means that a greater amount of sweat can be evaporated. In the case of sweat requirement for zero heat gain, this means that less sweat is required to bring the scalp down to its baseline temperature.

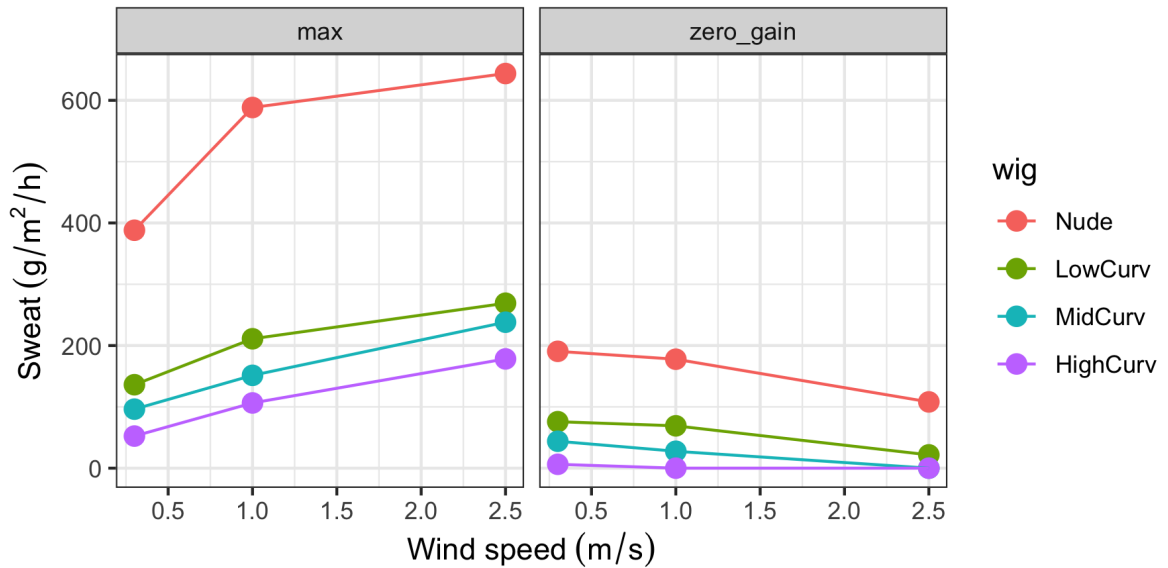


**Figure 5.4. Plot showing evaporative potential/requirement under different conditions.** The quantity of sweat that can be maximally evaporated (left) and that is required for zero heat gain (right) with various head coverings under three wind speeds.

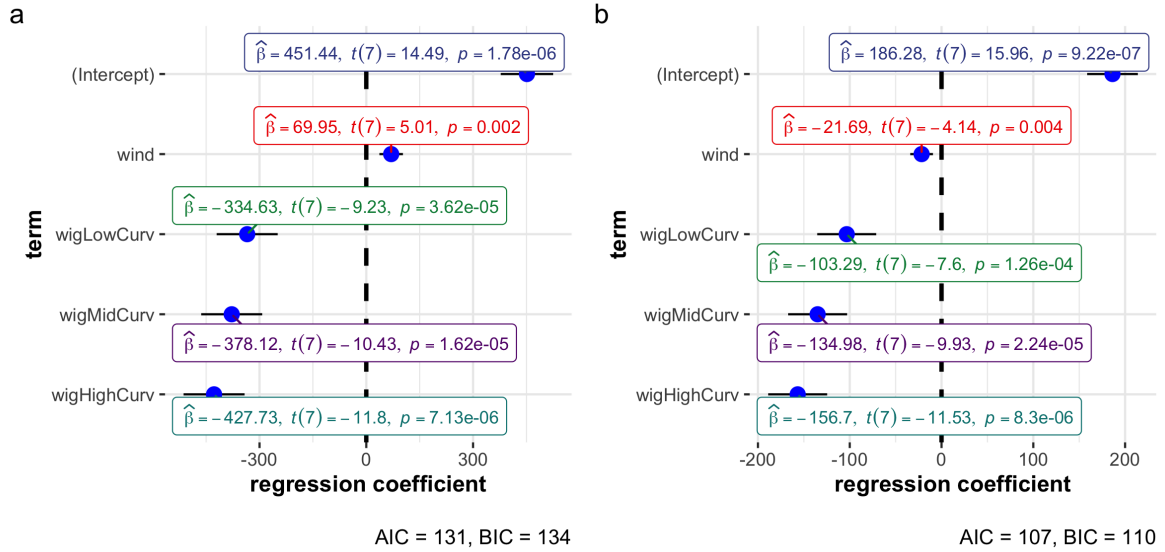


**Figure 5.5. Linear regression results for evaporative potential and requirements for heat loss.** Dot-and-whisker plots for linear regression of (a) maximum sweat potential and (b) sweat required for zero heat gain.

## 5.2.4 Thermocouple data interpretation issues on thermal manikins

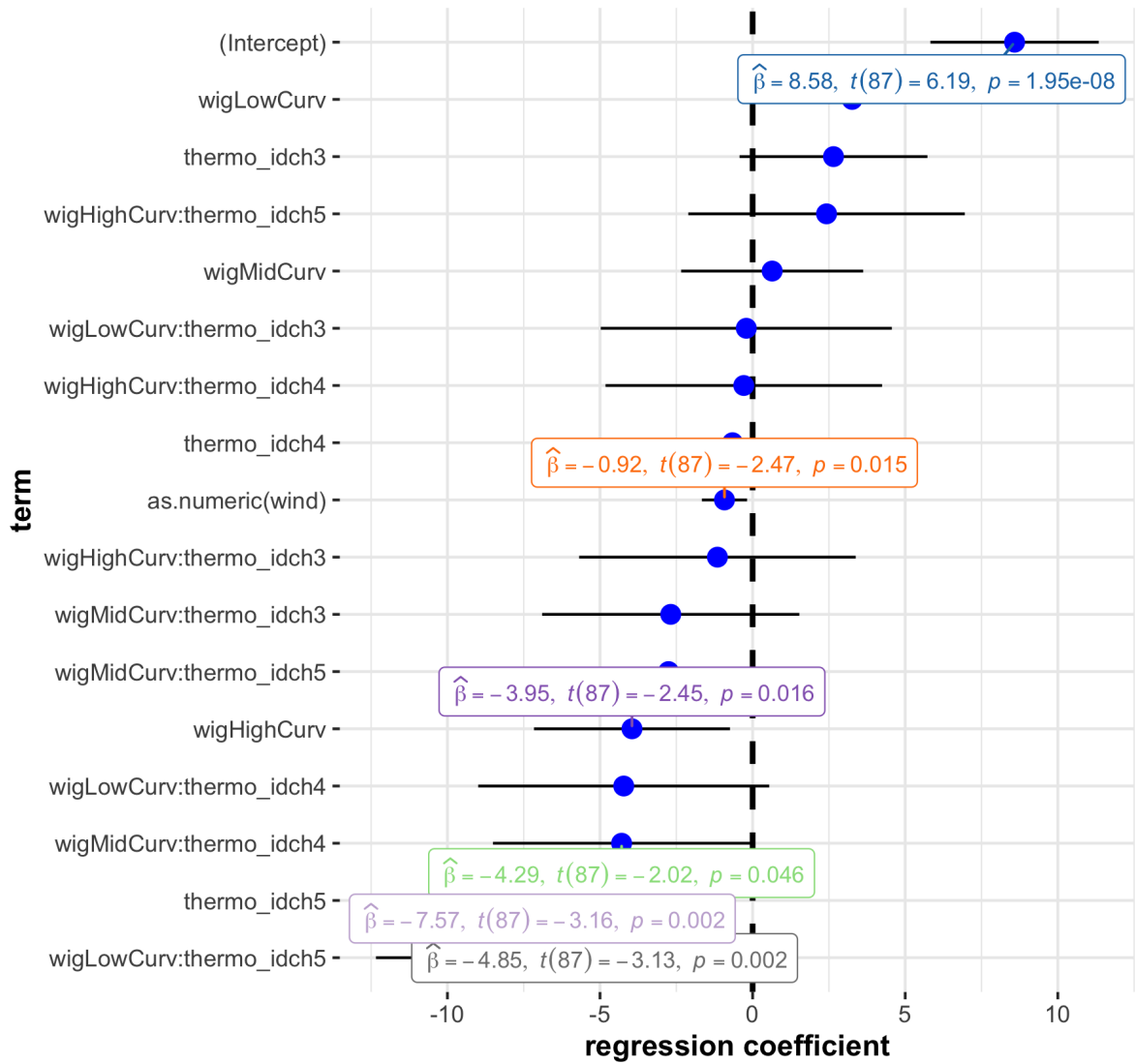
Thermocouples were placed along the midline of the thermal manikin (underneath wigs when one was worn). These are named by numbered channels from 1 to 5 (front to back; see diagram in Methods section). Channel 1 experienced some malfunctioning and is removed from the analyses. These measured the temperature at that point on the manikin’s scalp across experimental conditions. We then calculated solar influx as the temperature difference for that particular condition with and without solar radiation.

The baseline expectation would be that there is a net increase in temperature with the addition of solar radiation (as is apparent from the manikin data). However, our results show that there is considerable variation within individual conditions depending on the location of the thermocouple. Moreover, there is a consistent pattern showing a negative solar influx (i.e. lower temperature with radiation on) at the back of the head (see Figure 5.7). On a real (living) human scalp, such localized effects would be highly unlikely due to blood perfusion distributing the effect of the heat.

A linear model confirms that the strongest effect on solar influx is the interaction between the straight (low curvature) wig and thermocouple 5 which is placed at the back of the head (see Figures 5.6 and 5.12).

These results indicate an artifact in the data due to the thermal manikin's construction. The head region of the manikin is controlled as one whole. The thermal manikin reduces/increases its energy output to maintain the set skin temperature based on the average of each zone. Hence, if some regions within a zone are overheating, the entire zone will experience reduced heating from the manikin. Due to this, we find that the area least affected by solar exposure (as it is completely covered by hair) would have experienced a net decrease in temperature when other parts of the manikin head were overheating under solar exposure.

Despite these limitations, some interesting findings can be gleaned from these raw results. For example, we find that at  $T_{ambient} = 10^{\circ} \text{C}$ , a wind speed of 1m/s (equivalent to convection from walking), and no radiation, none of the trials reach the temperature threshold for thermal damage to the skin. However, with the added effect of radiation, many of the thermocouples picked up temperatures above various time-related exposure thermal thresholds that would lead to damage to the skin (see Figure 5.8).



AIC = 534, BIC = 581

Figure 5.6. Dot-and-whisker plot for linear regression on solar influx. Regression coefficient on x-axis with terms on the y-axis. Only significant terms are shown.

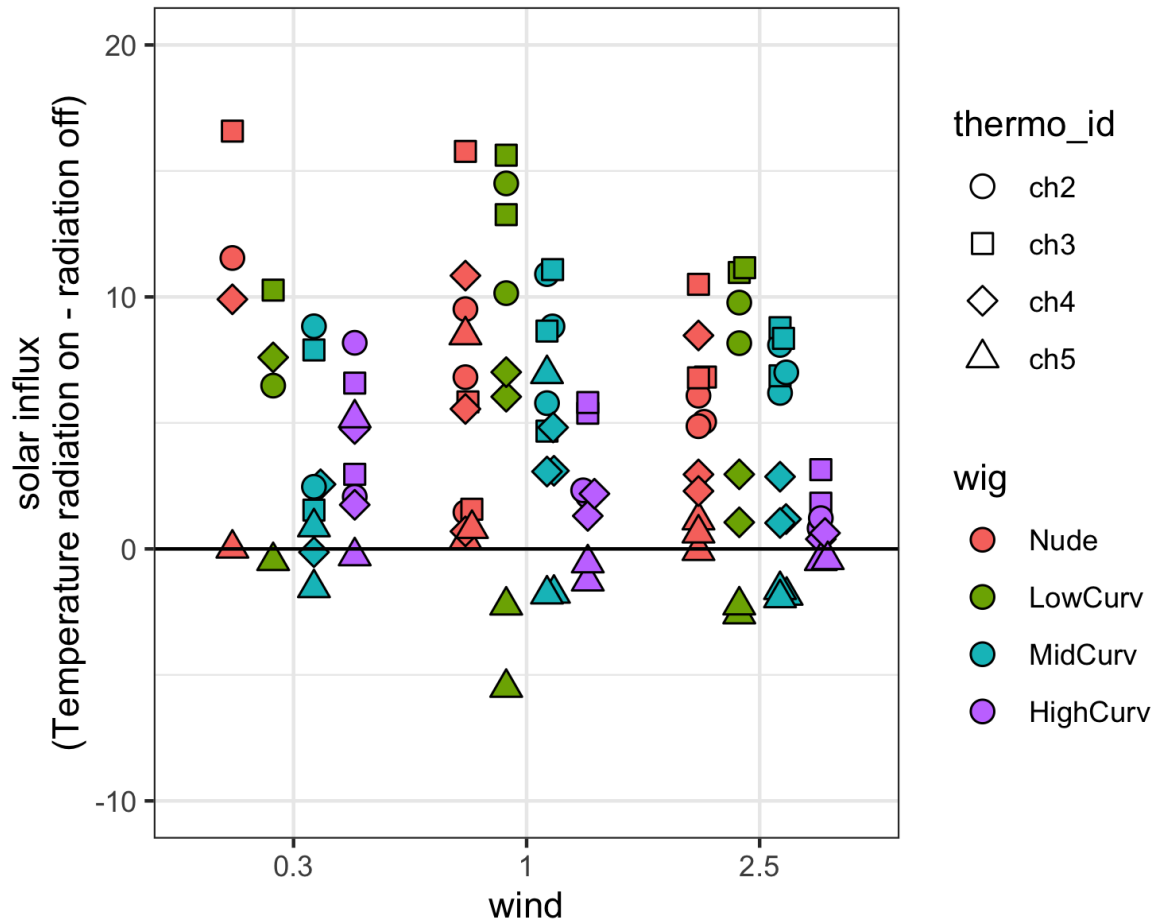


**Figure 5.7. Scatter plot of solar influx for different experimental conditions.** Line represents zero influx. Negative numbers represent negative solar influx (i.e. a higher temperature was found with no radiation than with radiation). Wigs are indicated by color and thermocouple ID is indicated by shape.

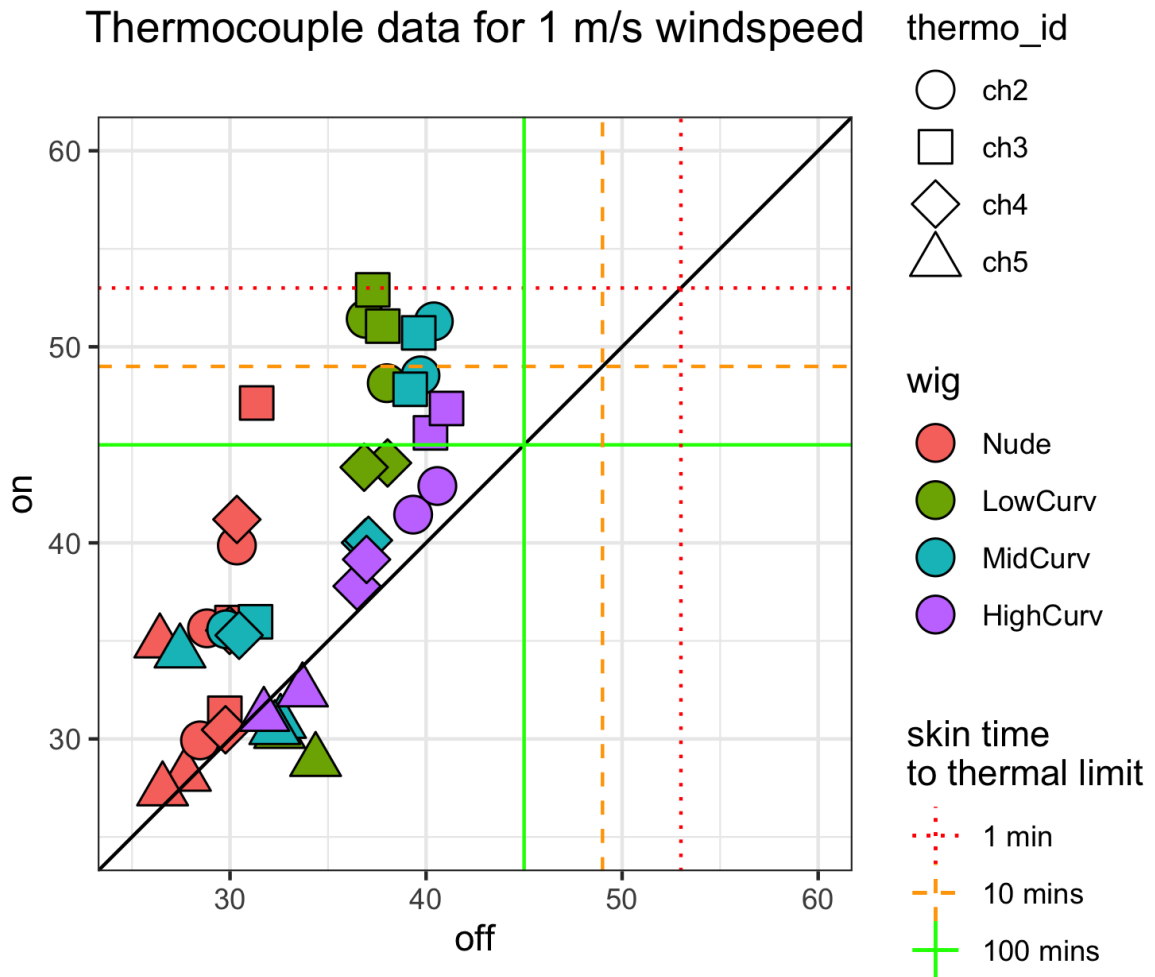


**Figure 5.8.** Thermocouple readings for across experiments for wind speed of  $1\text{ m/s}$ . The green line represents the cut off for burns sustained at that temperature after 100 minutes. The dashed and dotted orange lines represent that same limit but for burns sustained after only 10 and 1 minute respectively.

### 5.3 Discussion

The most striking observation from our results is the extent to which solar radiation increases heat load on a dry hairless scalp and the extent to which the level of hair curvature affects solar heating of the head (see Figure 5.1). In terms of direct heat

loss for the various experimental conditions, it is noteworthy that the only condition in which heat loss was negative (i.e., there was overall heat gain) was in a dry setting with solar radiation (see Figure 2), but, again, the extent of this was governed by hair curvature. This was also the condition in which differences between different levels of hair curvature were most pronounced, unlike other settings where the difference between hairlessness and hair (of any morphology) dwarfed the differences between wigs. It is also the one condition where a hairless scalp shows the lowest heat loss (or highest heat gain). When the scalp is saturated with water, it is clear that a hairless scalp is superior in terms of heat loss potential.

Using the dry and evaporative data, we were able to translate these results to the amount of sweat that could potentially be evaporated and the amount of sweat that would be required to attain heat balance (i.e., cancel out the heat gain from the solar radiation). From our data, it appears that the absence of hair is by far the best condition for maximum sweat evaporation, and hair curvature appears to be inversely correlated with sweat evaporation potential. However, when we consider how much additional evaporative cooling is required in each of these conditions, it emerges that a hairless scalp also necessitates more evaporative cooling due to the considerable amount of solar influx (Figure 5.4). As such, the relative disadvantage of tightly curled hair in maximum sweat potential becomes an advantage when we consider that less evaporative cooling is needed with such hair.

The literature on human scalp hair and sweating has generally regarded scalp hair as a hindrance to evaporative cooling (Cabanac & Brinnet, 1988; Falk, 1990; Shin et al., 2015; Coelho et al., 2010). Our study supports the view that the presence of hair reduces the efficiency of evaporative cooling. However, our study adds context to these findings, by taking into consideration the effect of solar radiation. Many of the studies on human responses to heat focus on exercise-induced hyperthermia at various ambient temperatures rather than hyperthermia from solar heat gain. As a result, many of the studies interpreting the effect of hair on heat loss cannot account for any beneficial effects in the presence of radiation. In our results, we see that, indeed, solar radiation influx is the prime factor that disadvantages a hairless scalp. This consideration is critical in understanding the evolution of scalp hair and of scalp hair form in humans. The genus *Homo* and anatomically modern humans, *H. sapiens*, evolved in equatorial African environments with high and relatively nonseasonal levels of solar radiation. Under these circumstances, passive heating of the head by solar radiation would be mitigated, possibly significantly, by tightly curled scalp hair.

Coelho et. al. (2010) provide a rare example of the evaluation of sweat rate and temperature in an outdoor setting under solar radiation exposure. While this approach results in more variation that cannot be controlled, it is closer to the environmental settings that we would wish to test from an evolutionary perspective. Coelho and colleagues found that sweat rate was indeed reduced in those with scalp hair, but, as all other temperature measurements were not significantly different between the hair and hairless conditions, one might conclude that to achieve equivalent heat loss to a scalp protected by hair, a hairless scalp requires more evaporative cooling. This would be in line with our results. In the environments in which humans evolved, solar radiation was uniformly high and free drinking water was limited to rivers and freshwater lakes. Under these conditions, and in the absence of technology for water storage, evolution would probably have favored adaptations for conservation of water. Scalp hair – particularly tightly curled and absorptive hair – would have maximized cooling, while reducing water loss, and prolonging the duration of strenuous, heat-producing physical activities between drinks of fresh water.

Nevertheless, our manikin study has certain limitations. The results should be interpreted with some caution as humans are subject to certain physiological constraints that do not affect the manikin. For example, despite the low ambient temperature (2 – 10°C) a number of thermocouples registered temperatures above 45°C and even 49°C - temperatures at which skin is damaged after exposure for 100 and 10 minutes respectively (Yarmolenko et al., 2011). Yet other thermocouples in the same experiment registered temperatures below 30°C, likely due to the fact that they were further from the direct path of the radiation. Such temperature discrepancies would not be possible on a living human's scalp (see Figure 5.8). Furthermore, we only have a limited range of human hair variability represented in our sample, due to the cost and availability of different human hair. The next logical steps to our work would therefore include expanding this range of hairs to account for variation beyond simply curvature (i.e. cross-sectional shape, porosity, density etc.). Additionally, we used a single dose of solar radiation. Our findings would be strengthened by ascertaining the relationship between quantity of radiation and hair morphology. Ultimately, the goal would be to validate these findings in trials involving human participants.

For researchers attempting to understand the evolution of early hominins and later human populations, these results relay critical information on the specific contexts where hair, and specifically tightly curled hair, may have been adaptive. Tightly curled hair has long been misleadingly associated with "wool" and our results demonstrate that,

counter to what this connotation might suggest, tightly curled hair does not form an insulating barrier for optimal heat retention. Rather its advantage lies in its ability to mitigate heat gain from solar radiation while maximizing heat loss. There remain many questions regarding the extent and significance of scalp hair in human thermoregulation when considered from a whole body heat loss perspective, but the results reported in this chapter represent the first steps towards a series of scientific investigations that will shed light on the effects of human scalp hair and its morphological variation on thermal load.

While we can (currently) only speculate at the timings of any hypothetical scalp and hair-related adaptations, it is worthwhile articulating some of the scenarios future research should consider. Mainly, the question is the sequence or combinations in which relevant traits emerged. Did scalp hair also disappear when hominins first evolved miniaturized hair follicles? Was the *appearance* of scalp hair a subsequent adaptation? Or was the *retention* of scalp a better descriptor of the evolutionary scenario? Similarly, we might ask whether tightly curled hair evolved simultaneously to the appearance/retention of scalp hair. Or, perhaps, the evolution of tightly curled hair happened hundreds of thousands of years later. Additionally, it would be crucial to investigate whether such hair morphology appeared only once in humans or whether there are examples of convergent evolution.

Based on our current knowledge of the hominin evolutionary history, a crucial period of time we may want to focus on is 2 million years ago, with the dispersal of *Homo erectus* and 80 thousand years ago with the dispersal of *Homo sapiens*. Between these two periods of time, we also suspect numerous dispersals leading to Neanderthal and Denisovan populations in Eurasia. Thus, an interesting point of consideration is whether the evolution of (tightly curled) scalp hair would have occurred prior to any hominin dispersals, or prior only to *Homo sapiens*' dispersal.

Some important factors framing the timing of scalp hair evolution are the evolution of "hairless" skin and large brains. The former is important as it implies thermoregulatory pressures and the latter as it presents an additional thermoregulatory constraint that scalp hair may have offered a solution for.

Our manikin study provides strong evidence for the potential adaptive value of scalp hair (especially if tightly curled) in the context of high solar heat load. However, any questions of timing or relative value for different hominins would require modelling of the various anatomies of these hominins. These would need to take into consideration skeletal robusticity (as this may have offered some benefits against heat gain, especially in the skull), but also brain size (which might point to increased risk of heat stroke). Additionally, the behavior of *Homo erectus*, Neanderthals, and *Homo sapiens* would have

played a critical role in their ability to culturally adapt to various climates. Consider the relative importance of such behavioral adaptations would help us better estimate when and where scalp hair (curled or otherwise) would have most likely provided a significant enough advantage to be called an evolutionary adaptation.

## 5.4 Methods

### 5.4.1 Materials & equipment

#### 5.4.1.1 Wigs

The global market of human hair limits feasible options for this project, so we decided to perform the experiments on three wigs made of untreated human hair reported to be of Chinese origin. A single wig is made of the hair of multiple individuals, however, in the process of production, hairs of uniform appearance are combined, resulting in less variation than would be observed across a natural scalp (Tarlo, 2017). To minimize variation between wigs, we used three naturally black human hair wigs of Chinese origin with 8” hair fibers (Figure 5.9). The principle difference between these wigs is that one is straight, one has been moderately curled, and another tightly curled.

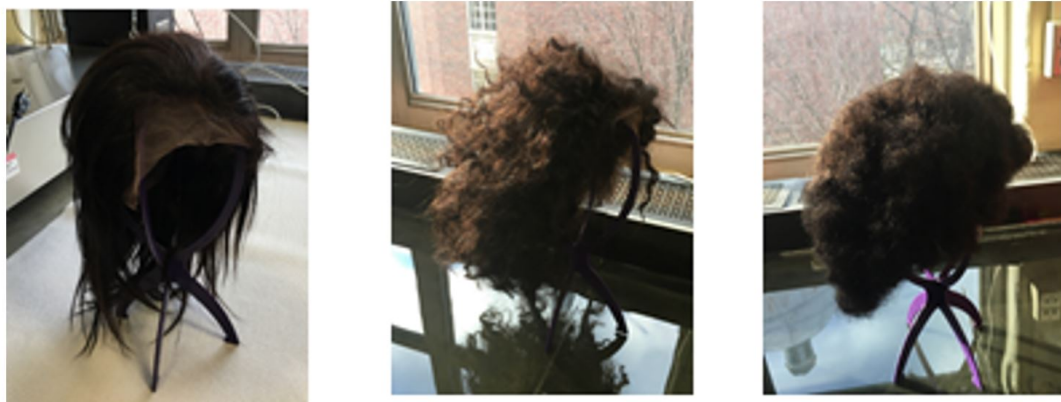


**Figure 5.9. Wigs used in experiments.** The wigs used in the experiment are made of human hair and were purchased from a purveyor who fashions different hair styles out of “Chinese virgin hair”. Reflectance measures were taken to ensure they were similar between the wigs and cross-sectional measures were checked from various points in the wig as an indicator of similarity across the wigs. The wigs are all made with hair fibers that are 8” long - the only difference is the tightness of the curl that was set in the wigs.

### 5.4.1.2 Equipment

The dry heat resistance experiments were carried out from October to November 2018, under the supervision of Dr. George Havenith and Dr. James Smallcombe at Loughborough University (Loughborough, UK).

The experiments used a thermal manikin (model “Newton”, Thermetrics, Seattle, Washington, USA). The “Newton” manikin is made of copper filled carbon-epoxy and features embedded wire elements that heat the surface of the manikin (with a maximum output of 800 W/m<sup>2</sup>). Dry heat loss experiments were conducted in a climate-controlled chamber in a custom-built wind tunnel. We carried out the experiments at wind speeds of ~0.3m/s, 1m/s, and 2.5m/s, roughly comparable to air movement when still, walking, and running, respectively. Humidity in the chamber was set to 40% and air temperature was set at 2°C and 10°C (for the 0.3m/s wind speed experiments).

The complete set of data were captured, but we only analyzed the data from the head zone of the manikin (out of 34 independently controllable zones on the manikin). A diagram and image of the set up are shown in Figures 5.10 and 5.11 respectively.

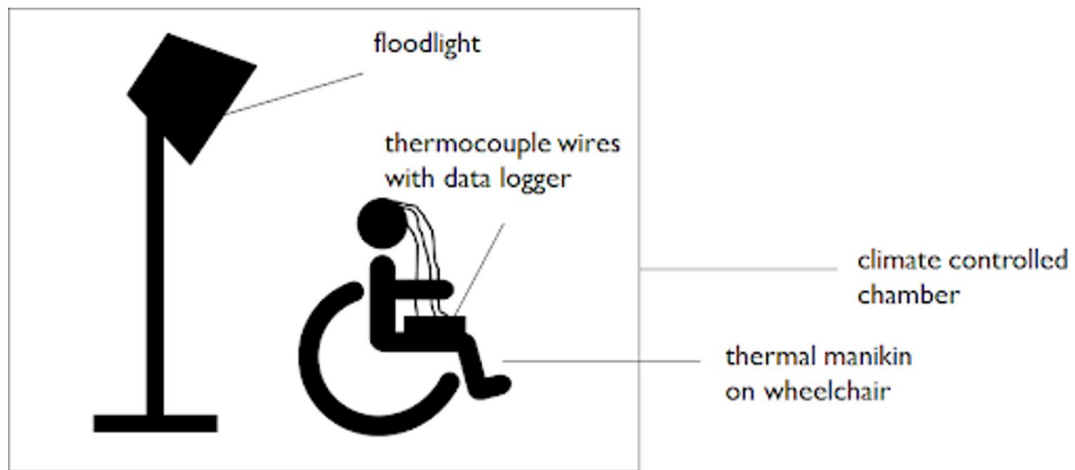


**Figure 5.10. Diagram of experimental setup.** The thermal manikin was sitting with its back towards the source of radiation.



**Figure 5.11. Image of experimental setup.** The set-up inside the climate-controlled chamber at Loughborough University.

Thermal manikins measure energy required to keep the manikin’s surface temperature at a user determined  $T_{skin}$ . As such, standards for manikin work dictate that (climate-chamber) conditions be set to maintain a minimum heat flux of  $20W/m^2$  hence low ambient temperatures in these experiments (International Organization for Standardization, 2015).

Using the raw manikin results, we were able to calculate the dry heat loss of the different wigs (American Society for Testing and Materials, 2004; Wang, Gao, Kuklane, & Holmér, 2011).

The evaporative heat loss experiments were carried out from May to August 2019 by Dr. James Smallcombe at Loughborough University. The experiments used the same equipment, but were set to capture heat exchange, rather than dry heat loss. The wet measurements involved completely saturating the manikin’s cotton “scalp” with water from a spray bottle and taking measurements with the temperature settings  $T_{manikin} = 34^{\circ}C$  and  $T_{ambient} = 34^{\circ}C$  or  $T_{manikin} = T_{ambient}$ . These settings allow for the isolation of evaporative heat loss.

Additionally, we gathered temperature readings from the manikin’s scalp with ther-

thermocouples which were placed along the midline of the thermal manikin (underneath wigs when one was worn). These measured the temperature at that point on the manikin's scalp across experimental conditions (see Figure 5.12).

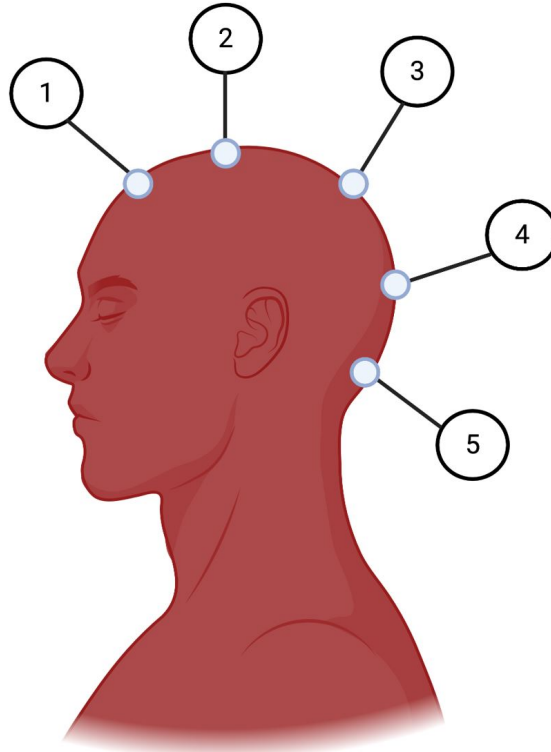


**Figure 5.12. Manikin with thermocouple placement.** Thermocouples were spaced evenly along the midline to capture temperature from multiple points on the head during the experiments.

#### 5.4.1.3 Analyses

For the analyses, we applied a correction to bring all the measurements to  $T_{ambient} = 30^{\circ}\text{C}$  with solar radiation. This process involved a number of steps.

##### **Step 1: Processing manikin data.**

First, the raw manikin data was processed by Dr. George Havenith to convert the manikin readings to heat loss in  $\text{W}/\text{m}^2$  (watts per meter squared) and thermal resistance in  $\text{m}^2 \cdot \text{K}/\text{W}$  (square meter kelvins per watt) for each region of the manikin and subsequently, the readings for each experiment were averaged for the head region.

##### **Step 2: Calculating heat loss for $4^{\circ}\text{C}$ and $30^{\circ}\text{C}$ .**

As measurements were taken across two different ambient temperatures, we first calculated the heat loss  $H$  for  $T_{ambient} = 4^{\circ}\text{C}$  and  $T_{ambient} = 30^{\circ}\text{C}$  using the mean thermal resistance for each condition (without radiation).

Heat loss for  $T_{ambient} = 4^{\circ}\text{C}$  was calculated as per equation 5.1 and heat loss for  $T_{ambient} = 30^{\circ}\text{C}$  was calculated as per equation 5.2:

$$H_{(4^{\circ}\text{C})} = 28/\text{m}^2 \cdot \text{K}/\text{W} \quad (5.1)$$

$$H_{(30^{\circ}\text{C})} = 5/\text{m}^2 \cdot \text{K}/\text{W} \quad (5.2)$$

### **Step 3: Calculating heat loss with solar radiation for $4^{\circ}\text{C}$ and $30^{\circ}\text{C}$ .**

To calculate the heat loss for each ambient temperature with solar radiation we used the net heat loss (solar influx), calculated as:

$$H_{solar\ influx} = H_{radiation\ on} - H_{radiation\ off} \quad (5.3)$$

and subtracted it from the heat loss for each temperature using equations 5.4 and 5.5 respectively.

$$H_{solar(4^{\circ}\text{C})} = H_{(4^{\circ}\text{C})} - H_{solar\ influx} \quad (5.4)$$

$$H_{solar(30^{\circ}\text{C})} = H_{(30^{\circ}\text{C})} - H_{solar\ influx} \quad (5.5)$$

These calculations take as a baseline the heat loss at their respective temperatures (without radiation) and subtract the heat loss attributed to the additional factor of heat gain from solar radiation. This solar influx is independent from temperature and thus does not itself require an adjustment to the ambient temperature but can be added post hoc. Therefore, the final calculations reflect the estimated heat loss at two different ambient temperatures with the added effect of heat gain from solar radiation.

### **Step 4: Calculating evaporative potential and evaporative requirement.**

Finally, we calculated the evaporative potential and requirements for different conditions by estimating this evaporation as a reflection of sweat in  $g/\text{m}^2/h$ . Both evaporative potential and requirements are calculated for  $T_{ambient(30^{\circ}\text{C})}$ .

**Calculating sweat requirements at 30°C.** Sweat requirements are calculated as the additional evaporative cooling required to cancel out heat gain, see equation 5.6

$$S_{zero\ gain} = \frac{H_{solar(30^{\circ}C)}}{2430 \cdot 3600} \quad (5.6)$$

**Calculating total evaporative heat loss at 30°C.** To calculate the maximum evaporative cooling potential  $S_{max}$ , first we added the heat loss attributed to evaporative cooling to the dry heat loss calculated, as per equation 5.7

$$H_{total(30^{\circ}C)} = H_{evaporative\ solar} + H_{dry\ solar(30^{\circ}C)} \quad (5.7)$$

**Calculating sweat potential at at 30°C.** Finally, we calculated evaporative maximum potential using equation 5.8.

$$S_{max} = \frac{H_{total(30^{\circ}C)-dry\ solar(30^{\circ}C)}}{2430 \cdot 3600} \quad (5.8)$$

Here  $H_{total(30^{\circ}C)-dry\ solar(30^{\circ}C)}$  represents the maximum evaporative potential under solar heat gain at 30°C and  $2430 \cdot 3600$  is the conversion to sweat in in  $g/m^2/h$ .

# Chapter 6 |

## Conclusion:

### Lessons learned and

### Future directions

#### 6.1 Deconstructing and reconstructing knowledge across disciplinary boundaries

A key theme that emerges from my work is the importance of transcending disciplinary boundaries in search of methodologies and unfamiliar sources of knowledge that may inform questions in biological anthropology. The collaborations that have made this doctoral research possible have highlighted the distinction between what is multidisciplinary, interdisciplinary and transdisciplinary. There are many different perspectives on what these terms encompass and how they are similar or different from each other (Brown & Dueñas, 2020).

For the purposes of this discussion, I want to delineate these three terms to emphasize various challenges and considerations in research that seeks to transcend disciplinary boundaries. If we define a discipline as a paradigm of knowledge production with its own community, ontological, epistemological and methodological practices, multidisciplinary is the parallel existence of disciplines that each engage in knowledge production regarding a common topic of interest creating a mosaic of distinct (and potentially complementary) perspectives. An interdisciplinary approach would, in my definition, be distinguished by the active engagement with differences between disciplines to come to a common resolution of a common question.

Finally, for something to be transdisciplinary or cross-disciplinary, it must be valid

across disciplines. In my use of these terms, transdisciplinarity is not something one can actively engage in, but rather, it can be a goal or end product of multi- and interdisciplinary work. Depending on the disciplines involved, different knowledge will fall into a common transdisciplinary category. The value of engaging in interdisciplinary work would be to identify what participating disciplines do not have in common and interrogate why these differences exist so we can synthesize new knowledge that can be accepted widely.

Thus, the distinction between multidisciplinary and interdisciplinarity lies in the quality and extent of collaboration. Deep and meaningful collaboration requires mutual respect, time, and self-reflexivity. Specifically, the ability to question one's own assumptions. In order to synthesize new knowledge across disciplinary boundaries, the first step is to deconstruct existing knowledge to its most basic units and identify assumptions that we can then interrogate.

Numerous factors influence the current paradigms that various disciplines find themselves in, including funding structures and historical particularities leading to branching and fusing of various disciplines. Collaborations across disciplinary boundaries can illuminate such unconscious influences and other assumptions that are not readily apparent to those within a specific paradigm. Even within disciplines, different perspectives serve as tools to expose lacunae in theory and practice. Once an oversight has been identified, breaking down the knowledge and identifying its origin and history serves simultaneously to help our collaborators understand our perspective and to expose issues that may have been inherited without adequate examination. Once the basic building blocks of our knowledge concerning a particular topic have been thoroughly interrogated across disciplines, it is possible to synthesize new transdisciplinary knowledge.

During my doctoral dissertation, I have investigated hair as a topic of common interest across anthropology, genetics, and environmental ergonomics. By breaking down the assumptions about the morphology of hair and testing assumptions about its thermal properties, I have been able to generate knowledge of transdisciplinary value, as well as new insights into this aspect of human evolution. Below, I reflect on the lessons learned and future directions for each of the projects.

## **6.2 Thermoregulation and the function of hair**

The work I present in Chapter 5 centers around the crucial question of solar heat gain and human thermoregulation. Thermoregulatory adaptations have been a primary focus

for anthropologists working to piece together the story of early human evolution. The loss of hair has received much attention in this context, but the role of scalp hair is often considered insignificant due to the small surface area that it covers. This view of human scalp hair as inconsequential expands beyond anthropology, as is illustrated by the dearth of literature on human hair and thermoregulation in other disciplines.

With my collaborators at Loughborough University, I carried out a number of experiments that attempted to remedy this gap by using well-established methodology from the field of environmental ergonomics in a novel context, namely, to test the thermal properties of human scalp hair. These trials demonstrated with surprising clarity that there was a considerable, measurable effect of scalp hair on the amount of heat gained by thermal manikin head. Even more surprising was the distinct directional effect of increasingly curled hair. The key takeaway from our experiments is that tightly curled hair, as a material, has a distinct set of thermal properties that, in fact, stand quite in contrast to the wool with which it is often erroneously compared. Moreover, our results suggest that any potential adaptive value to hair would be specific to a context where humidity was minimal and the heat source of concern was specifically radiative heat, rather than ambient heat or metabolic heat.

The experiments contributing to my doctoral research were a first venture into this unexplored territory. The results presented here are preliminary insights into the larger question of human scalp hair's thermoregulatory potential, but this work will prove instrumental in setting the foundation for future work by myself and others who wish to explore this question. Some immediate next steps include expanding the range of hair used in the experiments. Human hair wigs are a costly material and depending on the construction of the wig and the provenance of the hair, a single wig can cost upwards of 1000 USD. Our current experiments rely on hair that is artificially curled to different degrees, presumably, holding all (or much) other variation constant. Nevertheless, some of this other variation, including cross-sectional shape and porosity may respond significantly differently to the experimental settings we have used. An alternative avenue of research to be explored is the simulation of a wide range of hair fiber morphologies and use models from material science research to predict what the thermal properties would be.

Mathematical modelling has played an increasing role across disciplines and has been used to test specific hypotheses on human thermoregulation in evolutionary anthropology as well as other fields. These models will necessarily be part of a sophisticated approach to testing adaptive hypotheses. Discussing the adaptive potential of any trait in isolation is inherently limiting as selection acts on the entirety of an individual's phenotype. Results

informing specific physical effects of traits, like those presented in my work, are most effectively used in conjunction with models that take into consideration other aspects influencing thermoregulation, such as expected metabolic heat and paleoclimatic reconstructions (Hora et al., 2020; Ruxton & Wilkinson, 2011; Wheeler, 1985). An important focus in future work on the adaptive potential of human scalp hair will be the effect of solar heat gain and the brain, specifically. The large hominin brain is exceedingly sensitive to overheating and further exploring the differential response of body parts to heat will allow us to better understand what, if any, benefit there is to mitigating heat gain to the head compared to the rest of the body (Piil et al., 2020). Ultimately, the amalgamation of knowledge from all these various realms will serve to answer the principal question of adaptation in human evolution: did this trait affect our evolutionary fitness?

### **6.3 Genomic insights into human scalp hair morphology**

Poorly defined phenotypes critically hinder our ability to make sense of the biological factors that shape them on any fundamental level. The relationship between genome and phenome is mediated by many levels, each associated with their own omics (i.e., epigenomics, transcriptomics, proteomics, metabolomics). Many studies attempt to associate phenotype to genotype directly, but increasingly, researchers have sought to understand the interrelationships between all combinations of these different biological levels. However, the most “superficial” -omic level, the phenome, remains complex and abstract. Unlike these other -omic levels, the phenome does not describe something specific that can be studied with a finite set of methodologies. There is no universally accepted phenomic unit, nor can we realistically expect there to ever be.

There is a general awareness that phenotypes, however we define them, are abstractions of perceived properties emerging from underlying biological processes. There have been attempts to tackle this shortcoming, especially in medical and behavioral genetics, where deep phenotyping and endophenotyping have been proposed (Yehia & Eng, 2019; Insel & Cuthbert, 2009; Hasler, Drevets, Manji, & Charney, 2004; Walters & Owen, 2007; Weng, Shah, & Hripacsak, 2020; Tracy, 2008). Deep phenotyping could more accurately be described as extensive phenotyping, where studies give up large sample sizes in favor of a larger range of phenotypic information for each individual. The benefit of such an approach is that it allows for the investigation of biological factors that might co-vary due to intrinsic biological relationships between the phenotypes or due to some stratification

of another kind. On the other hand, endophenotypes have been used in behavioral and psychiatric genetics as an attempt to articulate more precise phenomic units that may be obfuscated by broader behavioral descriptors and psychiatric diagnoses. There is clearly an understanding that many traits are approximations of specific aspects of biological systems. But the extent to which those approximations deviate from reality, or how they might be affected by bias, is not always sufficiently appreciated.

In Chapter 4, I present work that illustrates how existing approaches to the genetic architecture of human scalp hair exemplify the issues of poorly defined phenotypes. The history of human scalp hair as a racialized trait plays a large part in the pervasiveness of classification systems that aggregate multiple aspects of hair into one-dimensional typological categories. For example, the persistent contrasting of “European”, “African” and “Asian” hair has led to the deep-rooted belief that the various characteristics of these stereotypes necessarily co-occur. Specifically, descriptions of their cross-sectional geometries have been used to explain the levels of curvature associated with those groups (i.e., that “Asian hair” is straight with a circular cross-section, “African hair” is tightly curled with a flat cross-section, and “European hair” is wavy with an intermediate cross-section).

The results I report in Chapter 4 show the extent to which phenotyping methods matter, especially in an admixed African-European population. The use of typical qualitative descriptors such as “straight”, “wavy”, “curly” and “frizzy” or “kinky” collapse a huge range of variation on the tightly curled end of the spectrum. This overemphasis of variation in the straighter range is similar to the disproportionate emphasis on variability in lighter skin according to classification systems like the Fitzpatrick scale. However, with our findings, I was able to demonstrate that homogenizing the variation that exists in “frizzy” or “kinky” hair is not justified by the genetic architecture of the trait. Moreover, the lack of correlation between curvature and cross-sectional shape (once ancestry was corrected for) directly challenged the oft-cited intrinsic relationship between the two factors.

Another interesting finding is that we replicated different previously reported loci with the different phenotypes. It is only with our new method of measuring curvature that we replicated a particular variant on Chromosome 20 (rs310644) that showed a promising allele distribution. This SNP showed an allele distribution where the ancestral allele (T) was most common across Eurasia, while the derived allele (C) was the predominant variant across African populations (and fixed in a number of them), as well as two Melanesian populations. This pattern is interesting for a number of reasons. First, tightly

curled hair is found at very high frequencies in these populations, so if hair curl in African populations and Melanesian populations has the same genetic architecture, we would expect to see this pattern. Second, the fact that it is the derived allele that is found in both of these populations may be important from an evolutionary perspective, because it suggests that tightly curled hair (if affected by this allele) may either not have present in the common ancestor of these contemporary human populations, or that there was some selective pressure against tightly curled hair in these populations. The ancestral vs. derived state of an allele is determined by comparing the variant to its homolog in *Pan troglodytes* assuming that whichever variant is present in *P. troglodytes* must be the allele present in the last common ancestor (LCA) between *Homo* and *Pan*. As we know that chimpanzees have straight hair, it is perhaps not unexpected that humans with tightly curled hair would have different alleles at the relevant sites. From a brief search on the UCSC genome browser, it appears that the T allele is fixed across the great apes and also in Denisovans (though it is not typed in available Neanderthal sequences). This suggests that the allele may be highly derived and specialized to African and Melanesian populations.

Together with the manikin work, there is good reason to pursue future work that centers on thermoregulatory adaptations. Specifically, an understanding of thermoregulatory adaptation as a suite of adaptive traits. As mentioned above, evolutionary genomics allows us to parse out in more detail the estimated times various traits have arisen (by tracing the appearance of causal variants). In the case of scalp hair, it will be particularly important to understand any correlations with various hominin dispersals. Beginning from the most recent population branches, we should investigate whether high-curvature variants are shared in distantly related populations (e.g. African and Melanesian populations) due to convergent evolution. Scenarios may be more complex than complete convergence or entirely attributable to a common ancestor, as scalp hair morphology is a complex trait. Depending on this scenario and on evidence of selection in the opposite direction in other populations (i.e. straighter hair in most Eurasian populations), we may be able to piece together an understanding of the extent to which hair has been shaped by selective pressures.

An important dimension between *Pan-Homo* genomic comparisons and genomic variation across *Homo sapiens*, is information that can be gleaned from archaic sequences. From the fossil record, we know that many archaic hominins dispersing into Eurasia were similar to later *Homo* (including *Homo sapiens* in skeletal anatomy. However, their soft-tissue morphology is unknown. With an understanding of loci that affect the epidermis,

but especially scalp hair morphology, we may be able to get a better understanding of when scalp hair (tightly curled or otherwise) evolved. If variants associated with tightly curled hair are unique to *Homo sapiens*, this may indicate an additional adaptive advantage in the species. Currently, it is hypothesized that the evolution of miniaturized hair follicles across the body coincided with the evolution of increased sweat gland density and darker pigmentation (Lu, Polak, Keyes, & Fuchs, 2016). These traits point to thermoregulatory adaptation to high solar heat load. However, it is unclear whether the retention or appearance of scalp hair occurred simultaneously. A better understanding of loci affecting the density of scalp hair especially, would allow us to pinpoint whether the minimization of solar heat gain demonstrated in our manikin study was part of this adaptive suite or the result of separate later selective events.

There are many future directions for this research, but as an immediate next step would be to reassess our sample using local ancestry estimations, rather than simple high-allele frequency differences. Additionally, I have access to South African and Papuan hair samples with associated genotypes that could prove useful in an attempt to replicate the associations from this preliminary effort. An alternative source of information may come from selection-based approaches. One of the key questions for hair morphology (specifically tightly curled hair) is whether it would have been present in the LCA of all humans. To elucidate the evolutionary history of hair morphology in humans, future work could look for differences on locus-specific branch length (LSBL) across keratin-associated genes and other candidate genes for hair morphology to compare LSBL across these regions compared to average LSBL across the genome.

## **6.4 Measuring hair to understand its biology**

Our findings on the genetic architecture of hair morphology would not have been possible without the development of novel high-throughput phenotyping methods. This project took by far the longest of all the projects presented in this dissertation, but it was a necessary investment of time and effort. Before this work, existing methods for quantifying hair fiber curvature and cross-sectional geometry were time and labor-intensive. The main issues were: 1) the absence of sample preparation methods for the measurement of hair curvature, 2) the unsuitability of embedding methods for tightly curled hair, and 3) the absence of software to automate the image analysis of samples. The sample preparation and image analysis issue caused a critical dilemma, because the validity and success of one could not be evaluated without the other. By investing in developing both

these branches of methodology, future work can now focus on improving a single aspect of these methods at a time.

The need for the methods to be high-throughput is in large part to provide alternatives to existing classification approaches used in hair-related research across disciplines. Because existing methods were so time-intensive and of uncertain repeatability, it was acceptable for many scientists to use what was (seemingly) a pragmatic simplification of the phenotype by describing its morphology according to qualitative terms or ancestry (or race) categories. The work presented in Chapter 3 illustrates why such terms are misleading and provides an alternative by showing multiple quantitative variables that have complex interrelationships. These methods are especially important to research that seeks to understand the biological processes underlying such variation as straight to curled hair. Without the ability to objectively quantify this variation, such research has relied on contrasting West African(-descendant) populations with (primarily) North European(-descendant) and East Asian(-descendant) concluding that the cross-sectional and follicular features of West African hair are universal determinants of curvature (Thibaut et al., 2005). By quantifying cross-sectional shape and curvature in an admixed African-European population, we demonstrated that such conclusions do not take into consideration the way in which certain traits are stratified by population (or ancestry) without necessarily having an intrinsic correlation.

Future directions for this research will involve the development of a Graphical User Interface to further expand the usability of our existing *fibermorph* software. Furthermore, it would be informative to carry out experiments across a number of aspects of the sample preparation protocol. For example, we could test the curvature of hair fibers cut down to different lengths. From our current protocol, we have noticed that hairs that have very eccentric (or flat) cross-sections may fall on their sides when cut below a particular length. This length itself may be an informative marker for hair morphology as a whole. Another line of inquiry is generating data on the variability of cross-sectional size and shape along a hair fiber. Because the methods we have developed for embedding and sectioning hair do not involve resin, we can easily slice off sections along a sample to image it and determine whether it is variable along its longitudinal axis. Finally, an important task would be to reach out to other researchers interested in quantifying hair morphology to learn how applicable our new methods are to challenges that they face and what could be done to foster a level of transdisciplinary uniformity for research on hair morphology.

## 6.5 Future directions in the study of hair and other racialized traits

This doctoral research strongly illustrates the extent to which racialized ideas have a pervasive effect on research in human biology, even when explicit measures are taken to avoid this. Scientific knowledge is generated on the basis of inherited knowledge and my research shows that an important path forward involves looking back and scrutinizing the assumptions that have remained unchallenged. Multiple findings in this dissertation exemplify our tendency to view traits as packages that travel with great fidelity through time and space. The ability to scientifically deconstruct phenotypes, like hair, allows us to explore and simulate possibilities that lie beyond our imagination.

Hair, along with other racialized traits, deserves further investigation that explicitly examines what quantifiable and perceivable aspects of phenotype people use (even unconsciously) as racial markers. In an attempt to distance itself from race, biological anthropology has relied heavily on demonstrating the (genetic) similarity of all humans, and the presence of certain kinds of phenotypic variation across purported racial groups. However, in focusing on what race *is not*, it has insufficiently explored what race *is*. As a result, the pivotal role that biological anthropologists played in constructing current concepts of race was not matched by an equal role in deconstructing those race concepts. In many cases, where explicitly racial terminology was used before, we now have the replacement of “race” with “population”, but without any change in the underlying conception of human biological variation. Or, equally problematic, a “colorblind” approach which does not mention aspects of human variation that connote race, but end up erasing non-European variation.

Understanding the grounds for racialization in the context of specific phenotypic variation will be key to determining the grounds for the durability of racial templates. As my doctoral work has shown, the biology of hair and our perception of it, necessarily call for a conscientious transdisciplinary approach to shed light on this complex and unique human phenotype.

# Appendix A |

## Chapter 3 Supplementary:

### Background information on hair morphology quantification

#### A.1 Previous work on cross-sectional geometry

The cross-sectional geometry of human scalp hair has been described in studies dating back to the 19th century (Pruner-Bey, 1864), but the methods for preparing samples for cross-sectional imaging are neither universally applied, nor universally applicable. To observe the cross-section of a hair, it must be cut perpendicularly to its longitudinal axis and magnified with a microscope. Typically, hairs are embedded in an epoxy resin, though examples of other embedding-media can be found (mainly paraffin, which is commonly used in histology). Whereas the width of a scalp hair fiber is on the order of micrometers ( 20um - 200um), its length can be orders of magnitude greater (up to multiple meters, but generally upwards of a few centimeters). Embedding thus facilitates the manipulation (sectioning) of this material. However, many individuals have scalp hair that is not straight. To ensure a perpendicular cut, curled hair fibers have to be stretched while the resin hardens; a process that takes upwards of 24 hours. Alternatively, great care has to be taken to find the correct angle for a perpendicular cut after embedding. Regardless, cutting epoxy resin is an additional challenge, as it requires expensive, specialized equipment (such as a microtome). There are no widely used protocols that make it possible for the full morphological range of human scalp hairs to be embedded successfully.

## A.2 Methods for embedding & sectioning hairs are laborious

For the cross-sectional study of hair, the main hindrance is the need to embed the hair in resin. Especially for tightly coiled hairs, there is a major obstacle in having to find a way to keep the hair taut for the 24 hours the resin requires to harden. Attempts at embedding are not consistently successful (see Figure A.1). The main alternative has been to place the hair between glass slides and record width along the length of the fiber. (Hrdy, 1973; Trotter, 1930) But this is an inferior alternative because it does not allow for the visualization of the cross-section, it only gives us the longitudinal diameter of the hair.



**Figure A.1. Example of hairs moving during resin drying process.** This is an image taken of a hair embedded using an older protocol that involved hooking the hairs along small strips of transparencies. Even with this precaution, hairs could move while the resin dried.

Some examples of existing protocols and methods for cross-sectional analysis include: Trotter (1930) uses the longitudinal diameter as a proxy for the cross-sectional shape and size:

“From each sample measurements were made on ten hairs chosen at random—thus a study of 3400 hairs from 340 individuals was made. Before measuring, the hairs were

dipped into a solution of equal parts of ether and 95 per cent alcohol and then thoroughly dried; this process removed all dust and extraneous matter. Measurements of the greatest and least diameters of the hair shafts were obtained by means of an ocular micrometer in the microscope (magnification X 120) used in conjunction with a hair rotator, similar in construction to the one described by Danforth(2). From these measurements were computed the hair index and the area of the cross-section of the shaft.”

Hrdy (1973) similarly described multiple measures of the cross-sectional diameter, which was used as a proxy for the cross-sectional geometry:

“(1) Average diameter. The average diameter was measured by placing the hair between glass slides and measuring with a micrometer-equipped microscope. The length of the hair was rapidly scanned and measured at many different places along the shaft, and the average value (in  $\mu$  m) recorded.”

Reis et al. (2020) use a method that involves bundling the hair before embedding and sectioning and show a step-by-step figure in their article:

“To overcome the flaws of other hair cross-section methods previously described,1, 3, 4 we used an epoxy embedding medium to maintain the hair strands intact and close together through the whole processing.

First, we prepared the embedding media—Agar 100 epoxy resin (Agar Scientific, Essex, UK)-using the fabricant recommended formulation to obtain hard blocks. We used a small drop to slightly embed each bundle of hair, keeping the hairs united and parallelly oriented. Each bundle was then left to rest for half an hour. This step is not mandatory but makes it easier to perform the next step. After this, we cut a small sample (about 0.5 cm in length) with the help of a scalpel and placed it in the molds, covering it with the rest of the embedding media. Polymerization at 60°C was then carried out for 24hours (Figure A.2). To finish, ultrathin sections (1250 nm) were cut using an ultramicrotome and stained with toluidine blue.”

Another example of more elaborate preparation of samples for study of the ultra-structure is seen in Koch et al. (2019):

“Each hair sample, consisting of approximately 20 terminal hairs, was tied together in a bundle to align the hairs longitudinally for embedding and cross-sectioning. The dehydration and fixation process typically employed for samples prepared for electron microscopy was not conducted prior to embedding as this process was found to dehydrate and potentially alter the structure of the cuticle during preliminary analyses. The hairs were air dried, embedded in Spurr’s resin, and placed in an oven at 60 degrees with desiccant to polymerize. Ultrathin sections ( 70 nm thick) were cut perpendicular to the

length of the hair shaft using a Leica ultramicrotome (Germany) and a Diatome Ultra diamond knife with a 35 degree blade. Sections were exposed to chloroform vapor to reduce section folding and potential deformation from impact with the cutting blade. Sections were collected onto Formvar supported slot grids, stained with a double staining procedure using lead citrate and uranyl acetate, and observed with a FEI (USA) Tecnai 1200 transmission electron microscope (TEM) with an accelerating voltage of 80 kV. Images of hair cross-sections were collected at  $4200\times$  magnification with a 20 percent overlap = in area. Montaging of the images was attempted; however, not all images aligned correctly.”

The methods we propose fall in between the efficient, but superficial measuring of longitudinal diameter and the meticulous but intensive, hand-washing of hairs and microtoming described in Reis et al. (2020) and Koch et al. (2019). Moreover, we provide more extensive video and still image guidance than we have found in the cross-sectional literature. This is to ensure that the protocol can be applied by any, regardless of previous experience or skill.

### **A.3 Previous work on curvature**

In contrast to cross-sections, the quantitative study of hairs longitudinal geometry has lagged behind. Longitudinal hair morphology ranges from a straight fiber, to a tightly coiled helix. A helix is a curve in 3-dimensional space that can be mathematically described by three parameters: arc length, curvature and torsion. The first attempt to operationalize the quantification of human scalp hair curvature appears relatively recently in the literature Hrdy’s (1973) curvature quantification method requires a hair to be pressed between two glass slides to collapse three-dimensional variation into two dimensions. Once between the slides, a transparent template with circles of known radius are placed over the sample and matched to the curves of the hair. Despite the introduction of these methods, it has only been rarely applied to research on human scalp hair. (Bailey & Schliebe, 1986; Lasisi et al., 2016; Loussouarn et al., 2007)

## A.4 Methods to quantify curvature have issues with replicability

Measuring curvature objective requires that the helical structure of non-straight hair fibers be reduced to two-dimensional curves. Previous curvature methods rely, without exception, on the subjective evaluation of the observer to one degree or another. (Mkentane et al., 2017; Loussouarn et al., 2007; Lasisi et al., 2016) Comparing hairs of different lengths is also a significant challenge. Depending on the method, a potential confounding factor is the greater number of points of measurement for hairs with high curvature as compared with low curvature (see Fig. A.2), involving potentially greater inter-observer variability in the number of and value of circles fitted to curves along a hair. Most importantly, of these existing methods, neither those for quantifying cross-section nor curvature could feasibly scale to the hundreds of samples many disciplines would need to phenotype.

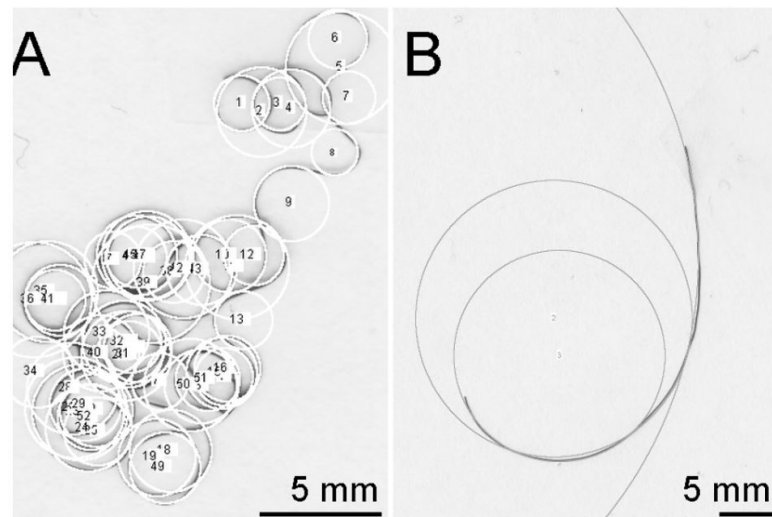


**Figure A.2. Example of discrepancy in number of measurements taken in high vs. low curvature hair with previous methods.** This image is from a previous publication (Lasisi et al., 2016) where circles were fitted to a hair’s curvature using ImageJ. This image shows the discrepancy in the number of data points gathered for tightly curled vs. straighter hair.

Hrды (Hrды, 1973) is the earliest published article describing a method of directly quantifying hair fiber curvature:

“(5) Average curvature. Each hair was placed between two glass slides,

allowing measurement of the curvature of hairs that vary in three dimensions. The radius of curvature of each curve of the hair was determined by placing a transparent template with circles of known radius over the sample and matching an arc of the appropriate circle with the curve. Average curvature itself is the inverse of the average radius of curvature; a high average curvature is represented by a high number.”

Bailey and Schliebe (1986) is a test of precision for Hrdy’s original 1973 method:

“Since that time, this measurement has been found to be useful in the forensic comparison of curly, human head hairs with certain modifications made to the original method. The method currently used by this laboratory consists of the following steps:

1. Placing the hair in boiling water to remove grooming agents and relax the hair;
2. Removing excess water and allowing the hair to dry at room temperature;
3. Placing the hair between two glass plates to reduce the curvature to two dimensions; and
4. Measuring the resultant curves with a circle template of known radius.

The average curvature is calculated as the inverse of the average radius in millimeters times 100. This measurement then ranges from 0 to 100 mm with the curlier hairs having the higher value. Straight hairs have an average radius of 100 mm or more and an average curvature of 0 mm. To help establish the precision of this method, a single, curly, Caucasian head hair was measured 30 times by one examiner, and independently, 30 times by a second examiner. The data comparing the results of these measurements are shown in Table 1.

The major sources of variation in the measurement are as follows:

1. Amount of drying the hair received after boiling;
2. Determination of which dimension was reduced when placed between the glass plates;
3. Judgment of the number of curves to be measured; and
4. Judgment of which circle radius gives the best fit.”

Loussouarn et al. (2007) describe a method that is derived from Hrdy's curvature method, but differing mainly in its decision to take only one measurement (the smallest) as representative of a sample's curvature. Additionally, they describe a number of steps that measure various aspects of curl, but are likely redundant and covarying with curvature. Moreover the final partition into the eight curl types appears to be somewhat arbitrary:

“The method requires very simple materials: two glass plates, tape, a simplified CD meter, a curl meter, and a ruler. The CD meter includes the four cut-off values derived from the segmentation tree for the classification of types I–IV. The curl meter is made of a 0.98-cm-diameter circle, allows the segmentation of types V and VI vs. VII and VIII. The ruler helps to constrain the hair to 80% of its length in order to separate type V from VI and VII from VIII. More precisely, this simplified method can be described in three steps. Initially, the hair is carefully laid on a glass plate, without applying any mechanical stress, in order to allow it to maintain its natural shape. A second glass plate is gently placed onto the hair, carefully avoiding any side shifting or sliding. The first step is the evaluation of the curvature using the CD meter. The area of the CD meter where the smallest curvature is located indicates whether the hair is type I, II, III, or IV (Fig. 3). If the smallest curvature is included in the filled circle, the hair is type V, VI, VII, or VIII. Two other steps are needed to classify the hair. The second step is the test of curliness using the curl meter. The curl meter is placed on the glass plate in order to determine whether or not the hair fits entirely inside the circle (Fig. 4). The third and last step consists of counting the number of wave crests. The cover plate is removed. One end of the hair is taped in front of 0 cm on the ruler and the other end is taped at 4 cm. The two ends of the hair are taped on the bottom glass plate. Each self-stick strip covers 0.5 cm of hair fiber, and the distance between the two tapes is fixed to 4 cm thanks to the ruler. After replacing the cover plate, the hair takes a sigmoid form from which the highest number of wave crests is counted (Fig. 5). Based on the curl meter result, and on the number of wave crests, the hair type (V, VI, VII, or VIII) can be defined with the following rules. If the entire hair is included in the curl meter and the number of crests is from one to five, the hair type is VII. If the entire hair is included in the curl meter and the number of crests is six or more, the hair type is VIII. If the entire

hair is not included in the curl meter and the number of crests is from one to three, the hair type is V. If the entire hair is not included in the curl meter and the number of crests is four or more, the hair type is VI.”

Lastly, Lasisi et al. (2016) propose something that can best be described as a direct digital application of Hrdy’s original curvature method:

“Single strands of hair were placed on a sheet of blank white paper, the application of mechanical stress was avoided to ensure unaltered curvature, and the paper was covered with a transparent sheet of acetate to facilitate a two-dimensional measurement. Three hairs were analyzed per person in order to provide a representative average for each individual. Samples were scanned using a flatbed scanner (CanoScan LiDE 600F) at a resolution of 1200 DPI. Curvature measurements were collected in ImageJ version 1.48. Each curve in a hair fiber was traced digitally, creating a separate data point from each curve. Curvature varied greatly among individuals, thus the number of measurements per hair varied from as few as two to as many as 60 (Fig. A.1). The mean, maximum, and minimum curve diameters from a single hair are then computed. Curvature is the inverse of the radius (curve diameter  $\div$  2), so the previously computed values yield a mean, maximum, and minimum curvature. The variable average curvature is the mean curvature averaged from the three hairs analyzed for a single individual. The variable irregularity is similarly calculated as an individual’s averaged maximum to minimum curvature ratio. Both average curvature and irregularity variables are derived from Hrdy (1973). Precise instructions for the method of curvature analysis described in this study have been made available (Supporting Information Document 2) and a depiction of the application of this digital method can be seen in Figure A.1.”

While Lasisi et al. 2016 presented an extensively documented methodology, this protocol was very laborious and did not include a washing step that was scalable.

# Appendix B |

## Chapter 3 Supplementary:

### Image analysis validation

#### B.1 Curvature

Here, we will evaluate the accuracy of *fibermorph* in estimating the length and curvature of hair using simulated data. See simulation script on GitHub at: [https://github.com/tinalasisi/2020\\_HairPheno\\_manuscript/blob/main/code/simhair.R](https://github.com/tinalasisi/2020_HairPheno_manuscript/blob/main/code/simhair.R).

The simulated data can be found at: [https://github.com/tinalasisi/2020\\_HairPheno\\_manuscript/blob/main/data/concat\\_simcurvature\\_Nov152020.csv](https://github.com/tinalasisi/2020_HairPheno_manuscript/blob/main/data/concat_simcurvature_Nov152020.csv).

We simulated arcs of various curvatures at a length of 1.57mm. There were 25 arcs per image.

##### B.1.1 Simulated vs. estimated curvature & length

To calculate the accuracy of our measurements, we compared the known parameters with the parameters estimated from our *fibermorph* package.

In Fig. B.1 **a** we see that there is a near perfect correlation between the simulated and estimated curvatures. Figure **b** shows the distribution of estimated hair lengths around the simulated length (red line).

We plot simulated curvature against estimated length to show the distribution of estimated length as a function of curvature.

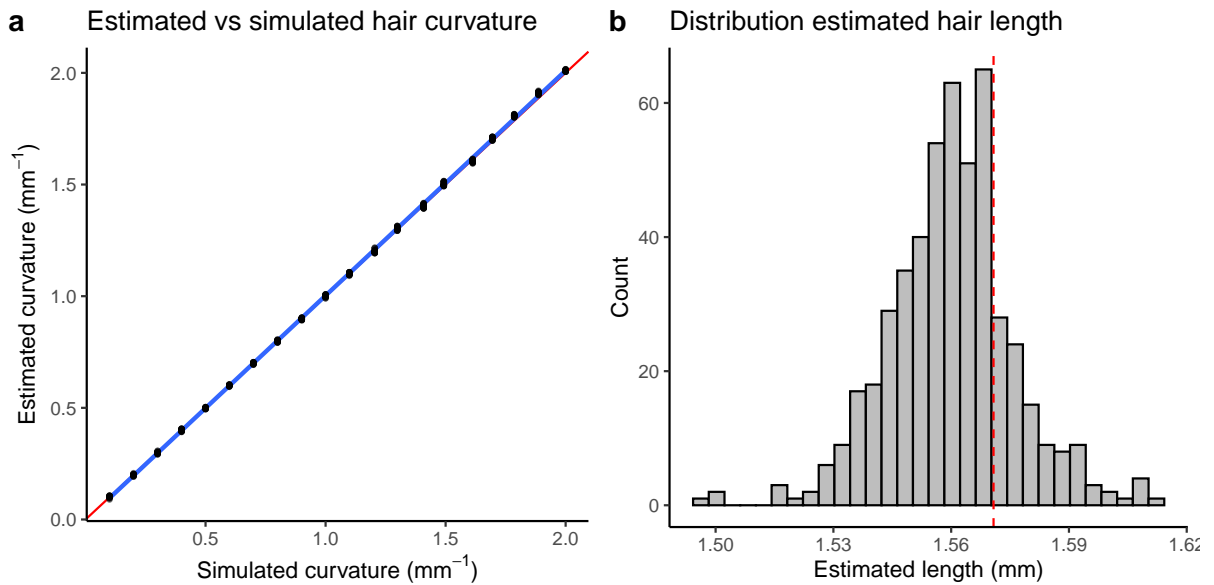


**Figure B.1. Error in estimated curvature and length a**, Scatter plot of correlation between simulated and estimated hair curvature (using *fibermorph*) and **b**, Histogram of distribution of estimated lengths with the red line showing the true simulated length.

Figure B.2 shows a broader range of error in the estimation of length in straighter hairs. This is likely a result of the majority of pixels being oriented in a manner that causes a divergence between the pixel length (number of pixels) and the real length that is being measured. We apply a correction for this known issue in image analysis, however, it is expected that there will still be some error. Note that each point in this figure represents an individual hair fragment within an image. This supports the notion that it is not the low curvature per se, but rather the combination of low curvature and specific orientations that increases the error in length estimation.

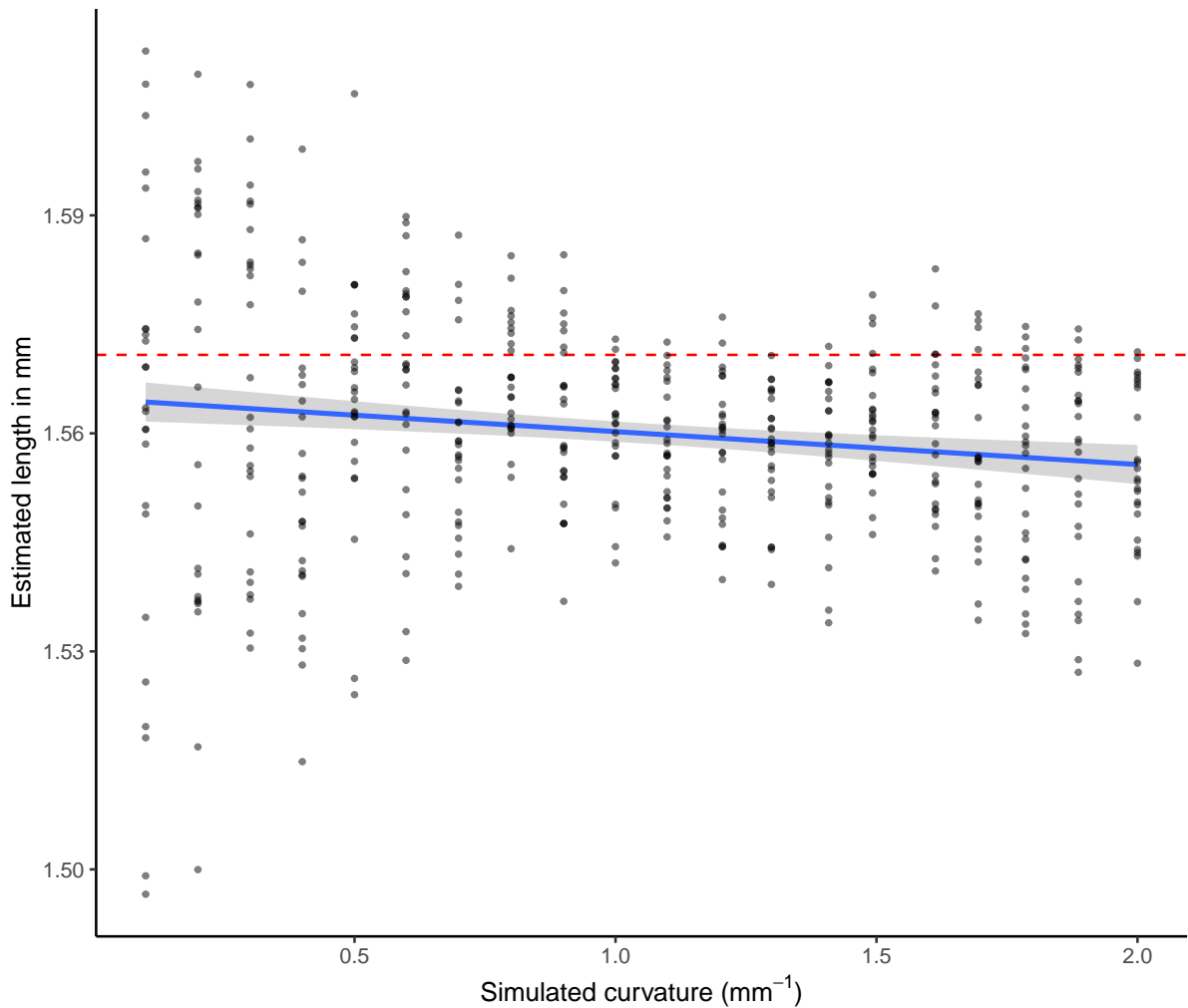


**Figure B.2. Simulated curvature vs estimated length** Simulated curvature on the x-axis and estimated length on the y-axis with a scatter plot showing a small negative correlation between the two, but a larger error in estimating length given a lower curvature.

### B.1.2 Measurement error in curvature and length

In addition to the correlations between simulated and estimated parameters, we calculate root mean square error (RMSE) and percent error as alternatives to investigate the measurement error of our package.

NB: we present the data summarized for each image (i.e. all 25 fragments) as we cannot provide a hair fragment to hair fragment comparison.

### B.1.2.1 Error statistics

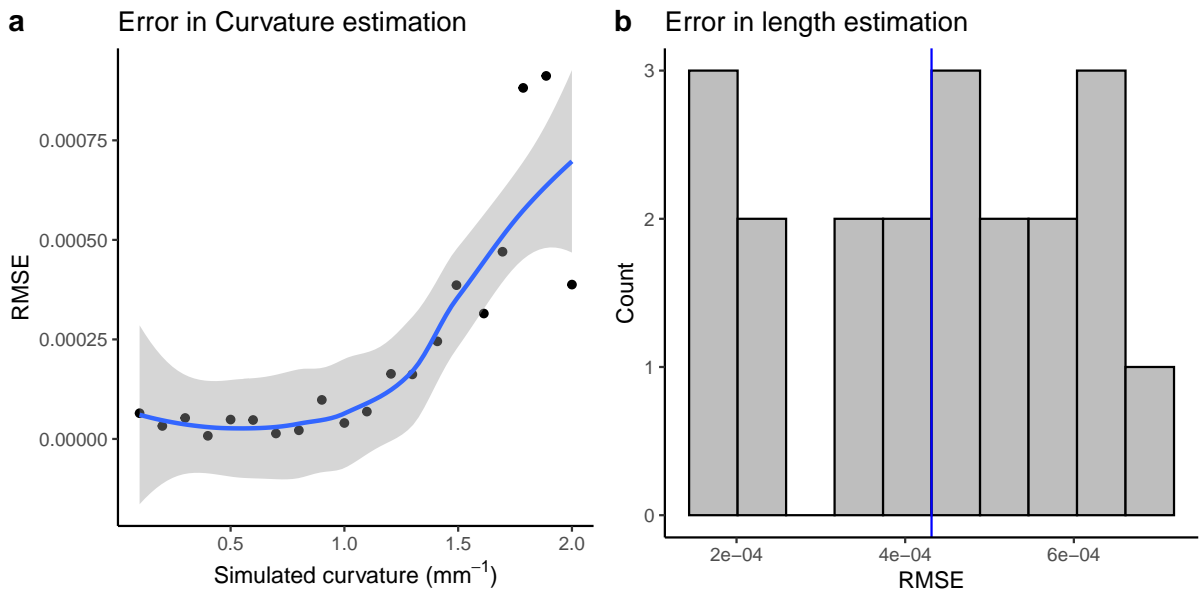
Below, we calculate the mean error values for both RMSE and percent error (See Table B.1). We see less than 1% error across the variables and RMSE of less than 0.0005.

Table B.1: RMSE and Percent Error per variable

var	mean.rmse	perent.error
curvature	0.0002210	0.4720430
length	0.0004312	0.6863358
radius	0.0004624	0.4626120

### B.1.2.2 Root mean square error

First, we plot the root mean square error for curvature and length (see Figure B.3). We then examine the relationship between curvature and RMSE of length (see Figure B.4) and we observe an increase in RMSE with curvature.



**Figure B.3.** Root mean square error for curvature and length **a**, Error in curvature estimation with simulated curvature on the x-axis and root mean square error (RMSE) on the y-axis and **b**, Histogram plot of distribution of RMSE for length estimation.

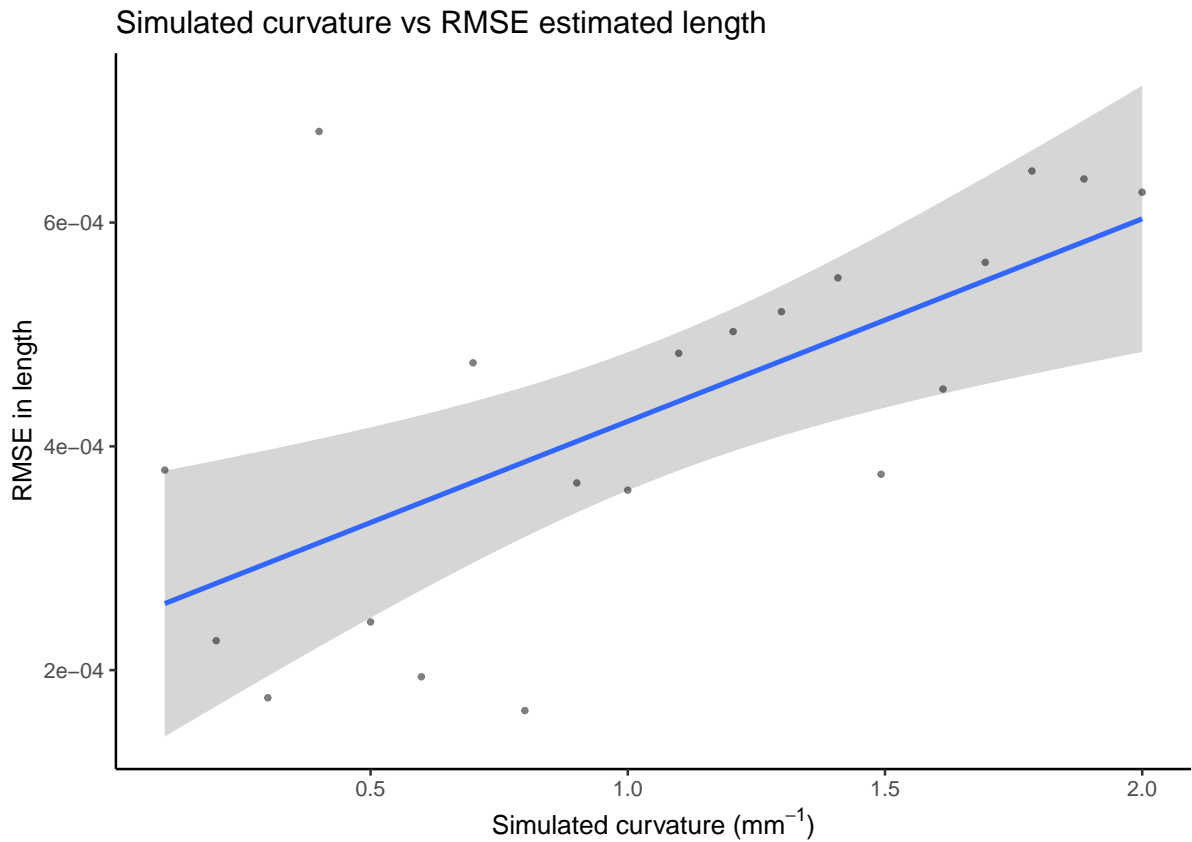


**Figure B.4. Correlation between curvature and RMSE for length** Simulated curvature on the x-axis and root mean square error (RMSE) on the y-axis. The scatter plot shows a positive correlation between the two suggesting that the tighter the curl, the more error there is in accurate estimation of the hair fiber length.

### B.1.2.3 Percent error

Below we plot the percent error for curvature and length (see Figure B.5). In comparing simulated curvature with length, we see that error appears to increase slightly with curvature if considering the data in terms of percent error (see Figure B.6).

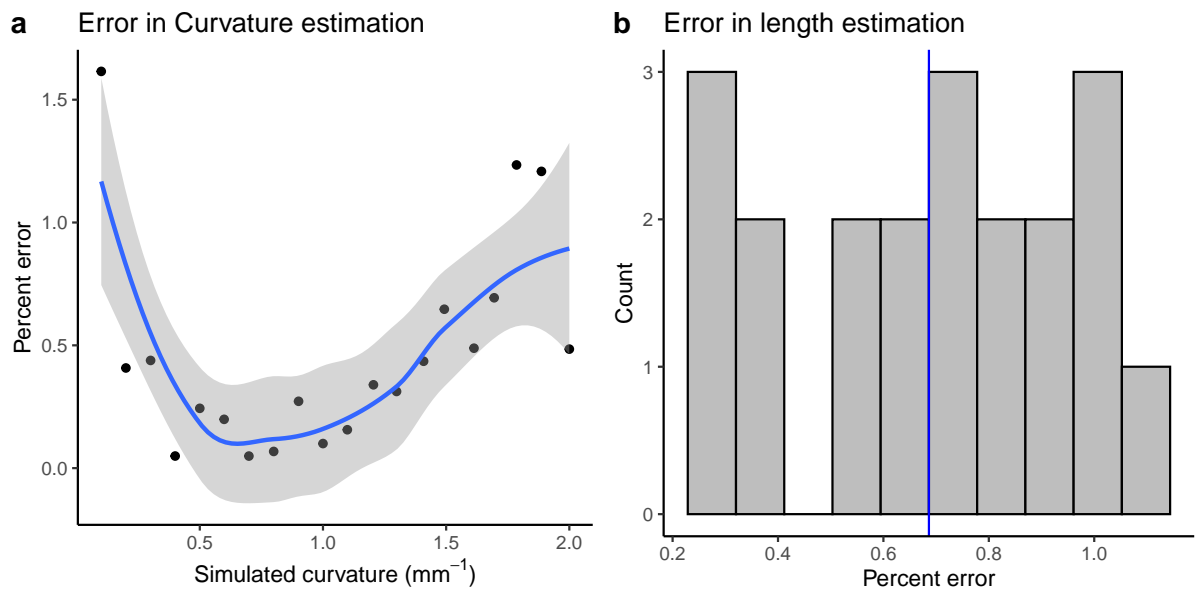


**Figure B.5. Percent error for curvature and length** **a**, Scatter plot of simulated curvature (x-axis) and percent error in curvature estimation (y-axis), and **b**, Histogram plot of distribution of percent error for length estimation

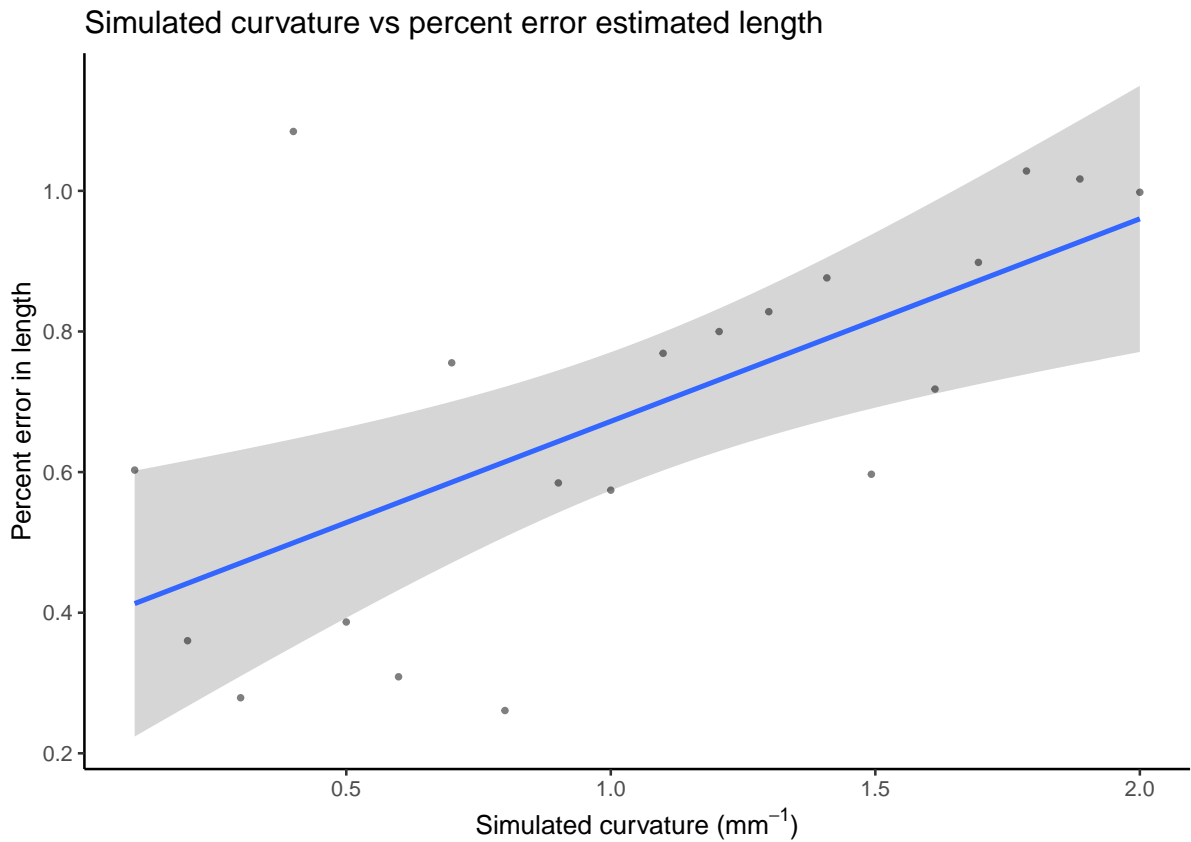


**Figure B.6. Correlation between curvature and percent error for estimated length** Simulated curvature on the x-axis is compared with the percent error in estimated length on the y-axis.

## B.2 Cross-section

The fibermorph section function estimates area, minimum diameter, maximum diameter and eccentricity for a given cross-sectional image. We tested the measurement error using randomly generated circles and non-circular ellipses. We see strong correlations between the estimated and simulated values for each cross-sectional parameter (see Figure B.7).

## B.2.1 Correlation between simulated and estimated section parameters

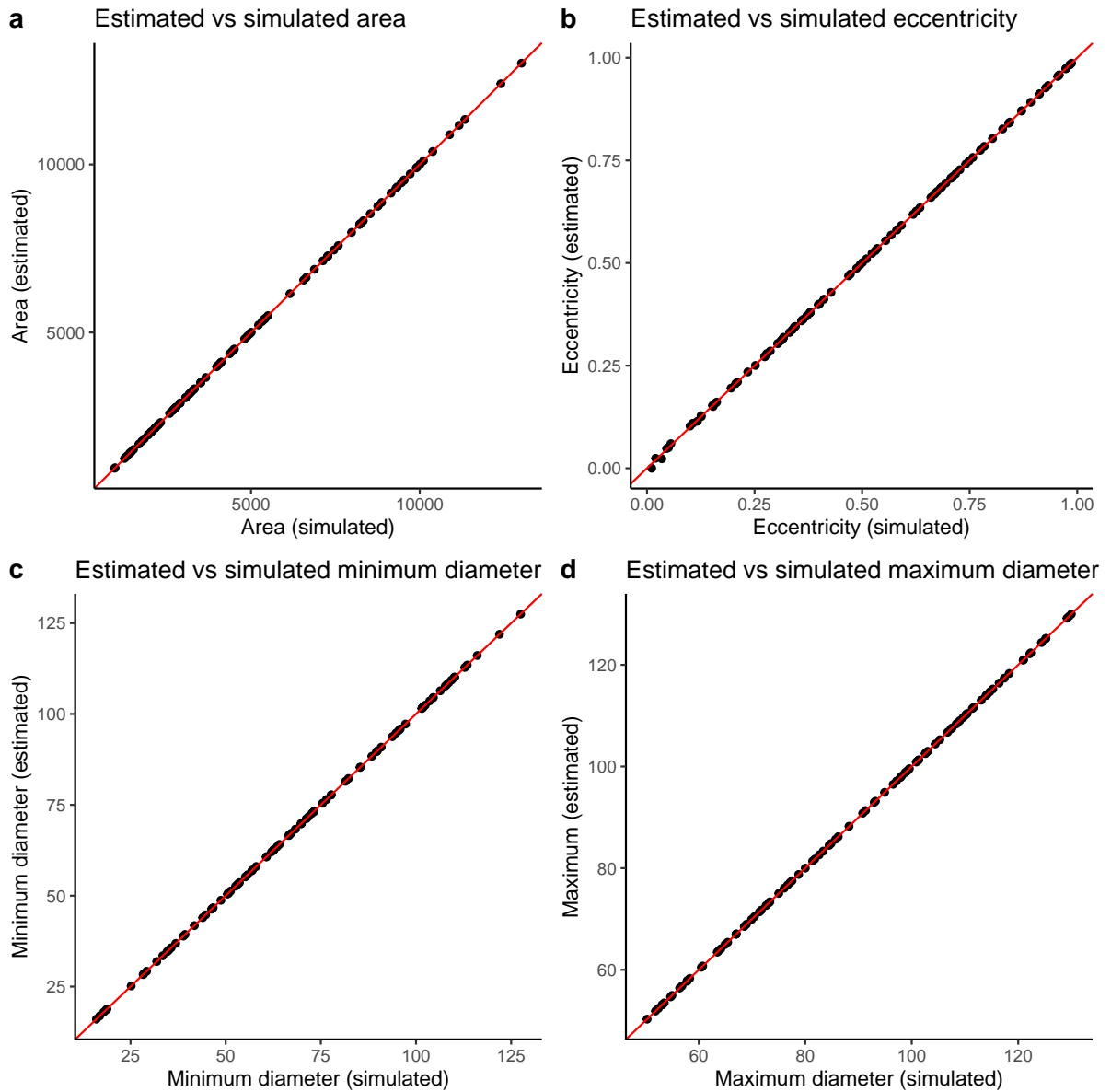


**Figure B.7. Correlation between simulated and estimated cross-sectional parameters** **a**, Correlation between simulated area (x-axis) and estimated area (y-axis), **b**, Correlation between simulated eccentricity (x-axis) and estimated eccentricity (y-axis), **c**, Correlation between simulated minimum diameter (x-axis) and estimated minimum diameter (y-axis), **d**, Correlation between simulated maximum diameter (x-axis) and estimated maximum diameter (y-axis)

## B.2.2 Measurement error for cross-sectional parameters

We calculate the percent error and RMSE for the cross-sectional parameters. First, we calculate mean error values for all parameters (see Table B.2). Percent error is considerably under 0.02% for each of the parameters with RMSE under 0.01 for all but area. As one of the simulated ellipses was a circle with an eccentricity of 0, any deviation from this produces an infinite percent error. So below we present the values removing this observation (see Table B.3).

Table B.2: RMSE and Percent Error per variable

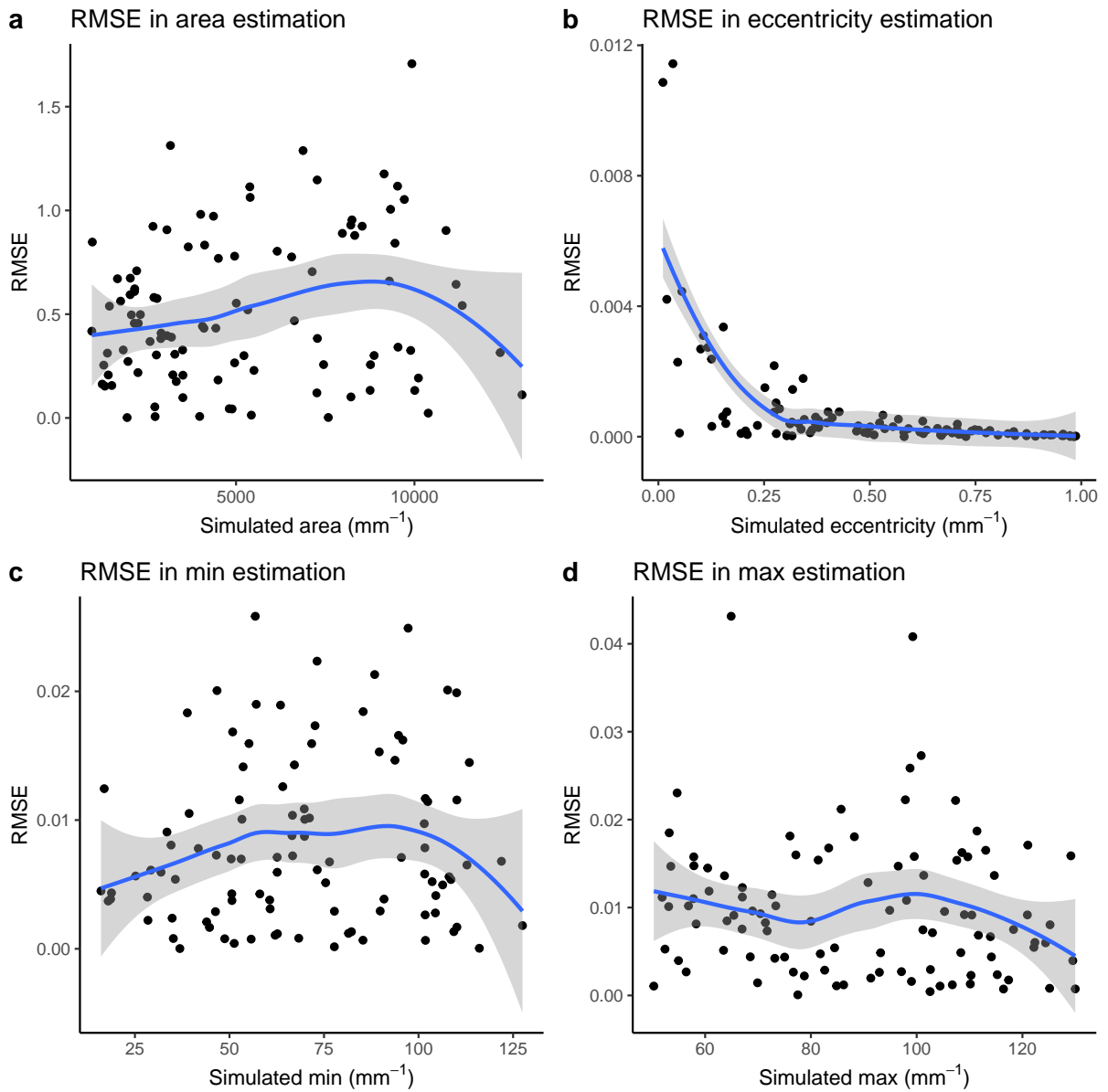
var	mean_rmse	perent_error
area	0.5136320	0.0137703
eccentricity	0.0007514	Inf
max	0.0097800	0.0120605
min	0.0080884	0.0136924

Table B.3: RMSE and Percent Error per variable

var	mean_rmse	perent_error
area	0.5136320	0.0137703
eccentricity	0.0006492	1.0066337
max	0.0097800	0.0120605
min	0.0080884	0.0136924

### B.2.2.1 Root mean square error

Below, we plot RMSE as a function of each parameter (see Figure B.8). There does not appear to be any overarching pattern in RMSE across the variables.



**Figure B.8. Correlation between simulated and RMSE for cross-sectional parameters, a,** Correlation between simulated area (x-axis) and RMSE of area (y-axis), **b,** Correlation between simulated eccentricity (x-axis) and RMSE of eccentricity (y-axis), **c,** Correlation between simulated minimum diameter (x-axis) and RMSE of minimum diameter (y-axis), **c,** Correlation between RMSE of maximum diameter (x-axis) and estimated maximum diameter (y-axis)

### **B.2.2.2 Percent error**

Below we plot the correlation between simulated values and percent error for each parameter (see Figure B.9). We observe a general decrease in percent error for each parameter.

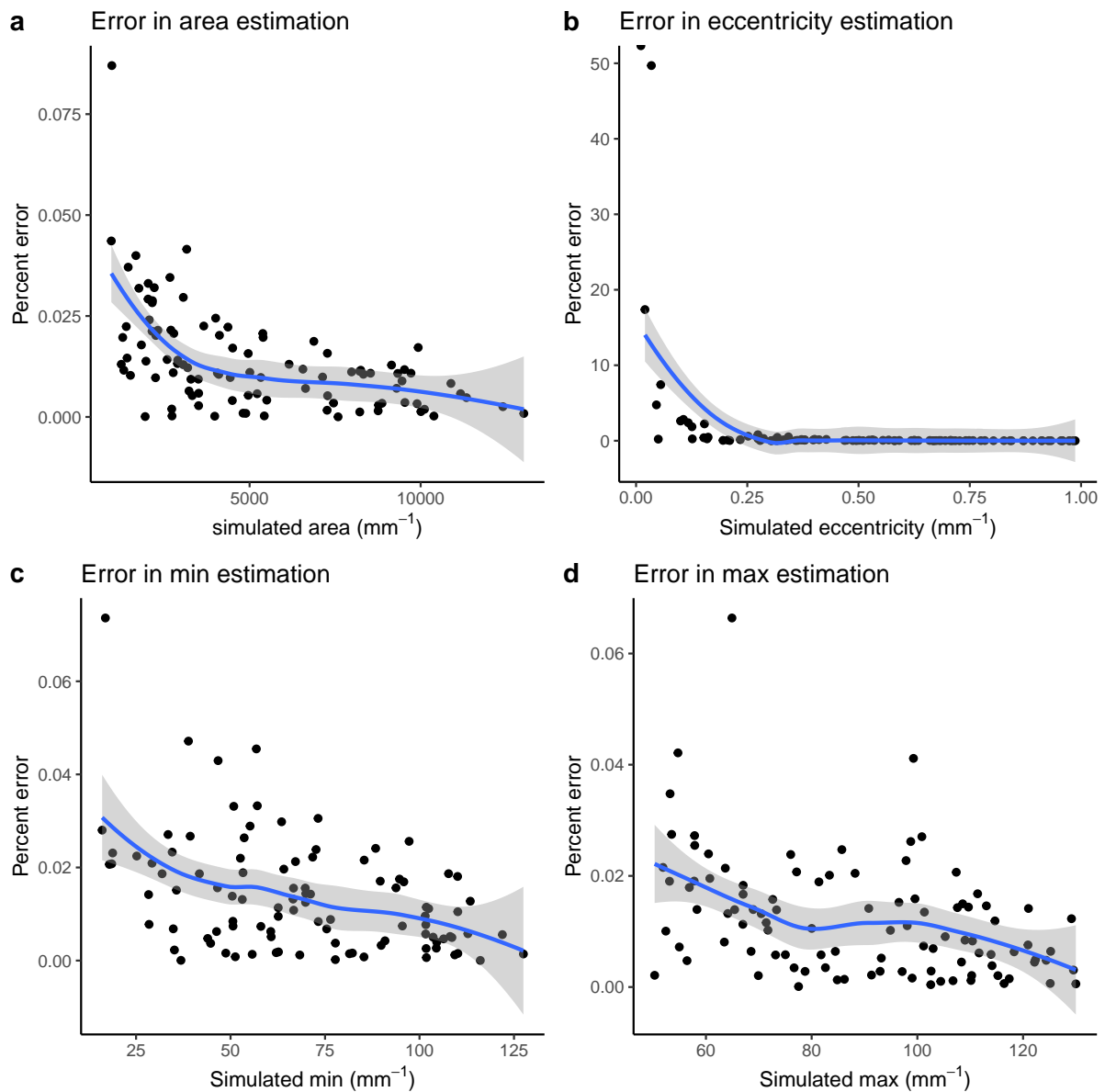


**Figure B.9. Correlation between simulated and percent error cross-sectional parameters, a,** Correlation between simulated area (x-axis) and percent error for area (y-axis), **b,** Correlation between simulated eccentricity (x-axis) and percent error for eccentricity (y-axis), **c,** Correlation between simulated minimum diameter (x-axis) and percent error for minimum diameter (y-axis), **c,** Correlation between percent error for maximum diameter (x-axis) and estimated maximum diameter (y-axis)

# Appendix C |

## Chapter 3 Supplementary:

### Biological significance of new methods

To explore the significance of quantifying hair fiber morphology, we explore the relationship between various quantitative hair traits, categorical data and genotype data on the same sample.

Our data consists of 193 individuals for whom we have quantitative hair phenotype data. In our first data quality control step, we filter to keep individuals who have more than 4 hair fragments in their curvature image and over 10% African ancestry. We calculate mean and median values for the cross-sectional data we have collected for individuals (~ 6 sectioned hair fibers). In our analyses, we use median values as they are less affected by intra-individual outliers.

#### C.1 Self-reported hair texture vs. quantitative hair curvature

We compare the self-reported hair texture with mean and median curvature for our sample (see Figure C.1). The single individual with a high mean curvature in the straight group is the result of an artefact in the image (see Figure C.2). The red arrow points to a stray fiber that likely contaminated the sample and was missed during imaging. Such potential outliers are the reason we chose to use the median curvature for a sample in our analyses.

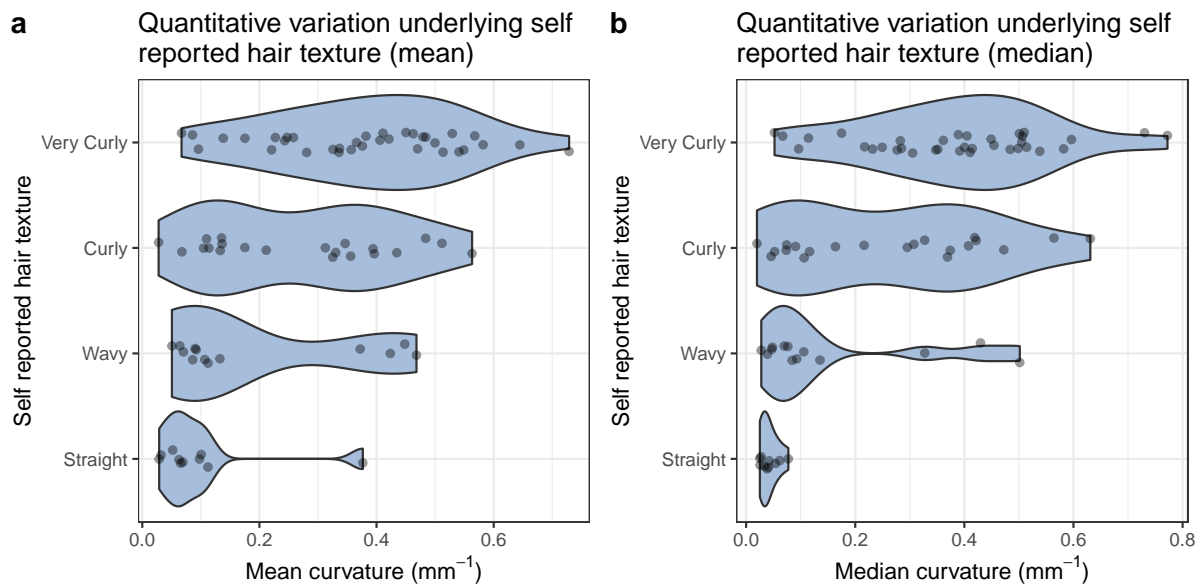


**Figure C.1. Self-reported hair texture vs. quantitative hair curvature** **a**, Mean hair fiber curvature (x-axis) and self-reported hair texture on (y-axis), **b**, Median hair fiber curvature (x-axis) and self-reported hair texture on (y-axis)

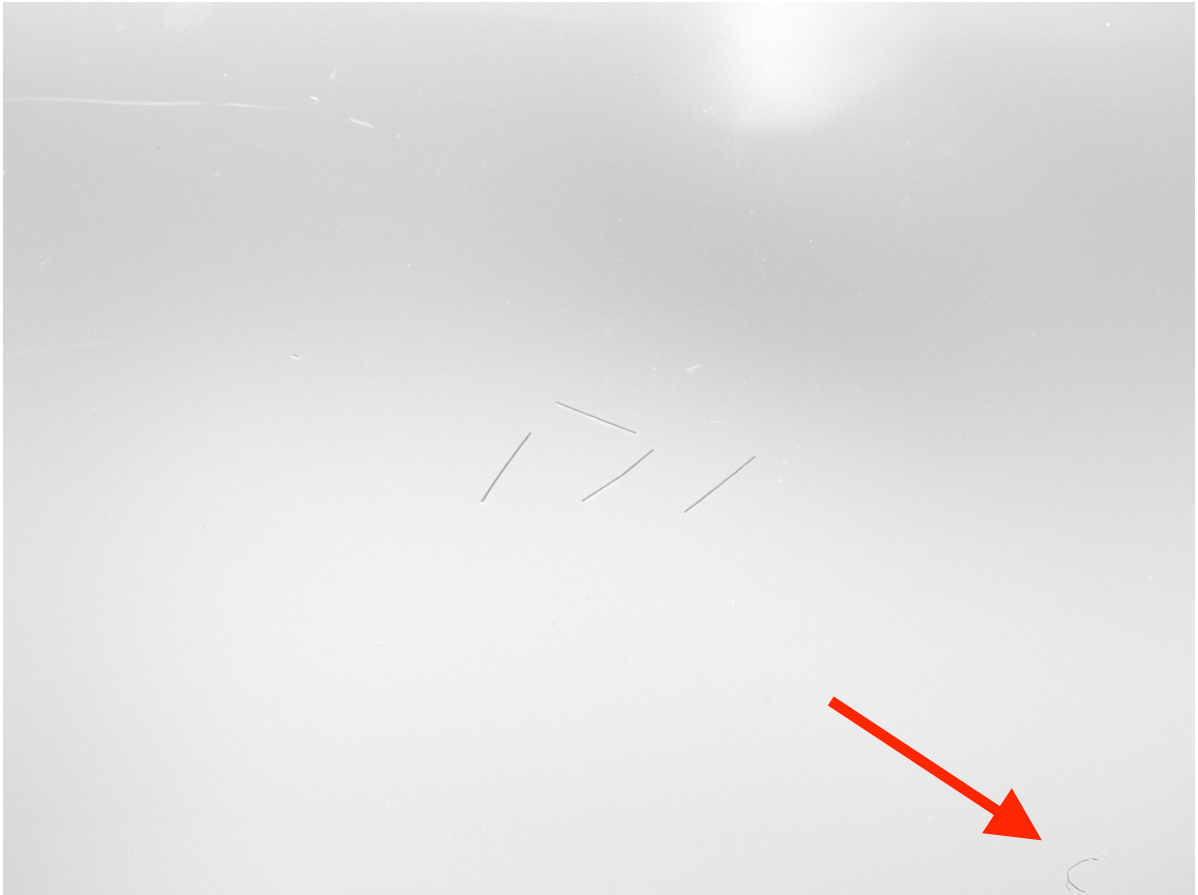


**Figure C.2. Image of hair sample with artefact biasing the measurement** Image of hair fibers used for curvature quantification with a red arrow pointing towards a stray fiber that appears to be contaminating the sample and biasing the curvature measurement.

## **C.2 Objective hair texture classification vs. quantitative curvature**

To explore how much data is lost when binning continuous variation, we compared mean and median curvature to classified hair texture. This classification is based on Loussouarn et al.'s (2007) paper.

While the authors propose a number of parameters to distinguish curlier hair types (based on number of twists and waves among other factors), their primary classification is based on curvature. We demonstrate that, regardless of additional parameters, a considerable range of curvature is obscured when collapsing hair variation according to their curvature thresholds.

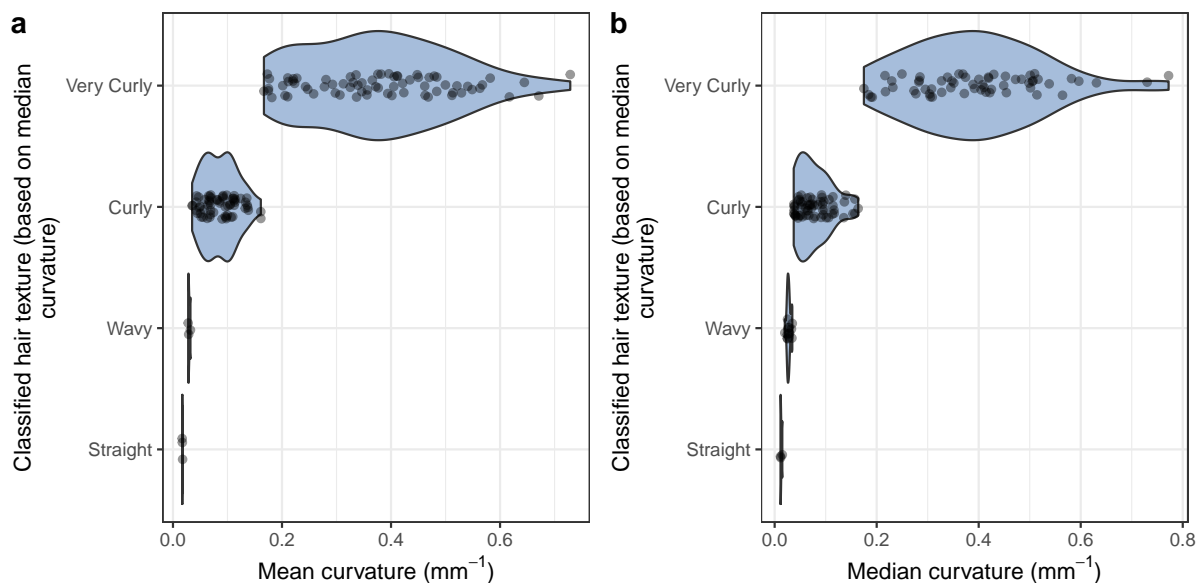


**Figure C.3. Objective hair classification vs. quantitative curvature** **a**, Mean hair fiber curvature (x-axis) and objectively categorized hair texture on (y-axis), **b**, Median hair fiber curvature (x-axis) and objectively categorized hair texture on (y-axis)

## C.3 Ancestry vs. hair morphology

We carried out a number of analyses using the genotype data collected for this diverse sample. In an admixed sample where a continuous trait has divergent distributions in the parental ancestry groups, the resulting admixed population can show a correlation between ancestry and that trait. Finding such a correlation suggests may imply a polygenic trait with high heritability.

### C.3.1 Admixture components

Our sample consists of admixed individuals with primarily African and European ancestry (see Figure C.4).

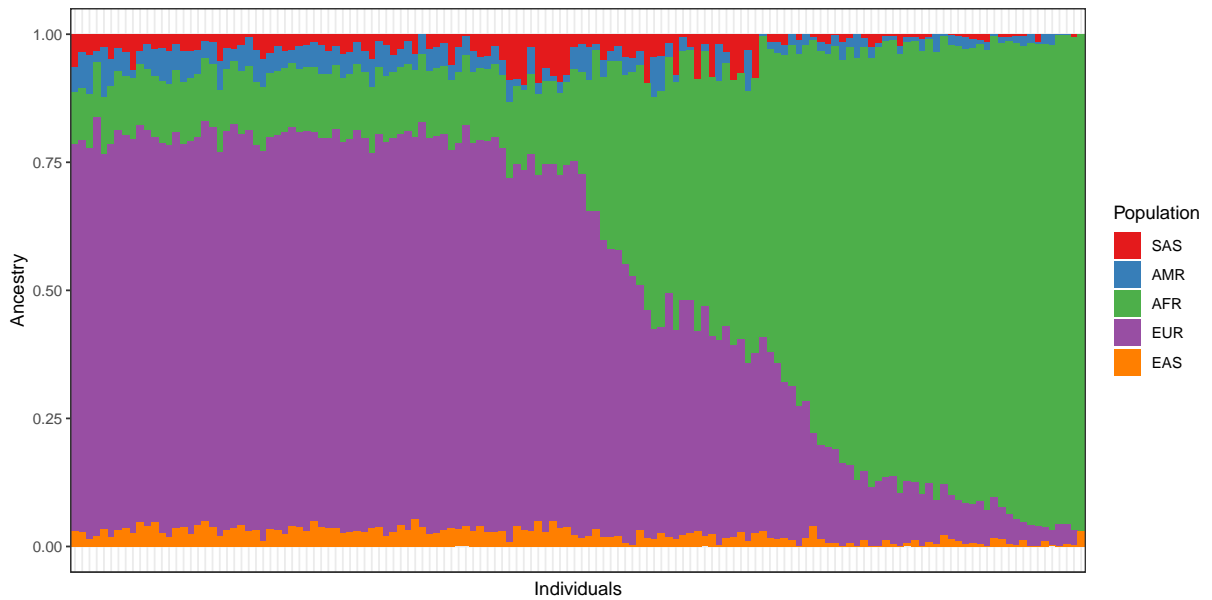


**Figure C.4. Admixture components for sample** Plot for K=5 ADMIXTURE of sample (n=192) with predominantly AFR and EUR ancestry. The colors represent ancestries that correspond to the following 1000 Genomes populations: - SAS = South Asian - AMR = American - AFR = African - EUR = European - EAS = East Asian. Each of these are meta-populations based on the grouping of multiple (sub)continental population groups in the 1000 Genomes repository.

### C.3.2 Ancestry vs. curvature

Here we plot the correlation between proportion of African ancestry and m-index, median curvature, and eccentricity (see Figure C.5).

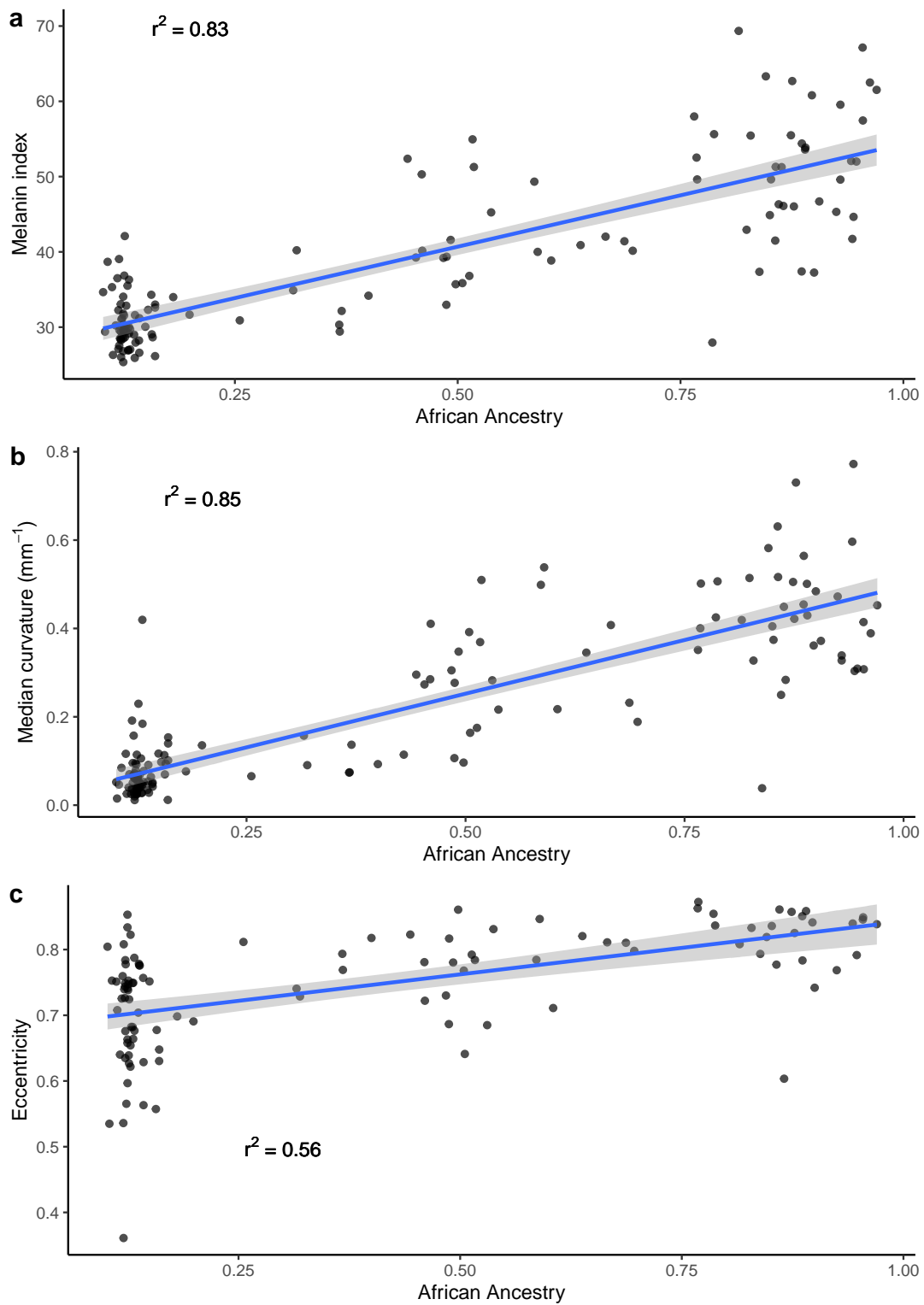


**Figure C.5. Percentage of African ancestry vs. M-index, curvature and eccentricity**  
**a**, African ancestry (x-axis) vs. Melanin Index (y-axis), **b**, African ancestry (x-axis) vs. median hair fiber curvature (y-axis), **c**, African ancestry (x-axis) vs. cross-sectional eccentricity (y-axis)

### C.3.3 Curvature vs. eccentricity

The relationship between cross-sectional shape (eccentricity) and curvature has long been debated. Due to the coincidence of cross-sectional shape and curvature in various populations that are often contrasted (i.e. East Asian vs. North European vs. West African), it has been unclear whether these traits have a causal relationship (specifically that higher eccentricity predicts higher curvature). In our admixed sample, we have the opportunity to test this question and fit a model between these traits with and without ancestry.

#### C.3.3.1 Uncorrected

First we examine the data without correcting for ancestry. If we consider the relationship between curvature and eccentricity without taking into account ancestry, we find that eccentricity is a significant predictor of curvature (see Figure C.6).

```
##
## Call:
## lm(formula = curv_median ~ eccentricity_median, data = df_curv_ecc)
##
## Residuals:
##      Min       1Q   Median       3Q      Max
## -0.2843 -0.1245 -0.0264  0.1125  0.4770
##
## Coefficients:
##              Estimate Std. Error t value Pr(>|t|)
## (Intercept)    -0.5682     0.1270  -4.474 1.94e-05 ***
## eccentricity_median  1.0284     0.1692   6.076 1.96e-08 ***
## ---
## Signif. codes:  0 '***' 0.001 '**' 0.01 '*' 0.05 '.' 0.1 ' ' 1
##
## Residual standard error: 0.1576 on 106 degrees of freedom
## Multiple R-squared:  0.2583, Adjusted R-squared:  0.2513
## F-statistic: 36.92 on 1 and 106 DF,  p-value: 1.959e-08
```

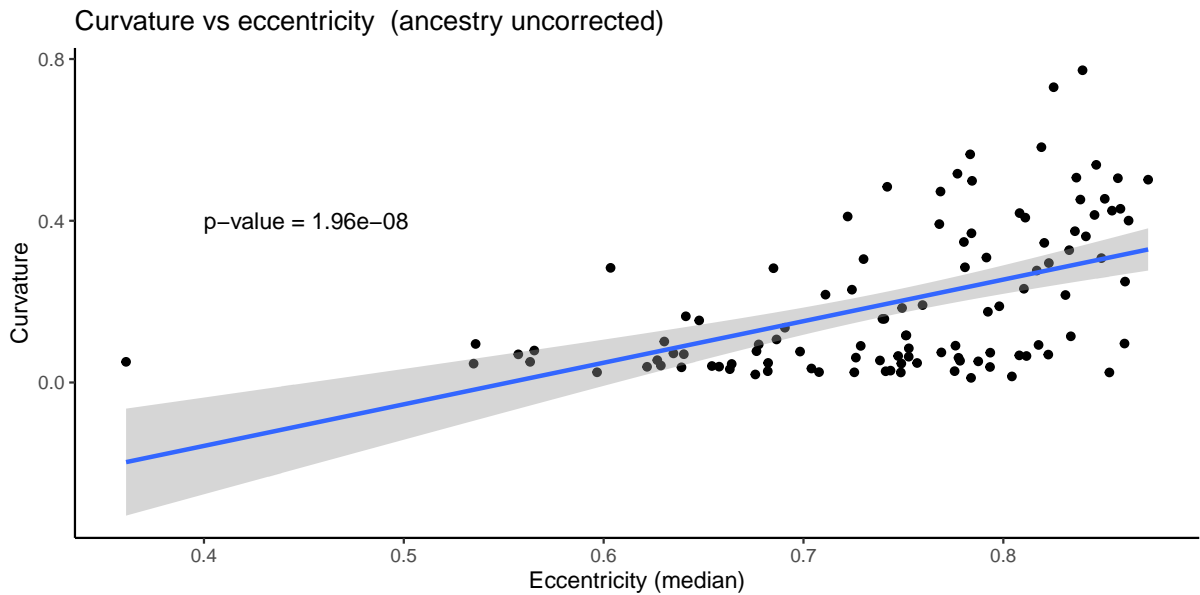


**Figure C.6. Curvature vs. eccentricity (without correction for ancestry)** Median eccentricity on the x-axis vs. median curvature on the y-axis show a positive correlation when they are plotted without correction for ancestry.

### C.3.3.2 Corrected

We then re-analyze the data with ancestry as a covariate and see that when we correct for ancestry, this correlation is no longer significant. This supports the idea that these traits may be independent (see Figure C.7).

```
##
## Call:
## lm(formula = curv_median ~ eccentricity_median + AFR, data = df_curv_ecc)
##
## Residuals:
##      Min       1Q   Median       3Q      Max
## -0.37902 -0.04122 -0.00657  0.03606  0.29971
##
## Coefficients:
##              Estimate Std. Error t value Pr(>|t|)
## (Intercept)   -0.07237    0.08661  -0.836   0.405
## eccentricity_median  0.10891    0.12511   0.871   0.386
## AFR             0.48101    0.03632  13.243 <2e-16 ***
```

```
## ---
## Signif. codes:  0 '***' 0.001 '**' 0.01 '*' 0.05 '.' 0.1 ' ' 1
##
## Residual standard error: 0.09693 on 105 degrees of freedom
## Multiple R-squared:  0.7222, Adjusted R-squared:  0.7169
## F-statistic: 136.5 on 2 and 105 DF,  p-value: < 2.2e-16
```

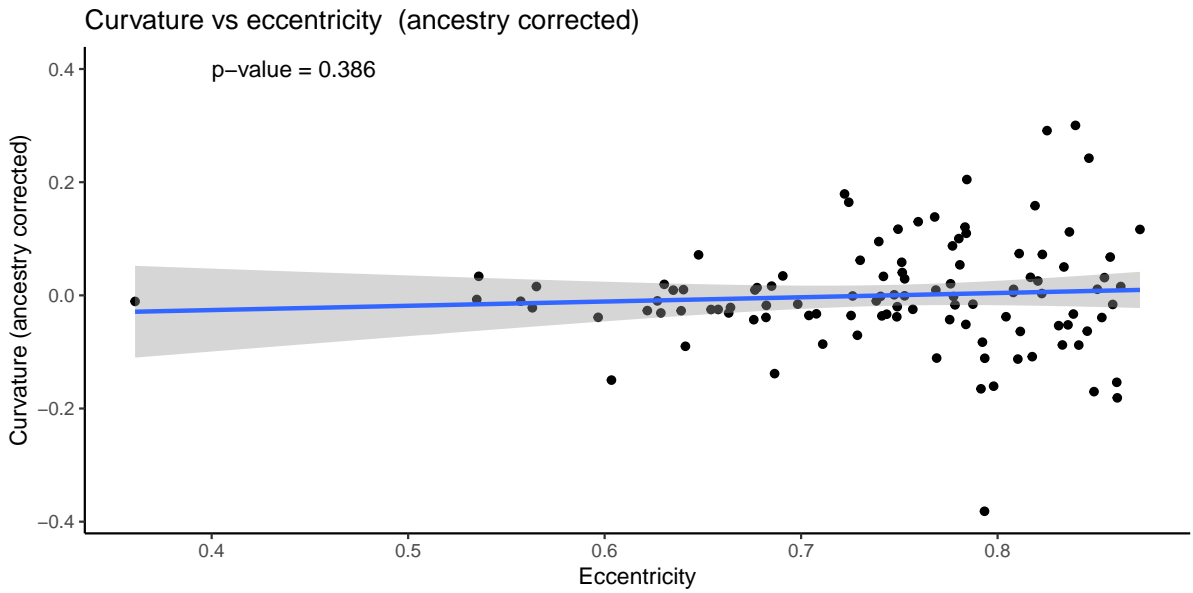


**Figure C.7. Curvature vs. eccentricity (with correction for ancestry)** Median eccentricity on the x-axis vs. median curvature on the y-axis show no correlation when they are plotted with correction for ancestry.

### C.3.4 Curvature vs. skin pigmentation

To demonstrate the potential effect of population stratification on traits, we compare hair curvature with skin pigmentation (m-index). These two traits are not biologically related, yet, in an admixed population, we may see a correlation that is due to population stratification of these polygenic traits.

#### C.3.4.1 Uncorrected

First we examine the relationship between curvature and skin pigmentation without correcting for ancestry (see Figure C.8). As expected, we see a significant correlation between the two traits.

```

##
## Call:
## lm(formula = curv_median ~ m_index, data = df_curv_mindex)
##
## Residuals:
##      Min       1Q   Median       3Q      Max
## -0.20715 -0.06804 -0.03471  0.04818  0.51483
##
## Coefficients:
##              Estimate Std. Error t value Pr(>|t|)
## (Intercept) -0.280232   0.041533  -6.747 4.91e-10 ***
## m_index      0.012887   0.001031  12.501 < 2e-16 ***
## ---
## Signif. codes:  0 '***' 0.001 '**' 0.01 '*' 0.05 '.' 0.1 ' ' 1
##
## Residual standard error: 0.1261 on 126 degrees of freedom
## Multiple R-squared:  0.5536, Adjusted R-squared:  0.5501
## F-statistic: 156.3 on 1 and 126 DF,  p-value: < 2.2e-16

```

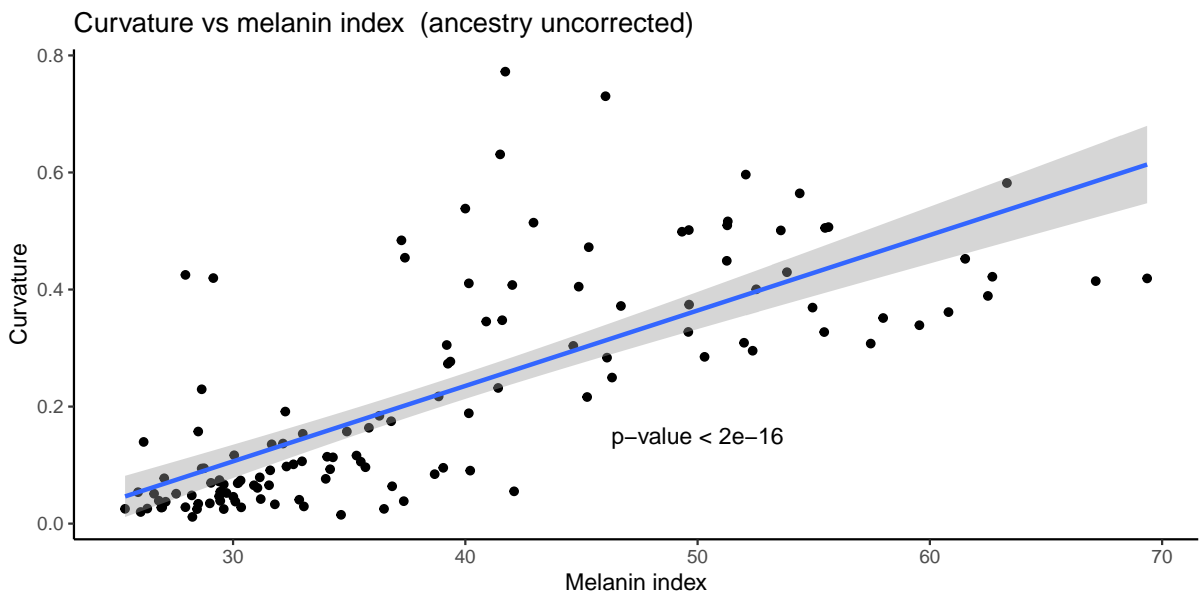


**Figure C.8. Curvature vs. M-index (without correction for ancestry)** Melanin Index on the x-axis vs. median curvature on the y-axis show a positive correlation when they are plotted without correction for ancestry.

### C.3.4.2 Corrected

We then apply a correction for ancestry and re-analyze the data (see Figure C.9. Like with curvature and eccentricity, the relationship between curvature and skin pigmentation is no longer significant when ancestry is taken into account.

```
##
## Call:
## lm(formula = curv_median ~ m_index + AFR, data = df_curv_mindex)
##
## Residuals:
##      Min       1Q   Median       3Q      Max
## -0.34321 -0.04877 -0.01348  0.03562  0.34806
##
## Coefficients:
##              Estimate Std. Error t value Pr(>|t|)
## (Intercept) -0.061501   0.042384  -1.451   0.149
## m_index      0.002734   0.001469   1.862   0.065 .
## AFR          0.406609   0.048561   8.373 9.63e-14 ***
## ---
## Signif. codes:  0 '***' 0.001 '**' 0.01 '*' 0.05 '.' 0.1 ' ' 1
##
## Residual standard error: 0.1014 on 125 degrees of freedom
## Multiple R-squared:  0.714, Adjusted R-squared:  0.7094
## F-statistic:  156 on 2 and 125 DF, p-value: < 2.2e-16
```

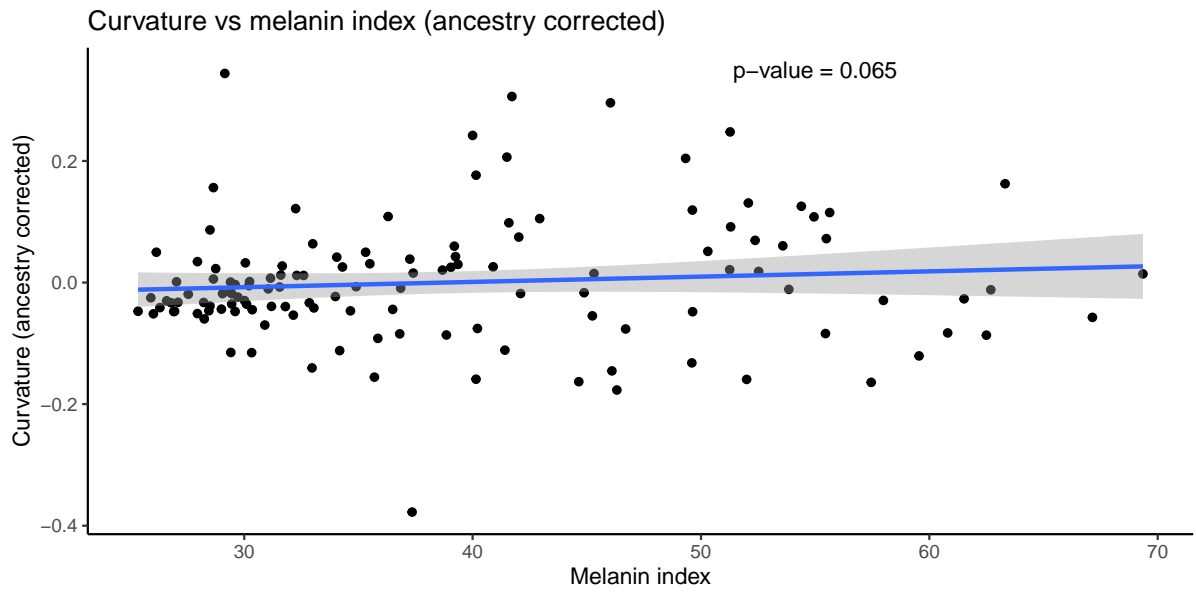


**Figure C.9. Curvature vs. M-index (with correction for ancestry)** Melanin Index on the x-axis vs. median curvature on the y-axis show no correlation when they are plotted with correction for ancestry.

# Appendix D |

## Chapter 4 Supplementary:

### Admixture & phenotype correlations

#### D.1 Admixture components

Our sample consists of admixed individuals with primarily African and European ancestry. We first calculated the ancestry for the entire ADAPT sample and then selected a subset based on whether they had  $>10\%$  AFR ancestry and  $<10\%$  non-EUR and non-AFR ancestry. Below we plot the ancestries for the admixed African-European sample that was phenotyped using the new hair quantification methods (see Figure. D.1). We subsequently use the African ancestry component from  $K=2$  which correlates strongly with the AFR ancestry estimate from  $K=5$  (see Figure D.2).

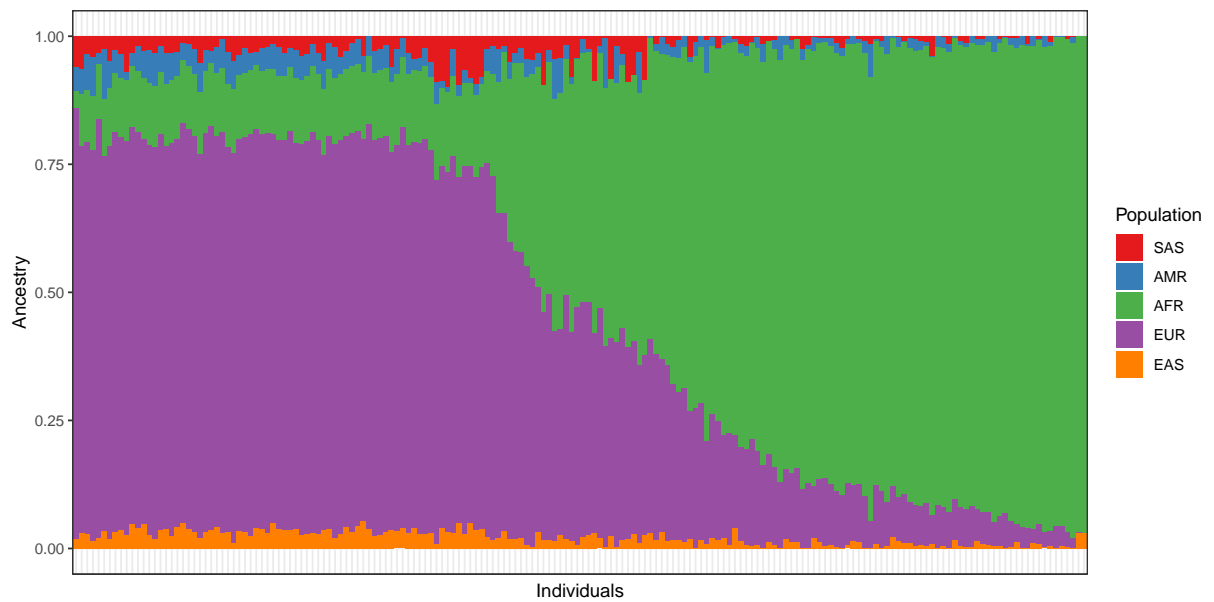


**Figure D.1. Admixture components for sample** Plot for K=5 ADMIXTURE of sample (n=192) with predominantly AFR and EUR ancestry. The colors represent ancestries that correspond to the following 1000 Genomes populations: - SAS = South Asian - AMR = American - AFR = African - EUR = European - EAS = East Asian. Each of these are meta-populations based on the grouping of multiple (sub)continental population groups in the 1000 Genomes repository.

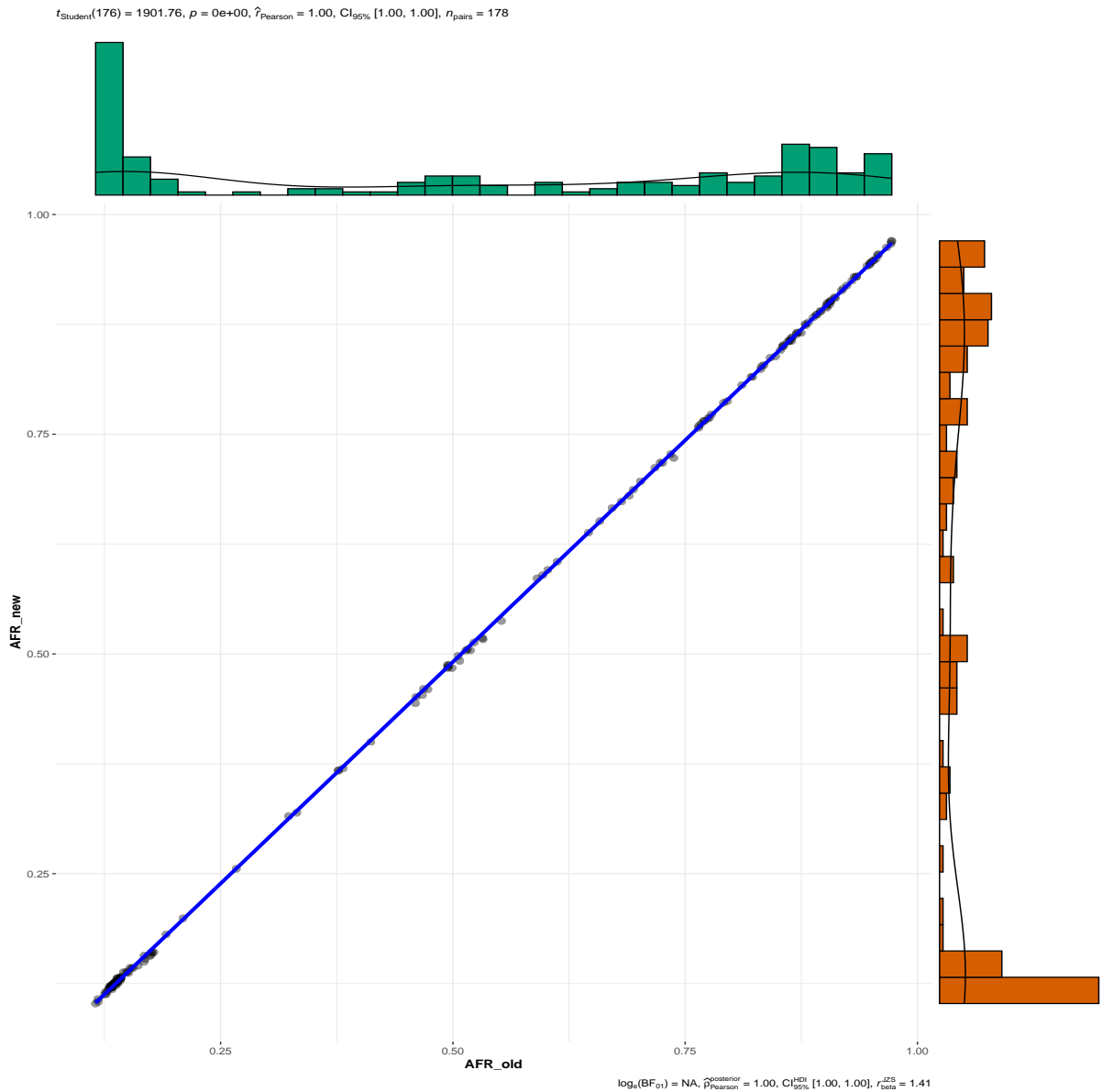


**Figure D.2. Correlation between different AFR calculations for the sample.** On the x-axis we have the proportion of AFR ancestry calculated with  $K=5$  and on the y-axis we have the proportion of AFR ancestry calculated with  $K=2$ . The two estimates are highly correlated with most of the variance being in the individuals with low AFR ancestry.

## D.2 Phenotypic distributions

Below we plot the distributions of various phenotypes (see Figure D.3). First we import data from previous work (Lasisi et al., 2016), with data on M-index, curvature and cross-sectional properties from individuals sampled in the UK from different ancestries. These

ancestries were inferred by questionnaires where participants reported the ethnicities and places of birth of their parents and grandparents. Here we group individuals with all four grandparents from African (and African ethnic identities) as African, individuals with all four grandparents from Europe (and European ethnic identities) as European, and individuals with at least three grandparents identifying as having Afro-Caribbean or African American ancestries as African Diaspora populations.

We plot the distributions as density plots (Figure D.4) and violin plots (Figure D.5) and scatter plots with regional ancestry details (Figure D.6). As expected, M-index and hair curvature are both divergent in their distributions when European and African participants are compared. Participants from the African Diaspora have distributions overlapping with both these populations, with higher densities overlapping with the African participants. Interestingly, no other phenotype shows such a pattern.

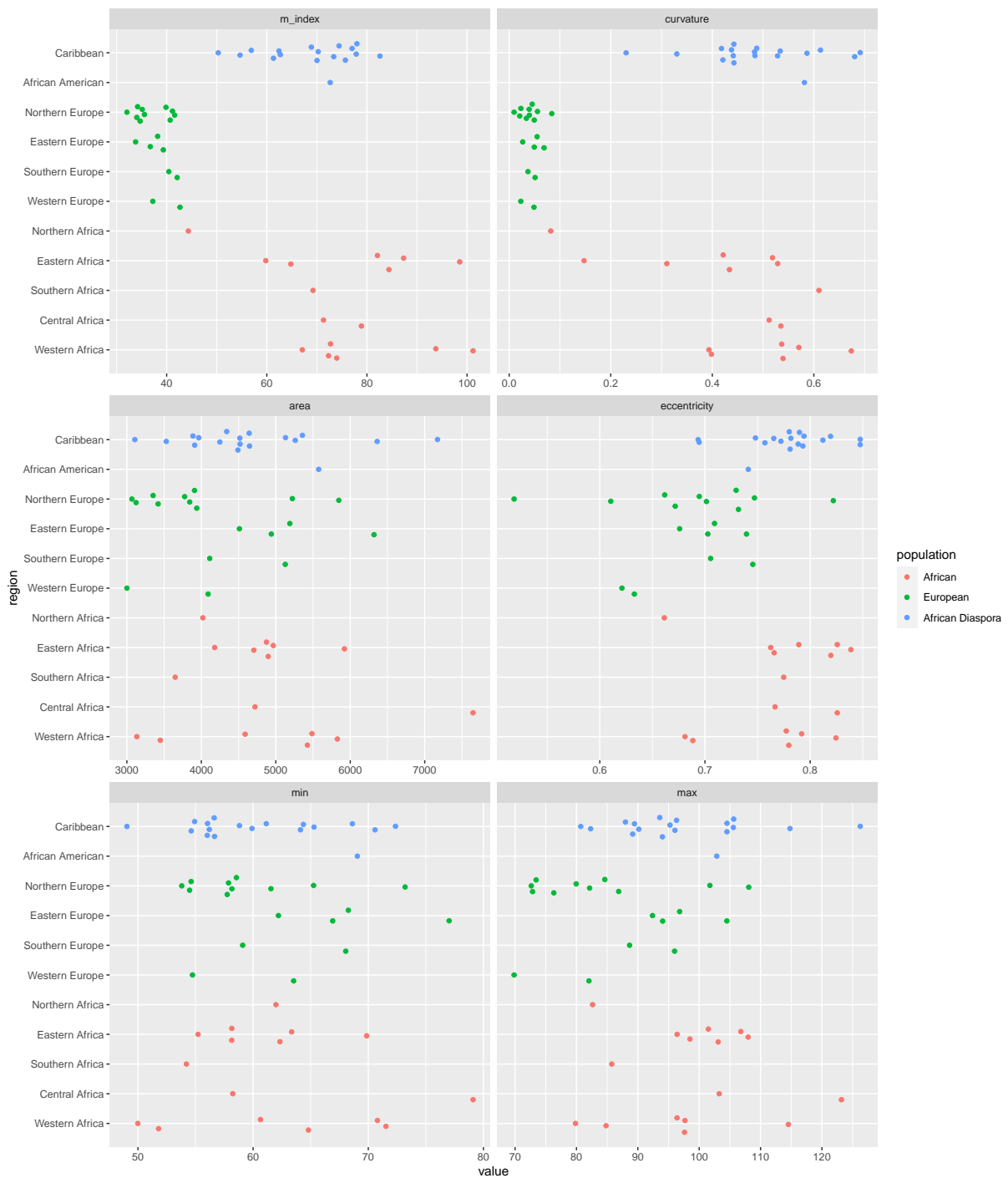


**Figure D.3.** Grouped scatter plots showing phenotypic distributions for each phenotype with regional details for the reference samples. **a**, Melanin Index **b**, median hair fiber curvature **c**, cross-sectional area **d**, cross-sectional eccentricity **e**, minimum diameter of cross-section **f**, maximum diameter of cross-section.

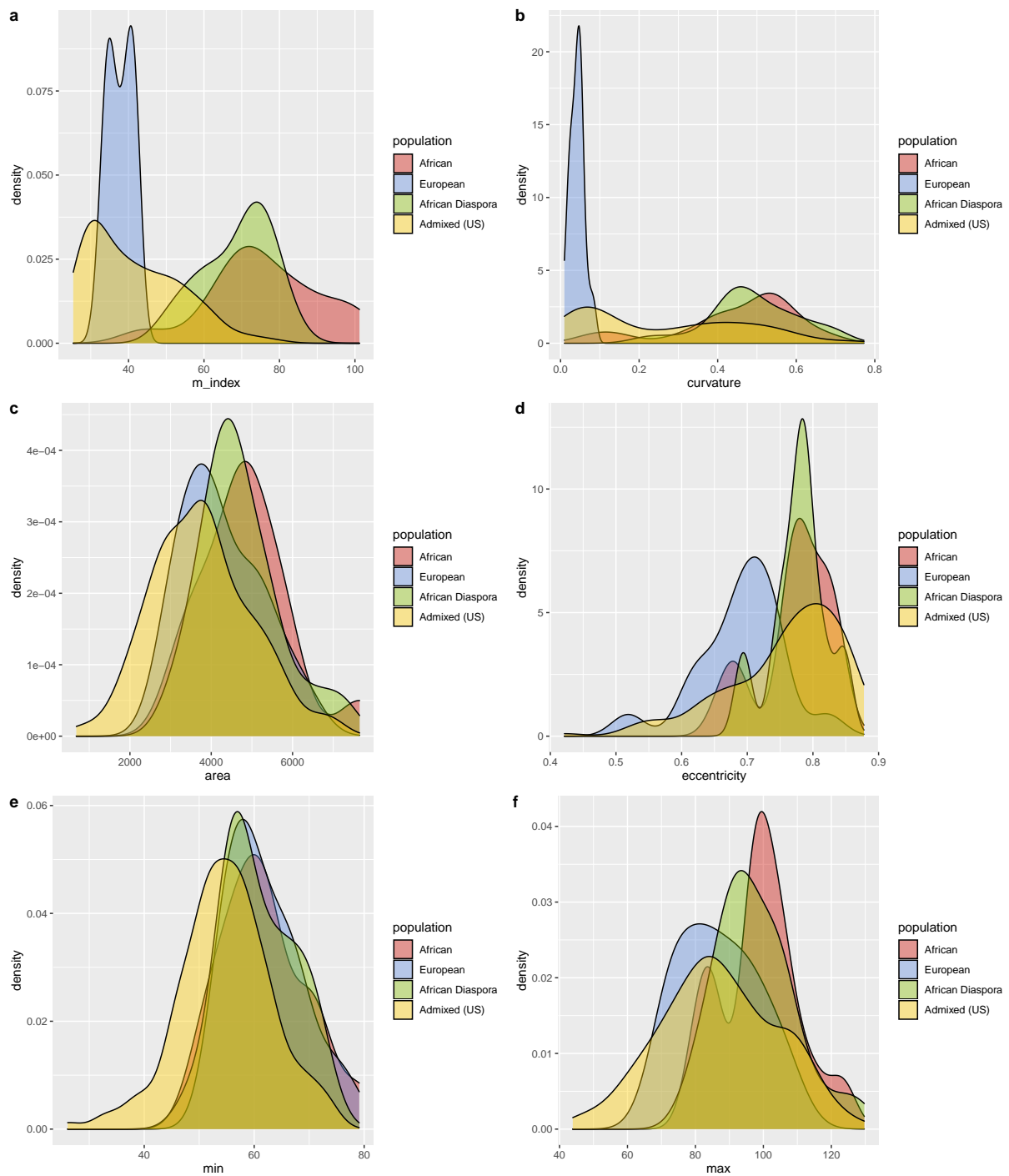


**Figure D.4.** Density plots showing phenotypic distributions for each phenotype for the reference samples and the current sample marked as Admixed (US). **a**, Melanin Index **b**, median hair fiber curvature **c**, cross-sectional area **d**, cross-sectional eccentricity **e**, minimum diameter of cross-section **f**, maximum diameter of cross-section.

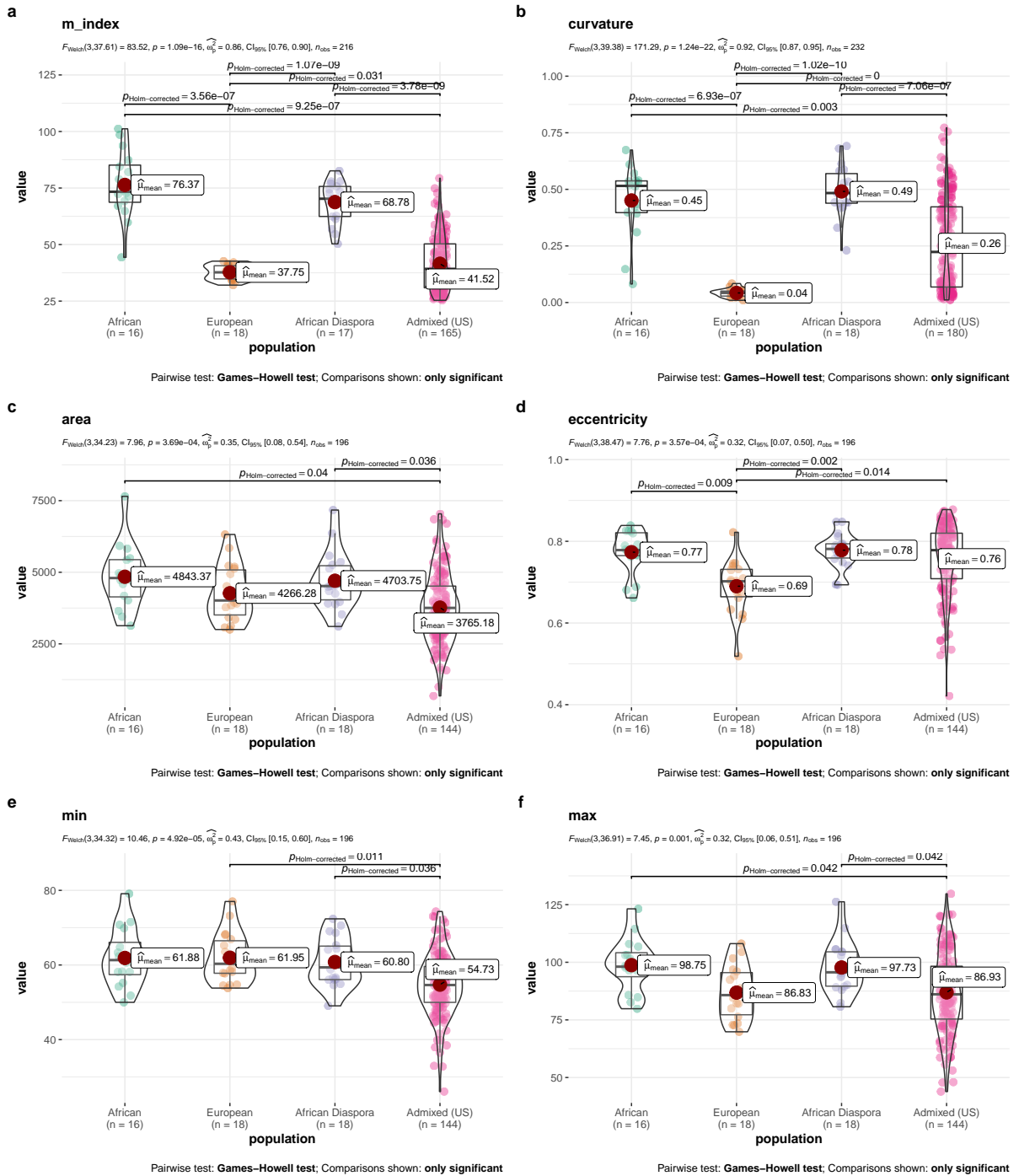


**Figure D.5. Violin plots showing phenotypic distributions for each phenotype for the reference samples and the current sample marked as Admixed (US). a, Melanin Index b, median hair fiber curvature c, cross-sectional area d, cross-sectional eccentricity e, minimum diameter of cross-section f, maximum diameter of cross-section.**



**Figure D.6.** Grouped scatter plots showing phenotypic distributions for each phenotype for the reference samples with regional details and the current sample marked as Admixed (US). **a**, Melanin Index **b**, median hair fiber curvature **c**, cross-sectional area **d**, cross-sectional eccentricity **e**, minimum diameter of cross-section **f**, maximum diameter of cross-section.

### **D.3 Sex differences**

The distribution of female/male-identified individuals is skewed, with a higher proportion of the sample being female (n=132 vs n=39 male). However, there appear to be no considerable differences in distribution between these sexes in our sample (see Figures D.7 and D.8).

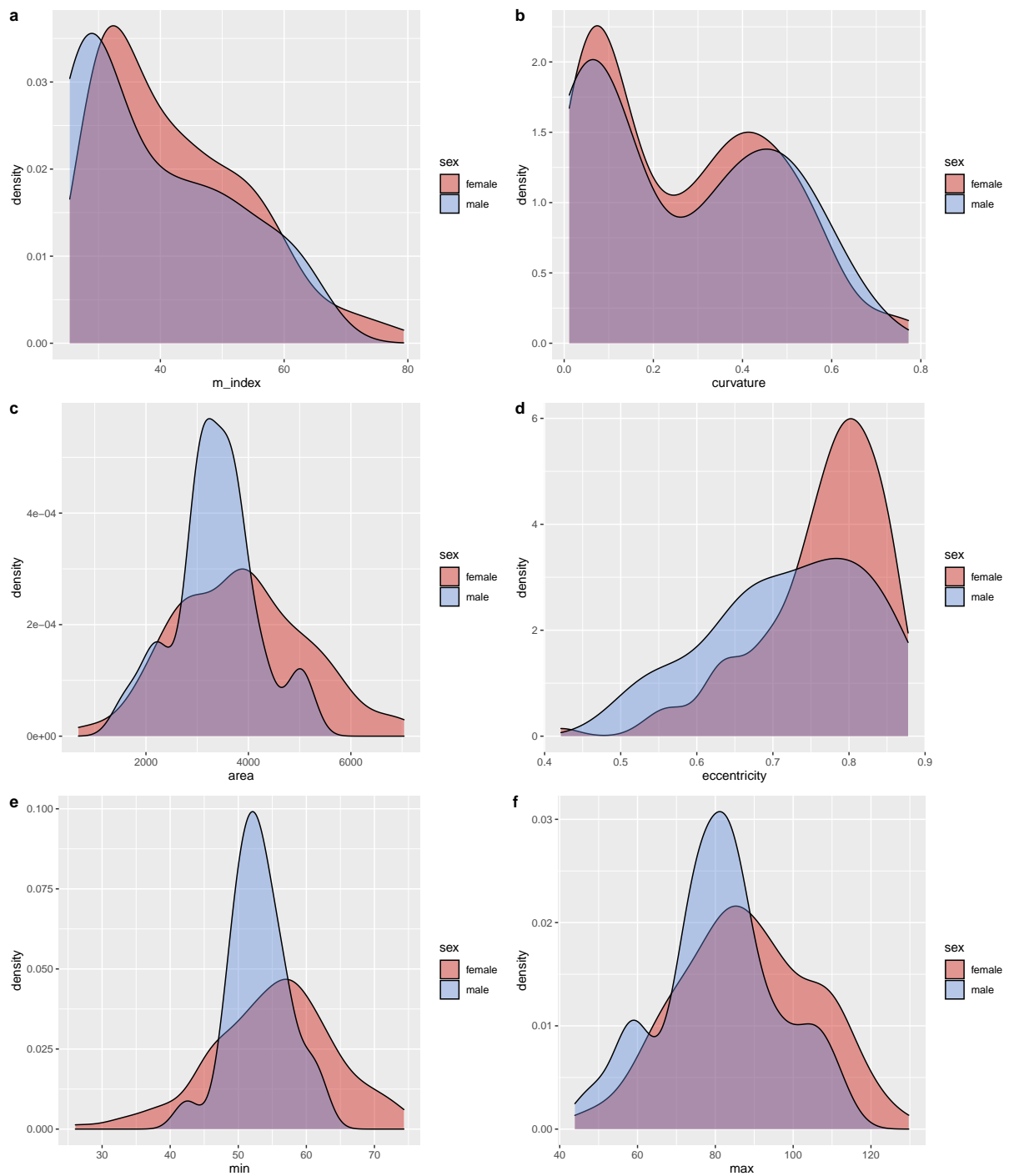


**Figure D.7.** Density plots showing phenotypic distributions for each phenotype per self-reported sex. **a**, Melanin Index **b**, median hair fiber curvature **c**, cross-sectional area **d**, cross-sectional eccentricity **e**, minimum diameter of cross-section **f**, maximum diameter of cross-section.

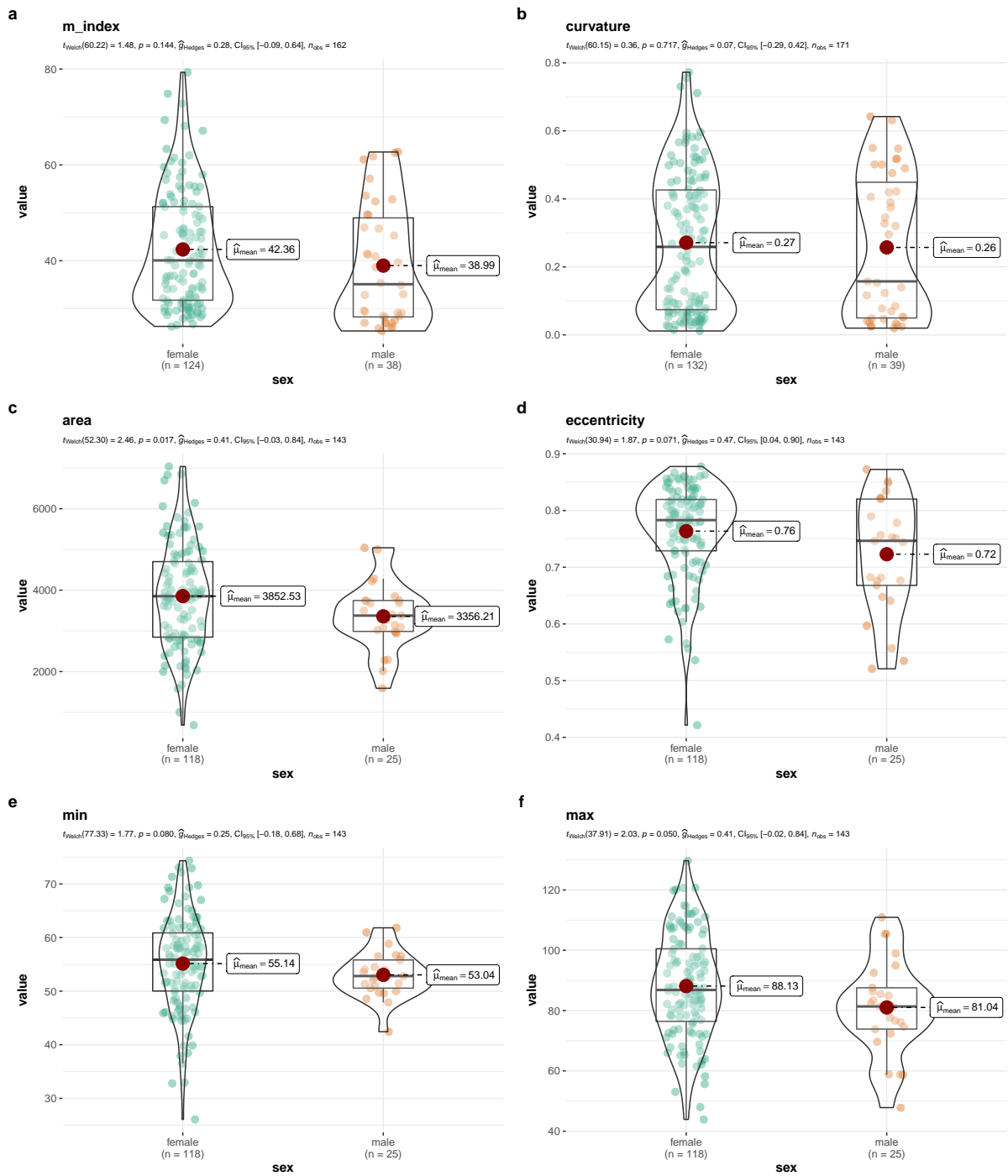


**Figure D.8. Violin plots showing phenotypic distributions for each phenotype per self-reported sex.** a, Melanin Index b, median hair fiber curvature c, cross-sectional area d, cross-sectional eccentricity e, minimum diameter of cross-section f, maximum diameter of cross-section.

## D.4 Ancestry vs. hair morphology

We carried out a number of analyses using the genotype data collected for this diverse sample. In an admixed sample where a continuous trait has divergent distributions in the parental ancestry groups, the resulting admixed population can show a correlation between ancestry and that trait. Finding such a correlation suggests may imply a polygenic trait with high heritability.

Here we plot the correlation between proportion of African ancestry and m-index, curvature, area, minimum diameter, maximum diameter, and area (using the median for each).

### D.4.1 Uncorrected

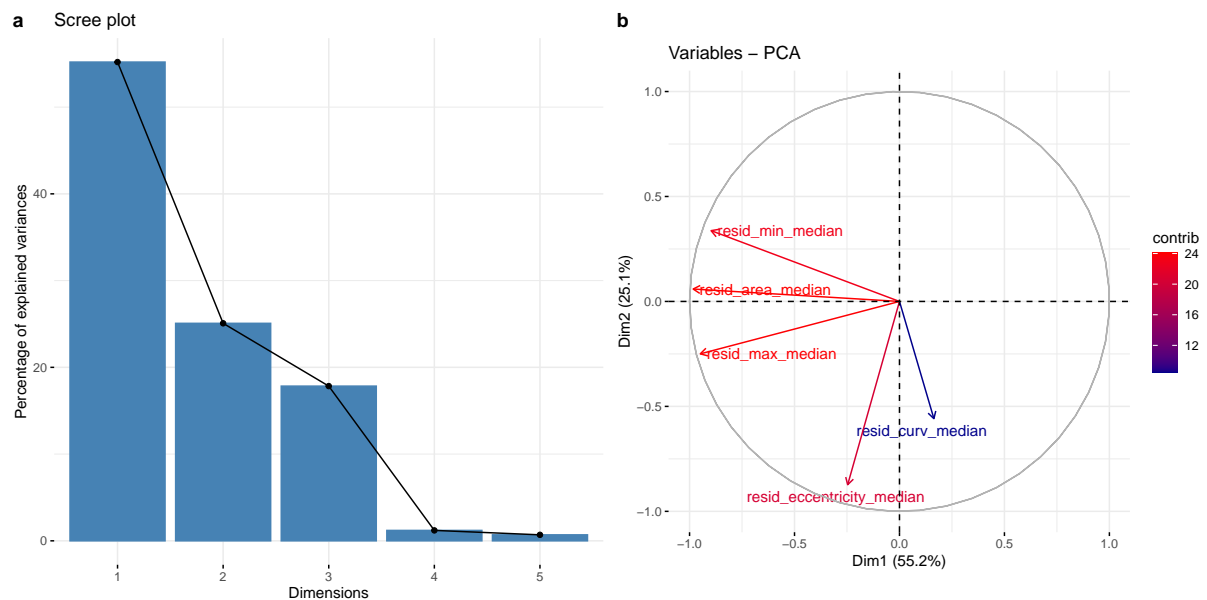


**Figure D.9. PCA results for quantitative hair phenotypes (without ancestry correction).** **a**, Scree plot showing the percentage of variance explained for each PC **b**, Contributing variables for first two PC dimensions.

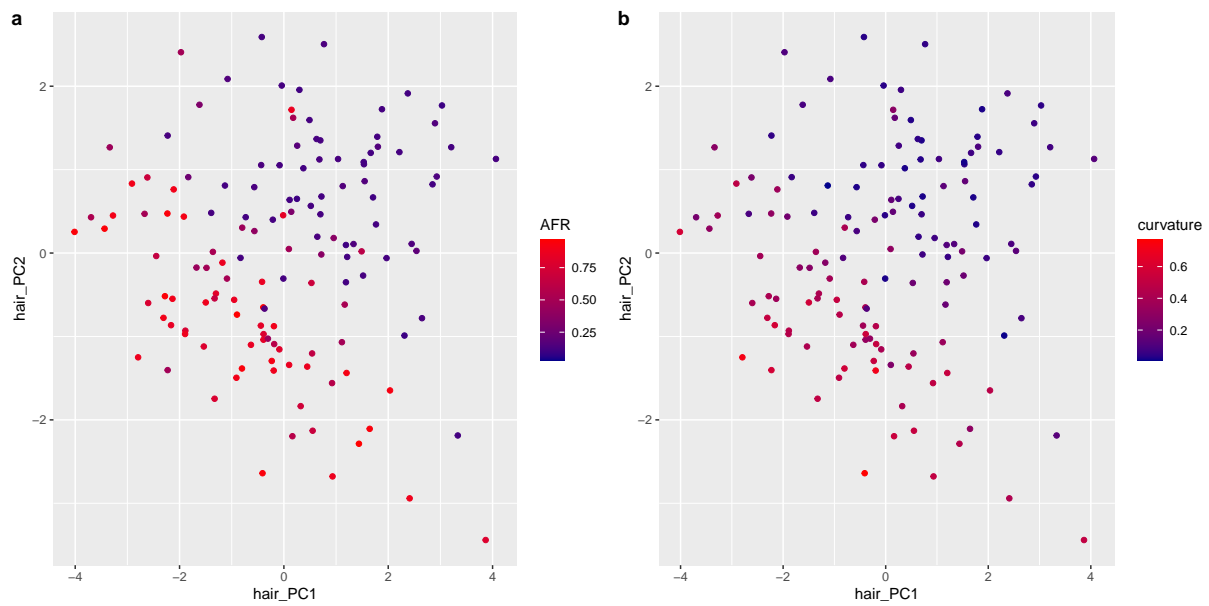


**Figure D.10. Scatter plot of individual PC scores along first two dimensions a,** Individual points colored according to proportion of AFR ancestry **b,** Individual points colored according to median hair fiber curvature

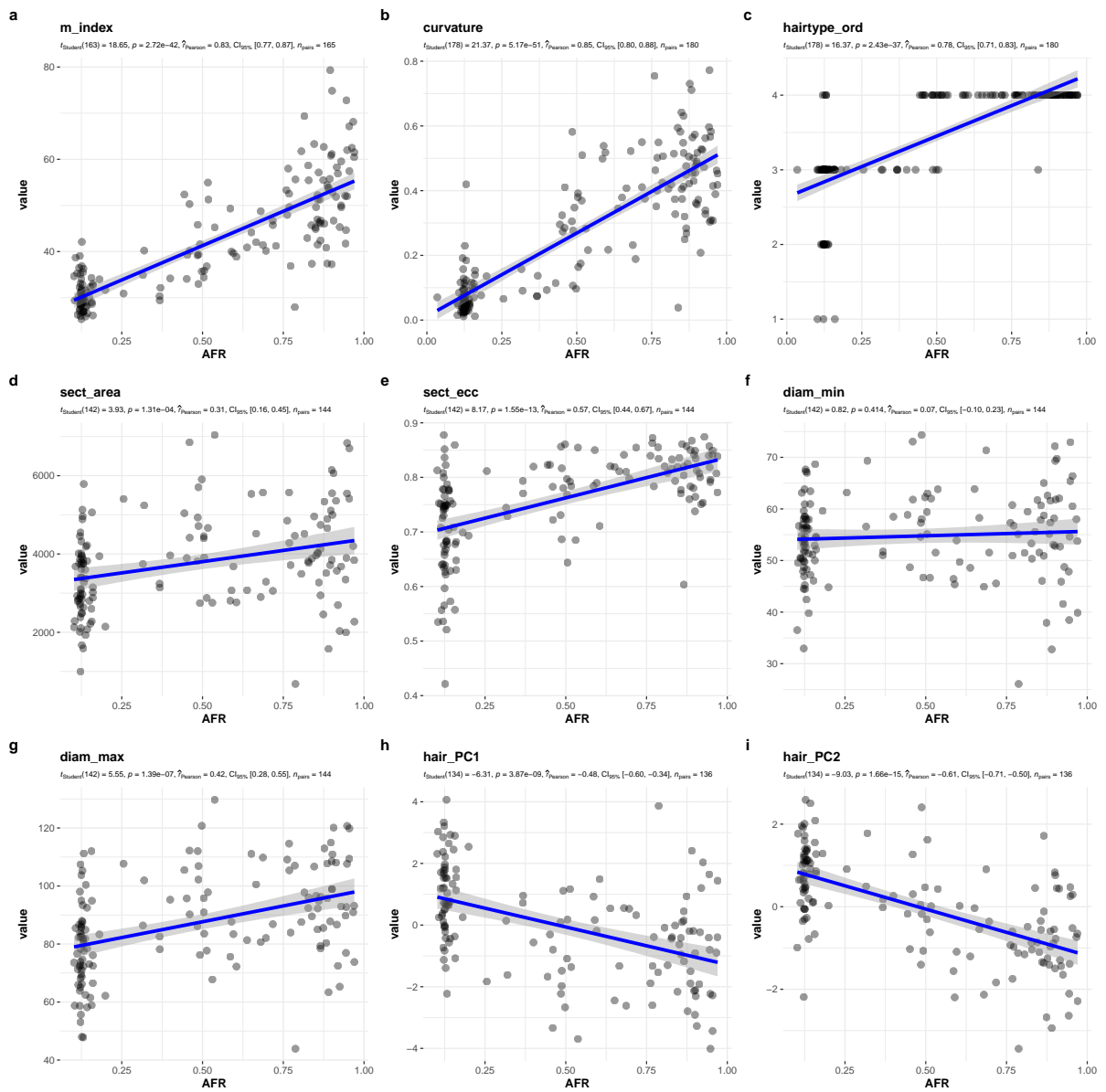
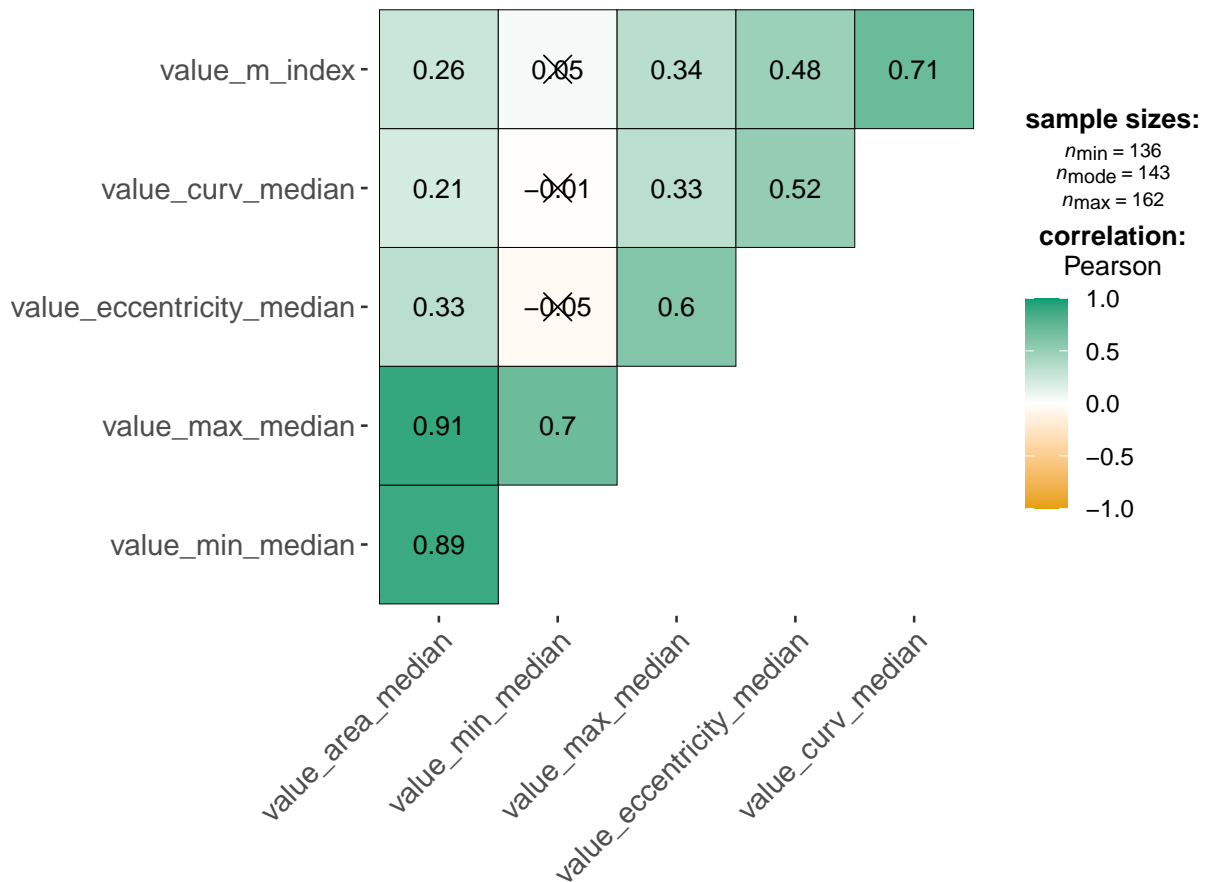


**Figure D.11. Scatter plots of all phenotypes against AFR ancestry** **a**, Melanin Index **b**, median hair curvature **c**, objectively classified hair texture **d**, cross-sectional area **e**, cross-sectional eccentricity **f**, minimum cross-sectional diameter **g**, maximum cross-sectional diameter **h**, PC1 for quantitative hair variables **i**, PC2 for quantitative hair variables.



X = non-significant at  $p < 0.05$  (Adjustment: Holm)

**Figure D.12. Correlation matrix of quantitative hair variables and Melanin Index.**

This correlation matrix shows the correlation between each of the phenotypes without correction for ancestry.

## D.4.2 Corrected

We repeat all of the analyses with a correction for ancestry. For the phenotypes, this means that we residualized the values against the proportion of AFR ancestry. We show the PCA results in Figures D.13, D.14 and the scatter plots of the phenotypic values against ancestry to demonstrate the correction (Fig. D.15), as well as the correlation matrix between the traits (Figure D.16). As we have taken ancestry out of the equation, we would not expect to see a correlation with AFR anymore, however, it is interesting that the first two PCs on residualized hair traits do not pick up a signal relating to curvature (Figure D.14). Similarly, the scatter plots comparing phenotypic value to AFR ancestry serve mostly to demonstrate the adequacy of the correction. However, it is

interesting to note that there is a surprisingly high range of variability in the individuals with low AFR ancestry for a number of phenotypes, including eccentricity (Figure D.15).

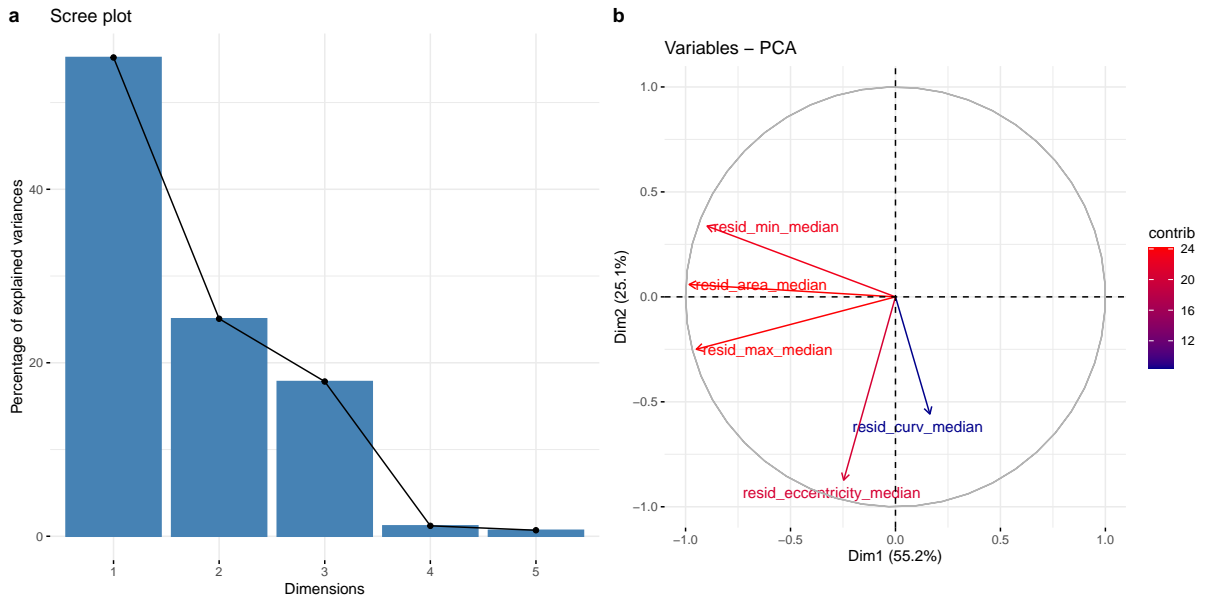


**Figure D.13. PCA results for quantitative hair phenotypes (with correction, using residualized phenotypic values).** **a**, Scree plot showing the percentage of variance explained for each PC **b**, Contributing variables for first two PC dimensions.

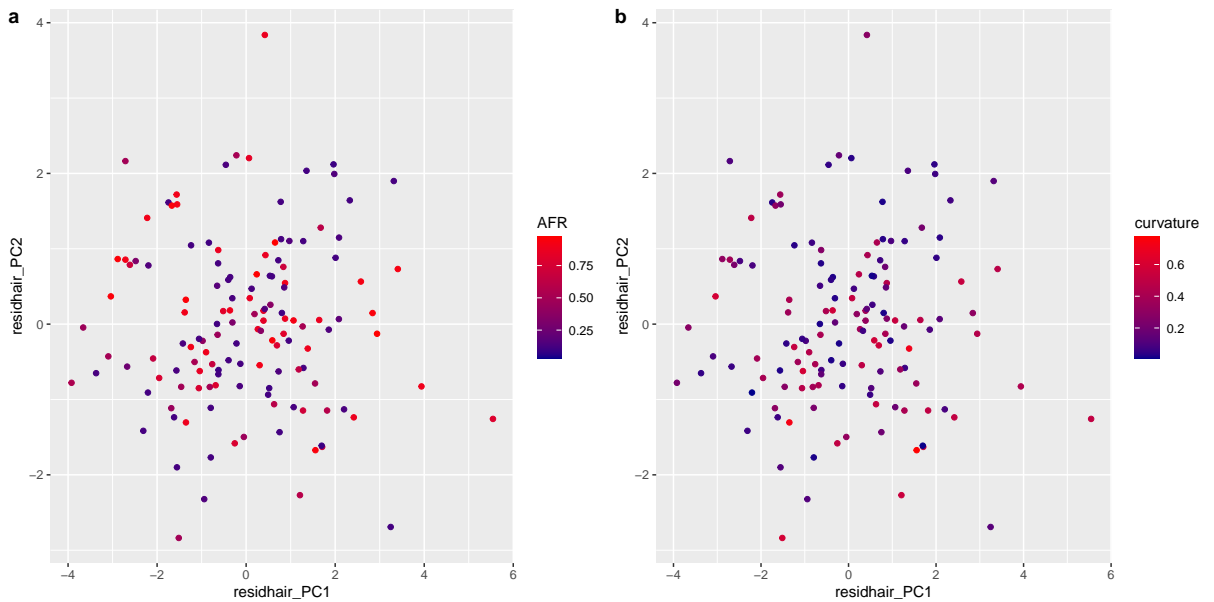


**Figure D.14. Scatter plot of individual PC scores along first two dimensions** **a**, Individual points colored according to proportion of AFR ancestry **b**, Individual points colored according to median hair fiber curvature

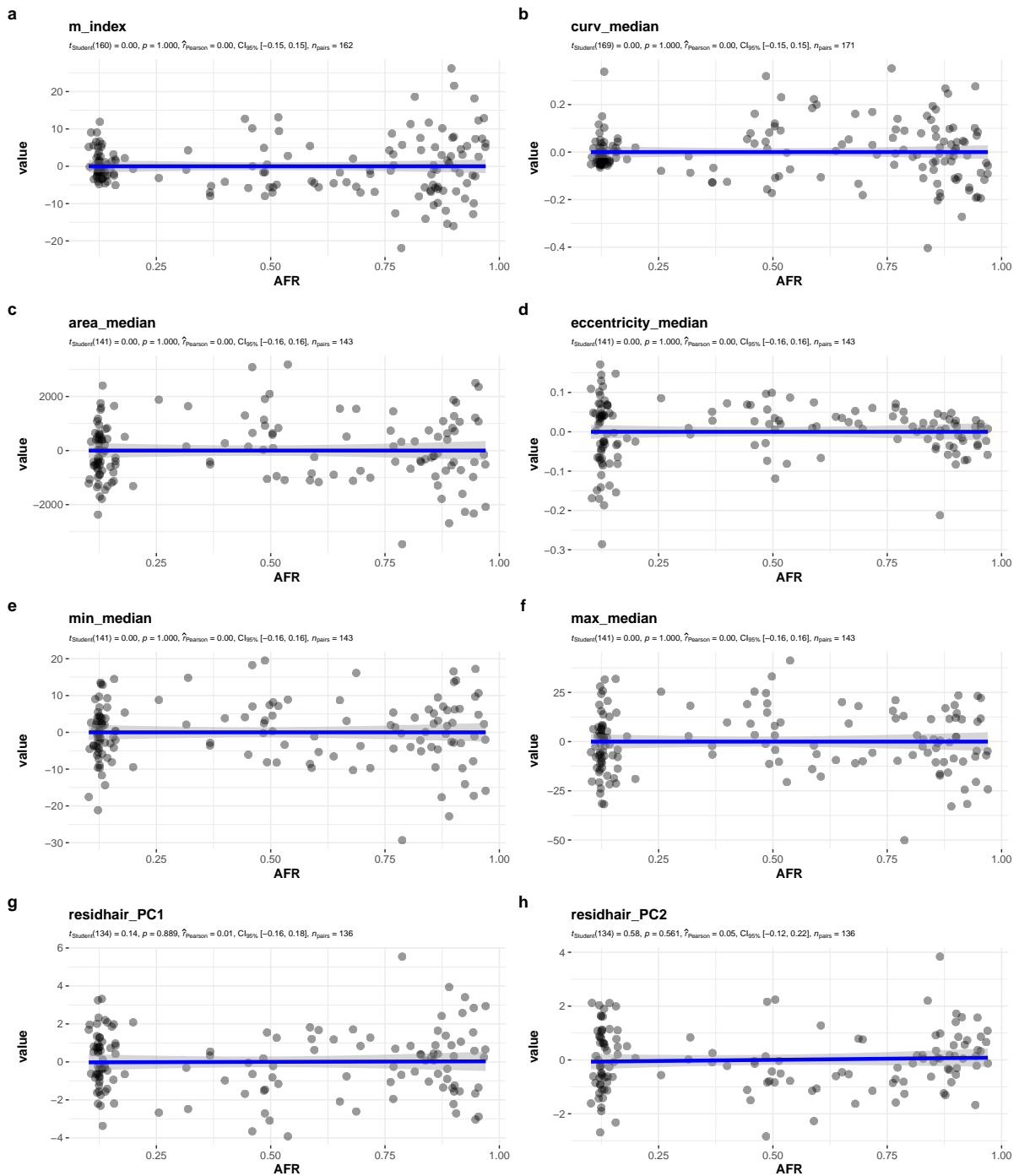
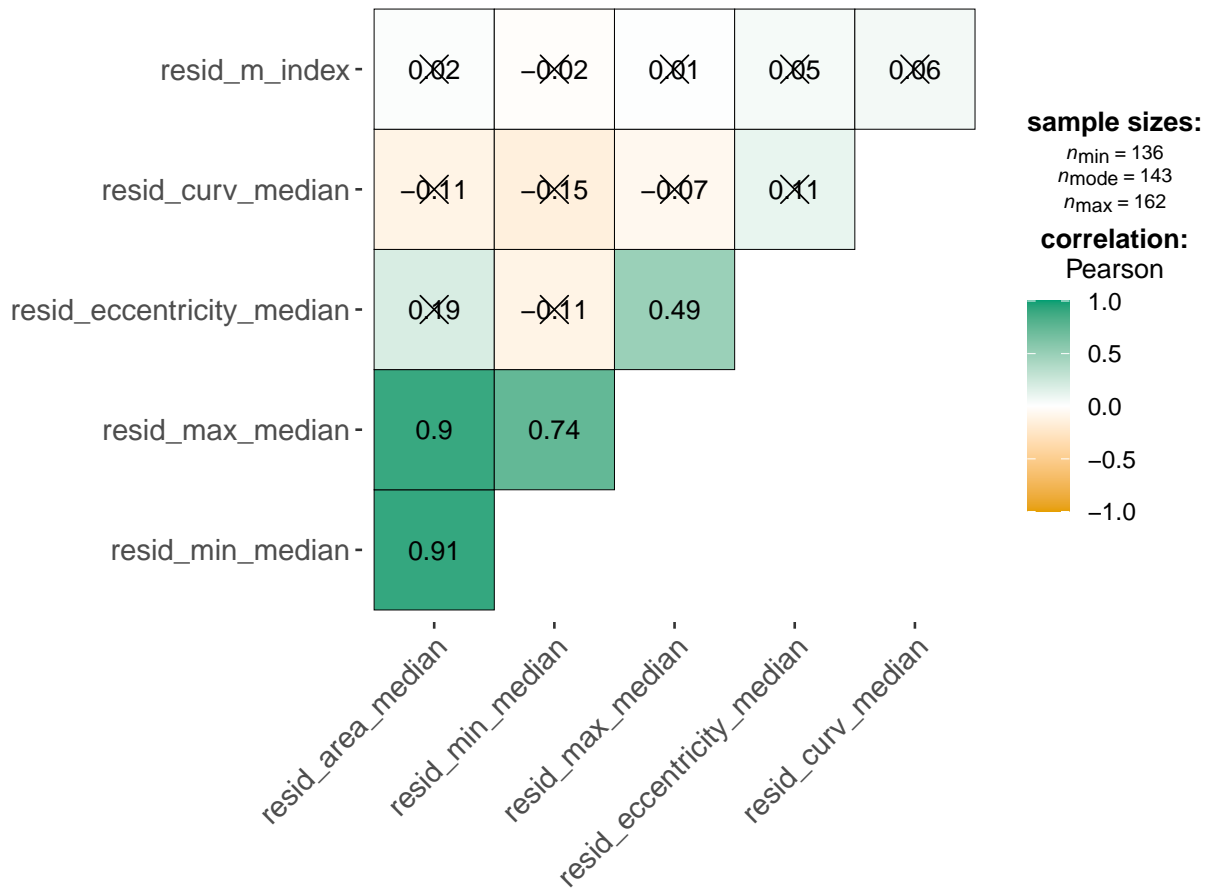


Figure D.15. Scatter plots of all phenotypes (residualized) against AFR ancestry a, Melanin Index b, median hair curvature c, objectively classified hair texture d, cross-sectional area e, cross-sectional eccentricity f, minimum cross-sectional diameter g, maximum cross-sectional diameter h, PC1 for quantitative hair variables i, PC2 for quantitative hair variables.



X = non-significant at  $p < 0.05$  (Adjustment: Holm)

**Figure D.16. Correlation matrix of quantitative hair variables and Melanin Index.** This correlation matrix shows the correlation between each of the phenotypes with correction for ancestry.

As a number of the cross-sectional traits appear to be correlated even after correcting for ancestry, we wanted to explore these relationships further and plot them below (Figure D.17).

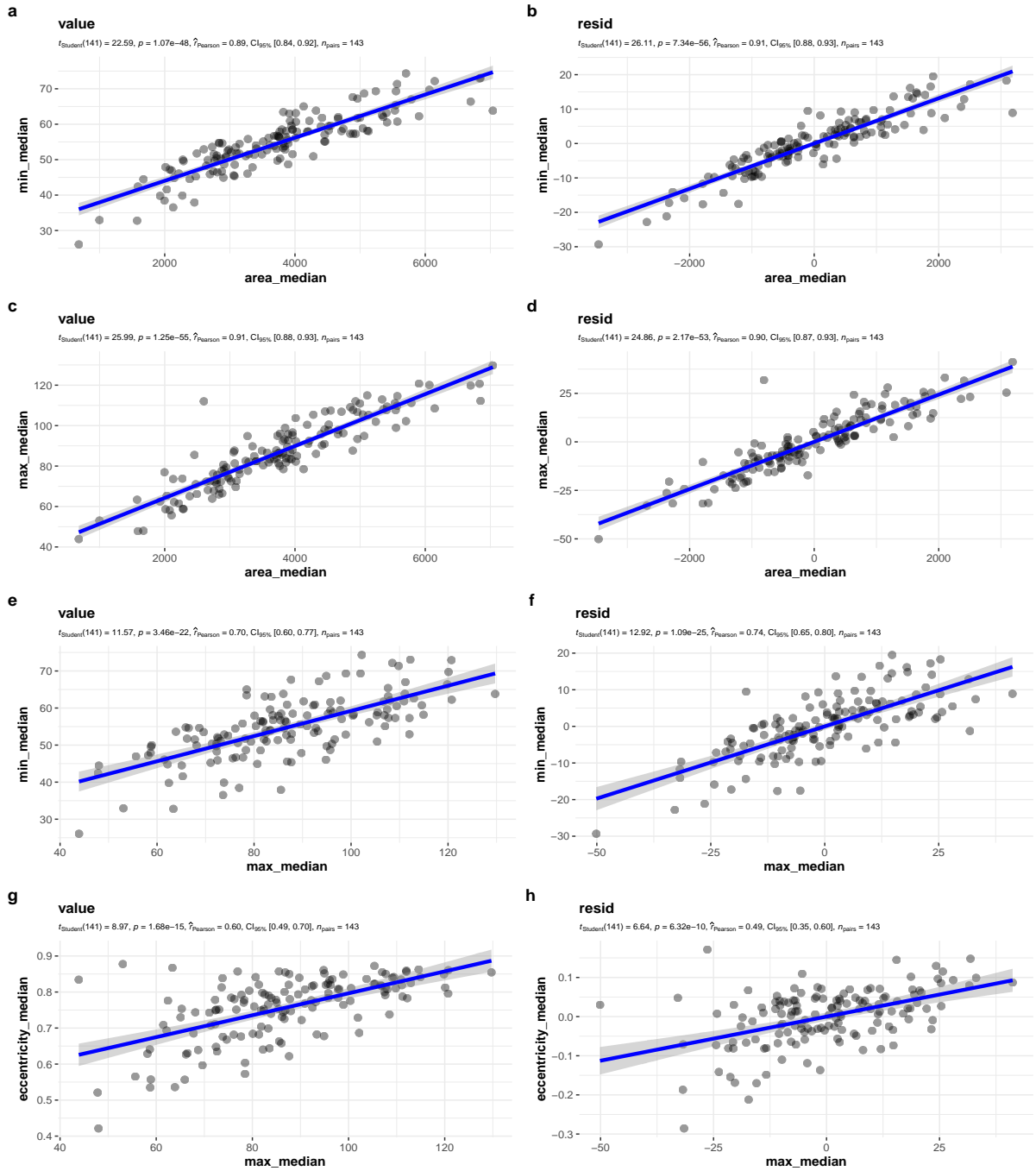


**Figure D.17.** Scatter plots of raw phenotypes of interest (left) against their residualized comparison (right) **a**, Cross-sectional area vs. minimum cross-sectional diameter **b**, Cross-sectional area vs. minimum cross-sectional diameter (residualized) **c**, Cross-sectional area vs. maximum cross-sectional diameter **d**, Cross-sectional area vs. maximum cross-sectional diameter (residualized) **e**, Maximum cross-sectional diameter vs. minimum cross-sectional diameter **f**, Maximum cross-sectional diameter vs. minimum cross-sectional diameter (residualized) **g**, Maximum cross-sectional diameter vs. cross-sectional eccentricity **h** Maximum cross-sectional diameter vs. cross-sectional eccentricity (residualized)

## D.5 Comparison with categorical

Finally, we compare the categorical data we have available for our sample with ancestry and quantitative curvature. We present the same scatter plot with AFR ancestry on the x-axis and median hair fiber curvature on the y-axis, but with objective classification overlaid and with self-reported hair texture (Figure D.18). We only had self-reported hair texture for a subset of the individuals and more information on the details of the objective classification can be found in Appendix C.

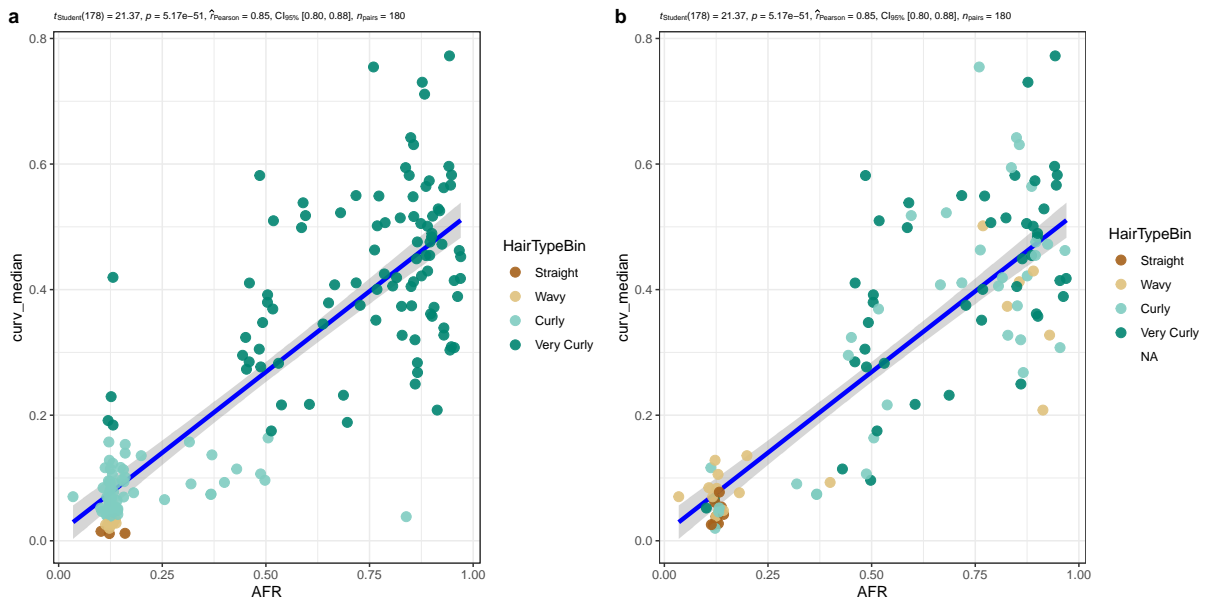


**Figure D.18. Categorical hair texture compared to quantitative hair curvature and proportion of AFR ancestry** **a**, Hair texture here is classified objectively according to cut offs suggested by Loussouarn et al. (2007) and **b**, shows hair texture according to participant self-report.

# **Appendix E | Chapter 4 Supplementary: Admixture & phenotype correla- tions for $> 15\%$ AFR ancestry**

## **E.1 Phenotypic distributions**

We repeat the analyses shown in Appendix D with a subset of individuals with  $>15\%$  AFR ancestry to demonstrate that the results stand despite the individuals included with low AFR ancestry.

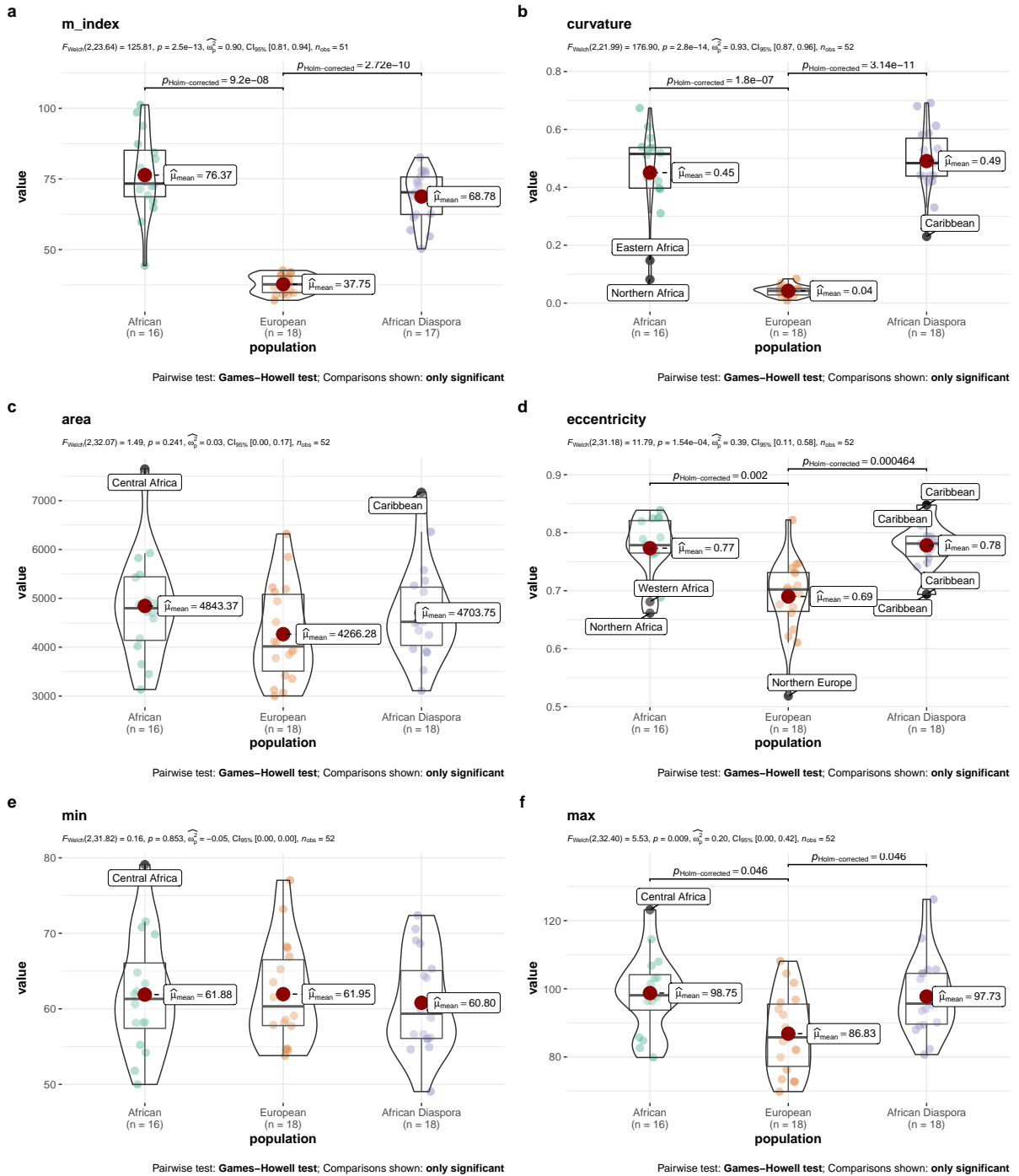


**Figure E.1. Violin plots showing phenotypic distributions for each phenotype for the reference samples. a, Melanin Index b, median hair fiber curvature c, cross-sectional area d, cross-sectional eccentricity e, minimum diameter of cross-section f, maximum diameter of cross-section.**

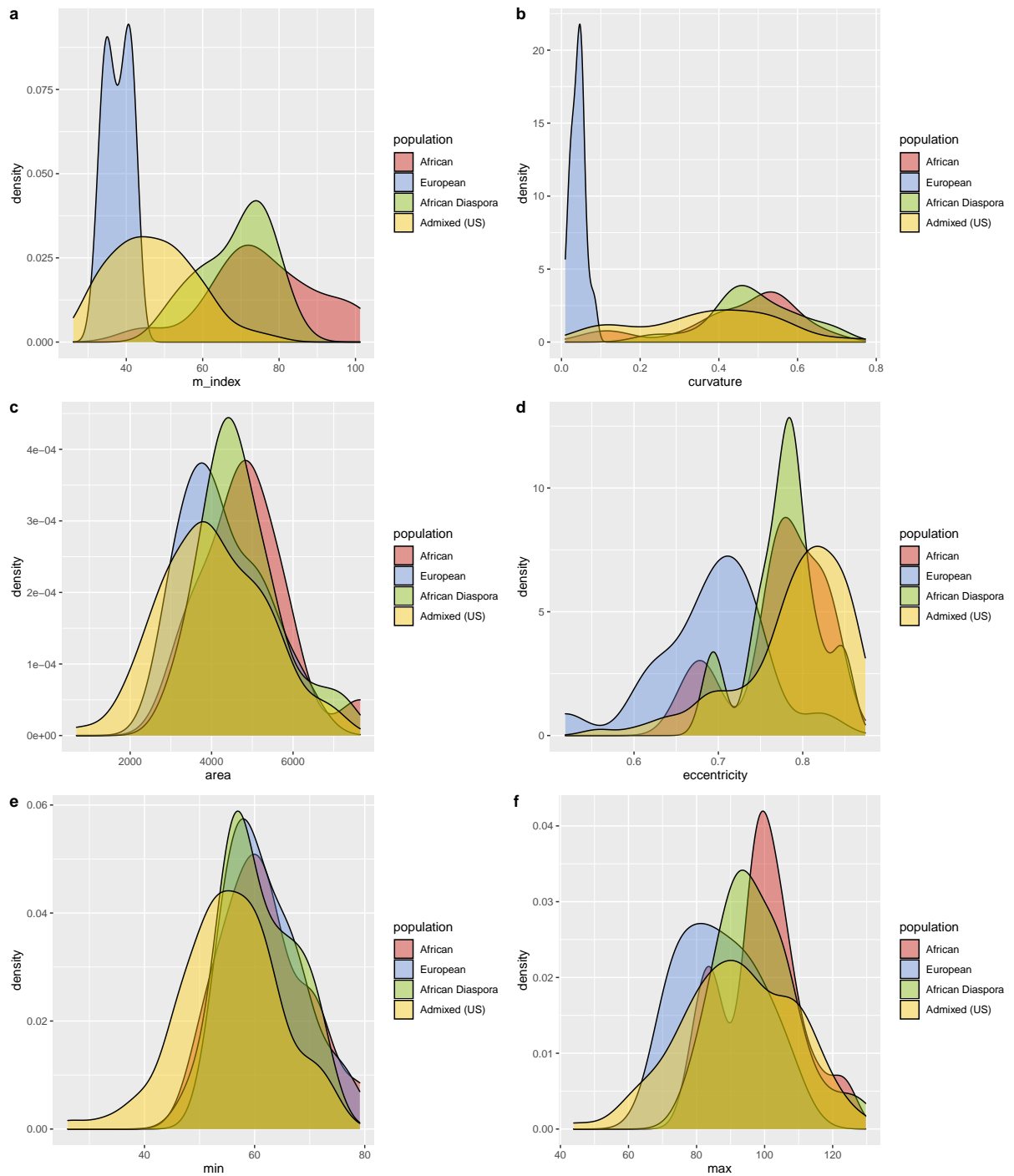


**Figure E.2.** Density plots showing phenotypic distributions for each phenotype for the reference samples and the current sample marked as Admixed (US). **a**, Melanin Index **b**, median hair fiber curvature **c**, cross-sectional area **d**, cross-sectional eccentricity **e**, minimum diameter of cross-section **f**, maximum diameter of cross-section.

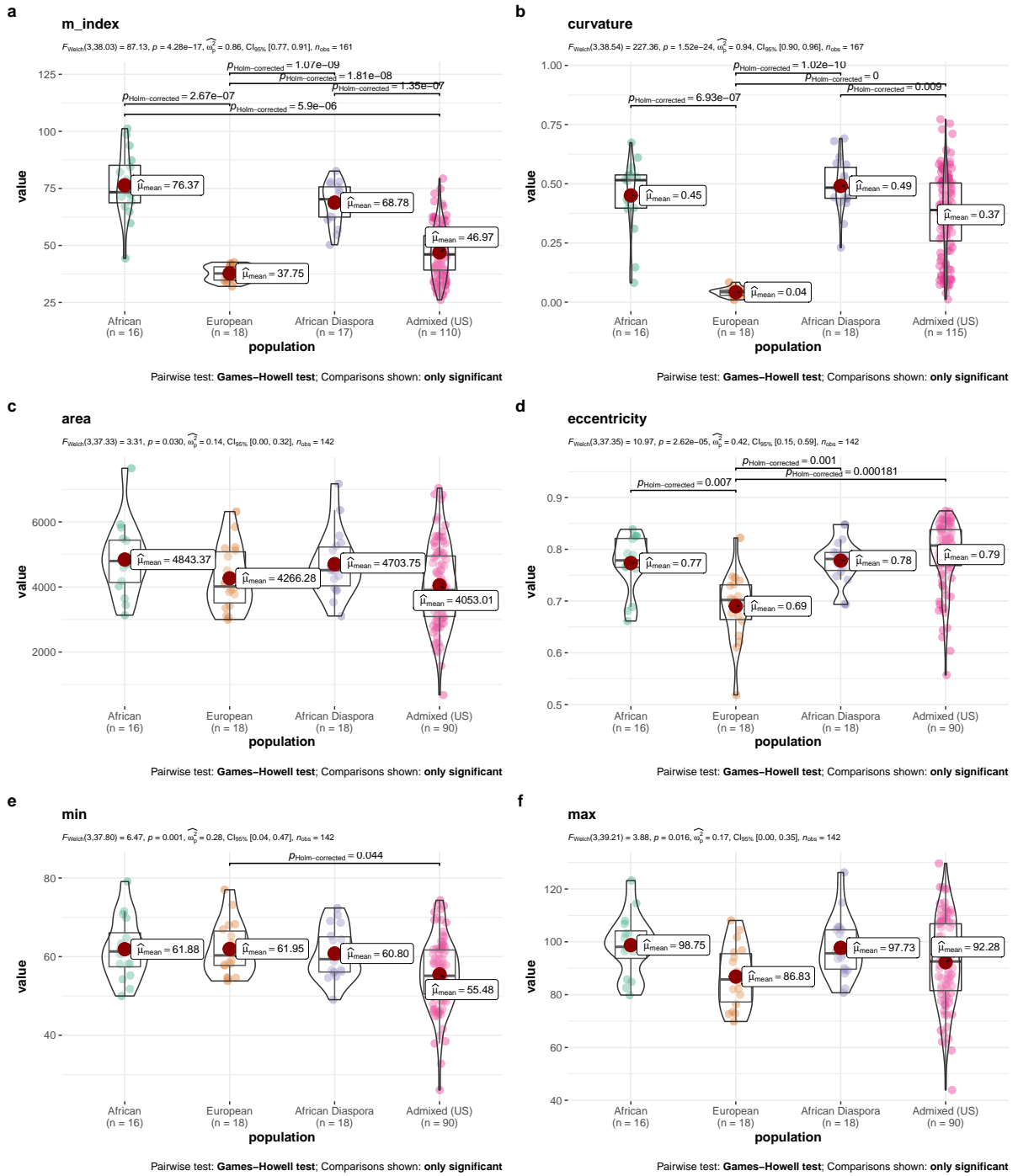


**Figure E.3. Violin plots showing phenotypic distributions for each phenotype for the reference samples and the current sample marked as Admixed (US). a, Melanin Index b, median hair fiber curvature c, cross-sectional area d, cross-sectional eccentricity e, minimum diameter of cross-section f, maximum diameter of cross-section.**

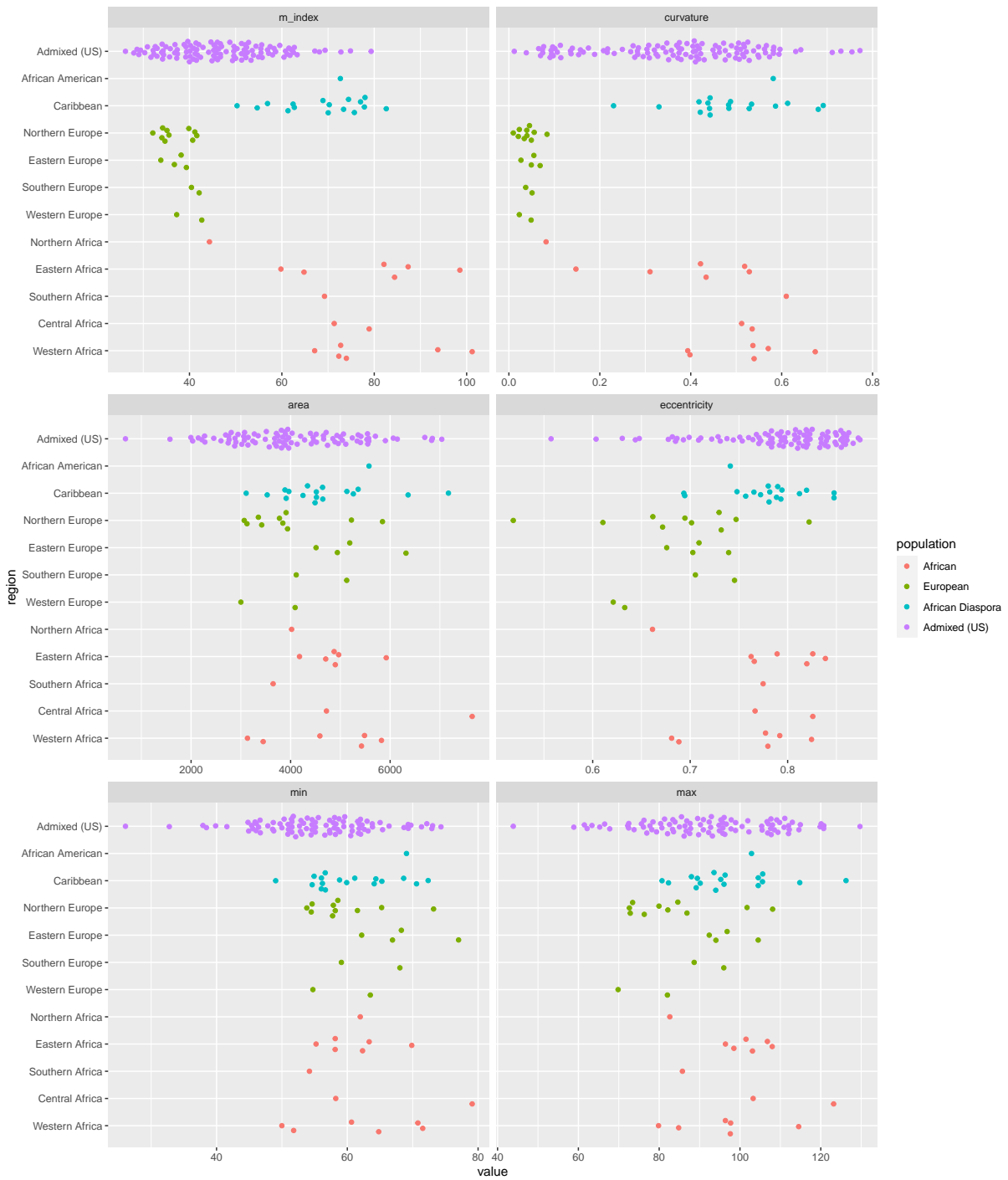


**Figure E.4.** Grouped scatter plots showing phenotypic distributions for each phenotype for the reference samples with regional details and the current sample marked as **Admixed (US)**. **a**, Melanin Index **b**, median hair fiber curvature **c**, cross-sectional area **d**, cross-sectional eccentricity **e**, minimum diameter of cross-section **f**, maximum diameter of cross-section.

## **E.2 Sex differences**

The distribution of female/male-identified individuals is skewed, with a higher proportion of the sample being female (n=89 and males being n=22). There appear to be no considerable differences in distribution between these sexes in our sample (see Figures E.5 and E.6).

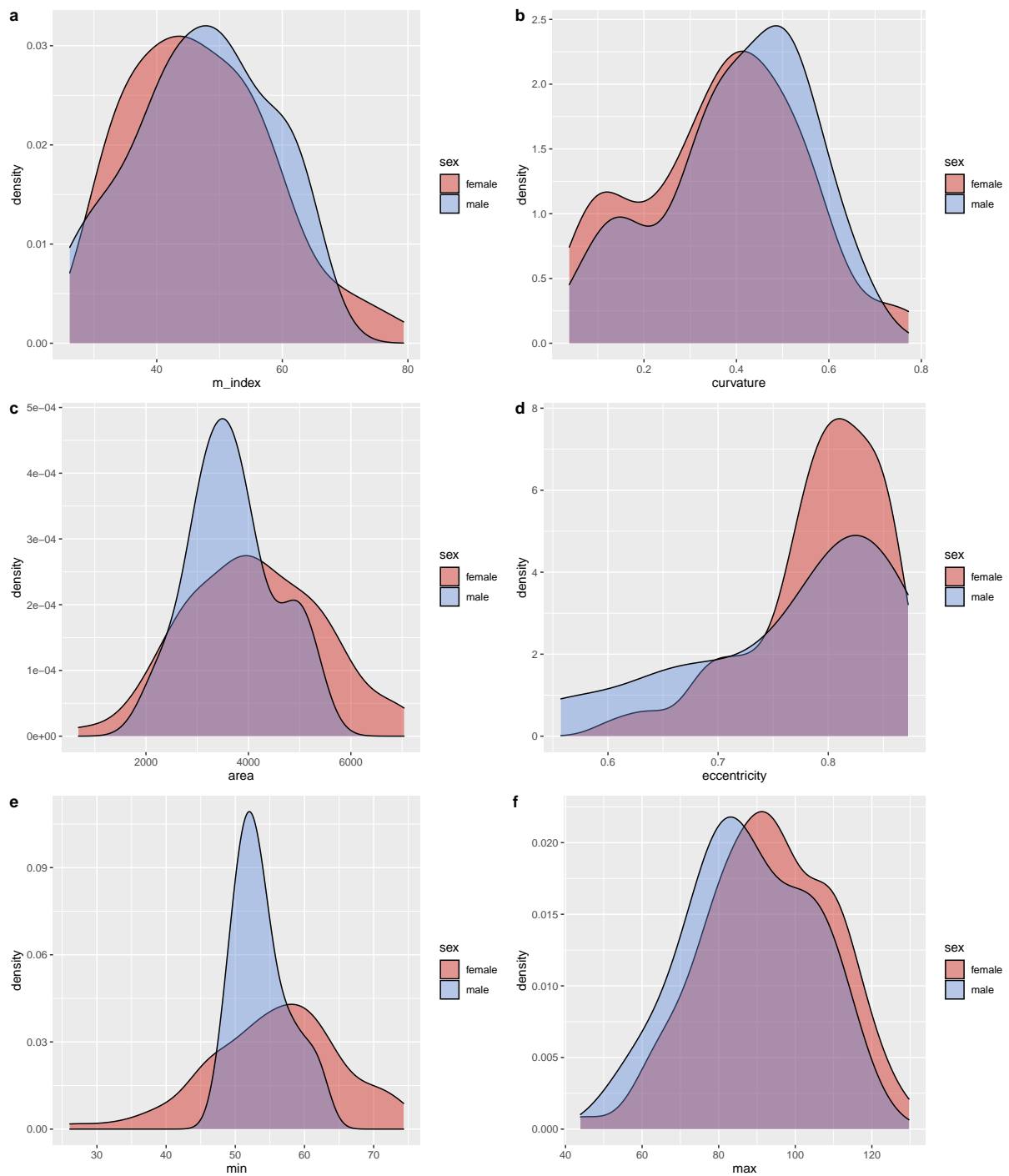


**Figure E.5. Density plots showing phenotypic distributions for each phenotype per self-reported sex. a, Melanin Index b, median hair fiber curvature c, cross-sectional area d, cross-sectional eccentricity e, minimum diameter of cross-section f, maximum diameter of cross-section.**

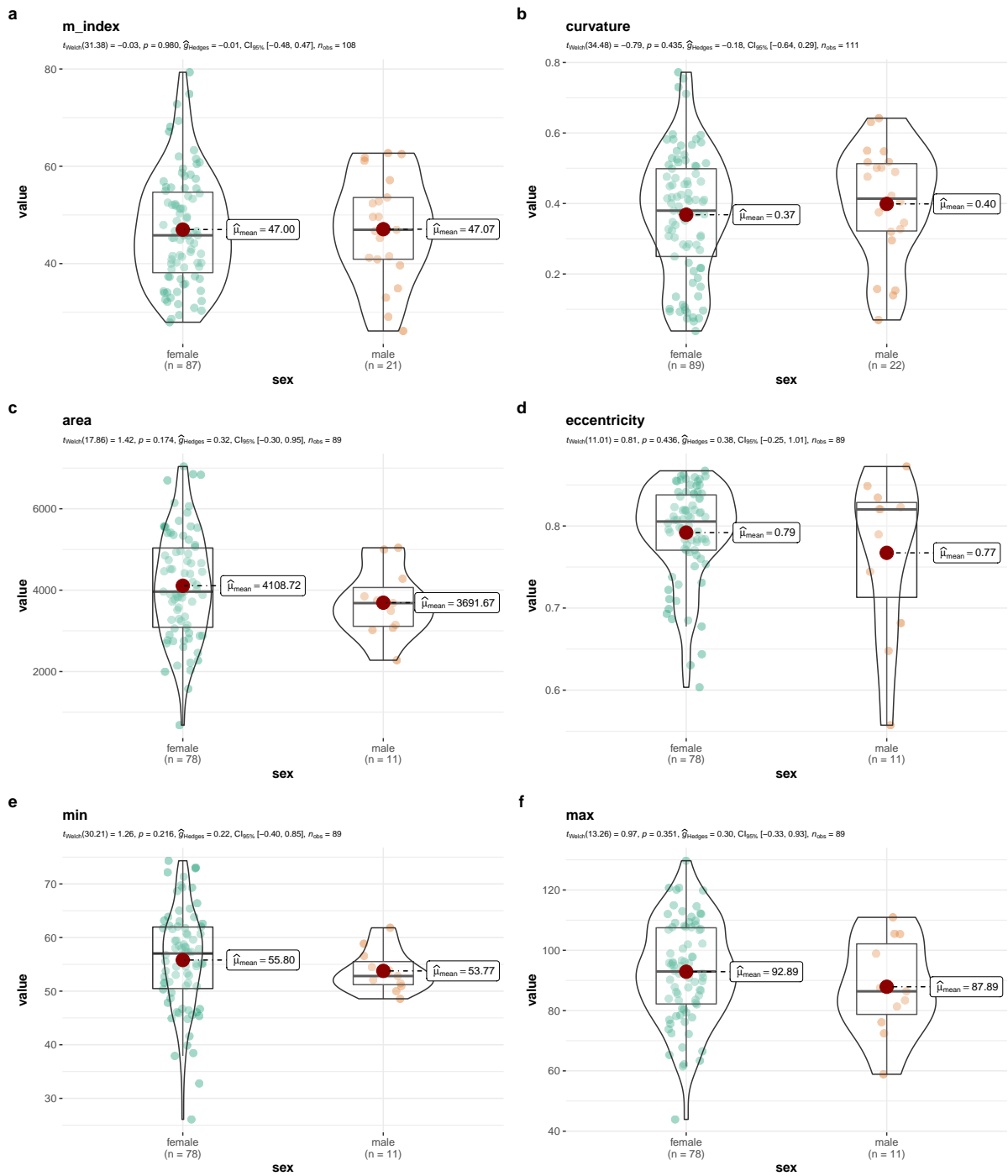


**Figure E.6. Violin plots showing phenotypic distributions for each phenotype per self-reported sex. a, Melanin Index b, median hair fiber curvature c, cross-sectional area d, cross-sectional eccentricity e, minimum diameter of cross-section f, maximum diameter of cross-section.**

## E.3 Ancestry vs. hair morphology

We carried out a number of analyses using the genotype data collected for this diverse sample. In an admixed sample where a continuous trait has divergent distributions in the parental ancestry groups, the resulting admixed population can show a correlation between ancestry and that trait. Finding such a correlation suggests may imply a polygenic trait with high heritability.

Here we plot the correlation between proportion of African ancestry and m-index, curvature, area, minimum diameter, maximum diameter, and area (using the median for each).

### E.3.1 Uncorrected

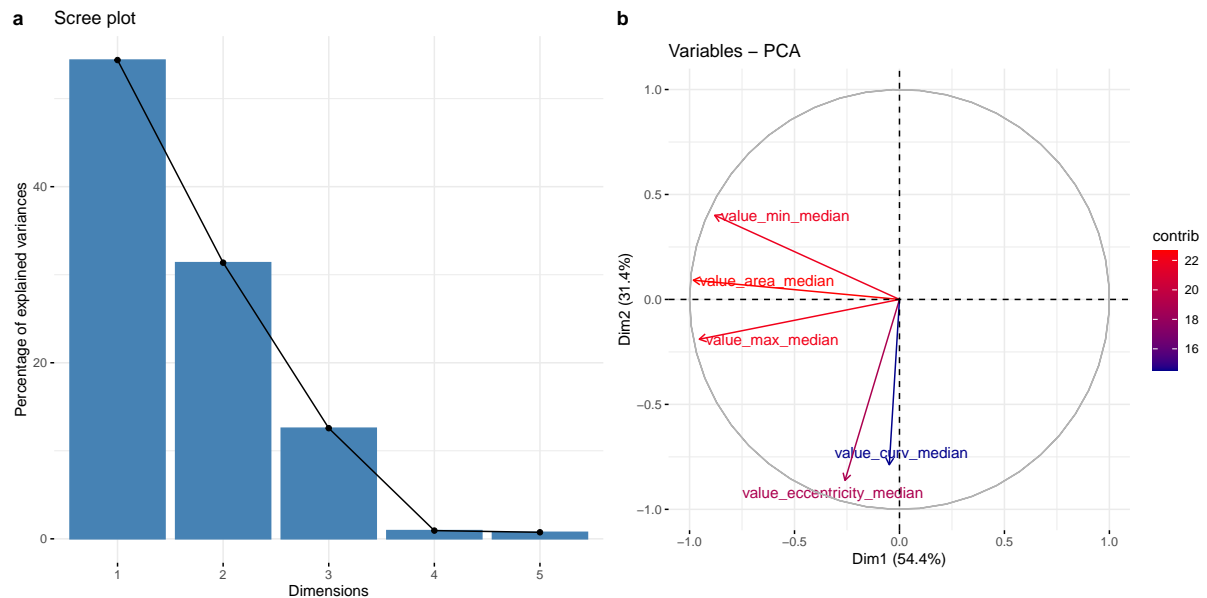


**Figure E.7. PCA results for quantitative hair phenotypes (without ancestry correction).** **a**, Scree plot showing the percentage of variance explained for each PC **b**, Contributing variables for first two PC dimensions.

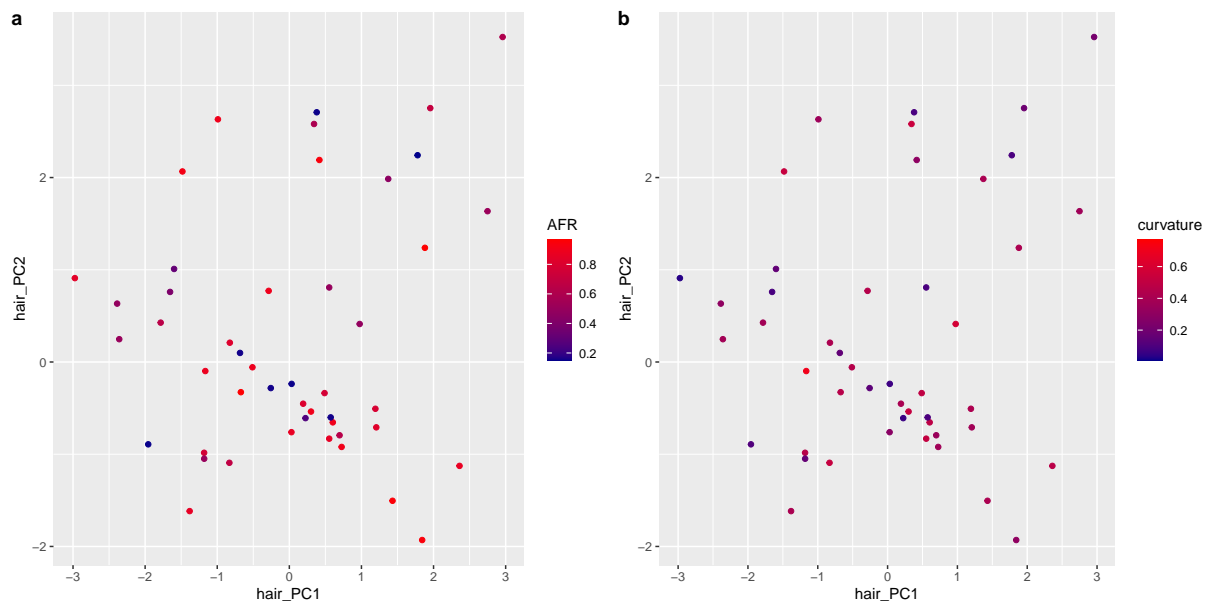


**Figure E.8. Scatter plot of individual PC scores along first two dimensions a,** Individual points colored according to proportion of AFR ancestry **b,** Individual points colored according to median hair fiber curvature

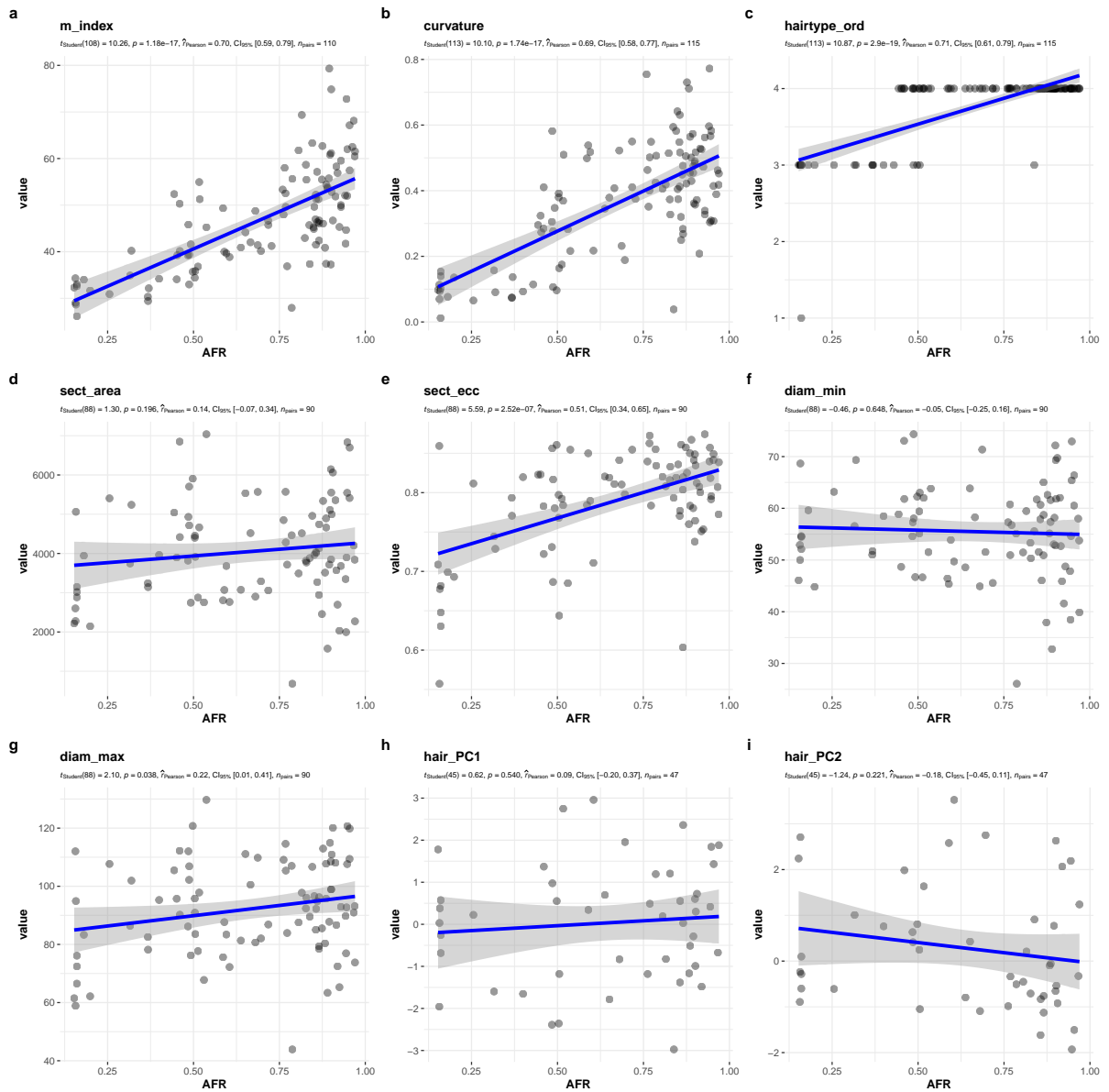


**Figure E.9. Scatter plots of all phenotypes against AFR ancestry a, Melanin Index b, median hair curvature c, objectively classified hair texture d, cross-sectional area e, cross-sectional eccentricity f, minimum cross-sectional diameter g, maximum cross-sectional diameter h, PC1 for quantitative hair variables i, PC2 for quantitative hair variables.**

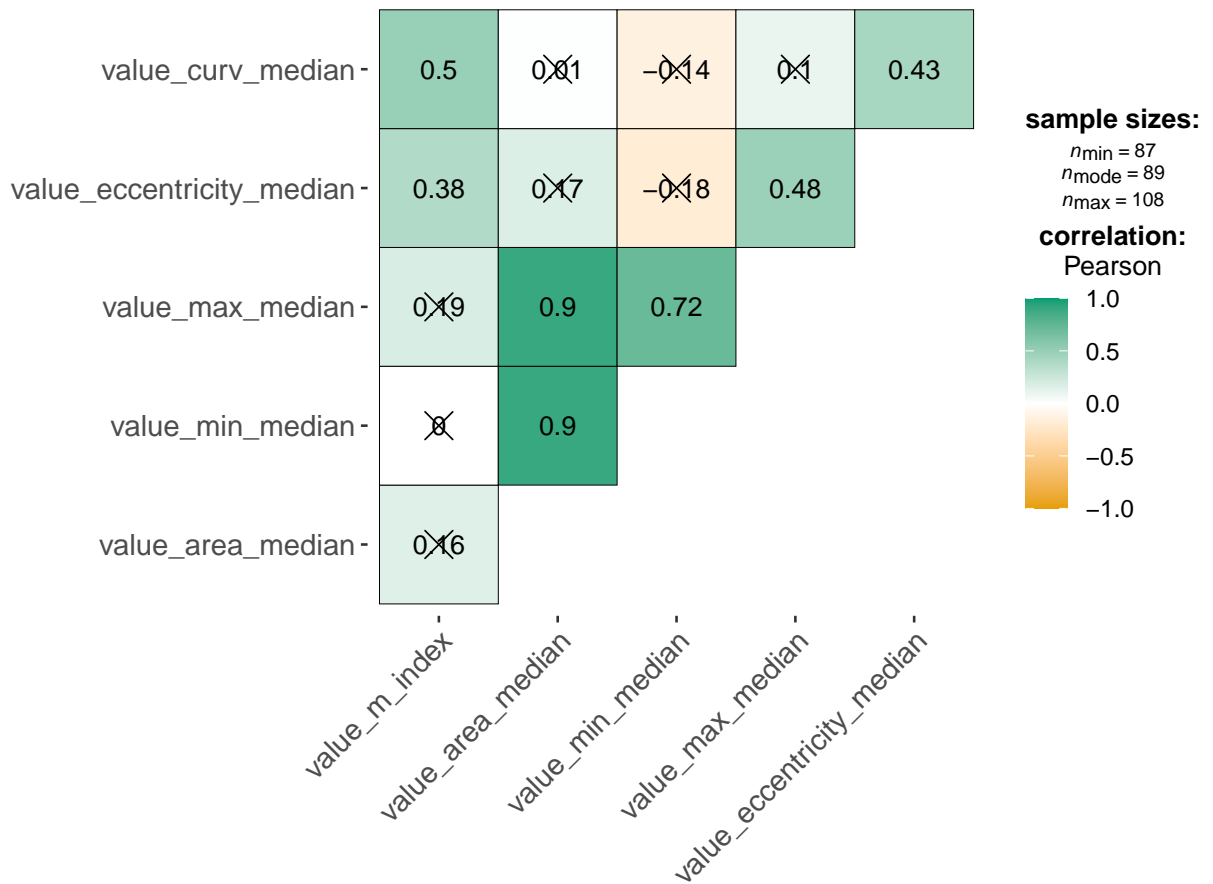


**Figure E.10. Correlation matrix of quantitative hair variables and Melanin Index.** This correlation matrix shows the correlation between each of the phenotypes without correction for ancestry.

### E.3.2 Corrected

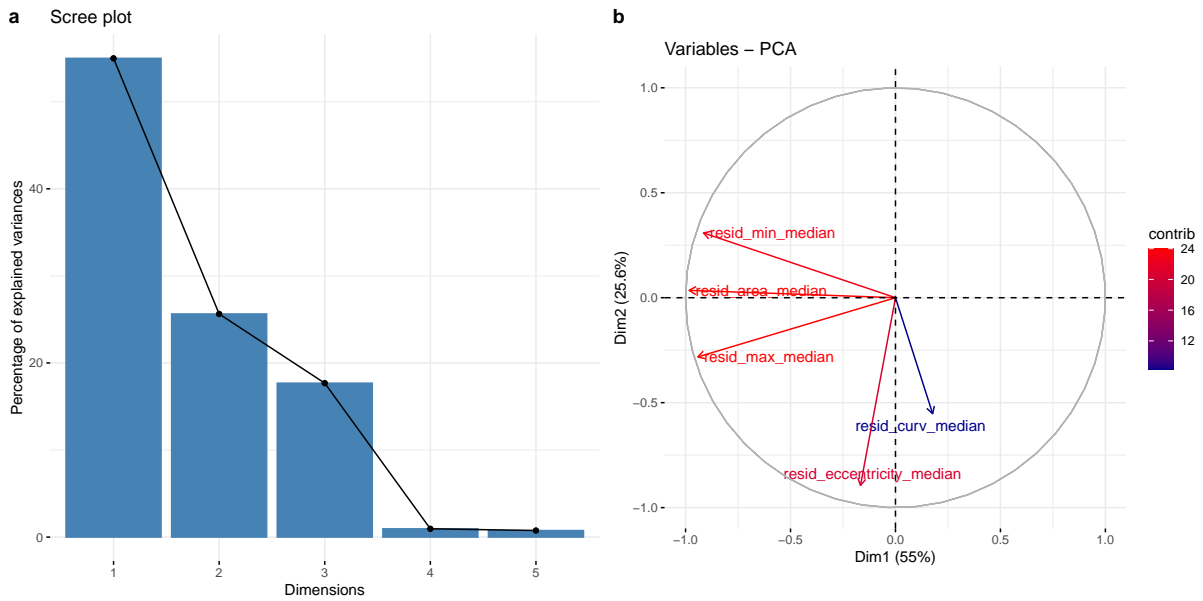


**Figure E.11. PCA results for quantitative hair phenotypes (with correction, using residualized phenotypic values).** **a**, Scree plot showing the percentage of variance explained for each PC **b**, Contributing variables for first two PC dimensions.

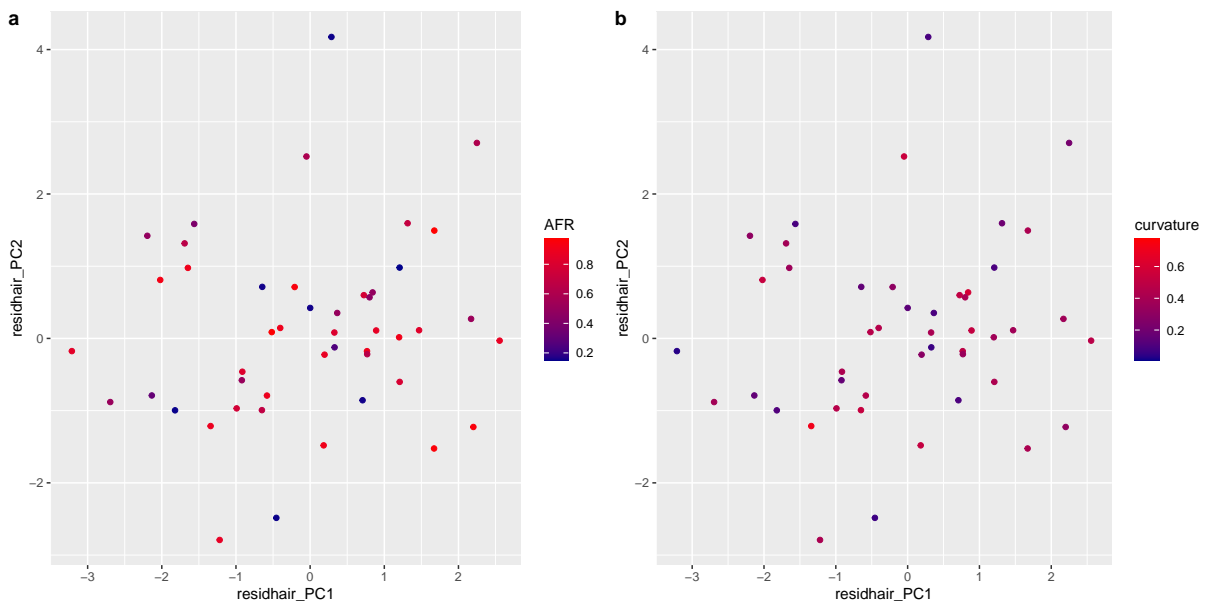


**Figure E.12. Scatter plot of individual PC scores along first two dimensions** **a**, Individual points colored according to proportion of AFR ancestry **b**, Individual points colored according to median hair fiber curvature

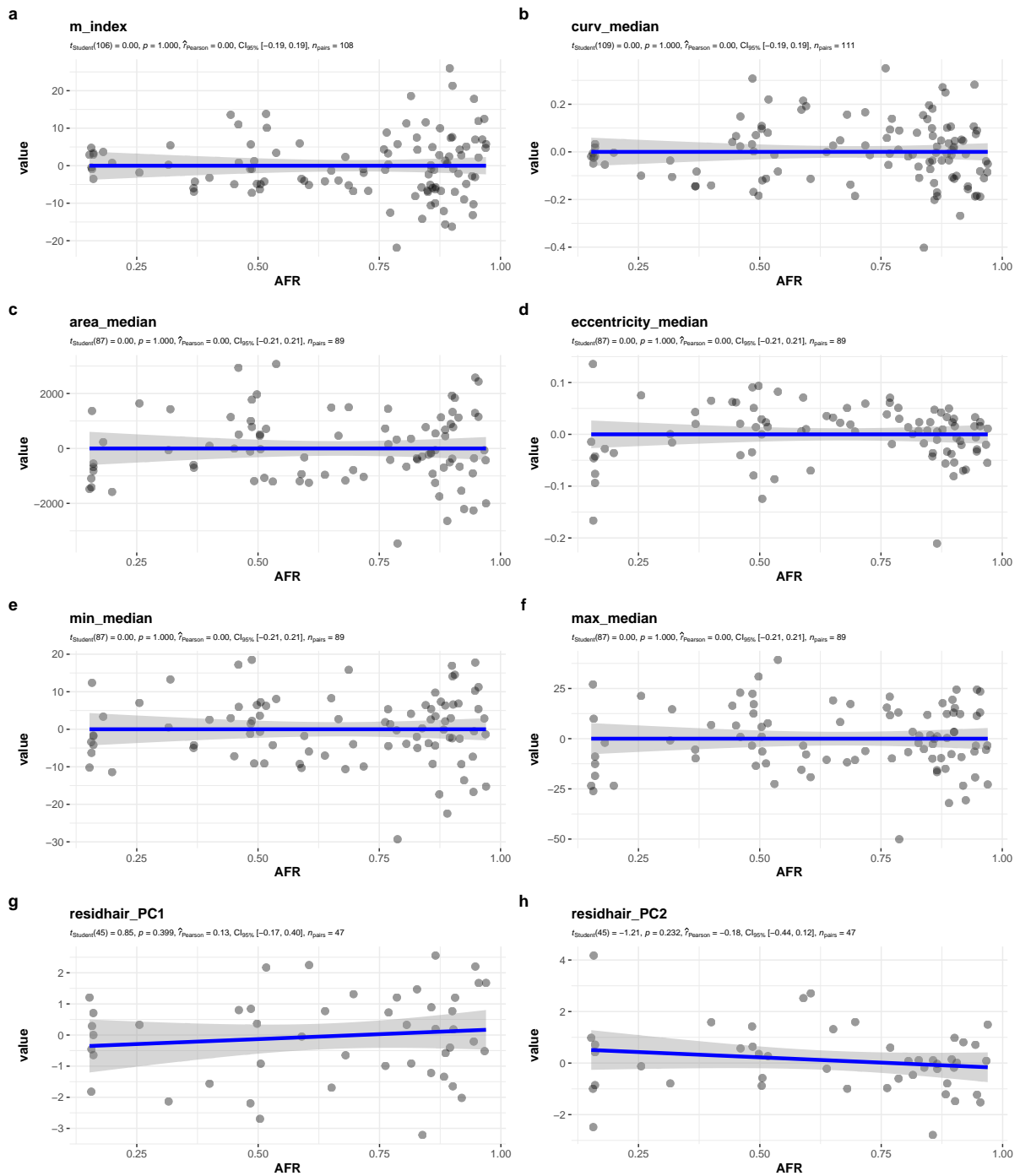
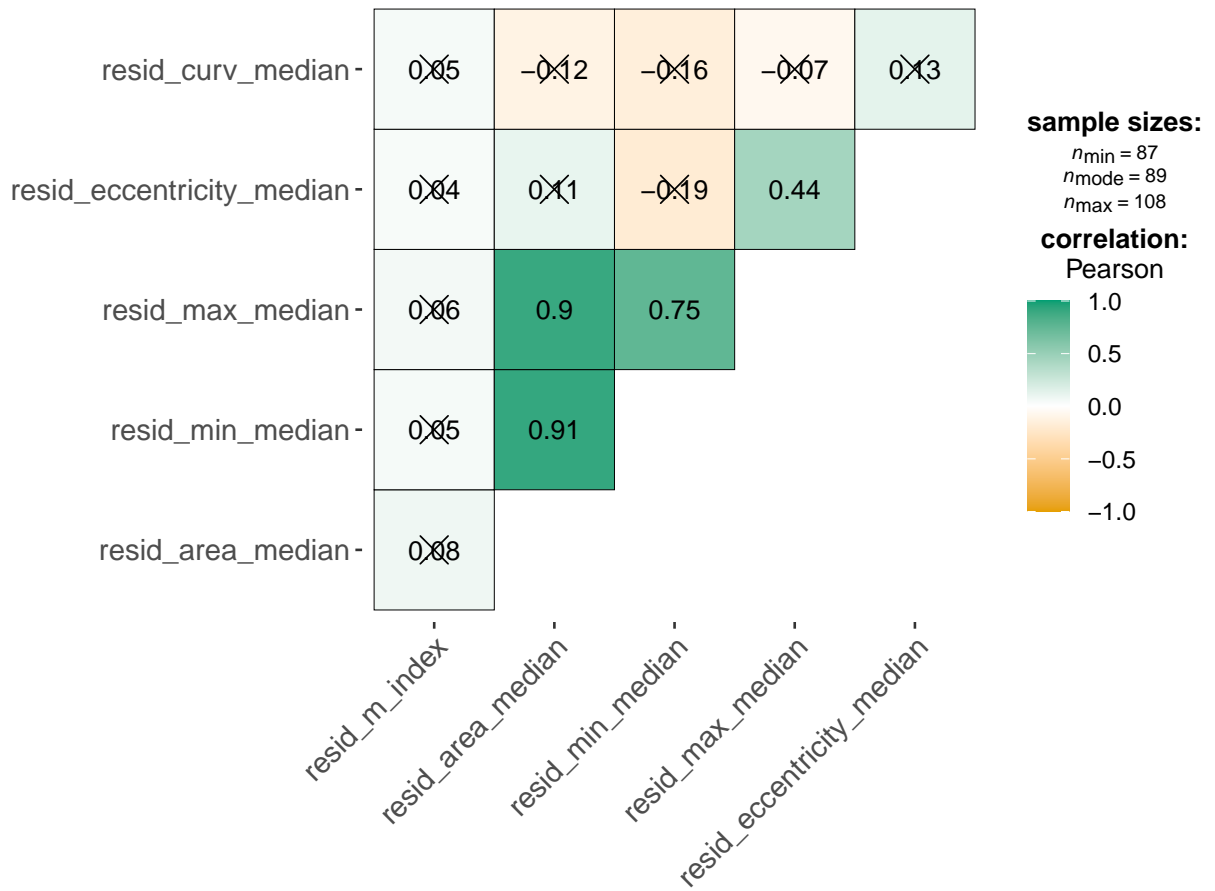


**Figure E.13.** Scatter plots of all phenotypes (residualized) against AFR ancestry **a**, Melanin Index **b**, median hair curvature **c**, objectively classified hair texture **d**, cross-sectional area **e**, cross-sectional eccentricity **f**, minimum cross-sectional diameter **g**, maximum cross-sectional diameter **h**, PC1 for quantitative hair variables **i**, PC2 for quantitative hair variables.



X = non-significant at  $p < 0.05$  (Adjustment: Holm)

**Figure E.14. Correlation matrix of quantitative hair variables and Melanin Index.** This correlation matrix shows the correlation between each of the phenotypes with correction for ancestry.

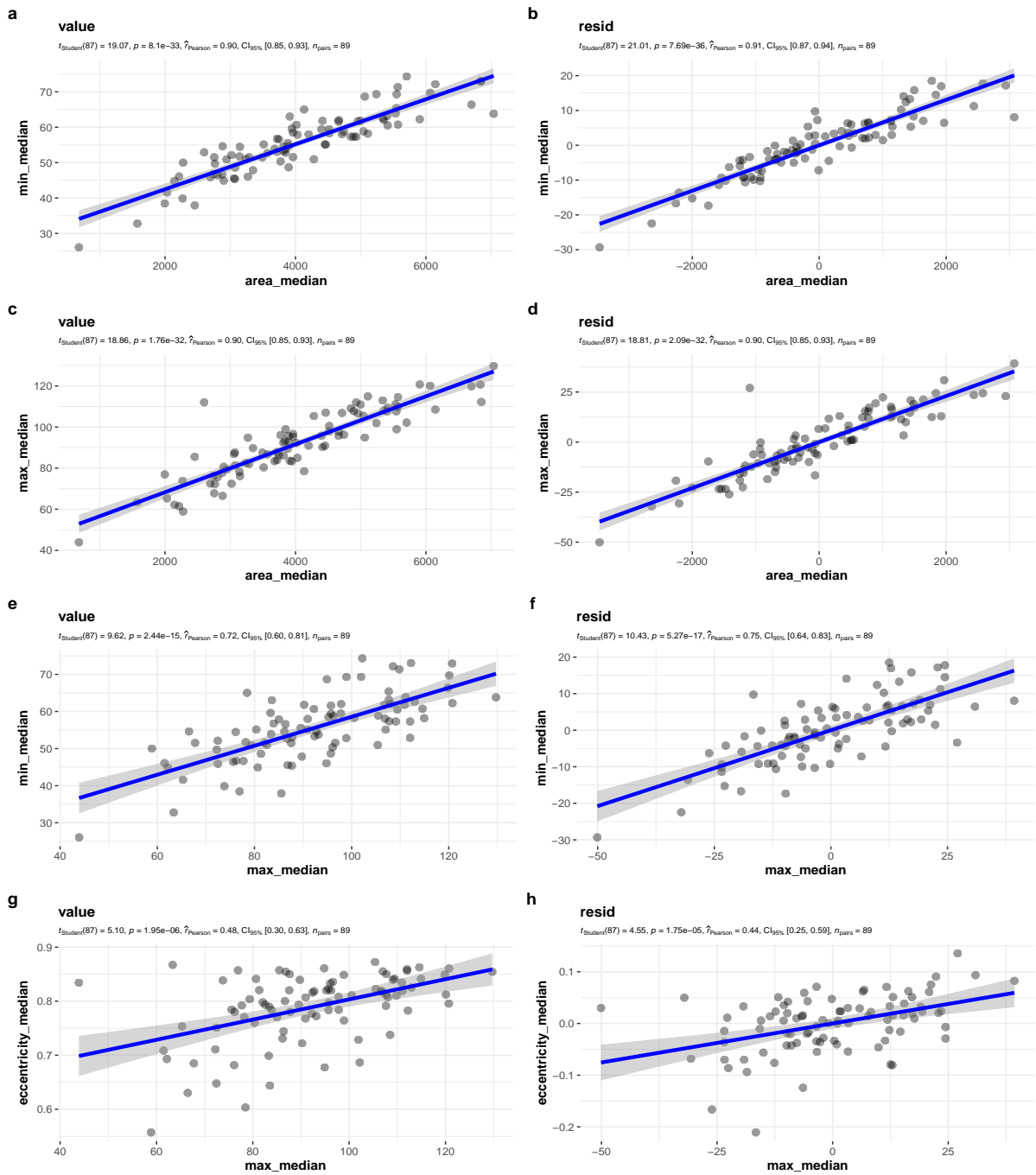


**Figure E.15.** Scatter plots of raw phenotypes of interest (left) against their residualized comparison (right) **a**, Cross-sectional area vs. minimum cross-sectional diameter **b**, Cross-sectional area vs. minimum cross-sectional diameter (residualized) **c**, Cross-sectional area vs. maximum cross-sectional diameter **d**, Cross-sectional area vs. maximum cross-sectional diameter (residualized) **e**, Maximum cross-sectional diameter vs. minimum cross-sectional diameter **f**, Maximum cross-sectional diameter vs. minimum cross-sectional diameter (residualized) **g**, Maximum cross-sectional diameter vs. cross-sectional eccentricity **h** Maximum cross-sectional diameter vs. cross-sectional eccentricity (residualized)

## E.4 Comparison with categorical

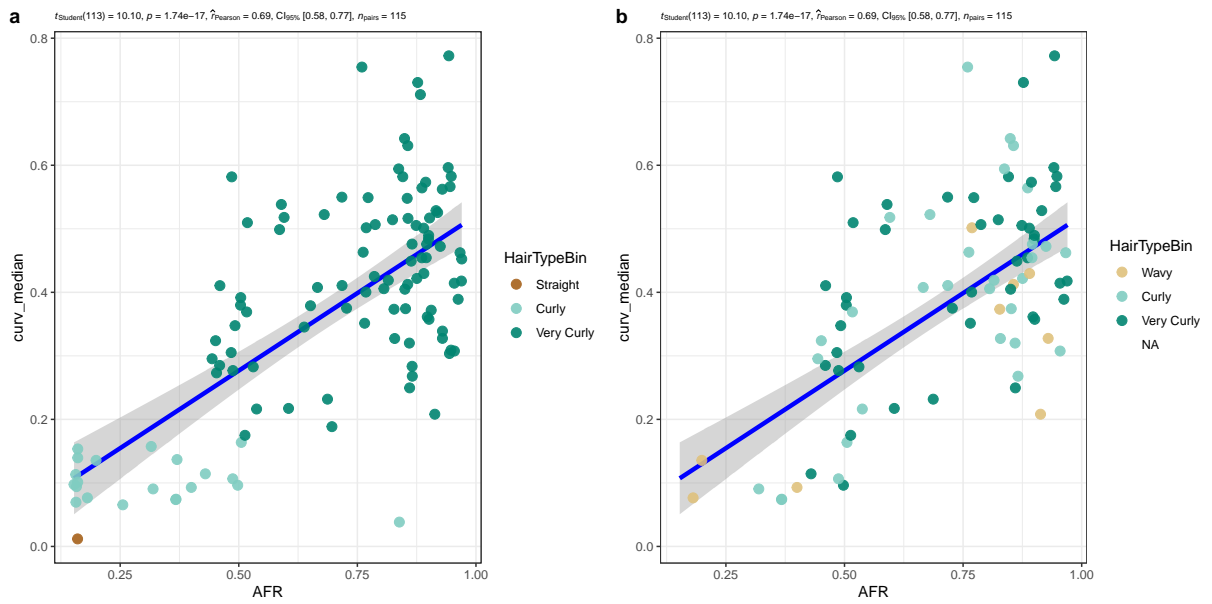


**Figure E.16. Categorical hair texture compared to quantitative hair curvature and proportion of AFR ancestry** **a**, Hair texture here is classified objectively according to cut offs suggested by Loussouarn et al. (2007) and **b**, shows hair texture according to participant self-report.

**Appendix F |**  
**Chapter 4 Supplementary:**  
**Genome-wide association**  
**results**

## F.1 QQ plots

Here we show the QQ plots for each phenotype.

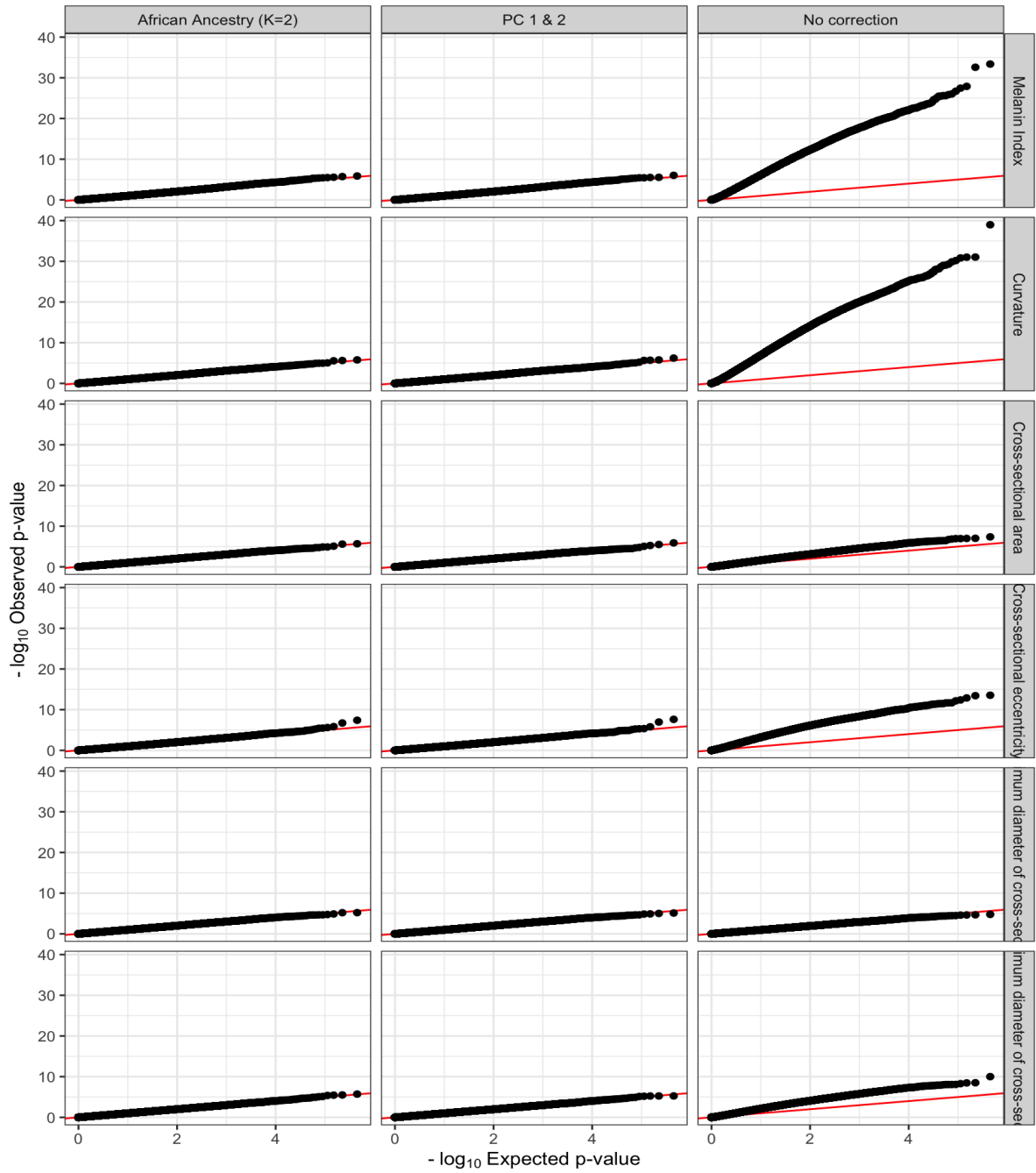


Figure F.1. QQ plots for various ancestry corrections and phenotypes. Columns represent different ancestry corrections and rows are different phenotypes.

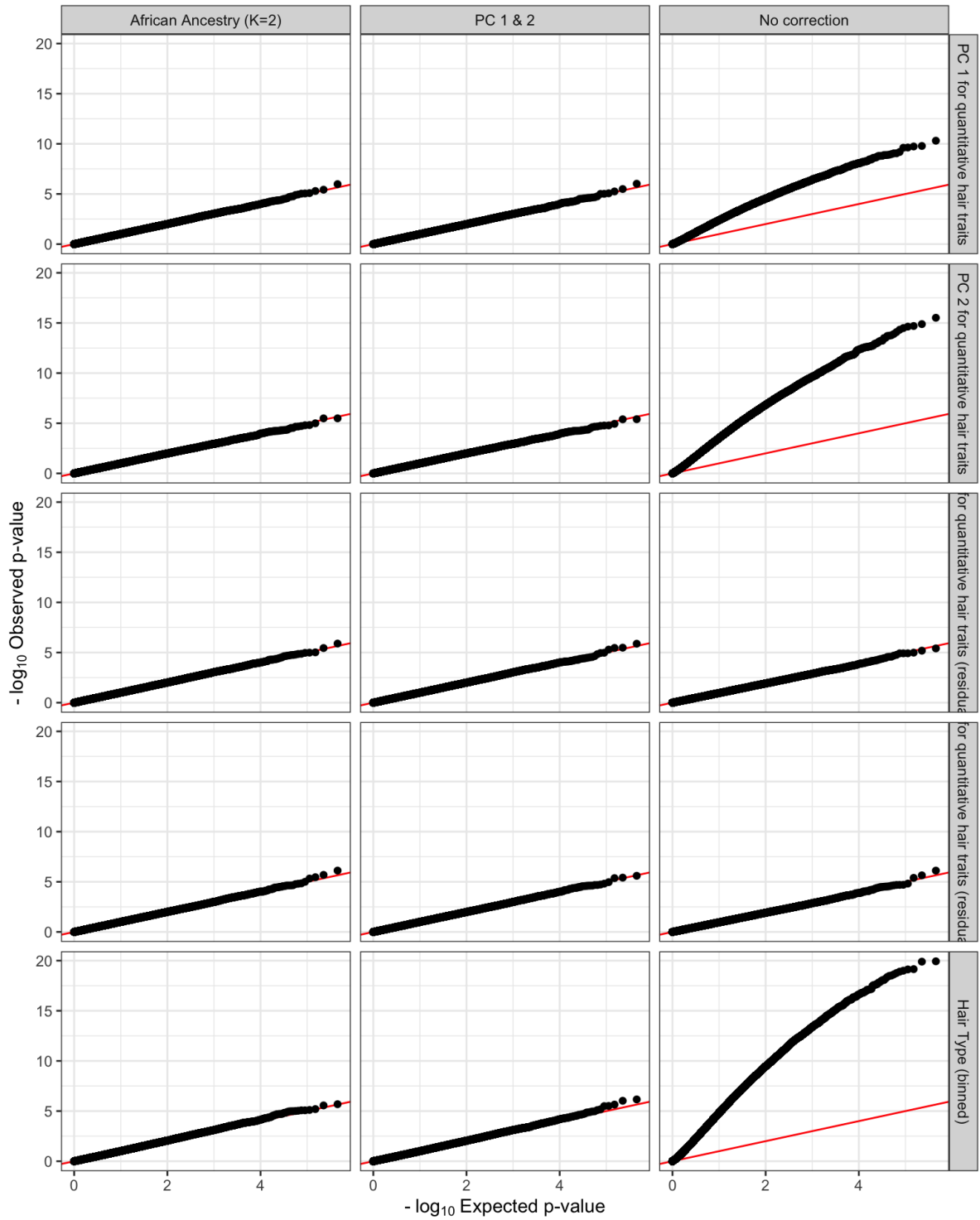


Figure F.2. QQ plots for various ancestry corrections and phenotypes. Columns represent different ancestry corrections and rows are different phenotypes.

**Table F.1.** Hair replicated SNPs

African Ancestry (K=2)	CHR	SNP	AI	BETA	GENES	trait	EA	BETA	meta	source
<b>Curvature</b>										
	4	rs168283	G	0.02996	NA	hair morphology	G	0.06000	Hair	GWAS meta-analysis
	4	rs6835769	T	-0.03237	NA	hair morphology	C	0.06000	Hair	GWAS meta-analysis
	20	rs310644	C	0.04549	NA	hair morphology	C	0.12000	Hair	GWAS meta-analysis
	4	rs1385130	G	-0.03378	NA	hair morphology	A	0.06000	Hair	GWAS meta-analysis
	20	rs310654	A	0.06317	NA	hair morphology	A	0.13000	Hair	GWAS meta-analysis
	20	rs310655	T	0.05144	NA	hair morphology	T	0.12000	Hair	GWAS meta-analysis
<b>Maximum diameter of cross-section</b>										
	14	rs12896399	T	-4.21000	AL133240.2 - SLC24A4	hair colour measurement, hair morphology measurement	NA	0.09375	GWAS	catalog
	15	rs12913832	G	-5.24700	HERC2, HERC2	hair colour measurement, hair morphology measurement	NA	0.34820	GWAS	catalog
	15	rs1129038	T	-5.38200	HERC2, HERC2	hair colour measurement, hair morphology measurement	NA	1.41855	GWAS	catalog
	1	rs6587673	A	4.69500	NA	hair morphology	G	0.05000	Hair	GWAS meta-analysis
	4	rs4975132	A	-5.33900	NA	hair morphology	G	0.05000	Hair	GWAS meta-analysis
	1	rs2146115	T	-5.80900	NA	hair morphology	T	0.08000	Hair	GWAS meta-analysis
<b>PC 1 for quantitative hair traits</b>										
	4	rs2627654	G	-0.47590	NA	hair morphology	G	0.06000	Hair	GWAS meta-analysis
	1	rs499697	G	0.50280	NA	hair morphology	G	0.08000	Hair	GWAS meta-analysis
	1	rs6700998	T	0.39780	NA	hair morphology	T	0.05000	Hair	GWAS meta-analysis
	1	rs6661961	T	0.40280	NA	hair morphology	T	0.05000	Hair	GWAS meta-analysis
<b>PC 2 for quantitative hair traits (residualized)</b>										
	1	rs17646946	A	-0.36470	NA	hair morphology	A	-0.22000	Hair	GWAS meta-analysis
<b>Hair Type (binned)</b>										
	4	rs1027444	G	0.17350	NA	hair morphology	G	0.06000	Hair	GWAS meta-analysis
	1	rs4845763	C	0.24880	NA	hair morphology	C	0.07000	Hair	GWAS meta-analysis
	1	rs12116609	T	-0.12370	NA	hair morphology	C	0.07000	Hair	GWAS meta-analysis
	4	rs345542	C	0.20960	NA	hair morphology	C	0.07000	Hair	GWAS meta-analysis
	1	rs12030667	A	0.15500	NA	hair morphology	A	0.06000	Hair	GWAS meta-analysis
	4	rs2035511	A	0.14700	NA	hair morphology	A	0.06000	Hair	GWAS meta-analysis
<b>PC 1 &amp; 2</b>										
	1	rs4240887	A	0.11280	NA	hair morphology	A	0.07000	Hair	GWAS meta-analysis

## F.2 Overlap with previously reported SNPs

Here we read in the GWAS results from Plink for each trait and cross-reference with a list of variants that were used in a meta-analysis on hair morphology (Liu et al, 2018 and the NHGRI-EBI GWAS Catalog). We check for overlap in significant SNPs between the meta-analysis, the catalog, and our sample for each of the phenotypes we used in the GWAS.

### F.2.1 Hair replicated SNPs

We replicated the following SNPs for hair morphology:

### F.2.2 Skin replicated SNPs

We replicated the following SNPs for skin pigmentation:

Table F.2. Skin replicated SNPs

CHR	SNP	A1	BETA	GENES	trait	EA	BETA	meta	source
<b>African Ancestry (K=2)</b>									
<b>Melanin Index</b>									
11	rs1042602	A	-2.367	TYR	skin pigmentation measurement	NA	0.227	GWAS catalog	
15	rs1426654	G	3.922	SLC24A5	skin pigmentation measurement	G	0.403	GWAS catalog	

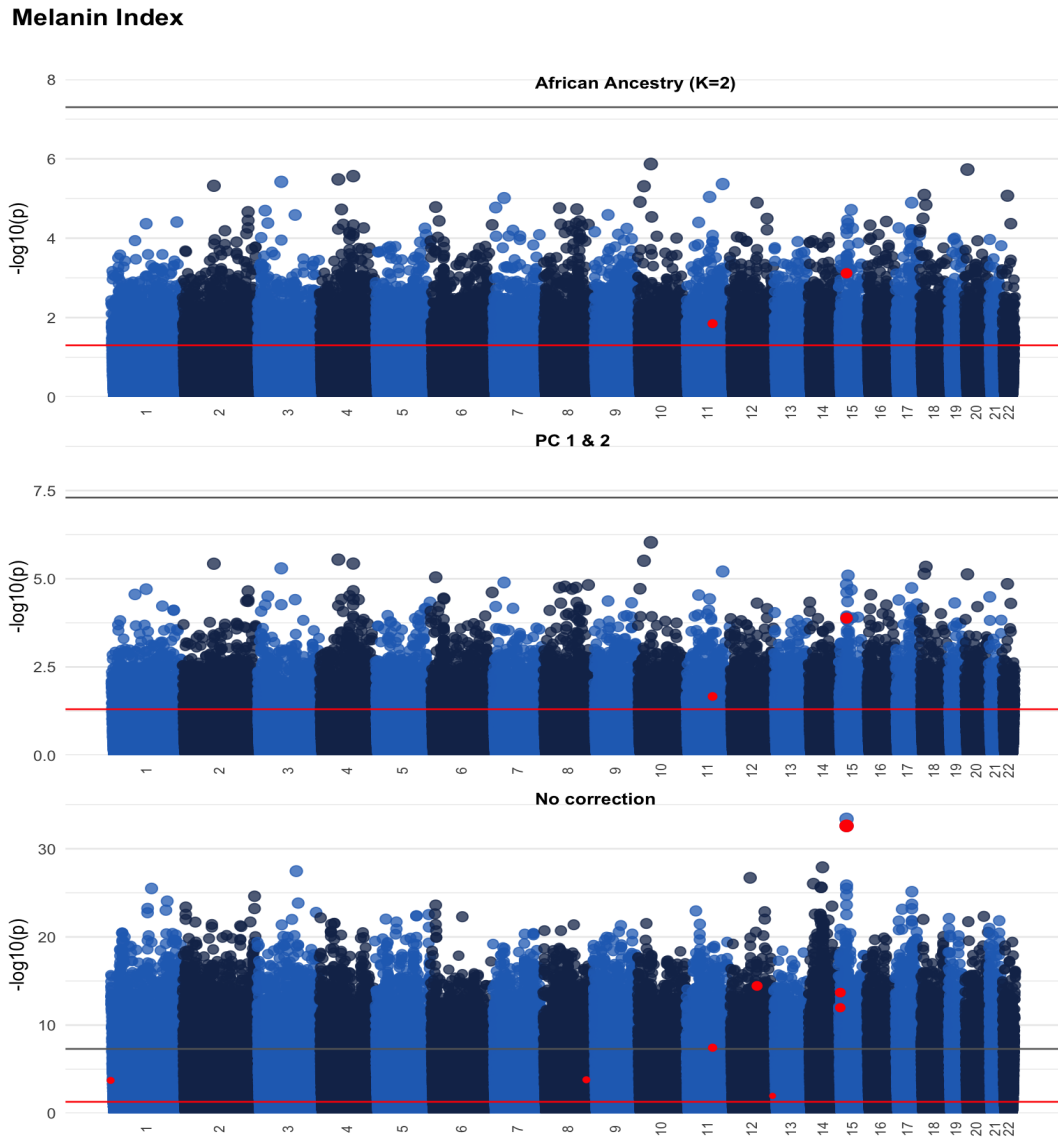
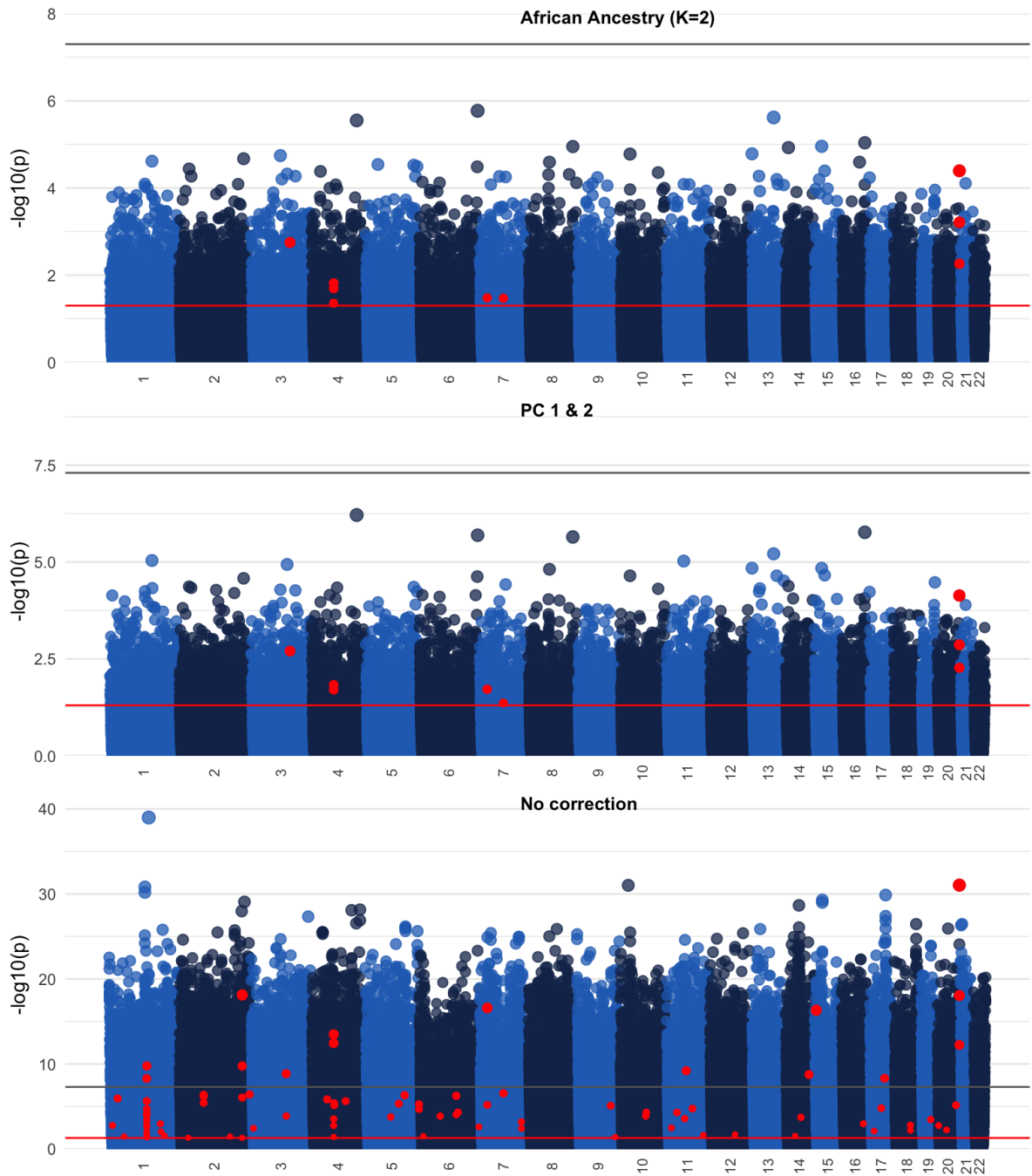


Figure F.3. Manhattan plot for Melanin Index. First row with correction for ancestry using AFR (K=2), second row using first 2 PCs to correct for ancestry, and last row shows plot without correction for ancestry. Highlighted are previously associated loci. Here we see *SLC24A5* on Chromosome 15.

## Curvature



**Figure F.4. Manhattan plot for median hair curvature.** First row with correction for ancestry using AFR ( $K=2$ ), second row using first 2 PCs to correct for ancestry, and last row shows plot without correction for ancestry. Highlighted are previously associated loci.

### Cross-sectional area

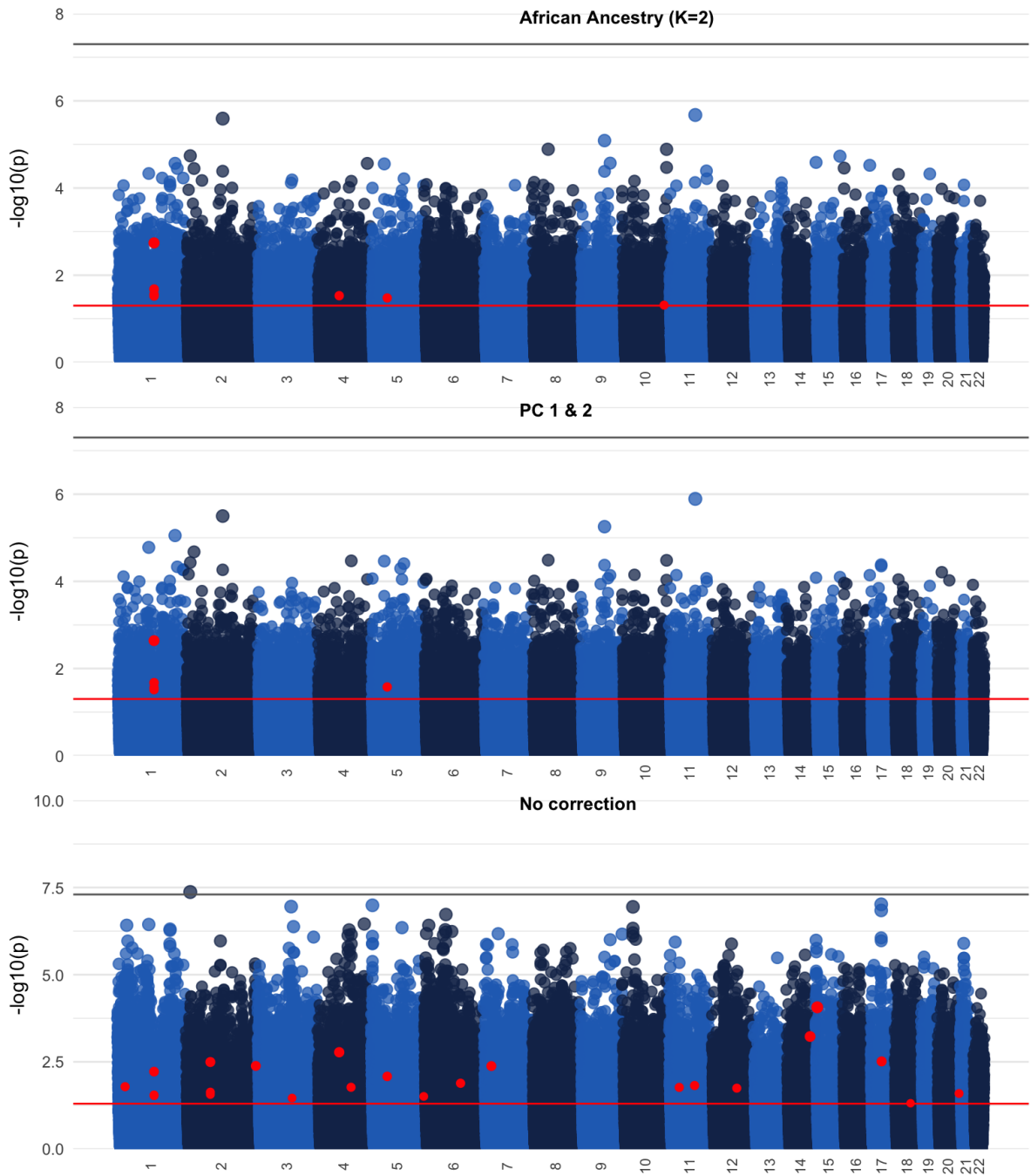


**Figure F.5.** Manhattan plot for cross-sectional area. First row with correction for ancestry using AFR ( $K=2$ ), second row using first 2 PCs to correct for ancestry, and last row shows plot without correction for ancestry. Highlighted are previously associated loci.

### Cross-sectional eccentricity

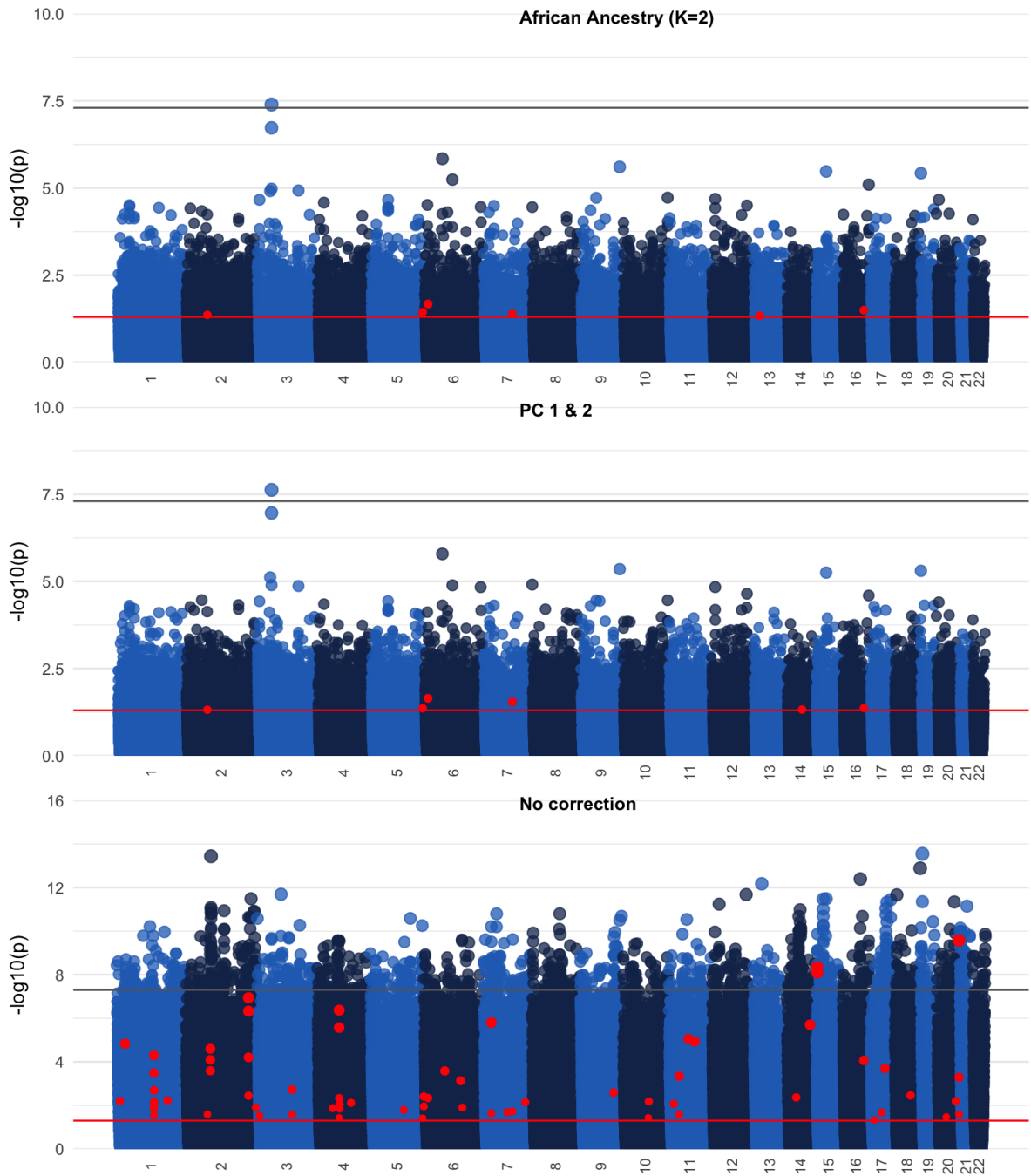


**Figure F.6. Manhattan plot for cross-sectional eccentricity.** First row with correction for ancestry using AFR ( $K=2$ ), second row using first 2 PCs to correct for ancestry, and last row shows plot without correction for ancestry. Highlighted are previously associated loci.

### Minimum diameter of cross-section

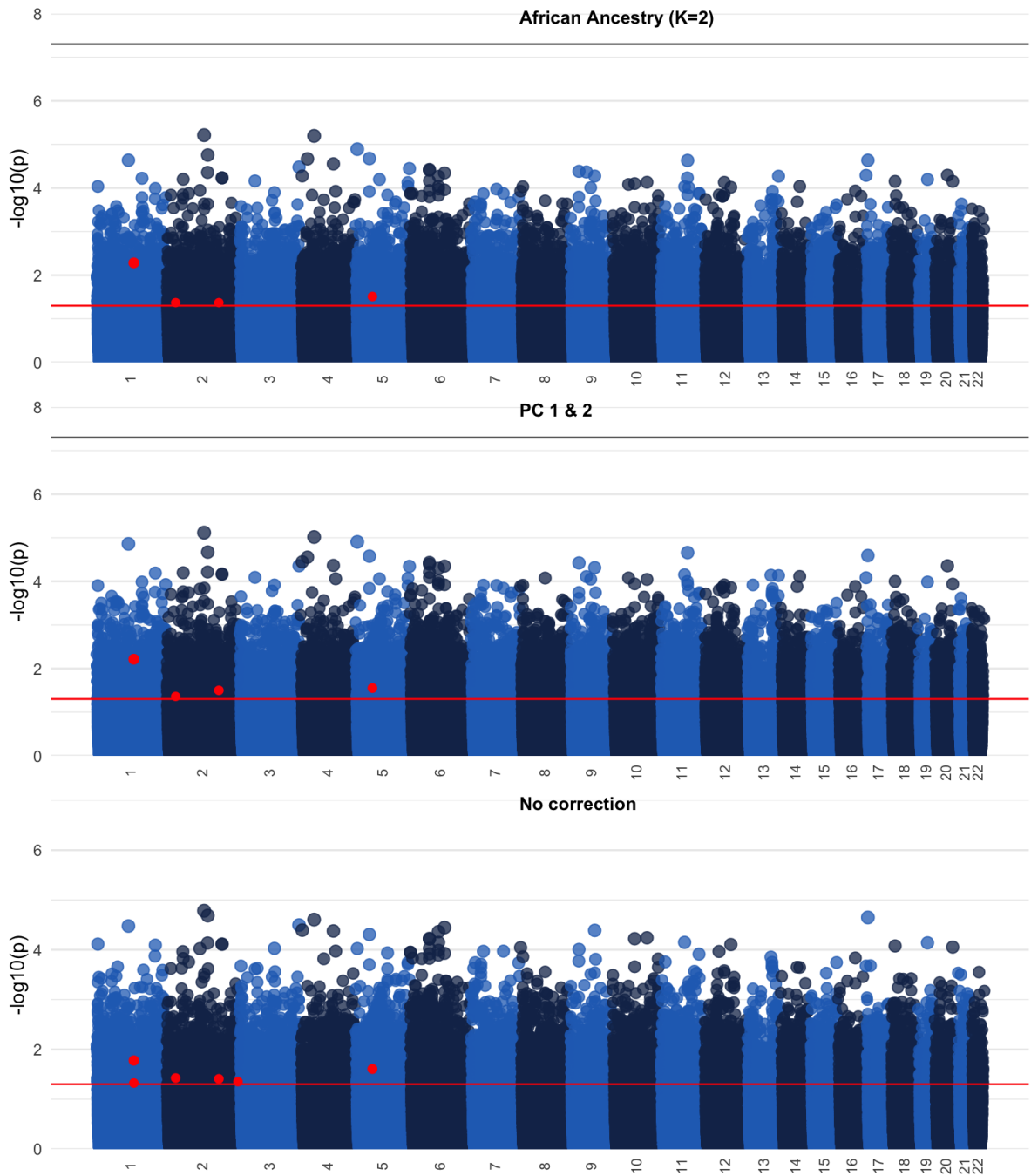


**Figure F.7. Manhattan plot for minimum cross-sectional diameter.** First row with correction for ancestry using AFR ( $K=2$ ), second row using first 2 PCs to correct for ancestry, and last row shows plot without correction for ancestry. Highlighted are previously associated loci.

### Maximum diameter of cross-section

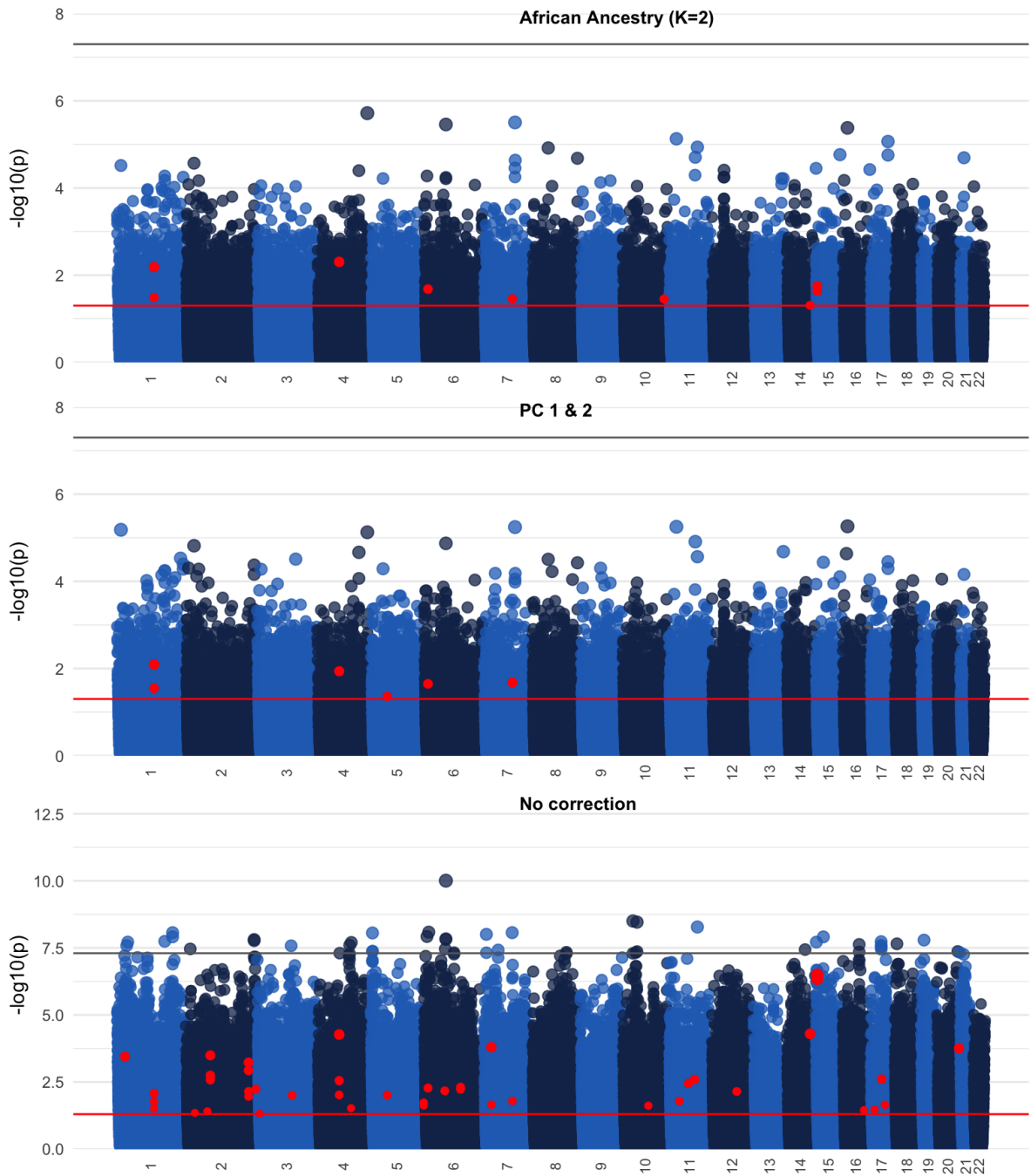


**Figure F.8. Manhattan plot for maximum cross-sectional diameter.** First row with correction for ancestry using AFR ( $K=2$ ), second row using first 2 PCs to correct for ancestry, and last row shows plot without correction for ancestry. Highlighted are previously associated loci.

### PC 1 for quantitative hair traits

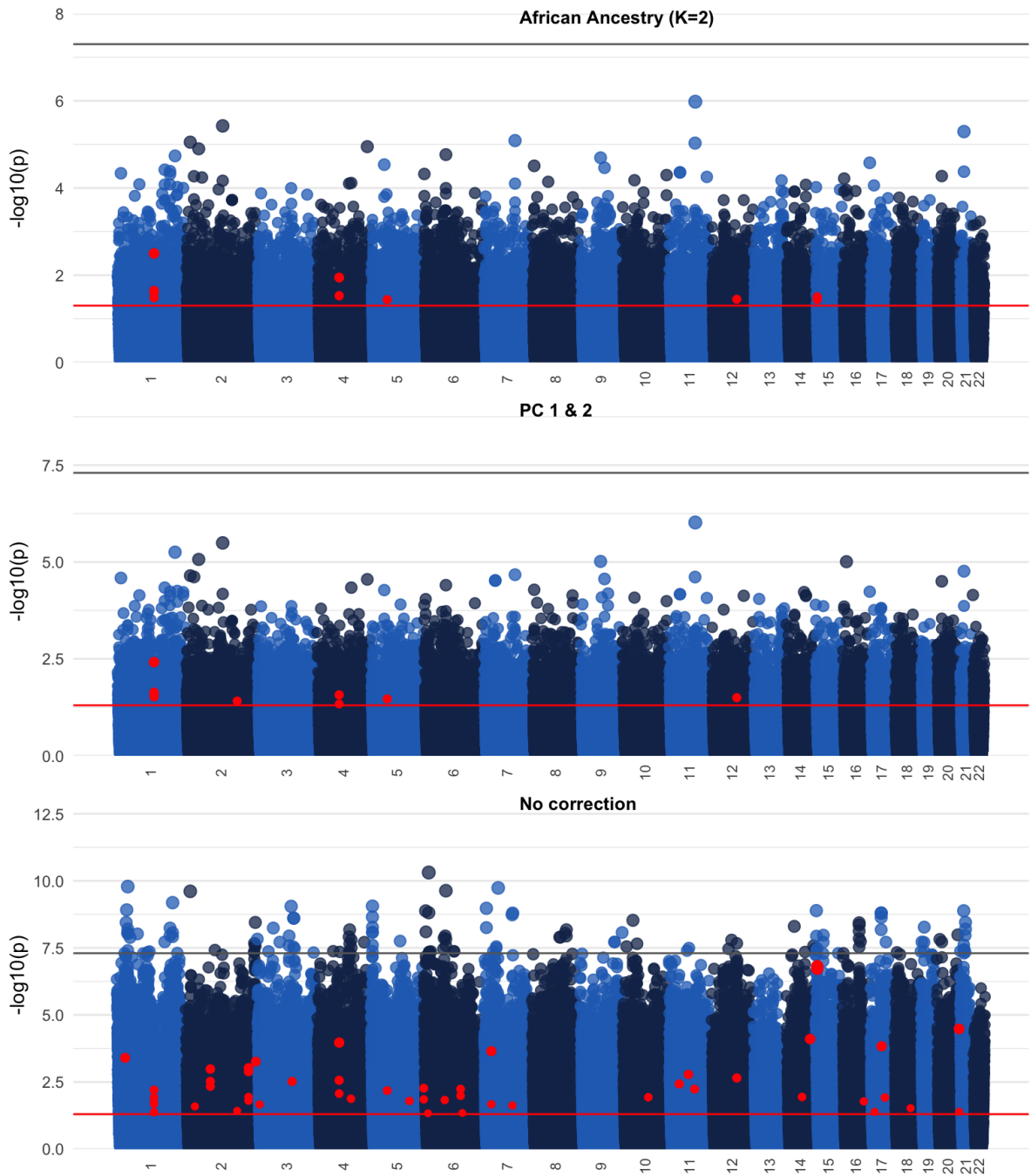


**Figure F.9.** Manhattan plot for PC1 on quantitative hair traits. First row with correction for ancestry using AFR ( $K=2$ ), second row using first 2 PCs to correct for ancestry, and last row shows plot without correction for ancestry. Highlighted are previously associated loci.

### PC 2 for quantitative hair traits

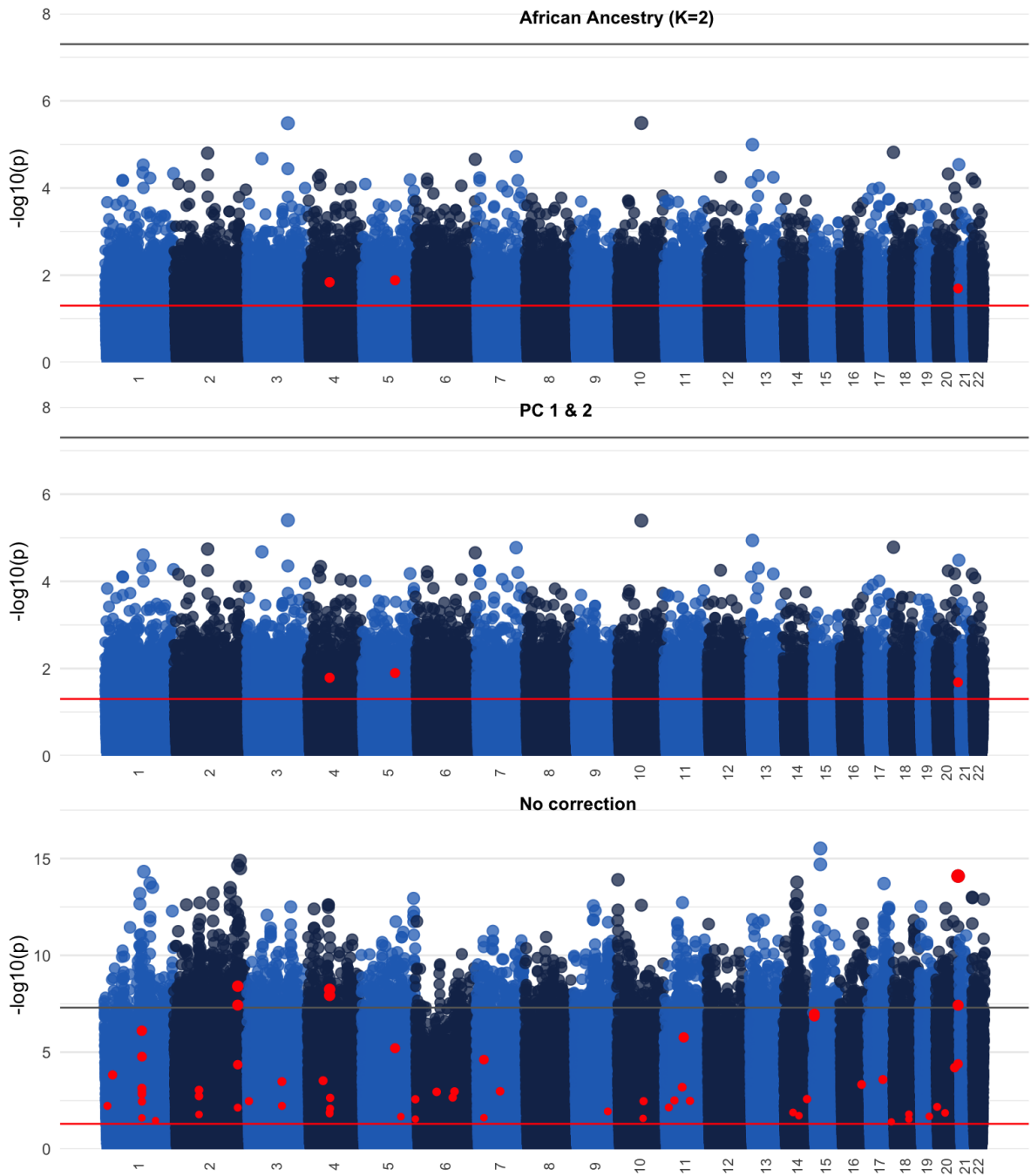


**Figure F.10.** Manhattan plot for PC2 on quantitative hair traits. First row with correction for ancestry using AFR ( $K=2$ ), second row using first 2 PCs to correct for ancestry, and last row shows plot without correction for ancestry. Highlighted are previously associated loci.

### PC 1 for quantitative hair traits (residualized)

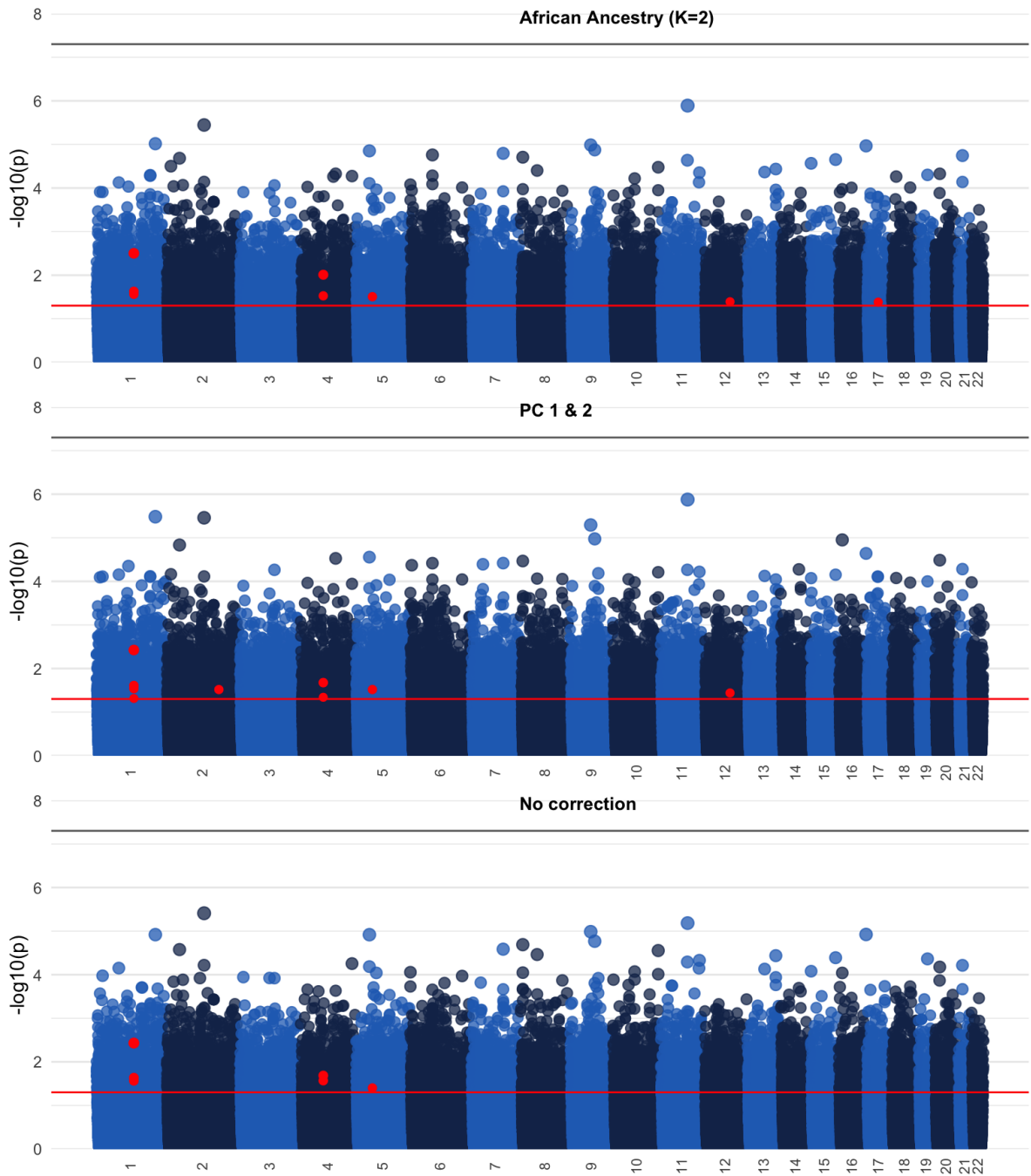


**Figure F.11.** Manhattan plot for PC1 on residualized quantitative hair traits. First row with correction for ancestry using AFR ( $K=2$ ), second row using first 2 PCs to correct for ancestry, and last row shows plot without correction for ancestry. Highlighted are previously associated loci.

### PC 2 for quantitative hair traits (residualized)

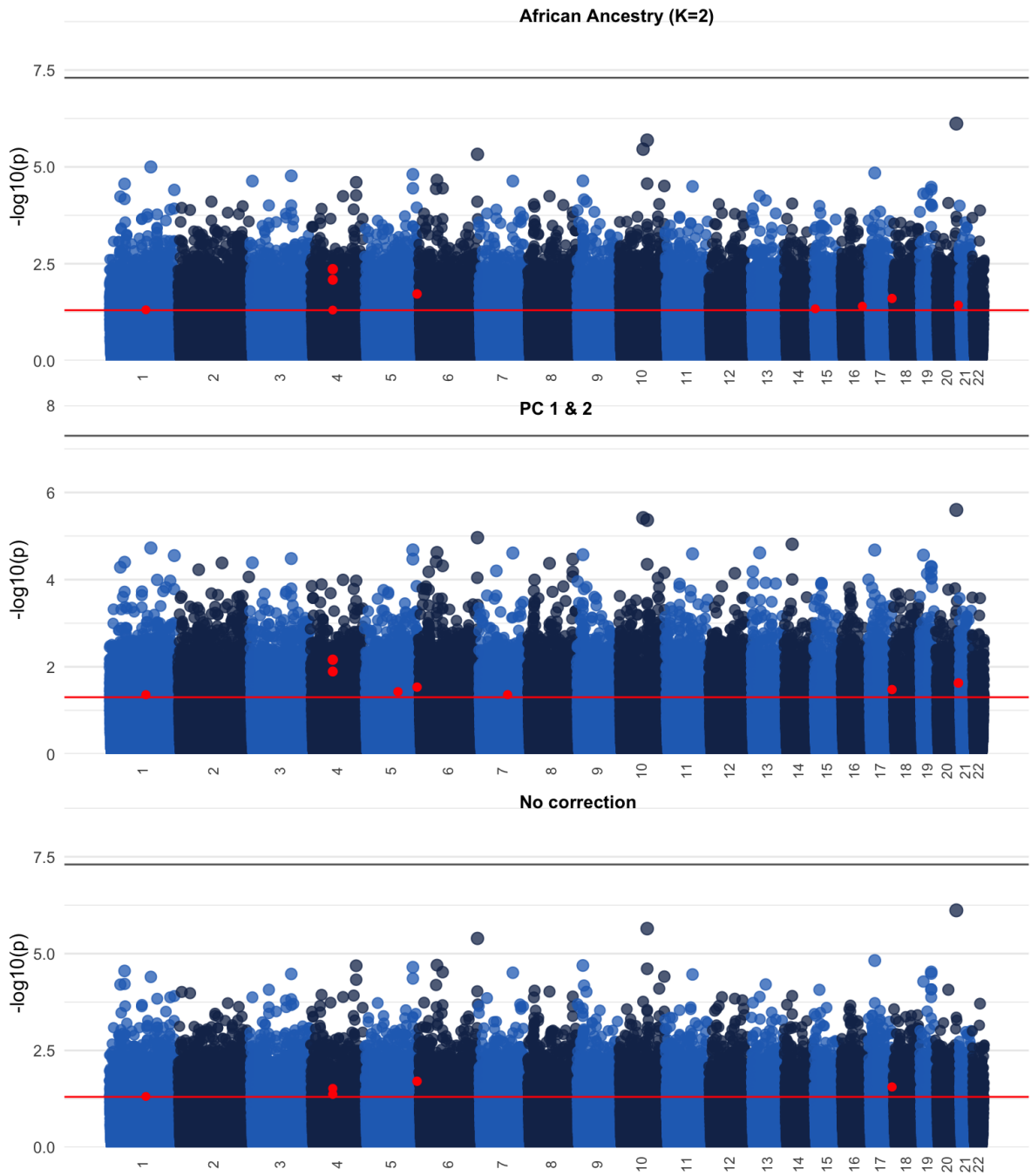


**Figure F.12.** Manhattan plot for PC2 on residualized quantitative hair traits. First row with correction for ancestry using AFR ( $K=2$ ), second row using first 2 PCs to correct for ancestry, and last row shows plot without correction for ancestry. Highlighted are previously associated loci.

### Hair Type (binned)

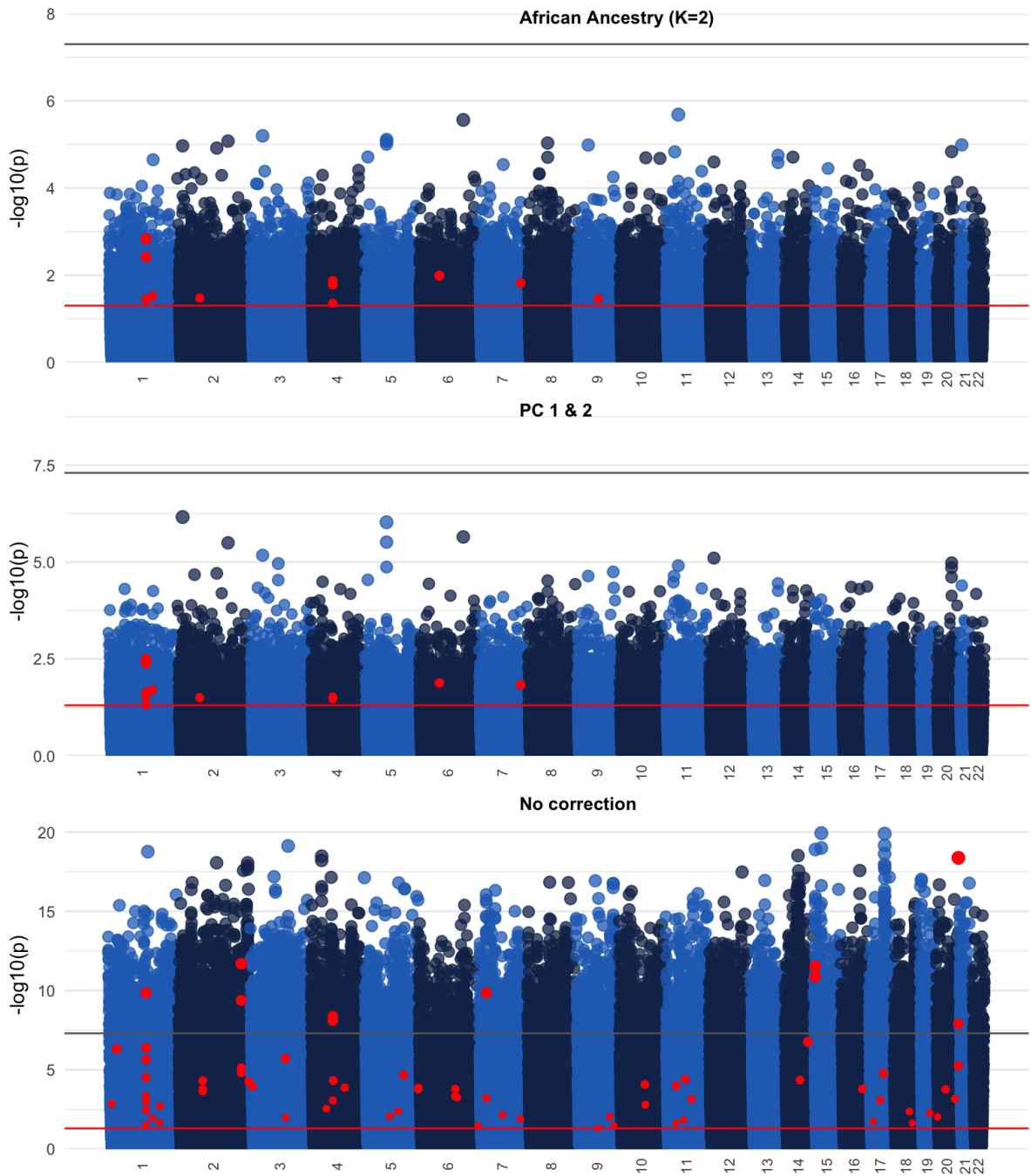


**Figure F.13.** Manhattan plot for objectively classified hair texture. First row with correction for ancestry using AFR ( $K=2$ ), second row using first 2 PCs to correct for ancestry, and last row shows plot without correction for ancestry. Highlighted are previously associated loci.

### **F.3 Admixture mapping**

Here, we read in frequency information for the SNPs in our association. Specifically, we select SNPs with high frequency differences between West Africans (YRI) and Europeans (CEU) as ancestry informative markers or AIMs.

## Melanin Index

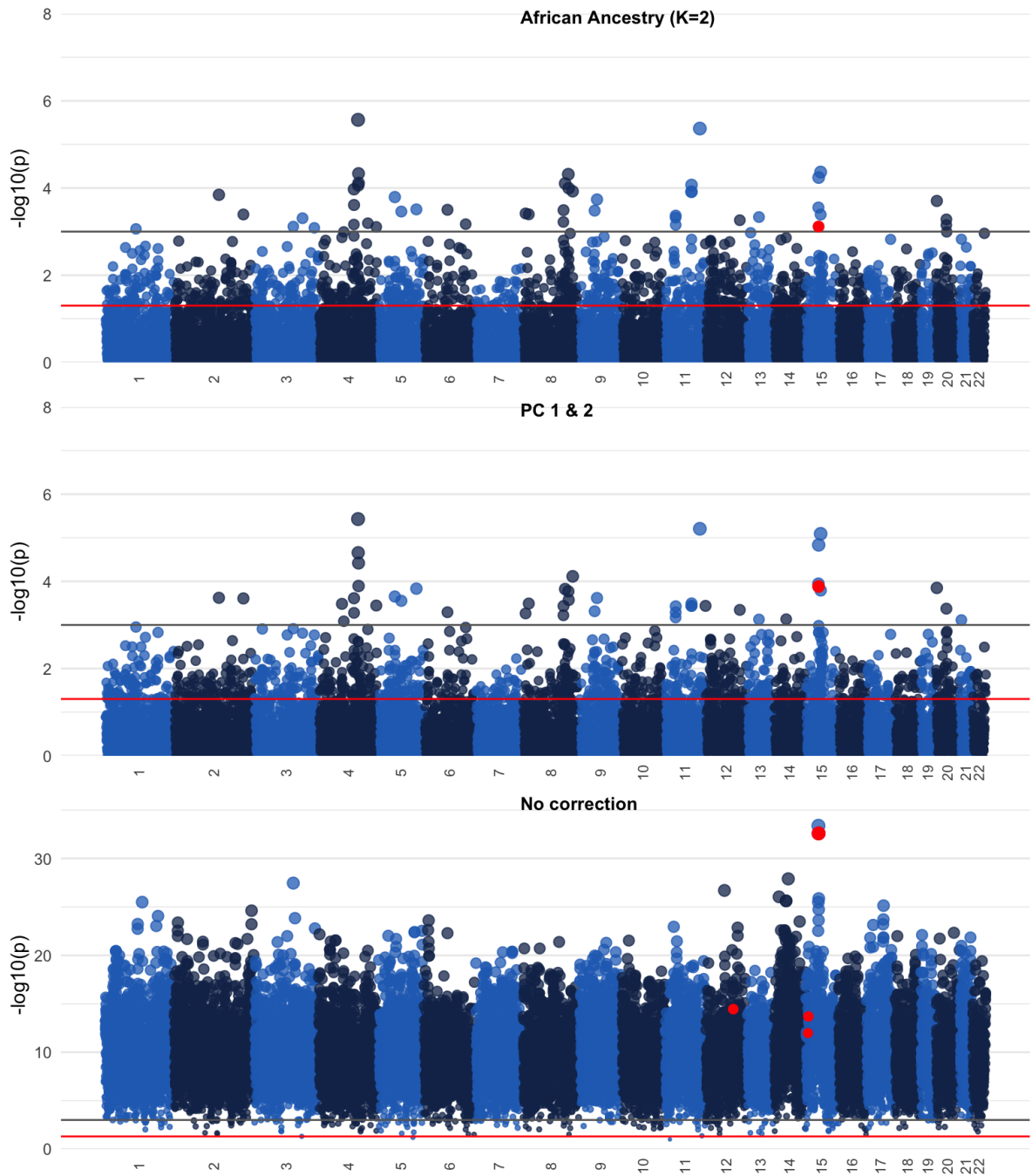


**Figure F.14.** Manhattan plot for Melanin Index on subset of alleles with high frequency difference between YRI-CEU. First row with correction for ancestry using AFR (K=2), second row using first 2 PCs to correct for ancestry, and last row shows plot without correction for ancestry. Highlighted are previously associated loci. The strongest highlighted signal is *SLC24A5*

## Curvature

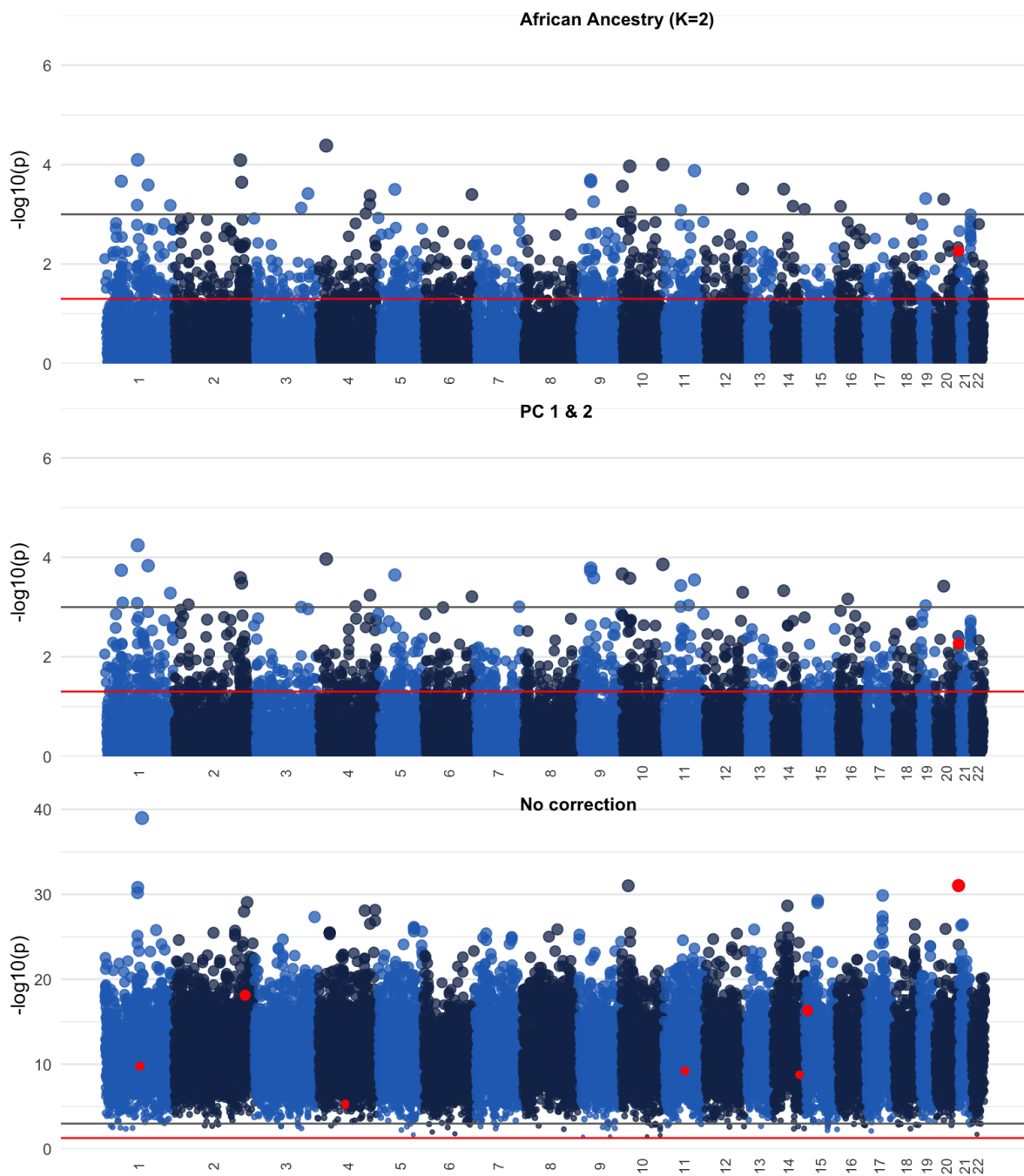


**Figure F.15.** Manhattan plot for median hair curvature on subset of alleles with high frequency difference between YRI-CEU. First row with correction for ancestry using AFR (K=2), second row using first 2 PCs to correct for ancestry, and last row shows plot without correction for ancestry. Highlighted are previously associated loci.

### Cross-sectional area

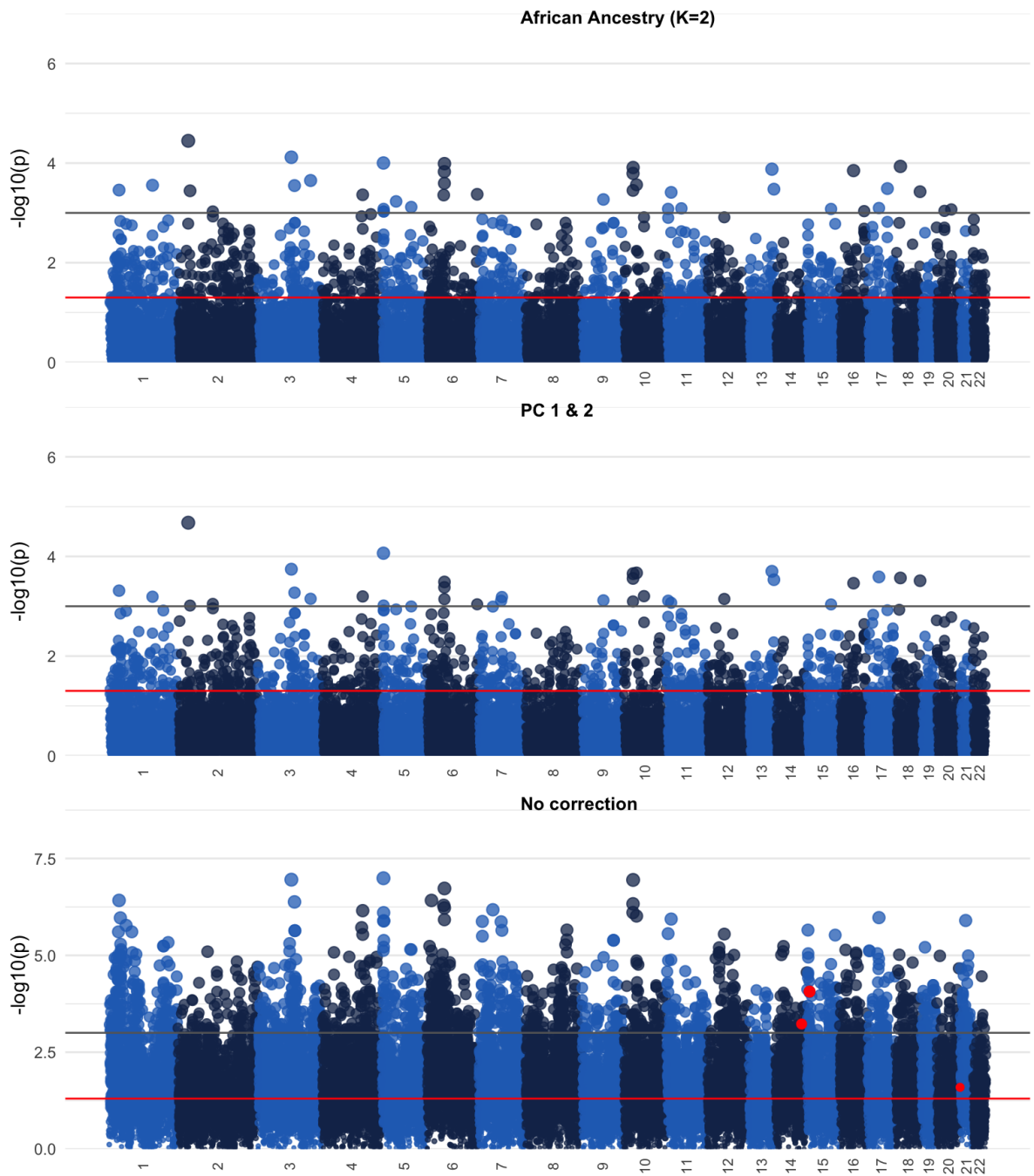


**Figure F.16.** Manhattan plot for cross-sectional area on subset of alleles with high frequency difference between YRI-CEU. First row with correction for ancestry using AFR (K=2), second row using first 2 PCs to correct for ancestry, and last row shows plot without correction for ancestry. Highlighted are previously associated loci.

## Cross-sectional eccentricity

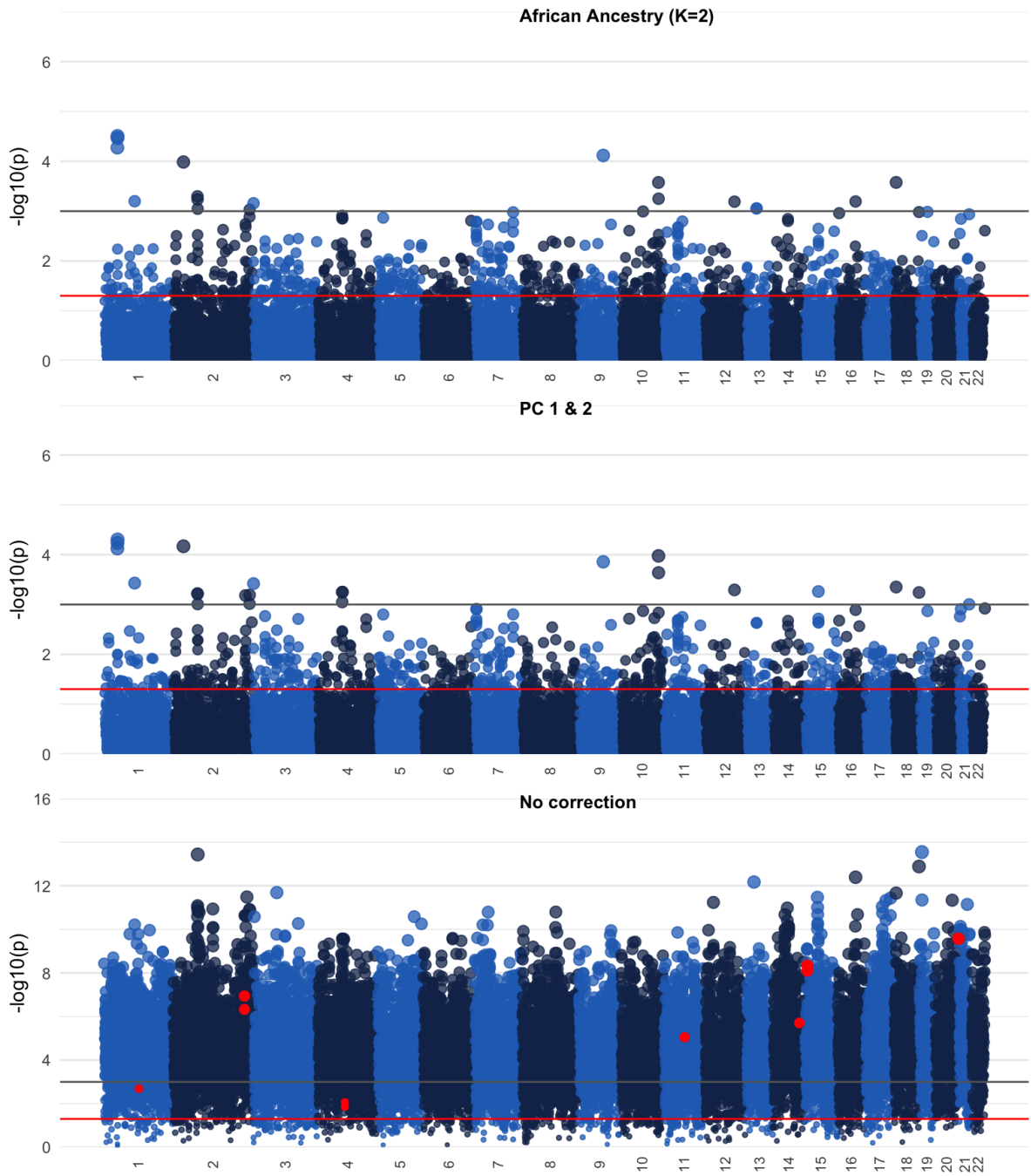


**Figure F.17.** Manhattan plot for cross-sectional eccentricity on subset of alleles with high frequency difference between YRI-CEU. First row with correction for ancestry using AFR (K=2), second row using first 2 PCs to correct for ancestry, and last row shows plot without correction for ancestry. Highlighted are previously associated loci.

### Minimum diameter of cross-section

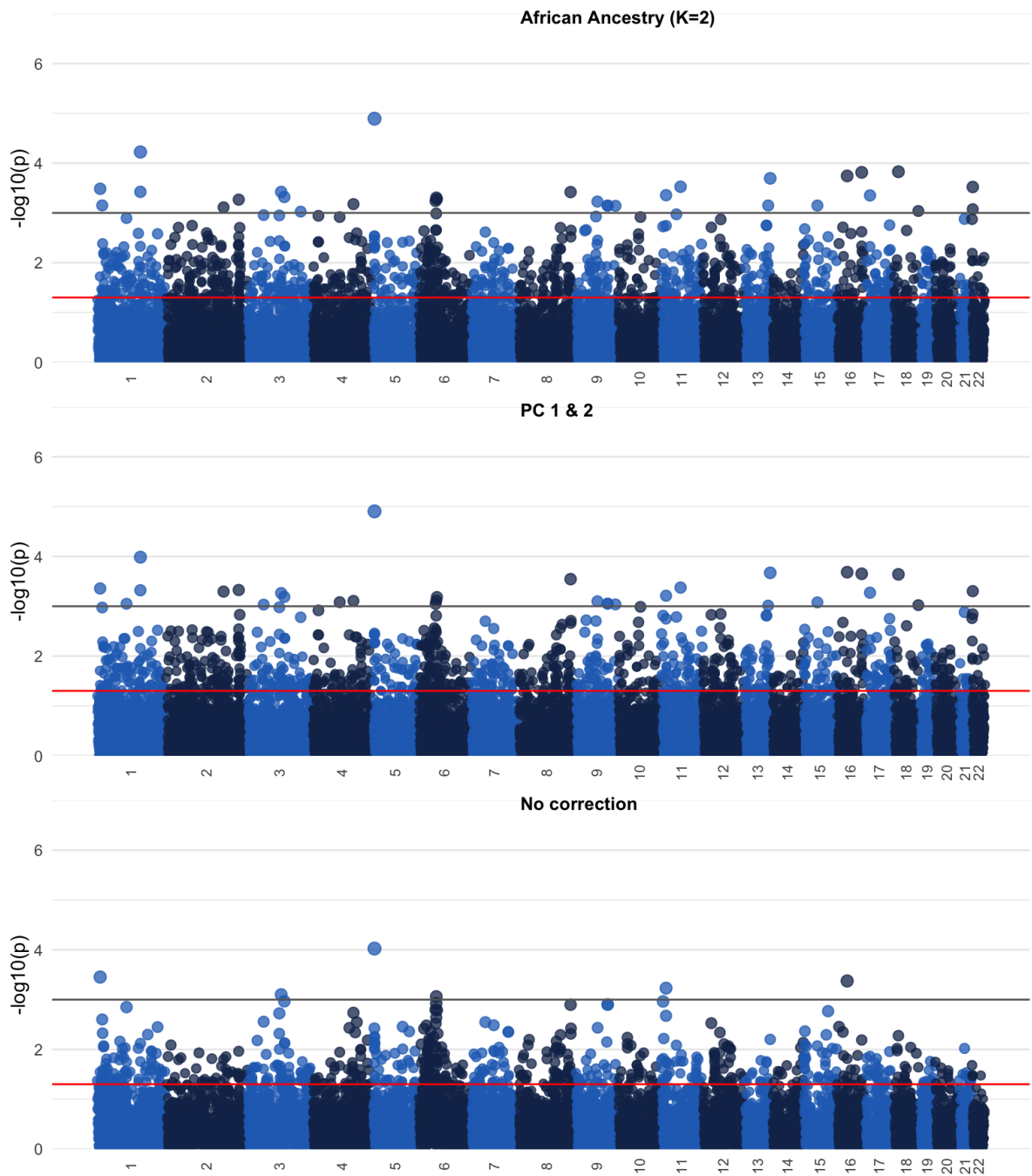


**Figure F.18.** Manhattan plot for minimum cross-sectional diameter on subset of alleles with high frequency difference between YRI-CEU. First row with correction for ancestry using AFR ( $K=2$ ), second row using first 2 PCs to correct for ancestry, and last row shows plot without correction for ancestry. Highlighted are previously associated loci.

### Maximum diameter of cross-section

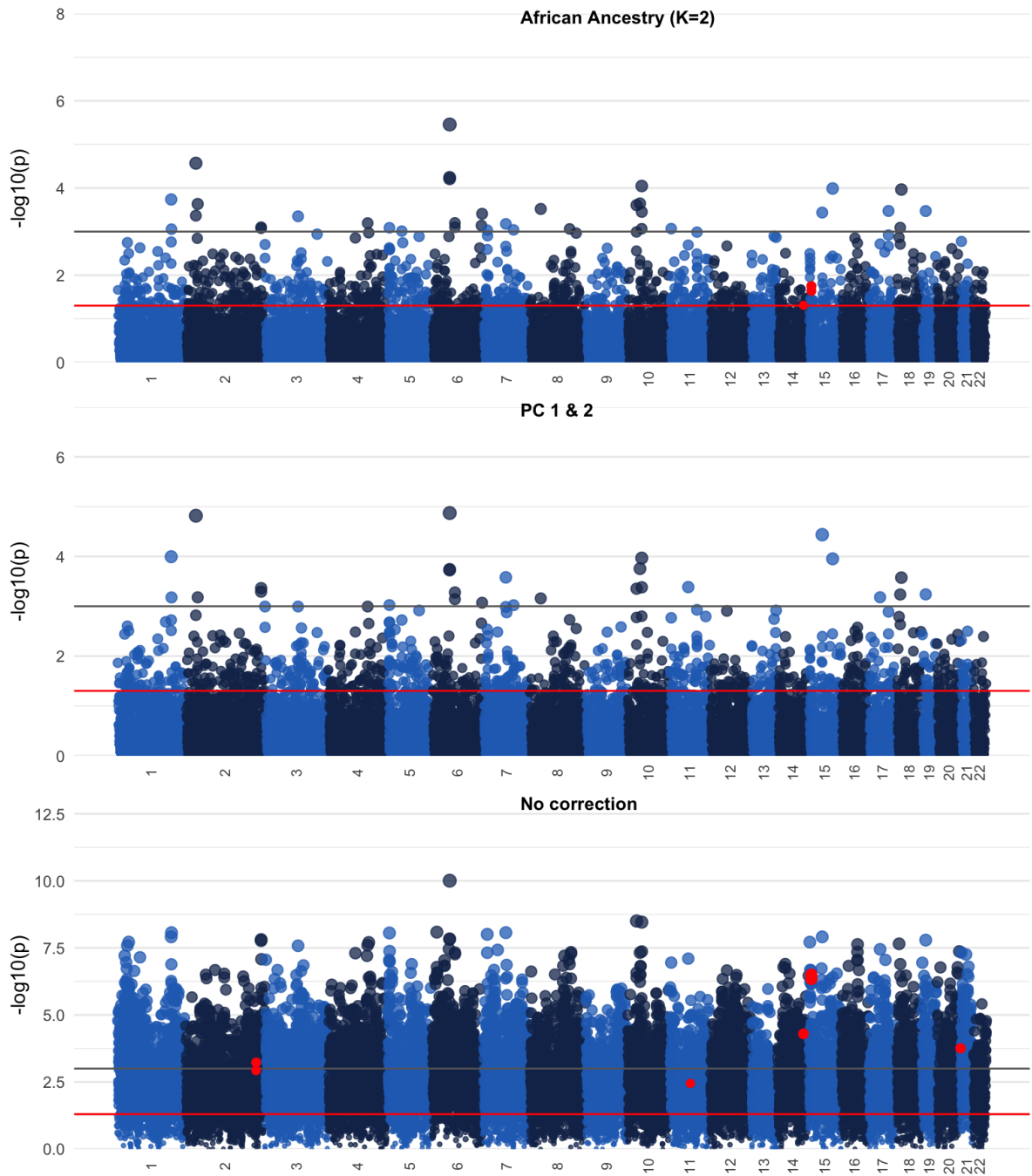


**Figure F.19.** Manhattan plot for maximum cross-sectional diameter on subset of alleles with high frequency difference between YRI-CEU. First row with correction for ancestry using AFR ( $K=2$ ), second row using first 2 PCs to correct for ancestry, and last row shows plot without correction for ancestry. Highlighted are previously associated loci.

### PC 1 for quantitative hair traits

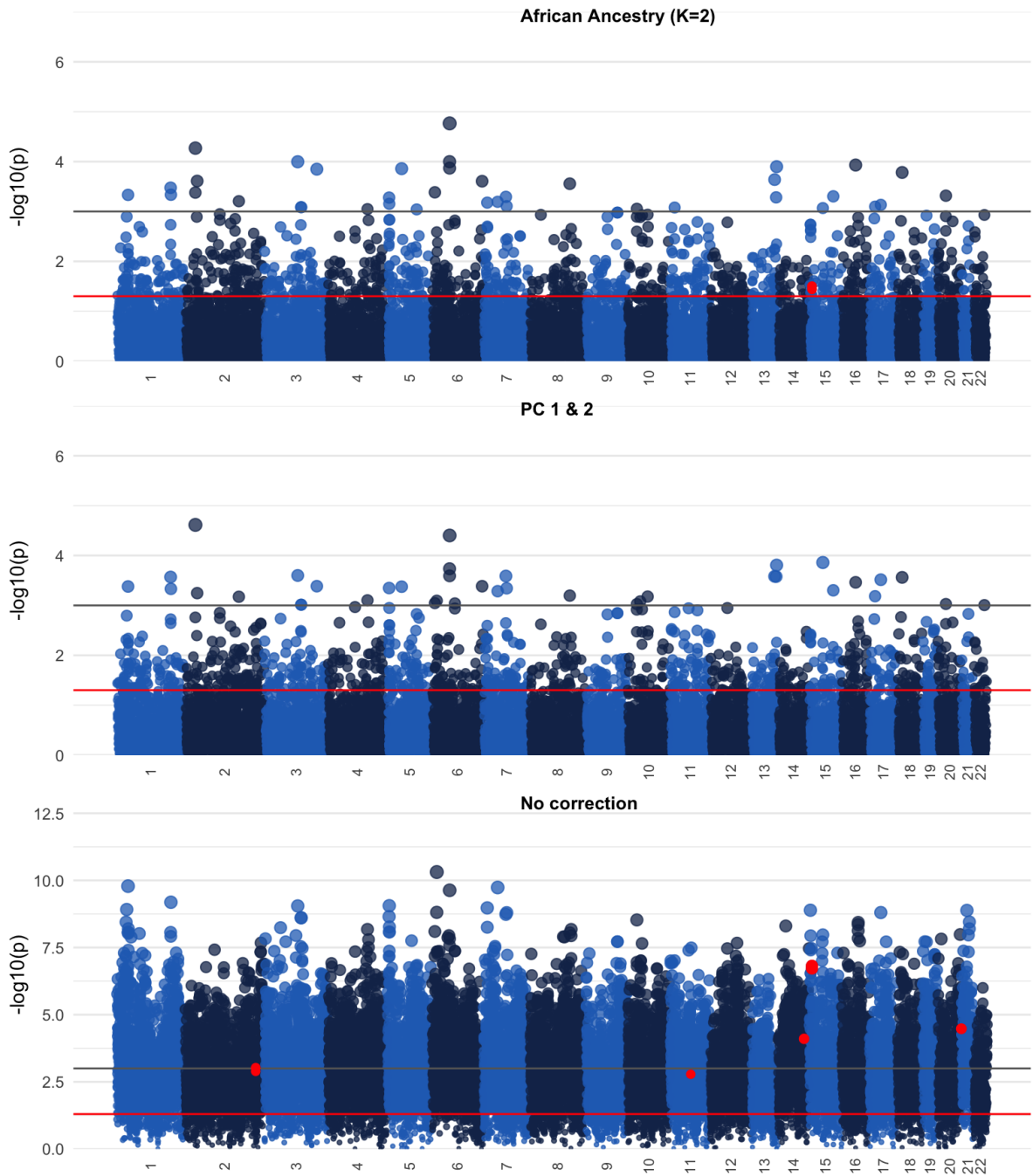


**Figure F.20.** Manhattan plot for PC1 for quantitative hair traits on subset of alleles with high frequency difference between YRI-CEU. First row with correction for ancestry using AFR ( $K=2$ ), second row using first 2 PCs to correct for ancestry, and last row shows plot without correction for ancestry. Highlighted are previously associated loci.

### PC 2 for quantitative hair traits

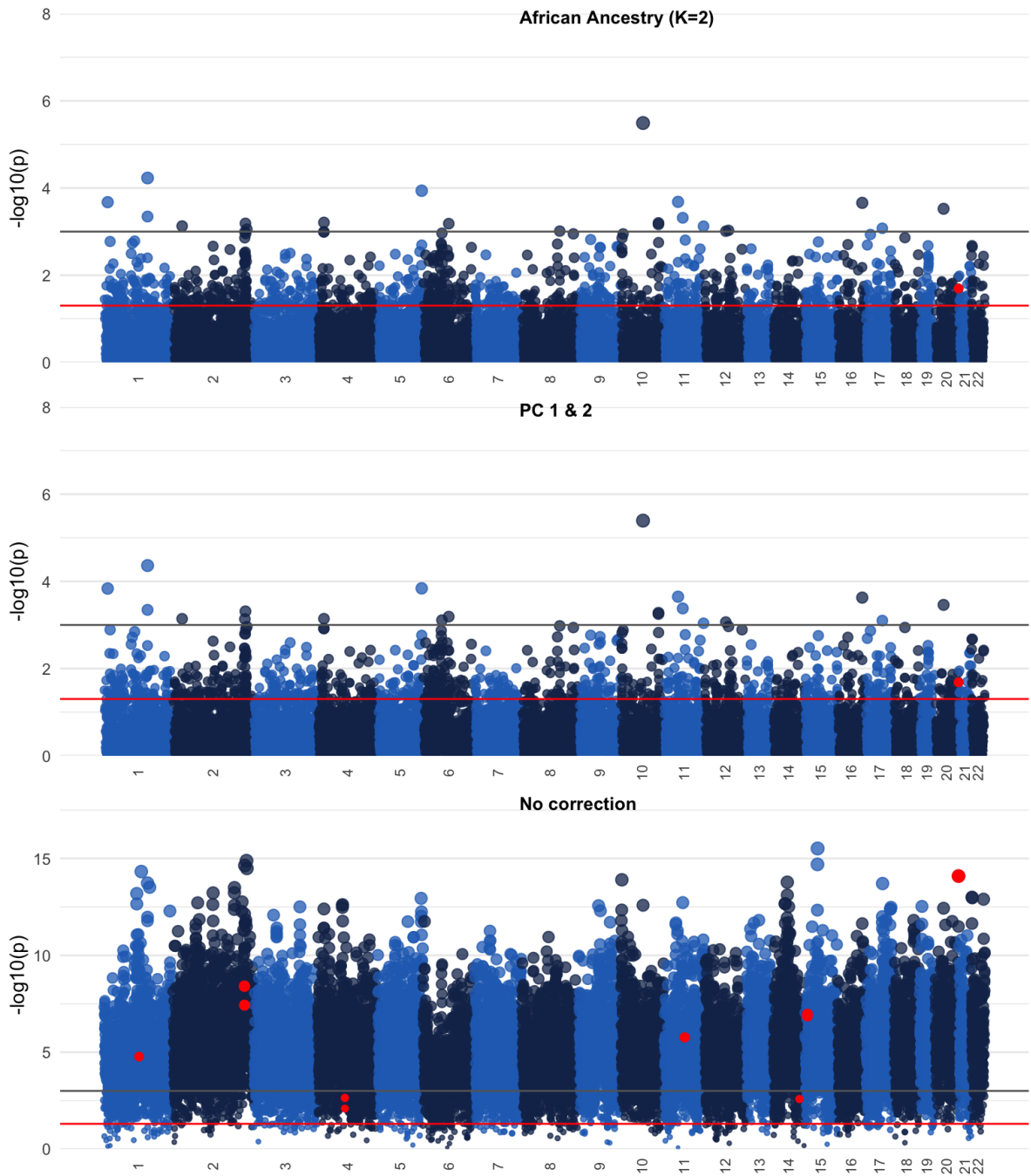


**Figure F.21.** Manhattan plot for PC2 for quantitative hair traits on subset of alleles with high frequency difference between YRI-CEU. First row with correction for ancestry using AFR ( $K=2$ ), second row using first 2 PCs to correct for ancestry, and last row shows plot without correction for ancestry. Highlighted are previously associated loci.

### PC 1 for quantitative hair traits (residualized)

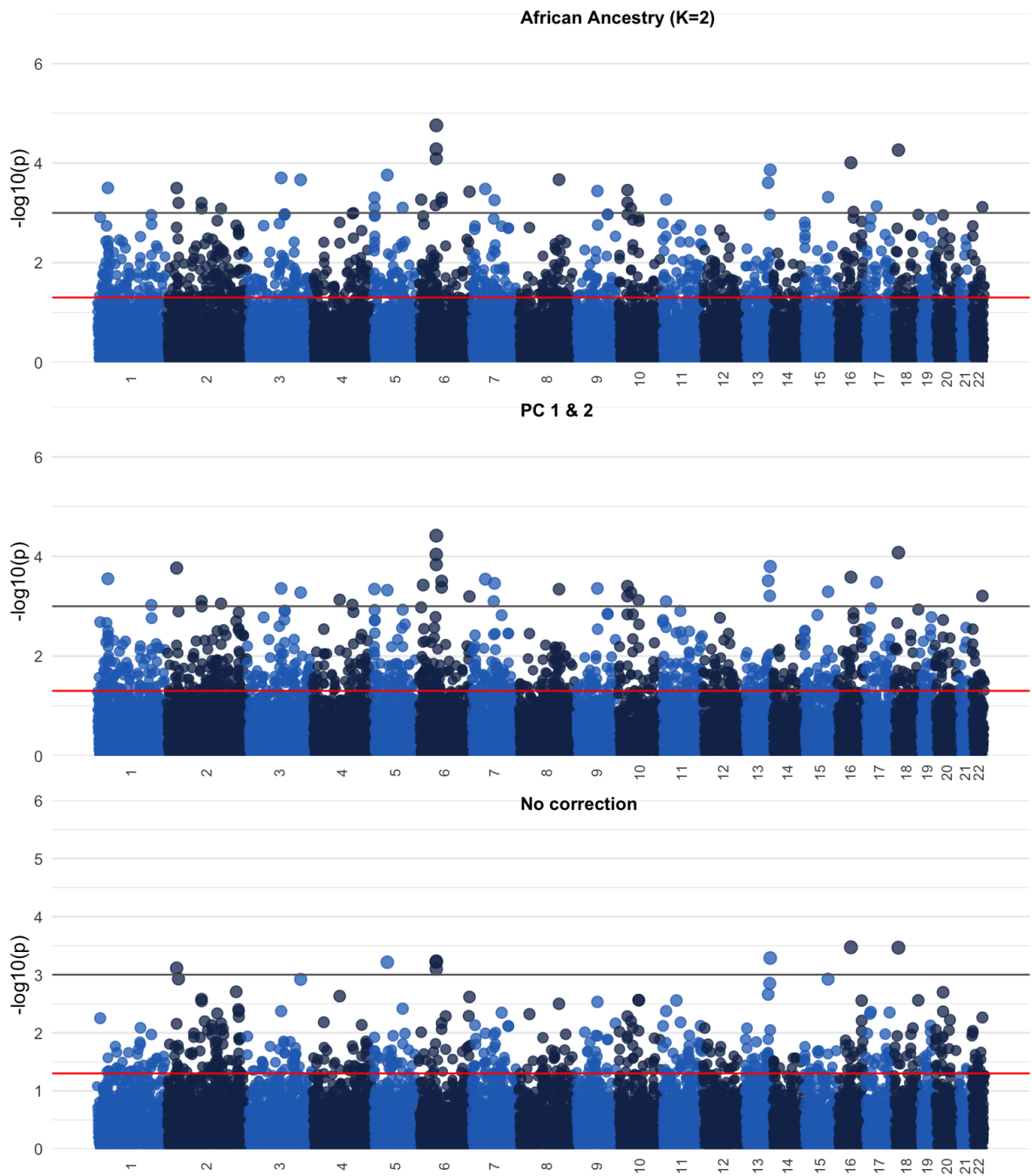


**Figure F.22.** Manhattan plot for PC1 for residualized quantitative hair traits on subset of alleles with high frequency difference between YRI-CEU. First row with correction for ancestry using AFR ( $K=2$ ), second row using first 2 PCs to correct for ancestry, and last row shows plot without correction for ancestry. Highlighted are previously associated loci.

### PC 2 for quantitative hair traits (residualized)

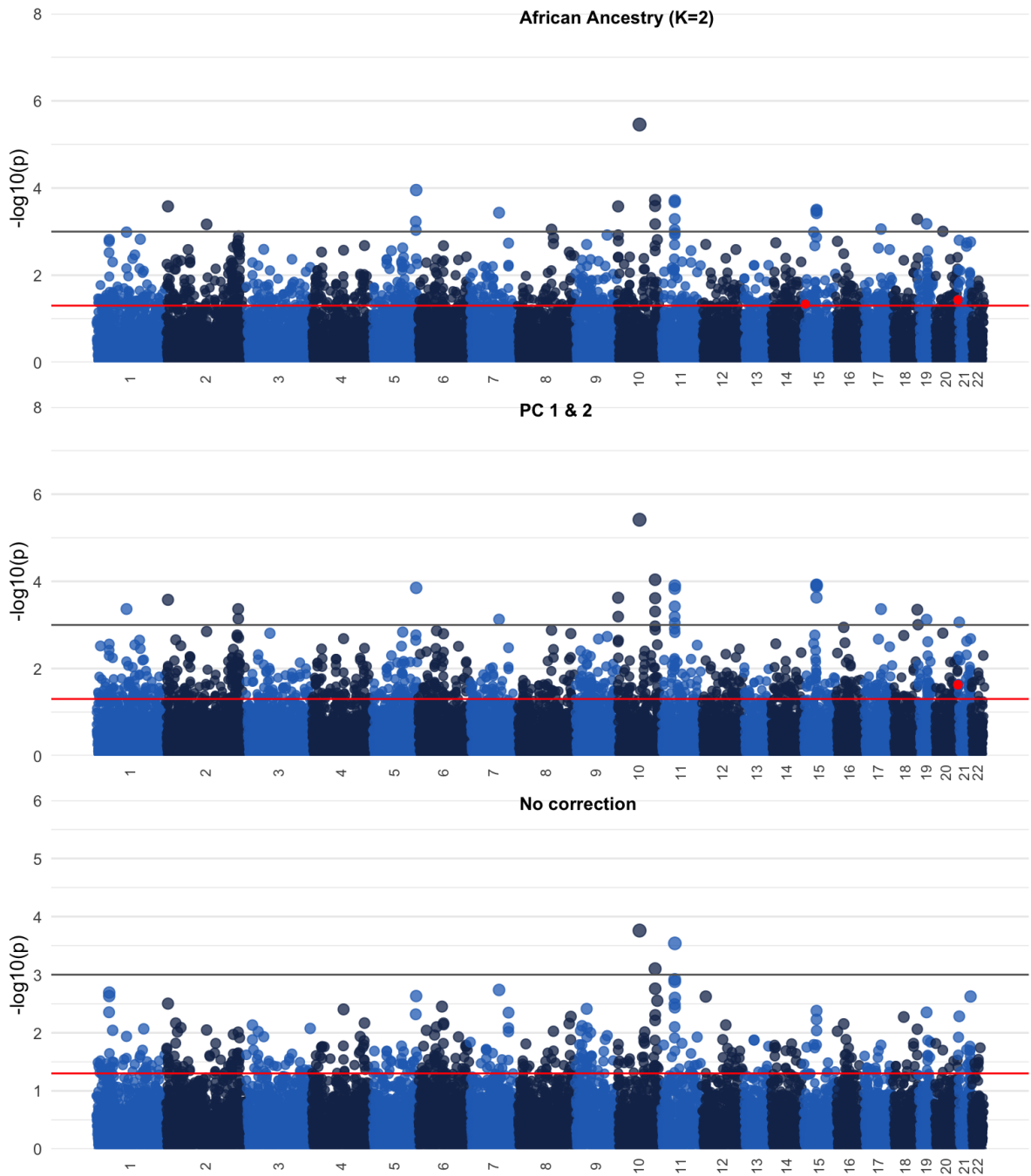


**Figure F.23.** Manhattan plot for PC2 for residualized quantitative hair traits on subset of alleles with high frequency difference between YRI-CEU. First row with correction for ancestry using AFR ( $K=2$ ), second row using first 2 PCs to correct for ancestry, and last row shows plot without correction for ancestry. Highlighted are previously associated loci.

### Hair Type (binned)

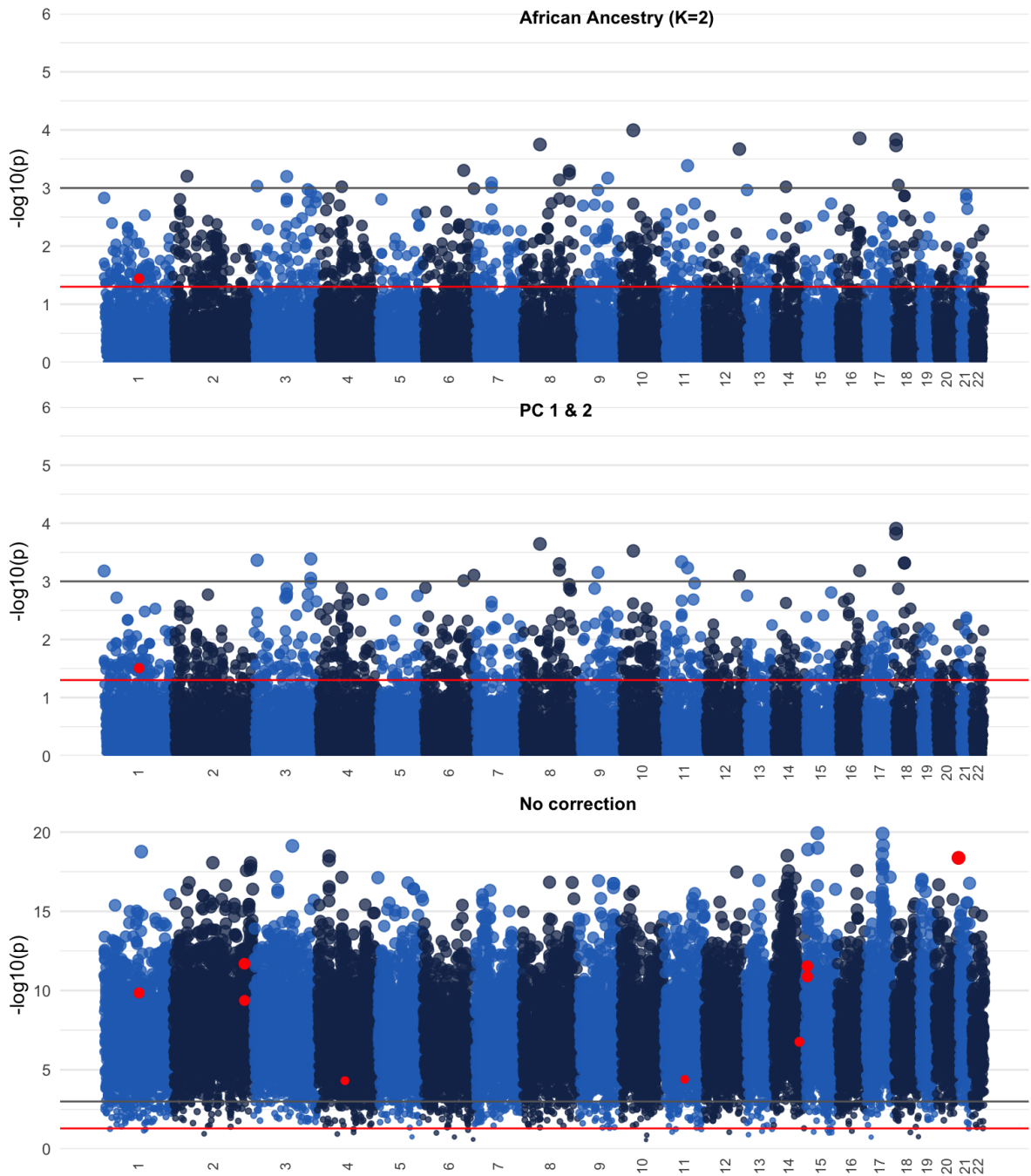


**Figure F.24.** Manhattan plot for objectively classified hair texture on subset of alleles with high frequency difference between YRI-CEU. First row with correction for ancestry using AFR ( $K=2$ ), second row using first 2 PCs to correct for ancestry, and last row shows plot without correction for ancestry. Highlighted are previously associated loci.

**Table F.3.** Hair novel SNPs

	CHR	SNP	BP	A1	BETA	STAT	P	a1_ceu	a2_ceu	maf_ceu	a1_yri	a2_yri	maf_yri	freq.diff
<b>African Ancestry (K=2)</b>														
<b>Curvature</b>														
	4	rs6841926	165700679	A	0.05385	3.597	0.0004190	A	G	0.080810	G	A	0.115700	0.803490
	10	rs7100028	131648687	G	-0.05544	-3.983	0.0000998	G	A	0.095960	A	G	0.157400	0.746640
<b>Cross-sectional eccentricity</b>														
	2	rs10173381	72544130	A	-0.03283	-3.395	0.0008977	G	A	0.212100	A	G	0.000000	0.787900
<b>PC 2 for quantitative hair traits</b>														
	10	rs1419138	119731281	C	0.48920	3.480	0.0006826	C	T	0.040400	T	C	0.087960	0.871640
	6	rs197902	95592790	C	0.46890	3.491	0.0006579	C	T	0.121200	T	C	0.092590	0.786210
	2	rs2251692	227589780	G	0.50320	3.404	0.0008814	A	G	0.232300	G	A	0.009259	0.758441
	5	rs2545801	176841339	C	0.47150	3.976	0.0001154	T	C	0.197000	C	T	0.050930	0.752070
<b>PC 2 for quantitative hair traits (residualized)</b>														
	10	rs10903929	3058348	A	0.59950	3.750	0.0002641	G	A	0.131300	A	G	0.055560	0.813140
<b>Hair Type (binned)</b>														
	3	rs1462797	110578521	C	0.23190	3.502	0.0006327	T	C	0.166700	C	T	0.069440	0.763860
<b>PC 1 &amp; 2</b>														
<b>PC 1 for quantitative hair traits</b>														
	6	rs6912993	10709075	C	-0.79970	-3.432	0.0008049	C	A	0.005051	A	C	0.166700	0.828249

### F.3.1 Hair novel SNPs

Below we show a list of SNPs that were significantly associated with various hair phenotypes in our sample. Here we arrange the list of significant SNPs from high to low frequency difference (YRI-CEU) and low to high P-values and present the top 10 SNPs (see Table F.3). Below we report all significant associations (see Table F.4).

**Table F.4.** Complete table of significant SNPs

African Ancestry (K=2)		CHR	SNP	BP	A1	BETA	STAT	P	a1_ceu	a2_ceu	maf_ceu	a1_yri	a2_yri	maf_yri	frq.diff
<b>Curvature</b>															
1	rs6588459	53511094	T	-0.05358	-3.780	0.0002157	T	C	0.050510	C	T	0.388900	0.560590		
1	rs1146353	116645757	C	-0.04514	-3.472	0.0006514	A	C	0.232300	C	A	0.083330	0.684370		
1	rs10924073	116919519	T	0.06068	4.039	0.0000804	T	C	0.040400	C	T	0.287000	0.672600		
1	rs7536647	176440645	T	0.05276	3.732	0.0002571	T	G	0.070710	G	T	0.347200	0.582090		
1	rs6682429	244811109	T	-0.04693	-3.469	0.0006591	G	T	0.469700	T	G	0.027780	0.502520		
2	rs2041915	206669214	A	0.05350	4.036	0.0000814	A	G	0.065660	G	A	0.365700	0.568640		
2	rs2302909	211503556	T	0.05230	3.766	0.0002263	T	G	0.080810	G	T	0.296300	0.622890		
3	rs7433098	144815506	T	0.04674	3.435	0.0007412	T	C	0.121200	C	T	0.375000	0.503800		
3	rs11929416	171791592	T	-0.05084	-3.622	0.0003829	T	C	0.045450	C	T	0.425900	0.528650		
4	rs6830171	25854036	C	-0.06757	-4.206	0.0000415	C	T	0.000000	T	C	0.435200	0.564800		
4	rs6847725	151547243	T	-0.04933	-3.362	0.0009640	T	C	0.050510	C	T	0.319400	0.525650		
4	rs2321377	165202724	T	-0.04356	-3.483	0.0006265	G	T	0.292900	T	G	0.143500	0.563600		
4	rs6841926	165700679	A	0.05385	3.597	0.0004190	A	G	0.080810	G	A	0.115700	0.803490		
5	rs2607378	67979800	T	0.05699	3.680	0.0003155	T	G	0.030300	G	T	0.319400	0.650300		
6	rs3799339	163726426	G	0.04319	3.610	0.0003996	G	A	0.222200	A	G	0.203700	0.574100		
9	rs10733325	16895610	C	0.05308	3.774	0.0002205	C	T	0.025250	T	C	0.449100	0.525650		
9	rs10733329	16895897	A	0.05318	3.795	0.0002034	A	G	0.025250	G	A	0.449100	0.525650		
9	rs10113990	23231298	C	0.05333	3.518	0.0005555	C	T	0.005051	T	C	0.486100	0.508849		
10	rs1570854	3418124	T	-0.04571	-3.716	0.0002721	C	T	0.313100	T	C	0.125000	0.561900		
10	rs12241514	21602923	A	0.05147	3.963	0.0001080	A	G	0.242400	G	A	0.171300	0.586300		
10	rs7067598	23217699	T	-0.04221	-3.377	0.0009035	C	T	0.242400	T	C	0.143500	0.614100		
10	rs7100028	131648687	G	-0.05544	-3.983	0.0000998	G	A	0.095960	A	G	0.157400	0.746640		
11	rs2863159	45197060	G	0.04756	3.405	0.0008228	G	A	0.136400	A	G	0.314800	0.548800		
11	rs670446	107472733	T	0.05080	3.909	0.0001325	T	C	0.085860	C	T	0.342600	0.571540		
12	rs11058115	125759099	G	-0.05327	-3.687	0.0003089	G	A	0.101000	A	G	0.384300	0.514700		
14	rs8009181	55583424	T	-0.05114	-3.679	0.0003115	T	C	0.010100	C	T	0.287000	0.702900		
14	rs847356	72780987	G	-0.04976	-3.459	0.0006823	A	G	0.434300	G	A	0.000000	0.565700		
14	rs7140253	107233999	G	0.04443	3.417	0.0007875	G	A	0.161600	A	G	0.208300	0.630100		
16	rs12934235	5697395	T	0.04147	3.456	0.0006879	T	C	0.313100	C	T	0.180600	0.506300		
19	rs10417922	17615609	C	-0.05094	-3.558	0.0004813	C	T	0.080810	T	C	0.384300	0.534890		
20	rs6106765	23995560	G	-0.05083	-3.549	0.0004977	G	A	0.141400	A	G	0.347200	0.511400		
<b>Cross-sectional area</b>															
1	rs7417775	31907102	A	606.40000	3.669	0.0003479	A	G	0.010100	G	A	0.398100	0.591800		
5	rs860987	4853391	G	503.50000	3.382	0.0009372	G	A	0.131300	A	G	0.175900	0.692800		
5	rs2650374	4859166	C	503.50000	3.382	0.0009372	C	T	0.131300	T	C	0.171300	0.697400		
10	rs2559524	22892152	A	608.10000	3.664	0.0003538	A	G	0.131300	G	A	0.319400	0.549300		
11	rs4334004	40890649	C	-567.60000	-3.425	0.0008106	C	T	0.131300	T	C	0.351900	0.516800		
16	rs8047238	82459672	A	-549.20000	-3.388	0.0009210	A	C	0.111100	C	A	0.273100	0.615800		
20	rs4810617	45762885	A	-497.60000	-3.411	0.0008523	A	G	0.121200	G	A	0.273100	0.605700		
<b>Cross-sectional eccentricity</b>															
1	rs710231	42204406	A	0.03621	4.172	0.0000531	G	A	0.348500	A	G	0.129600	0.521900		
1	rs2055953	42225580	T	0.03757	4.309	0.0000310	C	T	0.348500	T	C	0.148100	0.503400		
1	rs871343	42230685	G	0.03752	4.286	0.0000341	A	G	0.348500	G	A	0.106500	0.545000		
2	rs975612	72389334	T	-0.03054	-3.564	0.0005051	G	T	0.368700	T	G	0.032410	0.598890		
2	rs7565922	72441720	A	-0.03133	-3.523	0.0005797	G	A	0.318200	A	G	0.115700	0.566100		
2	rs10173381	72544130	A	-0.03283	-3.395	0.0008977	G	A	0.212100	A	G	0.000000	0.787900		
3	rs331894	336766	C	0.03361	3.471	0.0006930	T	C	0.424200	C	T	0.060190	0.515610		
9	rs979814	93106543	G	-0.03693	-4.079	0.0000760	G	A	0.095960	A	G	0.314800	0.589240		
12	rs7137194	99872660	C	0.03420	3.494	0.0006441	T	C	0.222200	C	T	0.240700	0.537100		
13	rs7995410	48753318	A	0.03074	3.401	0.0008791	G	A	0.414100	A	G	0.009259	0.576641		
13	rs2406804	48794188	C	0.03074	3.401	0.0008791	T	C	0.414100	C	T	0.009259	0.576641		
16	rs9888988	73495661	C	-0.03583	-3.494	0.0006393	T	C	0.186900	C	T	0.115700	0.697400		
18	rs648161	7042402	A	-0.03770	-3.744	0.0002647	G	A	0.393900	A	G	0.037040	0.569060		

Minimum diameter of cross-section

1	rs12140494	9600774	C	3.63300	3.686	0.0003277	C	T	0.232300	T	C	0.222200	0.545500
1	rs6429695	15273115	T	-3.98500	-3.465	0.0007066	G	T	0.393900	T	G	0.009259	0.596841
1	rs6665725	177136117	G	-4.26700	-3.645	0.0003773	G	A	0.065660	A	G	0.425900	0.508440
1	rs725416	177148159	A	-4.41900	-4.142	0.0000598	A	C	0.156600	C	A	0.245400	0.598000
2	rs2588888	178048763	G	-3.64700	-3.439	0.0007719	G	A	0.191900	A	G	0.291700	0.516400
2	rs992871	220689584	T	4.08200	3.542	0.0005413	C	T	0.409100	T	C	0.009259	0.581641
3	rs2160052	118641879	C	3.64200	3.577	0.0004795	C	T	0.136400	T	C	0.250000	0.613600
3	rs6767716	167907755	A	3.57500	3.380	0.0009413	G	A	0.151500	A	G	0.101900	0.746600
4	rs10029225	125732734	C	3.77900	3.483	0.0006662	C	T	0.161600	T	C	0.231500	0.606900
5	rs2134180	4734171	C	-4.65700	-4.526	0.0000128	T	C	0.363600	C	T	0.009259	0.627141
6	rs7762445	46461236	C	-4.21200	-3.524	0.0005773	T	C	0.474700	C	T	0.000000	0.525300
6	rs316144	52879695	C	-4.32400	-3.549	0.0005283	T	C	0.404000	C	T	0.004630	0.591370
8	rs7815277	131960656	C	4.16400	3.642	0.0003816	C	T	0.090910	T	C	0.291700	0.617390
9	rs7852195	81606411	T	-4.75400	-3.517	0.0005919	T	C	0.000000	C	T	0.453700	0.546300
9	rs7469847	118738595	G	3.99000	3.463	0.0007126	G	A	0.080810	A	G	0.412000	0.507190
9	rs7469818	118738647	C	3.99000	3.463	0.0007126	C	A	0.080810	A	C	0.407400	0.511790
9	rs1024277	134246225	T	-4.63700	-3.460	0.0007202	T	C	0.025250	C	T	0.425900	0.548850
11	rs4148640	17421714	G	-3.60700	-3.602	0.0004407	T	G	0.303000	G	T	0.120400	0.576600
11	rs4149180	62782278	T	-4.89800	-3.711	0.0002984	T	C	0.005051	C	T	0.407400	0.587549
13	rs7329271	104888924	C	-5.04700	-3.465	0.0007083	C	T	0.010100	T	C	0.435200	0.554700
13	rs9301388	110136564	C	4.02100	3.818	0.0002022	T	C	0.399000	C	T	0.013890	0.587110
15	rs1678983	48930645	C	-3.59400	-3.464	0.0007102	C	T	0.116200	T	C	0.370400	0.513400
16	rs4438310	25890171	A	4.68100	3.849	0.0001809	A	G	0.045450	G	A	0.407400	0.547150
16	rs1424052	82476144	A	-4.46300	-3.893	0.0001534	A	G	0.085860	G	A	0.398100	0.516040
17	rs9902289	12658023	G	-4.11000	-3.598	0.0004455	G	A	0.050510	A	G	0.370400	0.579090
18	rs11664142	75641491	A	-3.73000	-3.393	0.0009149	A	G	0.151500	G	A	0.208300	0.640200
22	rs5748167	19370586	C	-4.23200	-3.414	0.0008410	C	T	0.030300	T	C	0.430600	0.539100
22	rs5993624	19380714	C	-4.75800	-3.708	0.0003015	C	A	0.030300	A	C	0.356500	0.613200

**Maximum diameter of cross-section**

1	rs17021481	213985718	G	7.66200	3.845	0.0001831	G	A	0.106100	A	G	0.319400	0.574500
1	rs6681892	214089860	G	7.52400	3.401	0.0008797	G	T	0.060610	T	G	0.384300	0.555090
2	rs2723102	23527304	A	-8.54300	-3.609	0.0004307	A	G	0.080810	G	A	0.365700	0.553490
2	rs11125053	23701104	A	8.48300	4.344	0.0000270	G	A	0.353500	A	G	0.064810	0.581690
2	rs6732918	31009479	A	-6.88200	-3.780	0.0002327	A	G	0.176800	G	A	0.273100	0.550100
2	rs12613932	235670433	C	7.00700	3.417	0.0008383	C	T	0.141400	T	C	0.180600	0.678000
2	rs11903546	235670805	A	7.04000	3.432	0.0007921	A	C	0.141400	C	A	0.180600	0.678000
3	rs1355767	111416310	A	7.10600	3.598	0.0004460	A	G	0.277800	G	A	0.203700	0.518500
4	rs1040105	119284556	A	8.26800	3.500	0.0006381	A	G	0.065660	G	A	0.370400	0.563940
5	rs816480	4835205	A	7.05800	3.422	0.0008170	A	G	0.131300	G	A	0.152800	0.715900
5	rs32498	55548797	T	6.66900	3.370	0.0009742	C	T	0.298000	T	C	0.101900	0.600100
6	rs6921664	48321410	G	8.69000	4.134	0.0000615	G	A	0.045450	A	G	0.439800	0.514750
6	rs7755638	48329809	C	8.82800	4.154	0.0000569	C	T	0.045450	T	C	0.439800	0.514750
6	rs970048	48378266	G	9.67400	4.836	0.0000035	G	A	0.116200	A	G	0.379600	0.504200
6	rs1547251	83406107	T	-6.75500	-3.430	0.0007966	C	T	0.454500	T	C	0.004630	0.540870
6	rs2253003	83423397	T	-6.94100	-3.497	0.0006344	C	T	0.449500	T	C	0.004630	0.545870
6	rs16899333	167147083	T	-7.14100	-3.457	0.0007262	T	G	0.156600	G	T	0.333300	0.510100
6	rs1473500	168511016	T	-8.47300	-3.636	0.0003903	T	C	0.030300	C	T	0.342600	0.627100
7	rs7796918	8505405	A	8.10600	3.386	0.0009239	A	G	0.035350	G	A	0.449100	0.515550
7	rs7787692	91174263	A	8.14300	3.483	0.0006659	A	C	0.015150	C	A	0.430600	0.554250
7	rs7802845	111723488	G	-7.51600	-3.389	0.0009132	G	A	0.095960	A	G	0.342600	0.561440
8	rs483654	20809616	C	6.94200	3.708	0.0003022	T	C	0.308100	C	T	0.111100	0.580800
8	rs2935548	101680355	G	6.62000	3.404	0.0008683	G	A	0.095960	A	G	0.263900	0.640140
10	rs1750770	22926993	G	8.20800	3.763	0.0002473	G	A	0.166700	A	G	0.222200	0.611100
10	rs540878	30475054	G	7.88600	3.787	0.0002264	G	T	0.050510	T	G	0.398100	0.551390
10	rs773970	34813742	G	-6.52400	-3.408	0.0008590	A	G	0.308100	G	A	0.125000	0.566900
10	rs2477017	34911879	G	-8.05600	-4.036	0.0000900	A	G	0.318200	G	A	0.018520	0.663280
10	rs2490806	34918550	C	-7.65100	-3.664	0.0003531	T	C	0.318200	C	T	0.018520	0.663280
11	rs7102290	4995686	T	6.75400	3.410	0.0008556	T	C	0.131300	C	T	0.324100	0.544600
15	rs784417	49013011	G	7.13200	3.654	0.0003658	G	A	0.252500	A	G	0.213000	0.534500
15	rs7174749	81087552	A	7.17800	4.001	0.0001027	A	C	0.237400	C	A	0.245400	0.517200
17	rs1877822	63165077	G	-7.31100	-3.678	0.0003362	G	A	0.171700	A	G	0.236100	0.592200
18	rs600589	8831217	G	-6.53800	-3.425	0.0008092	A	G	0.272700	G	A	0.203700	0.523600
18	rs1787984	11972439	A	8.27400	3.987	0.0001085	G	A	0.252500	A	G	0.194400	0.553100
19	rs11557092	11257018	C	-6.82700	-3.677	0.0003377	T	C	0.227300	C	T	0.129600	0.643100

**PC 1 for quantitative hair traits**

1	rs522821	35741663	A	-0.88370	-3.591	0.0004645	A	G	0.055560	G	A	0.305600	0.638840
2	rs4668077	169439848	G	-0.74100	-3.507	0.0006220	A	G	0.176800	G	A	0.097220	0.725980
3	rs11539377	119219573	G	-0.77920	-3.426	0.0008193	G	A	0.020200	A	G	0.402800	0.577000
3	rs11916272	119242930	T	-0.77920	-3.426	0.0008193	T	C	0.020200	C	T	0.402800	0.577000
5	rs1209532	119392433	A	0.68490	3.395	0.0009086	G	A	0.454500	A	G	0.032410	0.513090
6	rs1765828	4646578	G	-0.70580	-3.626	0.0004129	G	T	0.075760	T	G	0.347200	0.577040
7	rs4723450	35948676	A	0.70300	3.499	0.0006399	G	A	0.358600	A	G	0.092590	0.548810
7	rs2724099	93435670	G	-0.86680	-3.440	0.0007796	G	A	0.085860	A	G	0.338000	0.576140
13	rs17367786	107935678	T	-0.67060	-3.558	0.0005210	C	T	0.434300	T	C	0.009259	0.556441
16	rs9933802	55429134	G	0.76770	3.972	0.0001172	G	T	0.075760	T	G	0.375000	0.549240
17	rs1015767	14458000	T	-0.69270	-3.434	0.0007978	C	T	0.292900	T	C	0.060190	0.646910
20	rs391040	22327111	A	-0.65820	-3.580	0.0004824	C	A	0.318200	A	C	0.171300	0.510500

**PC 2 for quantitative hair traits**

2	rs907864	20304899	T	-0.39780	-3.453	0.0007461	T	G	0.298000	G	T	0.189800	0.512200
2	rs13414424	222641193	C	0.44560	3.494	0.0006494	T	C	0.449500	C	T	0.032410	0.518090
2	rs2251692	227589780	G	0.50320	3.404	0.0008814	A	G	0.232300	G	A	0.009259	0.758441
4	rs207343	19036305	T	-0.52240	-3.508	0.0006183	T	C	0.075760	C	T	0.342600	0.581640
5	rs2545801	176841339	C	0.47150	3.976	0.0001154	T	C	0.197000	C	T	0.050930	0.752070
6	rs197902	95592790	C	0.46890	3.491	0.0006579	C	T	0.121200	T	C	0.092590	0.786210
8	rs4469413	92265638	G	-0.39480	-3.374	0.0009750	A	G	0.272700	G	A	0.175900	0.551400
10	rs2151962	72306822	G	0.58130	4.865	0.0000032	A	G	0.434300	G	A	0.055560	0.510140
10	rs1419138	119731281	C	0.48920	3.480	0.0006826	C	T	0.040400	T	C	0.087960	0.871640
10	rs1016112	119788183	C	-0.44990	-3.501	0.0006336	T	C	0.358600	C	T	0.087960	0.553440
11	rs7939125	39810064	A	-0.41290	-3.816	0.0002079	G	A	0.323200	A	G	0.143500	0.533300
11	rs11828333	131417551	C	-0.44900	-3.450	0.0007535	C	T	0.035350	T	C	0.421300	0.543350
12	rs7316843	71449811	T	-0.43480	-3.373	0.0009807	C	T	0.217200	T	C	0.226900	0.555900
12	rs17116007	76363748	T	0.47010	3.386	0.0009383	T	C	0.020200	C	T	0.430600	0.549200
17	rs7221641	58494204	T	-0.47310	-3.418	0.0008398	T	C	0.035350	C	T	0.463000	0.501650
20	rs3848799	23989930	T	0.51750	3.715	0.0003000	C	T	0.373700	T	C	0.000000	0.626300

**PC 1 for quantitative hair traits (residualized)**

2	rs843427	116219686	G	0.90430	3.504	0.0006279	G	A	0.045450	A	G	0.370400	0.584150
2	rs4530380	116238748	A	0.87300	3.426	0.0008177	A	G	0.045450	G	A	0.375000	0.579550
10	rs2559523	22893246	G	-0.82860	-3.509	0.0006172	G	A	0.131300	A	G	0.356500	0.512200
16	rs8045523	66973381	A	-0.73850	-3.384	0.0009443	A	G	0.161600	G	A	0.194400	0.644000

**PC 2 for quantitative hair traits (residualized)**

2	rs1656168	7877131	A	-0.56720	-3.751	0.0002636	G	A	0.242400	A	G	0.060190	0.697410
2	rs2709549	133440227	C	0.52000	3.480	0.0006818	A	C	0.429300	C	A	0.069440	0.501260
5	rs10516132	175282343	A	-0.50630	-3.523	0.0005886	A	G	0.151500	G	A	0.342600	0.505900
5	rs551657	176233792	T	-0.66420	-3.389	0.0009258	T	C	0.030300	C	T	0.226900	0.742800
7	rs1627354	107677984	A	0.62350	3.657	0.0003689	A	G	0.070710	G	A	0.319400	0.609890
8	rs1227664	80162053	C	0.54940	3.402	0.0008886	A	C	0.414100	C	A	0.000000	0.585900
10	rs10903929	3058348	A	0.59950	3.750	0.0002641	G	A	0.131300	A	G	0.055560	0.813140
10	rs853577	119821336	A	0.70280	3.850	0.0001890	A	G	0.040400	G	A	0.226900	0.732700
10	rs703422	119828177	G	-0.51940	-3.485	0.0006707	A	G	0.358600	G	A	0.083330	0.558070
11	rs1993836	39728091	A	-0.51560	-3.397	0.0009044	C	A	0.328300	A	C	0.125000	0.546700
11	rs10837222	39748212	T	-0.56160	-3.815	0.0002092	C	T	0.353500	T	C	0.027780	0.618720
11	rs1702585	39754355	A	-0.50080	-3.563	0.0005128	G	A	0.267700	A	G	0.203700	0.528600
15	rs809207	49026206	G	-0.48870	-3.685	0.0003334	G	A	0.176800	A	G	0.217600	0.605600
15	rs784411	49039797	C	-0.47930	-3.701	0.0003150	C	T	0.176800	T	C	0.231500	0.591700
15	rs8041414	49056670	G	-0.50200	-3.650	0.0003782	G	T	0.176800	T	G	0.189800	0.633400
18	rs4890939	75173558	G	-0.53620	-3.562	0.0005158	G	A	0.191900	A	G	0.296300	0.511800
19	rs4805612	31238357	T	0.52170	3.487	0.0006658	C	T	0.474700	T	C	0.004630	0.520670

**Hair Type (binned)**

2	rs1446296	38216416	T	-0.22970	-3.505	0.0006262	G	T	0.429300	T	G	0.000000	0.570700
3	rs17288498	7140857	G	0.21470	3.392	0.0009261	A	G	0.272700	G	A	0.060190	0.667110
3	rs1462797	110578521	C	0.23190	3.502	0.0006327	T	C	0.166700	C	T	0.069440	0.763860
4	rs6446825	73139890	T	-0.21000	-3.381	0.0009521	C	T	0.277800	T	C	0.092590	0.629610
6	rs6918767	139707585	C	-0.20890	-3.572	0.0004974	C	T	0.151500	T	C	0.250000	0.598500
7	rs260368	46463342	A	0.21160	3.428	0.0008135	C	A	0.176800	A	C	0.208300	0.614900
7	rs10278486	46551552	C	0.20720	3.374	0.0009733	T	C	0.191900	C	T	0.296300	0.511800
8	rs6474312	41008081	G	0.23390	3.858	0.0001783	A	G	0.469700	G	A	0.023150	0.507150
8	rs1386107	91872814	G	0.20030	3.462	0.0007254	A	G	0.232300	G	A	0.166700	0.601000
8	rs1402513	119660179	T	-0.22490	-3.568	0.0005039	C	T	0.419200	T	C	0.050930	0.529870
8	rs769322	119669368	G	-0.22180	-3.532	0.0005694	A	G	0.419200	G	A	0.055560	0.525240
9	rs2004725	108061875	C	-0.23930	-3.483	0.0006744	C	T	0.070710	T	C	0.425900	0.503390
10	rs12767581	29357507	G	-0.23160	-4.010	0.0001015	A	G	0.378800	G	A	0.000000	0.621200
11	rs892857	78707366	T	0.23400	3.625	0.0004123	C	T	0.308100	T	C	0.046300	0.645600
12	rs708849	117864216	C	-0.20920	-3.809	0.0002141	A	C	0.338400	C	A	0.106500	0.555100
14	rs9323364	60775701	C	0.19670	3.382	0.0009532	A	C	0.242400	C	A	0.032410	0.725190
16	rs12448290	80655883	T	-0.24180	-3.923	0.0001402	G	T	0.257600	T	G	0.175900	0.566500
18	rs475598	7027438	C	0.22050	3.848	0.0001853	T	C	0.388900	C	T	0.106500	0.504600
18	rs7237913	7029115	T	0.22520	3.912	0.0001463	C	T	0.388900	T	C	0.087960	0.523140
18	rs12454673	11817585	A	0.20660	3.402	0.0008878	G	A	0.373700	A	G	0.115700	0.510600

**PC 1 & 2****Curvature**

1	rs9887913	55462380	C	-0.05294	-3.408	0.0008191	C	T	0.020200	T	C	0.388900	0.590900
2	rs6743345	39443569	G	-0.04449	-3.383	0.0008876	G	A	0.166700	A	G	0.259300	0.574000
4	rs17040486	110400461	A	0.05712	3.360	0.0009602	A	G	0.000000	G	A	0.439800	0.560200
7	rs7810799	151734581	A	0.05002	3.355	0.0009783	A	G	0.025250	G	A	0.384300	0.590450
11	rs7107225	45006741	G	0.04555	3.360	0.0009767	G	A	0.055560	A	G	0.361100	0.583340
11	rs2036135	82448738	C	0.04415	3.374	0.0009150	C	T	0.252500	T	C	0.157400	0.590100
16	rs7188960	24719987	A	-0.04625	-3.464	0.0006850	A	G	0.085860	G	A	0.333300	0.580840

**Cross-sectional area**

11	rs7937649	5222379	G	479.60000	3.440	0.0007726	G	A	0.156600	A	G	0.333300	0.510100
12	rs7979812	56781444	A	586.40000	3.463	0.0007135	A	C	0.005051	C	A	0.449100	0.545849

**Cross-sectional eccentricity**

4	rs3117600	74731812	A	-0.02900	-3.396	0.0008964	G	A	0.272700	A	G	0.134300	0.593000
4	rs593641	74758439	G	-0.03100	-3.532	0.0005632	A	G	0.232300	G	A	0.120400	0.647300
4	rs569390	74760396	A	-0.03100	-3.532	0.0005632	G	A	0.232300	A	G	0.120400	0.647300
21	rs9983496	42586130	T	-0.03228	-3.366	0.0009912	C	T	0.469700	T	C	0.004630	0.525670

**Minimum diameter of cross-section**

1	rs4481881	107686418	T	-3.55500	-3.398	0.0008922	C	T	0.378800	T	C	0.046300	0.574900
3	rs33532	42415205	C	3.86000	3.386	0.0009255	C	T	0.075760	T	C	0.268500	0.655740
4	rs13108814	81351038	T	-3.42600	-3.419	0.0008276	T	G	0.197000	G	T	0.231500	0.571500

**Maximum diameter of cross-section**

11	rs2509984	62219776	A	8.31400	3.621	0.0004122	A	G	0.080810	G	A	0.398100	0.521090
17	rs8078799	41426948	A	8.59300	3.489	0.0006597	A	G	0.005051	G	A	0.425900	0.569049

**PC 1 for quantitative hair traits**

6	rs6912993	10709075	C	-0.79970	-3.432	0.0008049	C	A	0.005051	A	C	0.166700	0.828249
10	rs2578018	65839970	A	0.67390	3.488	0.0006647	A	C	0.166700	C	A	0.236100	0.597200
22	rs763100	45988571	A	0.77190	3.371	0.0009860	A	C	0.126300	C	A	0.185200	0.688500

**PC 2 for quantitative hair traits**

2	rs620698	220466199	G	-0.54980	-3.459	0.0007325	G	T	0.015150	T	G	0.328700	0.656150
6	rs239798	54805688	C	0.42840	3.442	0.0007768	C	A	0.176800	A	C	0.250000	0.573200

**PC 2 for quantitative hair traits (residualized)**

1	rs555095	110640433	A	-0.51630	-3.613	0.0004314	A	G	0.176800	G	A	0.254600	0.568600
2	rs10209807	222542378	A	0.48060	3.613	0.0004319	G	A	0.373700	A	G	0.125000	0.501300
10	rs7095234	3058952	G	-0.51280	-3.497	0.0006439	G	A	0.131300	A	G	0.314800	0.553900
11	rs10837260	39802603	C	-0.47160	-3.397	0.0009033	T	C	0.338400	C	T	0.013890	0.647710
18	rs9518	77288806	T	0.56570	3.370	0.0009895	C	T	0.166700	T	C	0.120400	0.712900
21	rs2823583	17416605	A	0.46530	3.410	0.0008665	C	A	0.393900	A	C	0.097220	0.508880

**Hair Type (binned)**

1	rs13303106	891945	G	0.21730	3.491	0.0006631	A	G	0.303000	G	A	0.078700	0.618300
3	rs4855054	181609741	C	0.18520	3.405	0.0008792	T	C	0.373700	C	T	0.111100	0.515200
3	rs10937074	181637333	C	0.20950	3.627	0.0004110	T	C	0.378800	C	T	0.037040	0.584160
6	rs4708459	168760569	A	0.20530	3.440	0.0007831	G	A	0.388900	A	G	0.060190	0.550910
8	rs6471261	91890170	G	0.20420	3.497	0.0006436	T	G	0.237400	G	T	0.213000	0.549600
9	rs10869083	74644462	C	-0.21300	-3.475	0.0007022	T	C	0.409100	C	T	0.023150	0.567750
11	rs6485802	48051442	A	-0.21260	-3.594	0.0004614	C	A	0.252500	A	C	0.041670	0.705830
18	rs12956949	35171653	A	0.20240	3.580	0.0004836	G	A	0.383800	A	G	0.074070	0.542130
18	rs7505519	35172316	A	0.20240	3.580	0.0004836	G	A	0.383800	A	G	0.074070	0.542130

# Appendix G |

## Chapter 5 Supplementary:

### Thermal manikin experiment results

#### G.1 Heat loss (4°C)

The dry measurements were taken at two different temperatures - one with  $T_{manikin} = 34^{\circ}C$  and  $T_{ambient} = 8^{\circ}C$ , and another with  $T_{manikin} = 38^{\circ}C$  and  $T_{ambient} = 4^{\circ}C$ .

The second set of temperature options was found to be necessary with the straight (low curvature) wig in the  $0.3\ m/s$  wind speed setting with the radiation on because the manikin would overheat to the point where no heat loss could be measured. We then made sure to conduct all the  $0.3\ m/s$  wind speed experiments with this second option.

In the preparation of the data, we applied a correction to bring all the measurements to the same temperature, i.e.  $T_{ambient} = 4^{\circ}C$ .

The wet measurements are based on heat exchange rather than dry heat loss. These measurements were taken with the temperature settings  $T_{manikin} = 34^{\circ}C$  and  $T_{ambient} = 34^{\circ}C$  or  $T_{manikin} = T_{ambient}$ . The measurements have been converted to heat loss for comparative purposes (see Figure G.1).

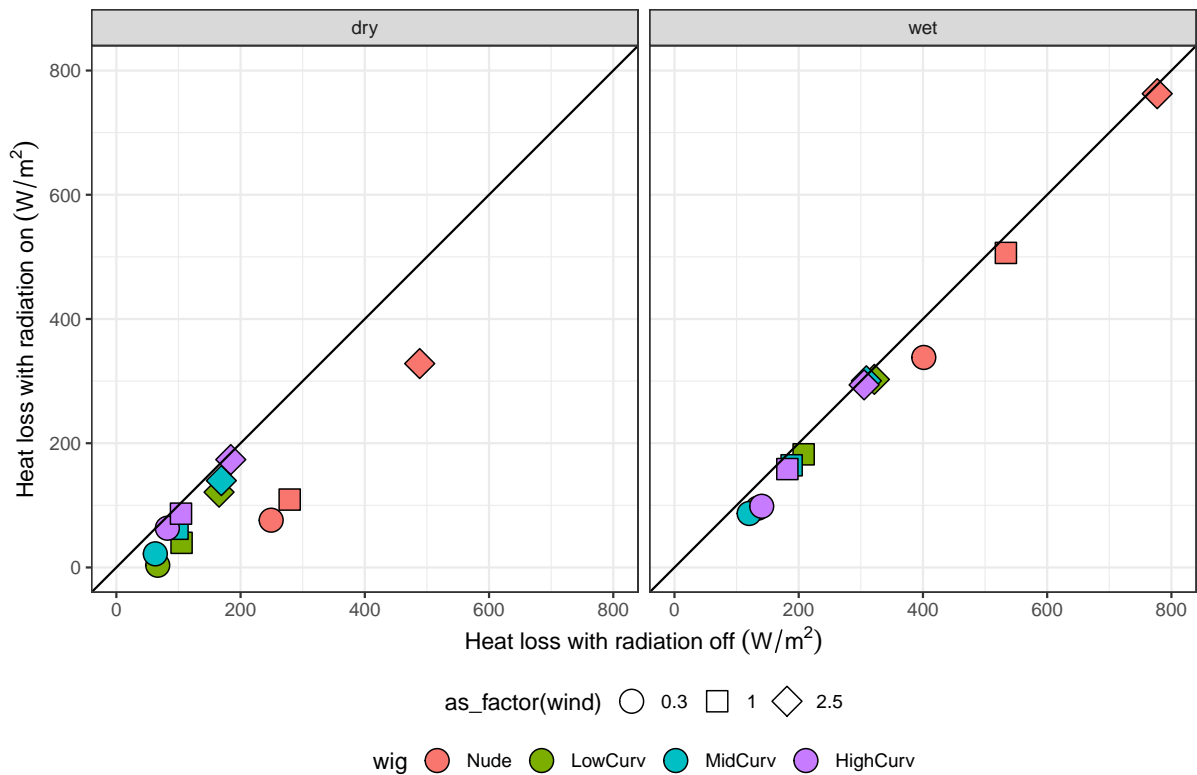


**Figure G.1.** Comparison of dry heat loss and wet heat loss (dry + evaporative) for various head coverings at three wind speeds with radiation on and off at 4C. Heat loss with radiation off (x-axis) vs. heat loss with radiation on (y-axis) for dry (left) and wet (right) experiments. Wigs are indicated by color and wind speed is indicated by shape.

### G.1.1 Linear model

We created a linear model for heat loss using wet/dry, radiation, wind speed and head covering (wig type) as independent variables. Additionally, we include possible interactions between wet/dry, radiation and wig type.

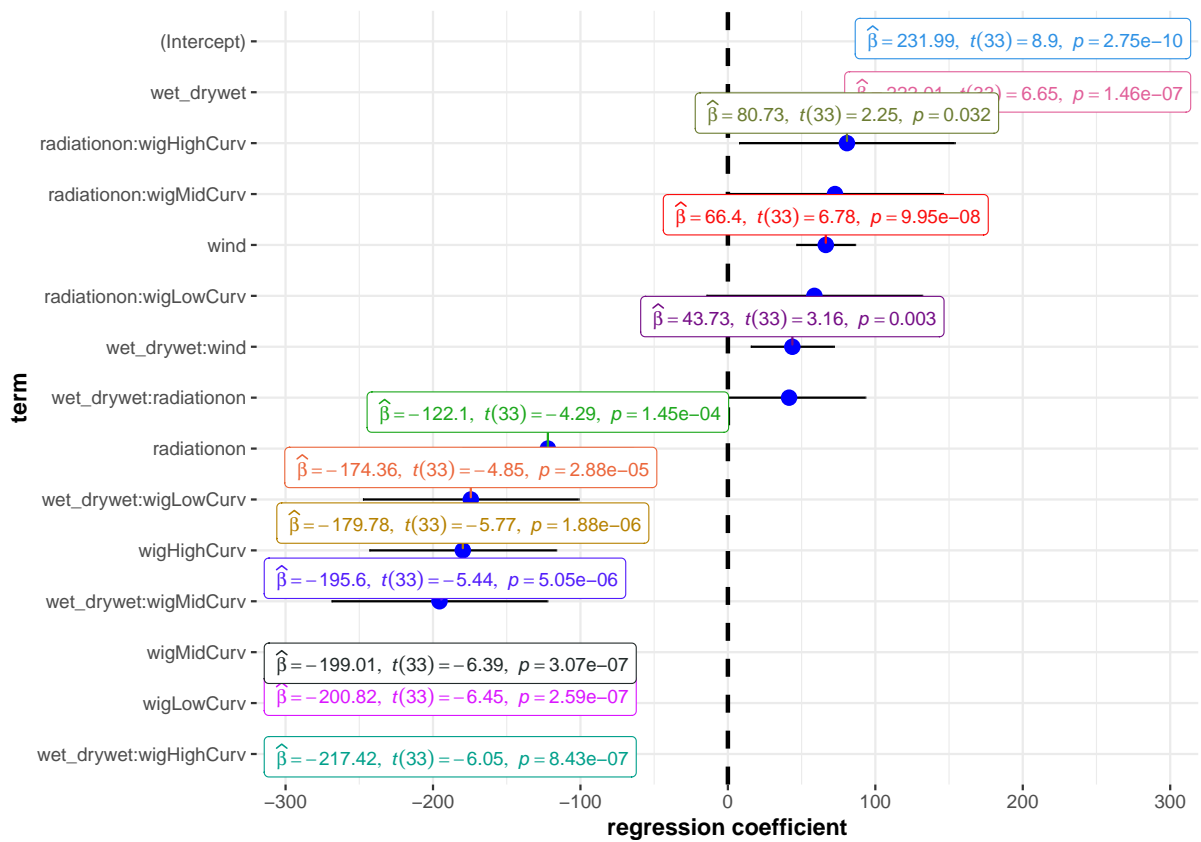
Below, our results show that the most significant variables are wig and radiation, with marginal significance in radiation and the interaction between radiation and wig type (see also Figure G.2).

```
##
## Call:
## lm(formula = heatloss4c ~ wet_dry + radiation + wind + wig +
##     wet_dry * wind + wet_dry * wig + wet_dry * radiation + radiation *
##     wig, data = df_4c_influx_long)
```

```

##
## Residuals:
##      Min       1Q   Median       3Q      Max
## -85.683 -26.449   4.191  16.538 113.977
##
## Coefficients:
##              Estimate Std. Error t value Pr(>|t|)
## (Intercept)      231.985     26.064   8.901 2.75e-10 ***
## wet_drywet       222.015     33.410   6.645 1.46e-07 ***
## radiationon     -122.100     28.430  -4.295 0.000145 ***
## wind              66.402      9.796   6.778 9.95e-08 ***
## wigLowCurv     -200.820     31.143  -6.448 2.59e-07 ***
## wigMidCurv     -199.010     31.143  -6.390 3.07e-07 ***
## wigHighCurv    -179.780     31.143  -5.773 1.88e-06 ***
## wet_drywet:wind   43.734     13.854   3.157 0.003399 **
## wet_drywet:wigLowCurv -174.364     35.961  -4.849 2.88e-05 ***
## wet_drywet:wigMidCurv -195.597     35.961  -5.439 5.05e-06 ***
## wet_drywet:wigHighCurv -217.417     35.961  -6.046 8.43e-07 ***
## wet_drywet:radiationon  41.506     25.428   1.632 0.112133
## radiationon:wigLowCurv  58.664     35.961   1.631 0.112332
## radiationon:wigMidCurv  72.647     35.961   2.020 0.051545 .
## radiationon:wigHighCurv  80.733     35.961   2.245 0.031588 *
## ---
## Signif. codes:  0 '***' 0.001 '**' 0.01 '*' 0.05 '.' 0.1 ' ' 1
##
## Residual standard error: 44.04 on 33 degrees of freedom
## Multiple R-squared:  0.9542, Adjusted R-squared:  0.9347
## F-statistic: 49.09 on 14 and 33 DF, p-value: < 2.2e-16

```



AIC = 514, BIC = 544

**Figure G.2.** Dot-and-whisker plot for regression analysis of heat loss Regression coefficient on the x-axis with different terms on the y-axis. Only significant results shown.

Viewed as an ANOVA, we confirm that the main significant variables in our model are radiation, wind speed and wig type, while there is a marginal significance ( $<0.05$ ) for the interaction for radiation \* wig type and wet/dry\* wig type.

##	Df	Sum Sq	Mean Sq	F value	Pr(>F)
## wet_dry	1	274771	274771	141.649	1.74e-13 ***
## radiation	1	28037	28037	14.453	0.000588 ***
## wind	1	314980	314980	162.378	2.71e-14 ***
## wig	3	589784	196595	101.348	< 2e-16 ***
## wet_dry:wind	1	19330	19330	9.965	0.003399 **
## wet_dry:wig	3	89034	29678	15.299	2.07e-06 ***
## wet_dry:radiation	1	5168	5168	2.664	0.112133
## radiation:wig	3	11989	3996	2.060	0.124503
## Residuals	33	64013	1940		

```
## ---
## Signif. codes:  0 '***' 0.001 '**' 0.01 '*' 0.05 '.' 0.1 ' ' 1
```

## G.2 Solar influx (4°C)

We can also look specifically at the effect of the radiation by subtracting the measurements with radiation off from those with radiation on.

From the plots below, it is apparent that the experiments with a “Nude” manikin scalp show a considerably different pattern than any of the wigs.

Interestingly, in the dry experiments, the effect of solar radiation appears to cluster more by wig, while the wet experiments show a solar influx that is more patterned by wind speed (see Figure G.3).

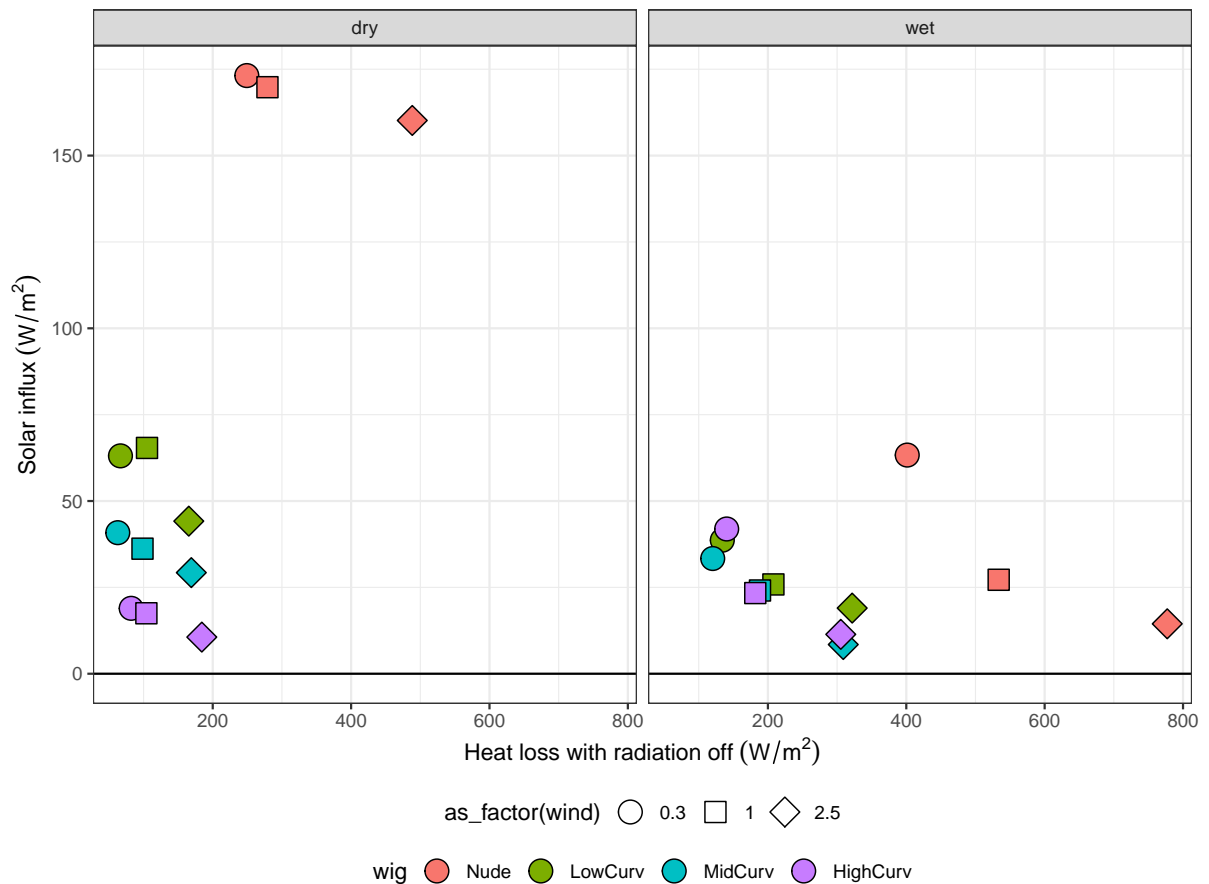


**Figure G.3. Scatter plot of solar flux across experiments.** This plot shows the solar influx as a function of heat loss in the radiation off state. The horizontal line is at zero showing that all values are positive.

Below, we plot the same net heat loss as a function of wind speed. Similarly, we see that, in the dry experiments, there is a very clear effect of wig type and no hair, while the wet experiments show a much more pronounced effect of wind speed (see Figure G.4).

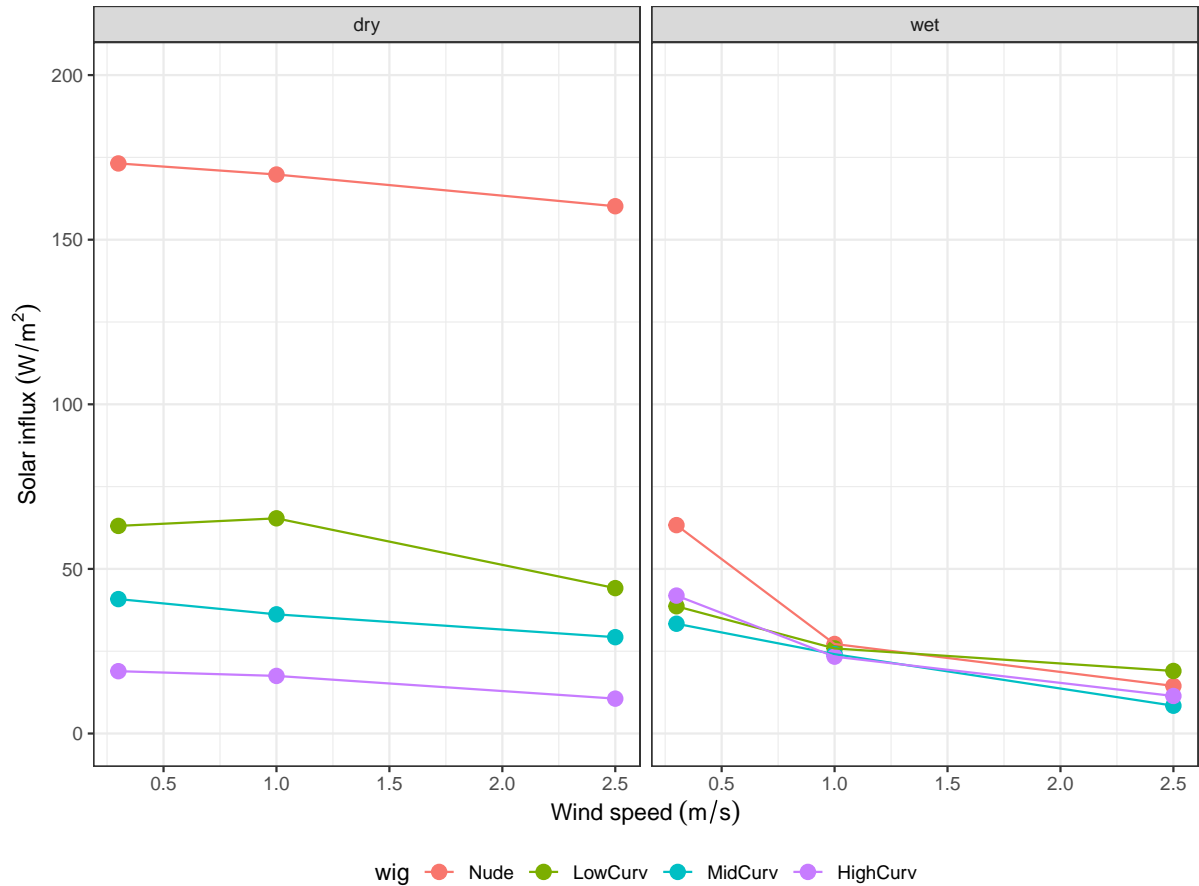


**Figure G.4. Solar influx as a function of wind speed** Wind speed is shown on the x-axis with solar influx on the y-axis. Wigs are indicated by different colors.

## G.2.1 Linear model

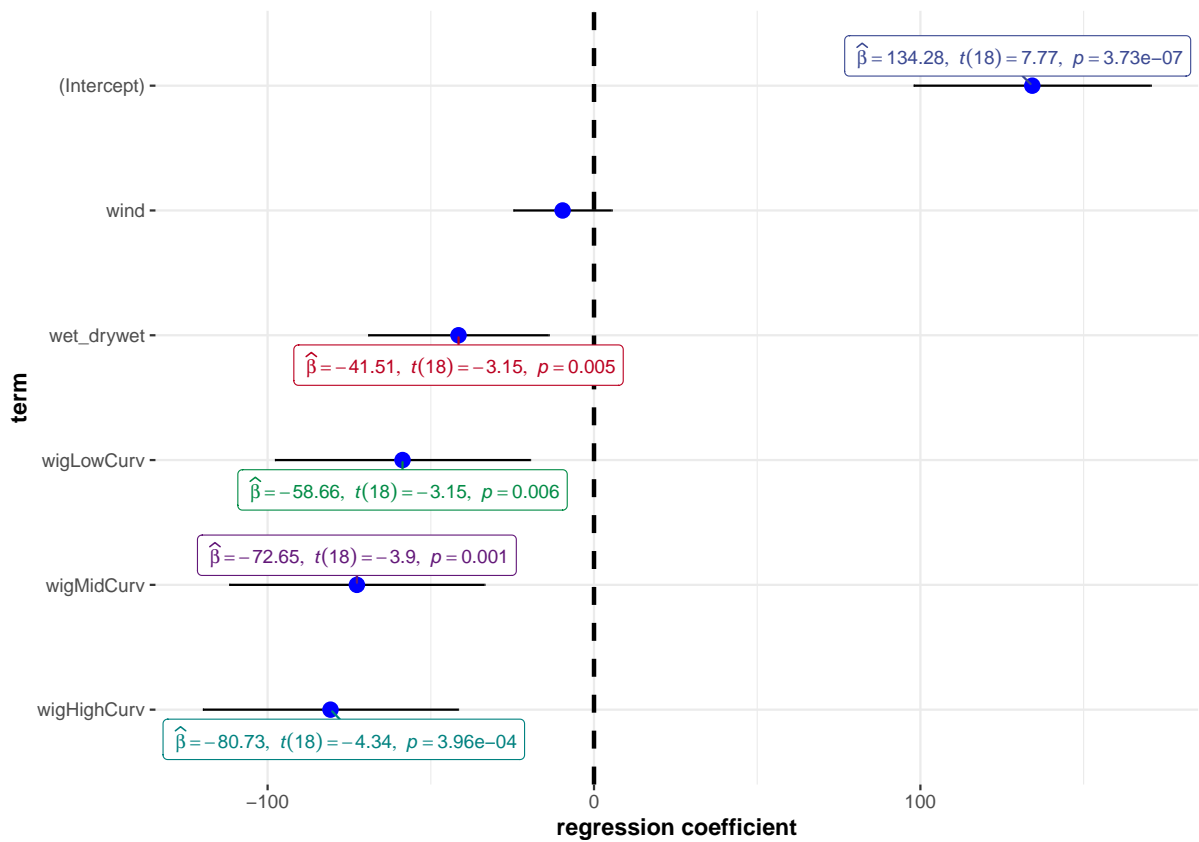
We test the effect of the predictor variables with a linear model (see Figure G.5) and find that wig type and wet vs. dry have a significant effect on solar influx, but that wind speed does not.

```
##
## Call:
## lm(formula = net_w_m2_4C ~ wind + wig + wet_dry, data = df_4c_influx_wide)
##
```

```

## Residuals:
##      Min       1Q   Median       3Q      Max
## -55.958 -18.162   0.361  17.313  49.925
##
## Coefficients:
##              Estimate Std. Error t value Pr(>|t|)
## (Intercept)  134.278     17.290   7.766 3.73e-07 ***
## wind          -9.615      7.170  -1.341 0.196600
## wigLowCurv  -58.664     18.611  -3.152 0.005512 **
## wigMidCurv -72.647     18.611  -3.904 0.001041 **
## wigHighCurv -80.733     18.611  -4.338 0.000396 ***
## wet_drywet   -41.506     13.160  -3.154 0.005490 **
## ---
## Signif. codes:  0 '***' 0.001 '**' 0.01 '*' 0.05 '.' 0.1 ' ' 1
##
## Residual standard error: 32.23 on 18 degrees of freedom
## Multiple R-squared:  0.6592, Adjusted R-squared:  0.5646
## F-statistic: 6.964 on 5 and 18 DF,  p-value: 0.000883

```



AIC = 242, BIC = 250

**Figure G.5. Dot-and-whisker plot of linear regression on solar influx.** Regression coefficient shown on the x-axis with terms on the y-axis. Only significant terms are shown

This is seen more clearly in the ANOVA.

```
##           Df Sum Sq Mean Sq F value Pr(>F)
## wind      1   1868    1868    1.798 0.19660
## wig       3  23977    7992    7.692 0.00163 **
## wet_dry   1  10336   10336    9.948 0.00549 **
## Residuals 18  18703    1039
## ---
## Signif. codes:  0 '***' 0.001 '**' 0.01 '*' 0.05 '.' 0.1 ' ' 1
```

### G.3 Heat loss (30°C)

Below we plot the heat loss for 30°C (see Figure G.6).

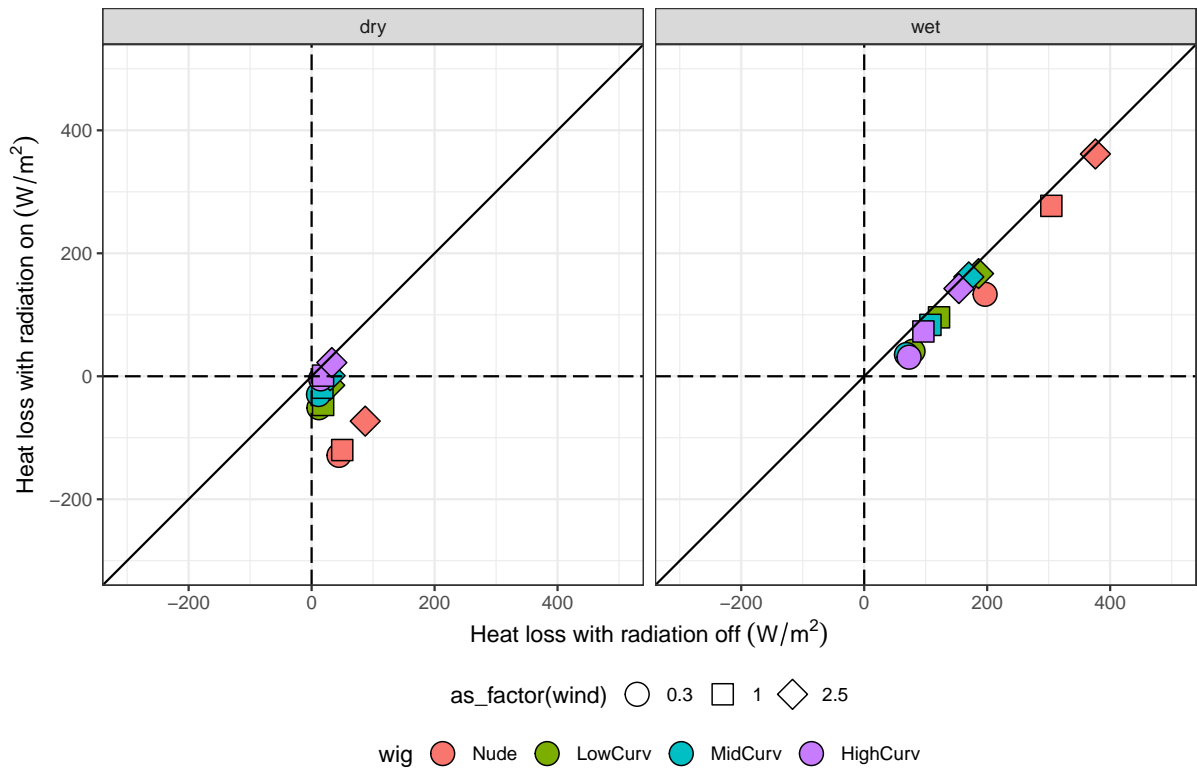


**Figure G.6. Comparison of dry heat loss and wet heat loss (dry + evaporative) for various head coverings.** Shown for three wind speeds with radiation on and off at 30°C. Solid line represents  $x=y$  and dashed lines represent 0 intercept for each axis.

### G.3.1 Linear model

We created a linear model for heat loss using wet/dry, radiation, wind speed and head covering (wig type) as independent variables. Additionally, we include possible interactions between wet/dry, radiation and wig type.

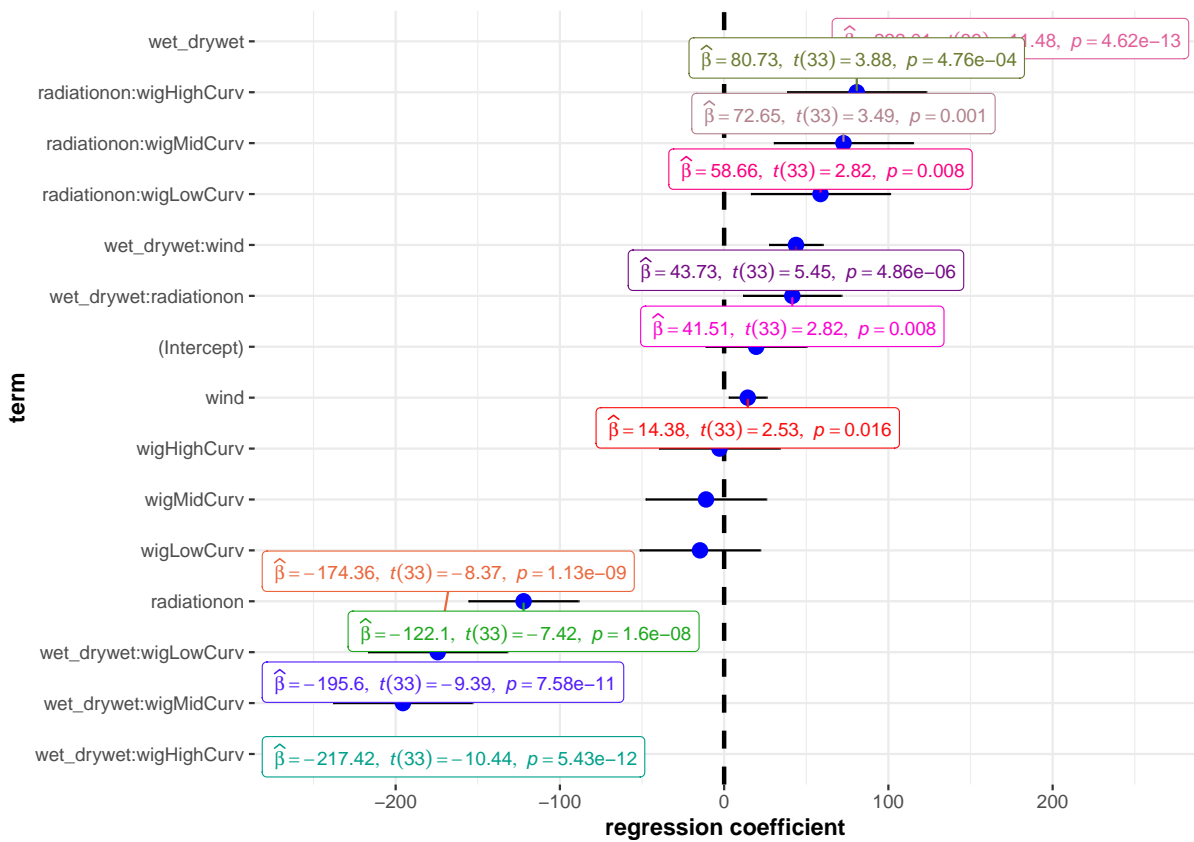
Below, our results show that the most significant variables are wig and radiation, with marginal significance in radiation and the interaction between radiation and wig type (see also Figure G.7).

```
##
## Call:
## lm(formula = heatloss30C ~ wet_dry + radiation + wind + wig +
##     wet_dry * wind + wet_dry * wig + wet_dry * radiation + radiation *
##     wig, data = df_30C_influx_long)
##
## Residuals:
```

```

##      Min      1Q  Median      3Q      Max
## -62.340 -10.624  -1.509  11.063  58.101
##
## Coefficients:
##
##              Estimate Std. Error t value Pr(>|t|)
## (Intercept)      19.502     15.092   1.292 0.205265
## wet_drywet      222.015     19.346  11.476 4.62e-13 ***
## radiationon    -122.100     16.462  -7.417 1.60e-08 ***
## wind            14.376      5.672   2.534 0.016190 *
## wigLowCurv    -14.703     18.033  -0.815 0.420724
## wigMidCurv    -11.046     18.033  -0.613 0.544368
## wigHighCurv   -2.820      18.033  -0.156 0.876707
## wet_drywet:wind  43.734      8.022   5.452 4.86e-06 ***
## wet_drywet:wigLowCurv -174.364     20.823  -8.374 1.13e-09 ***
## wet_drywet:wigMidCurv -195.597     20.823  -9.393 7.58e-11 ***
## wet_drywet:wigHighCurv -217.417     20.823 -10.441 5.43e-12 ***
## wet_drywet:radiationon  41.506     14.724   2.819 0.008085 **
## radiationon:wigLowCurv  58.664     20.823   2.817 0.008118 **
## radiationon:wigMidCurv  72.647     20.823   3.489 0.001398 **
## radiationon:wigHighCurv  80.733     20.823   3.877 0.000476 ***
## ---
## Signif. codes:  0 '***' 0.001 '**' 0.01 '*' 0.05 '.' 0.1 ' ' 1
##
## Residual standard error: 25.5 on 33 degrees of freedom
## Multiple R-squared:  0.961, Adjusted R-squared:  0.9444
## F-statistic: 58.01 on 14 and 33 DF, p-value: < 2.2e-16

```



AIC = 461, BIC = 491

**Figure G.7.** Dot-and-whisker plot for regression analysis of heat loss Regression coefficient on the x-axis and terms on the y-axis. Only significant results shown.

Viewed as an ANOVA, we confirm that the main significant variables in our model are radiation, wind speed and wig type, while there is a marginal significance ( $<0.05$ ) for the interaction for radiation \* wig type and wet/dry\* wig type.

##	Df	Sum Sq	Mean Sq	F value	Pr(>F)
## wet_dry	1	274771	274771	422.464	< 2e-16 ***
## radiation	1	28037	28037	43.107	1.84e-07 ***
## wind	1	53104	53104	81.647	1.92e-10 ***
## wig	3	46773	15591	23.971	2.02e-08 ***
## wet_dry:wind	1	19330	19330	29.721	4.86e-06 ***
## wet_dry:wig	3	89034	29678	45.630	7.67e-12 ***
## wet_dry:radiation	1	5168	5168	7.946	0.00808 **
## radiation:wig	3	11989	3996	6.144	0.00194 **
## Residuals	33	21463	650		

```
## ---
## Signif. codes:  0 '***' 0.001 '**' 0.01 '*' 0.05 '.' 0.1 ' ' 1
```

## G.4 Solar influx (30°C)

We can also look specifically at the effect of the radiation by subtracting the measurements with radiation off from those with radiation on.

From the plots below, it is apparent that the experiments with a “Nude” manikin scalp show a considerably different pattern than any of the wigs.

Interestingly, in the dry experiments, the effect of solar radiation appears to cluster more by wig, while the wet experiments show a solar influx that is more patterned by wind speed (see Figure G.8).

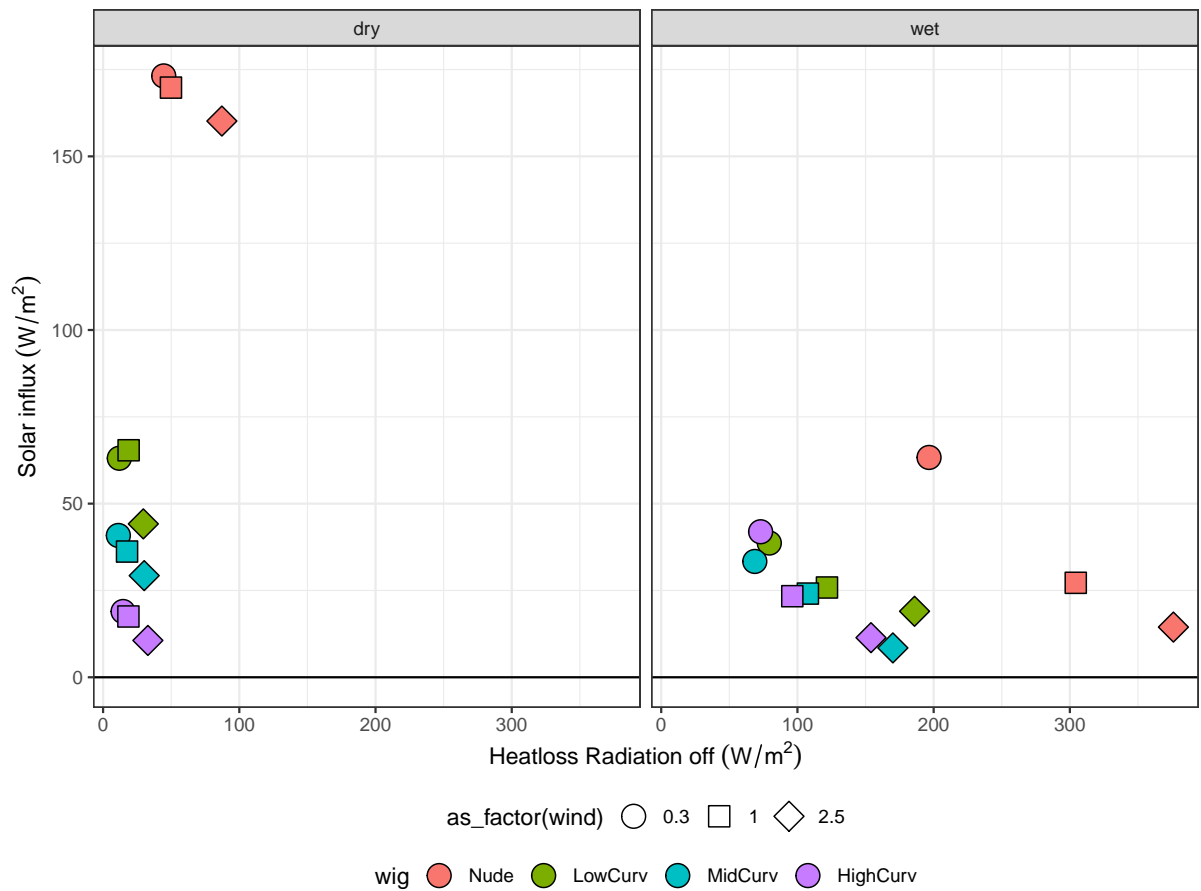


**Figure G.8. Scatter plot of heat loss and solar influx across experiments.** This plot shows the solar influx as a function of heat loss in the radiation off state. The horizontal line is at zero showing that all values are positive.

Below, we plot the same net heat loss as a function of wind speed. Similarly, we see that, in the dry experiments, there is a very clear effect of wig type and no hair, while the wet experiments show a much more pronounced effect of windspeed (see Figure G.9).

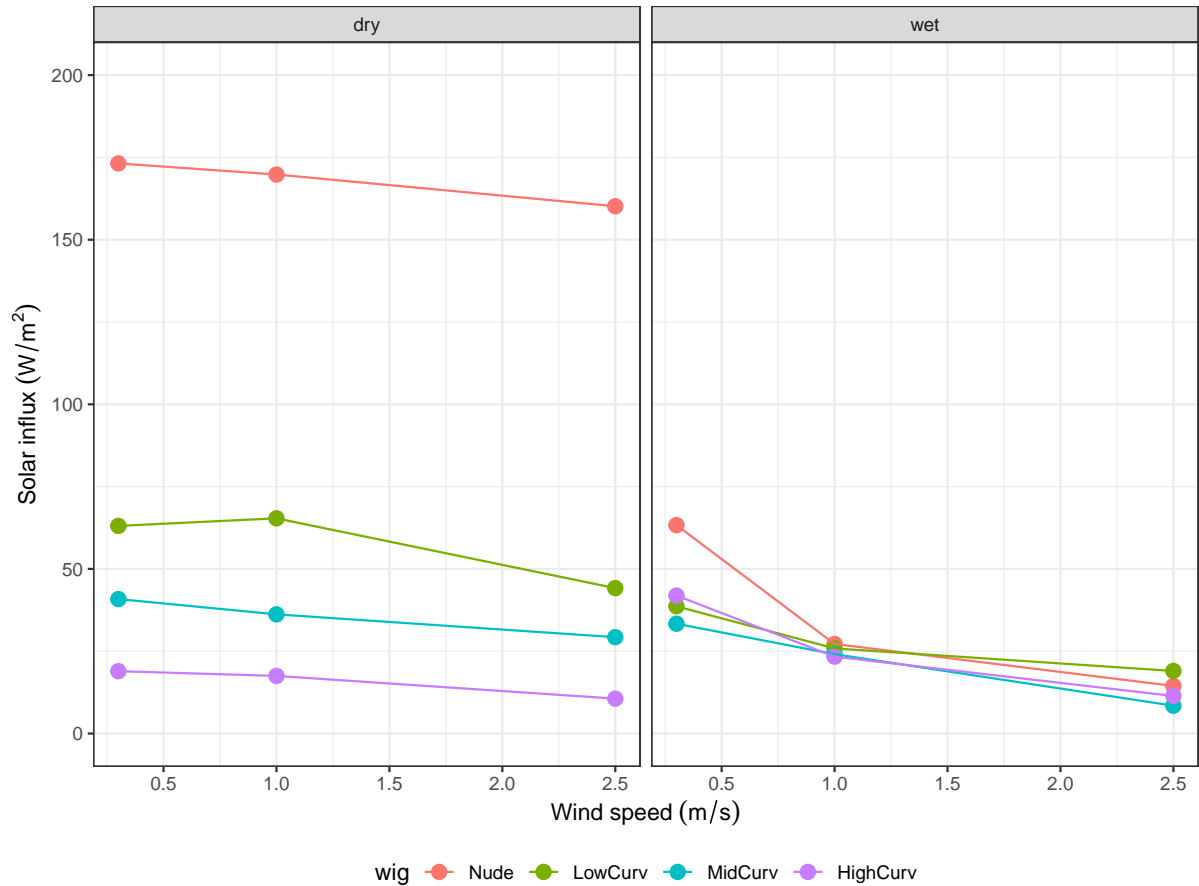


**Figure G.9. Solar influx as a function of wind speed.** Wind speed is shown on the x-axis with solar influx on the y-axis. Wigs are indicated by color.

### G.4.1 Linear model

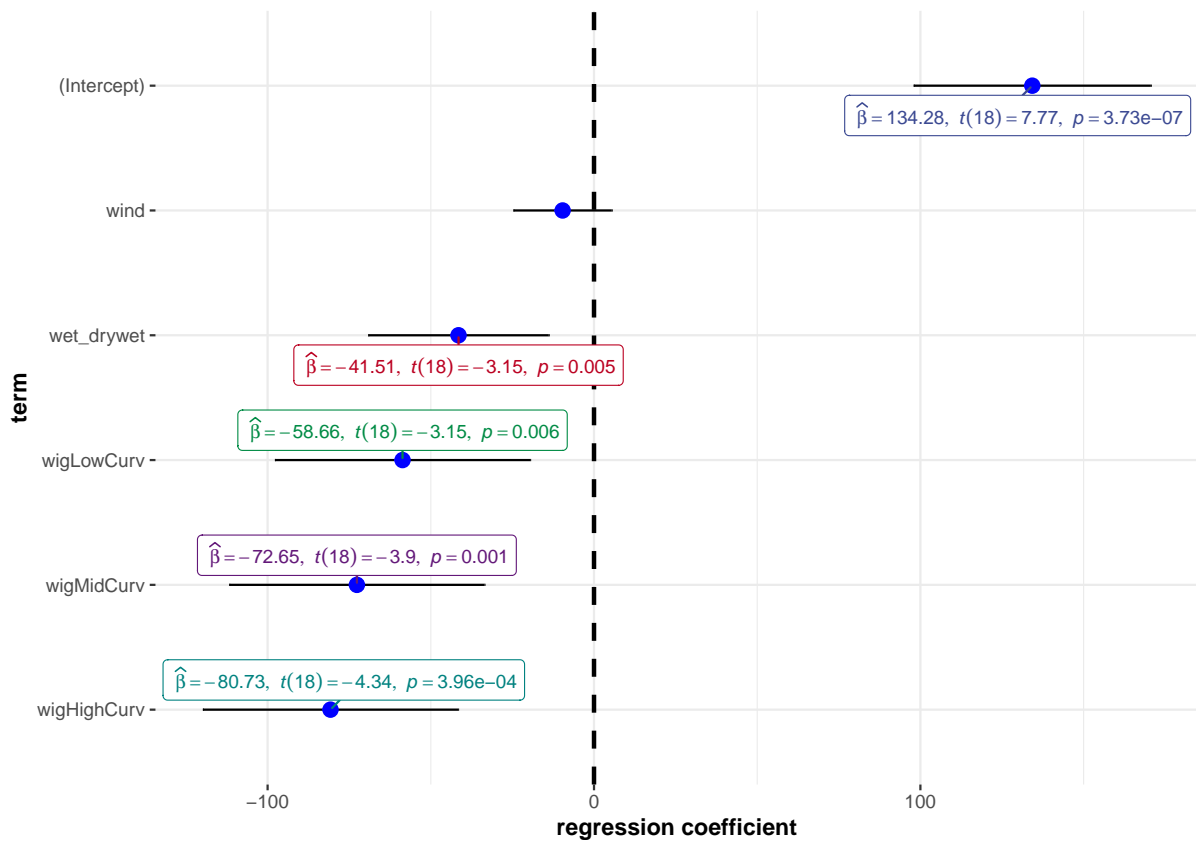
We test the effect of the predictor variables with a linear model (see Figure G.10) and find that wig type and wet vs. dry have a significant effect on solar influx, but that wind speed does not.

```
##
## Call:
## lm(formula = net_w_m2_30C ~ wind + wig + wet_dry, data = df_30C_influx_wide)
##
```

```

## Residuals:
##      Min       1Q   Median       3Q      Max
## -55.958 -18.162   0.361  17.313  49.925
##
## Coefficients:
##              Estimate Std. Error t value Pr(>|t|)
## (Intercept)  134.278     17.290   7.766 3.73e-07 ***
## wind          -9.615      7.170  -1.341 0.196600
## wigLowCurv  -58.664     18.611  -3.152 0.005512 **
## wigMidCurv  -72.647     18.611  -3.904 0.001041 **
## wigHighCurv -80.733     18.611  -4.338 0.000396 ***
## wet_drywet   -41.506     13.160  -3.154 0.005490 **
## ---
## Signif. codes:  0 '***' 0.001 '**' 0.01 '*' 0.05 '.' 0.1 ' ' 1
##
## Residual standard error: 32.23 on 18 degrees of freedom
## Multiple R-squared:  0.6592, Adjusted R-squared:  0.5646
## F-statistic: 6.964 on 5 and 18 DF,  p-value: 0.000883

```



AIC = 242, BIC = 250

**Figure G.10. Dot-and-whisker plot of linear regression on solar influx.** Regression coefficient is shown on the x-axis with terms on the y-axis. Only significant results are shown.

This is seen more clearly in the ANOVA.

```
##           Df Sum Sq Mean Sq F value  Pr(>F)
## wind           1    1868     1868   1.798 0.19660
## wig            3   23977     7992   7.692 0.00163 **
## wet_dry        1   10336    10336   9.948 0.00549 **
## Residuals    18   18703     1039
## ---
## Signif. codes:  0 '***' 0.001 '**' 0.01 '*' 0.05 '.' 0.1 ' ' 1
```

## G.5 Effect of radiation and evaporation (30°C)

Here are plots for the total heat losses recalculated for an ambient temperature of 30°C.

What becomes apparent now is that there is a substantial heat gain in the dry condition once solar radiation is added (bottom left). In both wet conditions and without the effect of radiation, the absence of hair clearly associates with higher heat loss see Figure G.11).

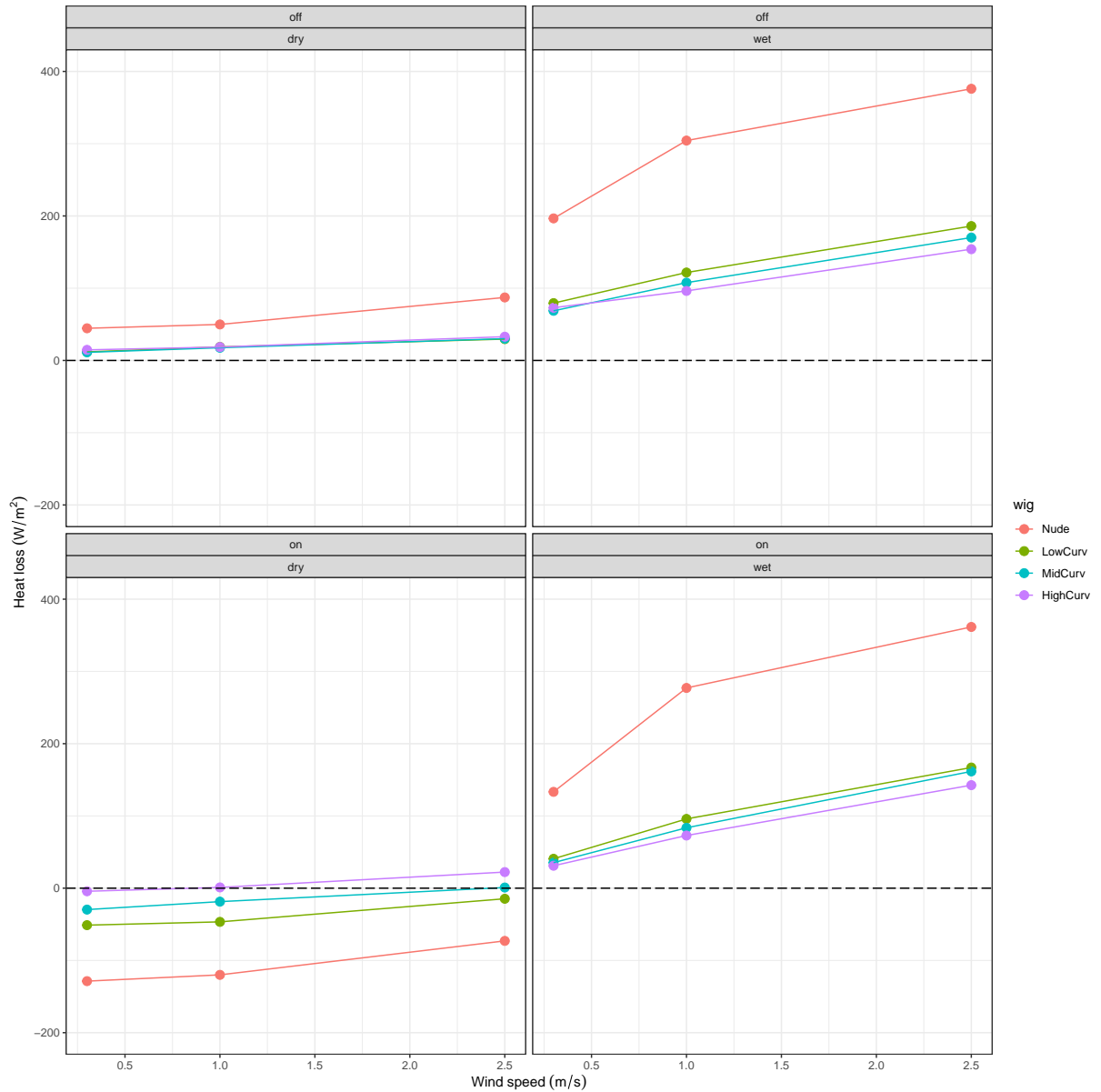


**Figure G.11. Plot of wind speed and heat loss in different experimental conditions.** Heat loss with radiation off/on (top to bottom) and in dry and wet conditions (left to right) calculated for ambient temperature of 30°C. Dashed line represents  $y=0$ .

## G.5.1 Linear model

### G.5.1.1 Separate wet and dry lm

We repeated the linear model for wet and dry conditions separately (see Figure G.12).

We found a striking difference between the effects seen in the dry and wet conditions. The dry condition showed that radiation had the single strongest negative effect on heat loss, while the interaction between solar radiation and high curvature wig showed the highest positive effect on heat loss. All terms were found to be significant.

Conversely, for the wet conditions, none of the interactions between wig and solar radiation were significant with wind providing the single positive significant effect on heat loss and the wigs reducing heat loss with increased curvature.

```
##
## Call:
## lm(formula = heatloss30C ~ wind + wig + radiation + radiation *
##     wig, data = df)
##
## Residuals:
##      Min       1Q   Median       3Q      Max
## -8.9391 -5.6930  0.1225  3.7185 16.5050
##
## Coefficients:
##              Estimate Std. Error t value Pr(>|t|)
## (Intercept)      42.308      4.964   8.523 3.92e-07 ***
## wind              14.376      1.719   8.365 4.95e-07 ***
## wigLowCurv     -40.460      6.309  -6.413 1.17e-05 ***
## wigMidCurv     -40.862      6.309  -6.476 1.05e-05 ***
## wigHighCurv    -38.470      6.309  -6.097 2.04e-05 ***
## radiationon    -167.711      6.309 -26.582 4.95e-14 ***
## wigLowCurv:radiationon  110.178      8.923  12.348 2.92e-09 ***
## wigMidCurv:radiationon  132.278      8.923  14.825 2.29e-10 ***
## wigHighCurv:radiationon 152.033      8.923  17.039 3.17e-11 ***
## ---
## Signif. codes:  0 '***' 0.001 '**' 0.01 '*' 0.05 '.' 0.1 ' ' 1
##
## Residual standard error: 7.727 on 15 degrees of freedom
```

```
## Multiple R-squared:  0.9848, Adjusted R-squared:  0.9767
## F-statistic: 121.8 on 8 and 15 DF,  p-value: 3.084e-12
```

While the wet condition was most affected by wind speed and saw a negative correlation between heat loss and increasingly curled hair.

```
##
## Call:
## lm(formula = heatloss30C ~ wind + wig + radiation + radiation *
##     wig, data = df)
##
## Residuals:
##      Min       1Q   Median       3Q      Max
## -67.851  -7.214   5.306   9.583  35.295
##
## Coefficients:
##
##              Estimate Std. Error t value Pr(>|t|)
## (Intercept)      218.712     17.905  12.215 3.39e-09 ***
## wind              58.110       6.199   9.374 1.16e-07 ***
## wigLowCurv     -163.310     22.757  -7.176 3.20e-06 ***
## wigMidCurv     -176.828     22.757  -7.770 1.23e-06 ***
## wigHighCurv    -184.586     22.757  -8.111 7.26e-07 ***
## radiationon      -34.983     22.757  -1.537  0.145
## wigLowCurv:radiationon    7.150     32.184   0.222  0.827
## wigMidCurv:radiationon   13.017     32.184   0.404  0.692
## wigHighCurv:radiationon   9.433     32.184   0.293  0.773
## ---
## Signif. codes:  0 '***' 0.001 '**' 0.01 '*' 0.05 '.' 0.1 ' ' 1
##
## Residual standard error: 27.87 on 15 degrees of freedom
## Multiple R-squared:  0.946, Adjusted R-squared:  0.9172
## F-statistic: 32.86 on 8 and 15 DF,  p-value: 3.792e-08
```

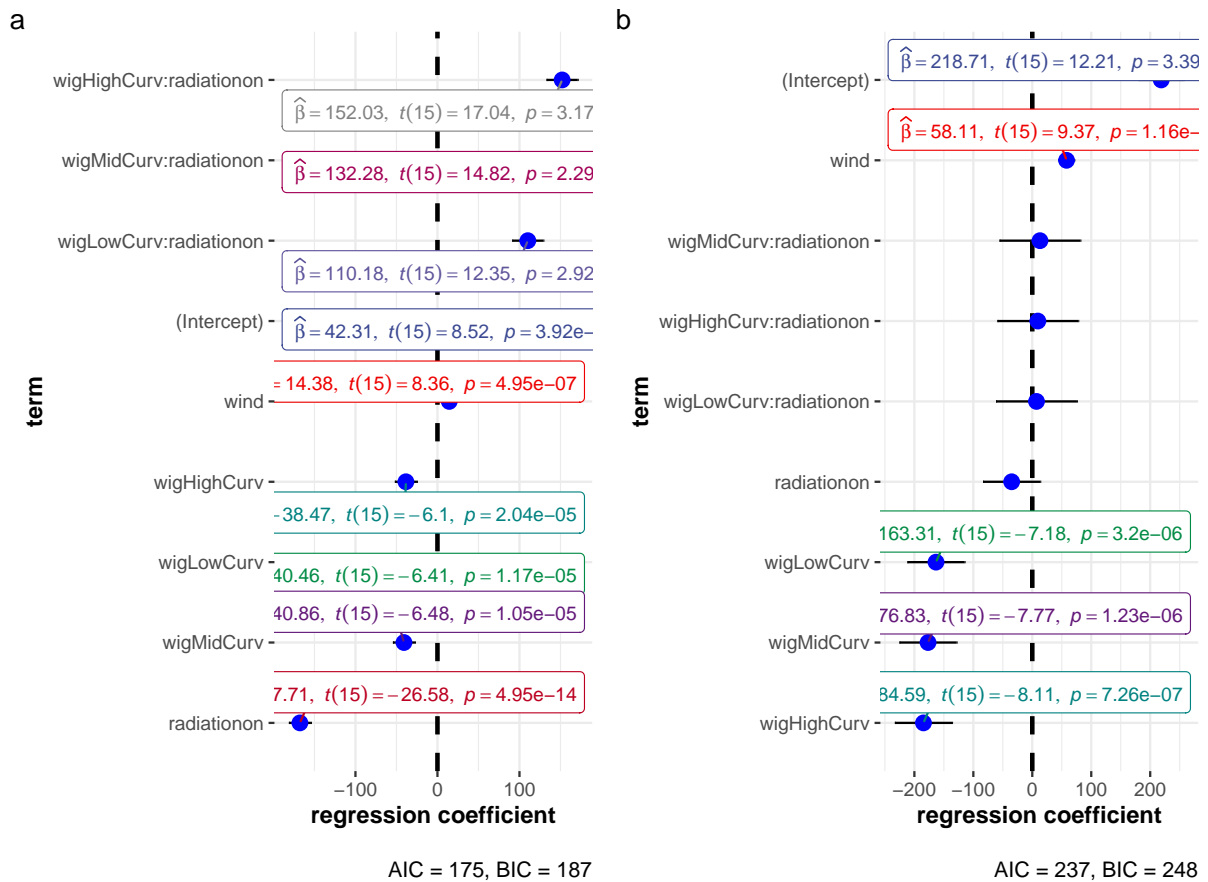


**Figure G.12. Dot-and-whisker plot of linear models for heat loss at 30°C.** Regression coefficients shown on the x-axis with terms on the y-axis and separate plots for for (a) dry and (b) wet conditions

We present the linear models in an ANOVA table below. The ANOVA for the dry linear model is as follows:

##		Df	Sum Sq	Mean Sq	F value	Pr(>F)			
##	wind	1	4178	4178	69.97	4.95e-07	***		
##	wig	3	4578	1526	25.56	3.81e-06	***		
##	radiation	1	28640	28640	479.64	8.44e-13	***		
##	wig:radiation	3	20768	6923	115.94	1.34e-10	***		
##	Residuals	15	896	60					
##	---								
##	Signif. codes:	0	'***'	0.001	'**'	0.01	'*' 0.05	'.' 0.1	' ' 1

For wet, we see:

```

##           Df Sum Sq Mean Sq F value    Pr(>F)
## wind           1  68256   68256  87.865 1.16e-07 ***
## wig            3 131229   43743  56.309 2.14e-08 ***
## radiation      1   4565    4565   5.876  0.0284 *
## wig:radiation  3    136     45   0.058  0.9808
## Residuals     15 11653     777
## ---
## Signif. codes:  0 '***' 0.001 '**' 0.01 '*' 0.05 '.' 0.1 ' ' 1

```

## G.6 Inferred effect of heat loss through sweating at 30°C

Here, we plot the sweat rate potential (left) and the sweat rate required to cancel out heat gain at  $T_{ambient} = 30^{\circ}C$ .

What emerges is that while heat loss potential is higher without hair as a barrier (i.e. the “nude” condition), the *potential* sweat far exceeds the physiologically possible sweat rate for humans. The plot for zero heat gain shoes that a nude scalp requires the most sweat and this requirement is inversely correlated with hair curvature (see Figure G.13).

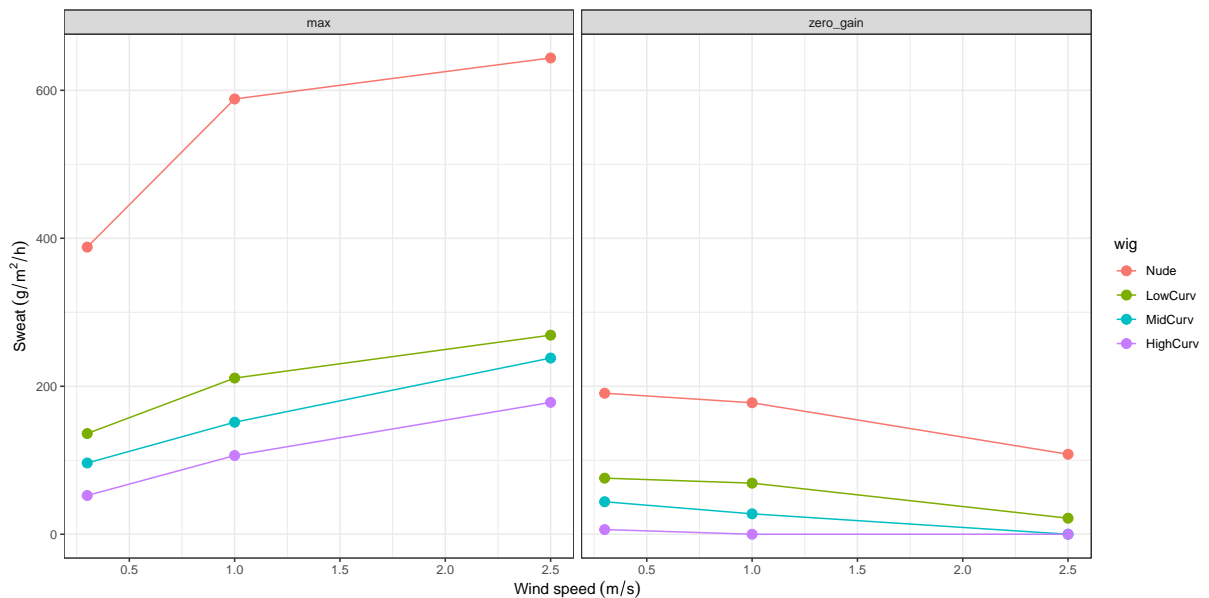


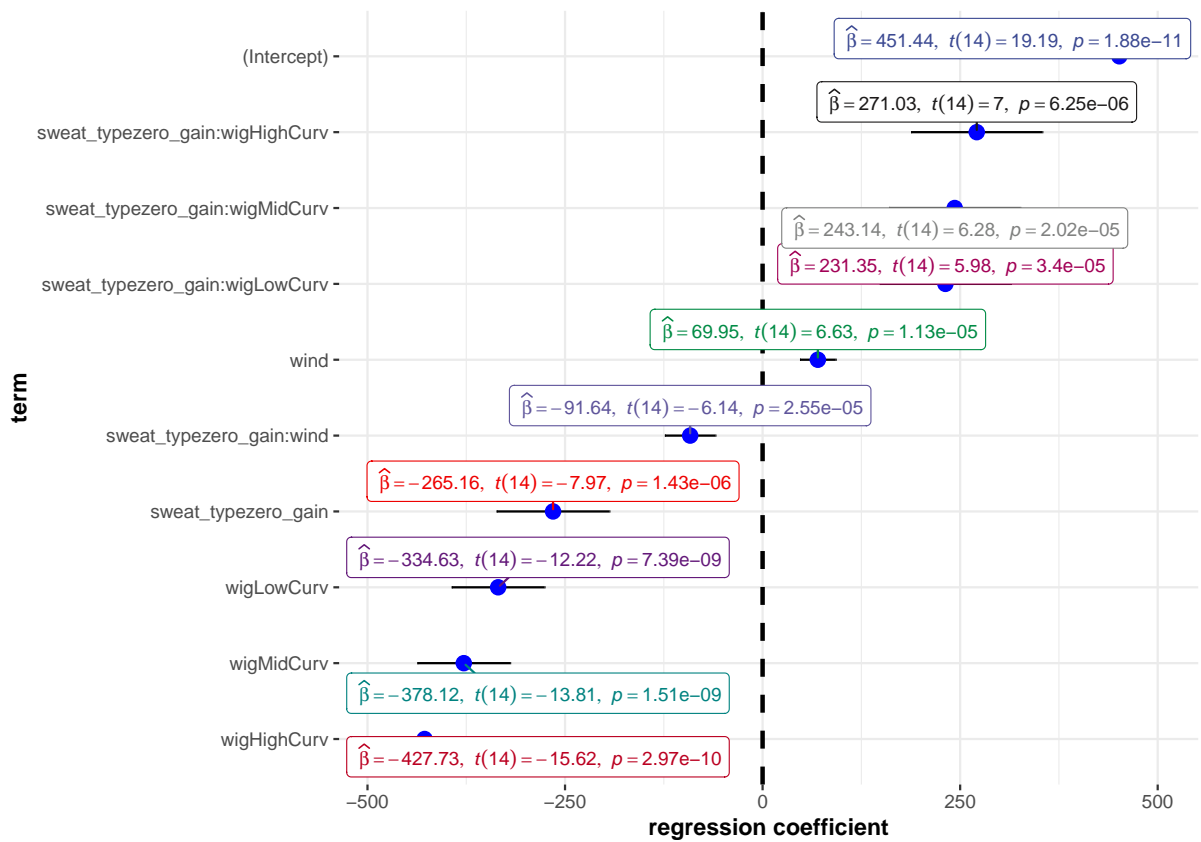
**Figure G.13. Plot of maximum sweat potential and required sweat in various experimental conditions** The quantity of sweat that can be maximally evaporated (left) and that is required for zero heat gain (right) with various head coverings under three wind speeds

## G.6.1 Linear model

### G.6.1.1 Combined wet and dry lm

In a linear model we see that all variables and interactions significantly affect quantity of sweat (see Figure G.14).

```
##
## Call:
## lm(formula = sweat ~ sweat_type + wind + wig + sweat_type * wind +
##     sweat_type * wig, data = sweat_merge_df)
##
## Residuals:
##      Min       1Q   Median       3Q      Max
## -84.325  -8.444   0.644  11.302  66.908
##
## Coefficients:
##
##              Estimate Std. Error t value Pr(>|t|)
## (Intercept)         451.44      23.52  19.192 1.88e-11 ***
## sweat_typezero_gain -265.16      33.27  -7.971 1.43e-06 ***
## wind                69.95      10.55   6.632 1.13e-05 ***
## wigLowCurv        -334.63      27.38 -12.222 7.39e-09 ***
## wigMidCurv        -378.12      27.38 -13.811 1.51e-09 ***
## wigHighCurv       -427.73      27.38 -15.623 2.97e-10 ***
## sweat_typezero_gain:wind    -91.64      14.92  -6.143 2.55e-05 ***
## sweat_typezero_gain:wigLowCurv  231.35      38.72   5.975 3.40e-05 ***
## sweat_typezero_gain:wigMidCurv  243.14      38.72   6.279 2.02e-05 ***
## sweat_typezero_gain:wigHighCurv 271.03      38.72   7.000 6.25e-06 ***
## ---
## Signif. codes:  0 '***' 0.001 '**' 0.01 '*' 0.05 '.' 0.1 ' ' 1
##
## Residual standard error: 33.53 on 14 degrees of freedom
## Multiple R-squared:  0.9768, Adjusted R-squared:  0.9619
## F-statistic: 65.57 on 9 and 14 DF,  p-value: 6.781e-10
```



AIC = 246, BIC = 259

Figure G.14. Dot-and-whisker plot of linear model for quantity of sweat with wind, wig and sweat type as independent predictors. Regression coefficient on the x-axis and terms on the y-axis. Only significant values shown

```
##           Df Sum Sq Mean Sq F value    Pr(>F)
## sweat_type      1  227816   227816   202.61 1.02e-09 ***
## wind            1   11770    11770    10.47 0.00598 **
## wig             3  310798   103599    92.14 1.86e-09 ***
## sweat_type:wind  1   42434    42434    37.74 2.55e-05 ***
## sweat_type:wig   3   70720    23573    20.97 1.91e-05 ***
## Residuals      14   15741     1124
## ---
## Signif. codes:  0 '***' 0.001 '**' 0.01 '*' 0.05 '.' 0.1 ' ' 1
```

### G.6.1.2 Separate max and zero gain

We repeat the tests with maximum sweat potential and zero heat gain separately (see Figure G.15).

Maximum sweat potential shows a strongly significant effect from wig type and wind speed.

```
##
## Call:
## lm(formula = sweat ~ wind + wig, data = df)
##
## Residuals:
##      Min       1Q   Median       3Q      Max
## -84.325 -12.663   4.806  13.887  66.908
##
## Coefficients:
##              Estimate Std. Error t value Pr(>|t|)
## (Intercept)   451.44      31.15  14.493 1.78e-06 ***
## wind           69.95      13.97   5.008 0.00155 **
## wigLowCurv  -334.63      36.26  -9.230 3.62e-05 ***
## wigMidCurv  -378.12      36.26 -10.429 1.62e-05 ***
## wigHighCurv -427.73      36.26 -11.797 7.13e-06 ***
## ---
## Signif. codes:  0 '***' 0.001 '**' 0.01 '*' 0.05 '.' 0.1 ' ' 1
##
## Residual standard error: 44.4 on 7 degrees of freedom
## Multiple R-squared:  0.9656, Adjusted R-squared:  0.946
## F-statistic: 49.15 on 4 and 7 DF,  p-value: 3.301e-05
```

This is confirmed with an ANOVA.

```
##              Df Sum Sq Mean Sq F value    Pr(>F)
## wind           1  49450   49450   25.08 0.00155 **
## wig            3 338191  112730   57.17 2.74e-05 ***
## Residuals      7  13803    1972
## ---
## Signif. codes:  0 '***' 0.001 '**' 0.01 '*' 0.05 '.' 0.1 ' ' 1
```

Sweat quantity for zero heat gain also shows highly significant effects for wind and wig type. However, the main difference appears to be in the directionality of the effect of wind.

```
##
## Call:
## lm(formula = sweat ~ wind + wig, data = df)
##
## Residuals:
##      Min       1Q   Median       3Q      Max
## -23.9713  -7.2857  -0.7838   8.5270  24.6396
##
## Coefficients:
##              Estimate Std. Error t value Pr(>|t|)
## (Intercept)  186.276     11.674  15.956 9.22e-07 ***
## wind         -21.688       5.235  -4.143 0.004333 **
## wigLowCurv -103.285     13.588  -7.601 0.000126 ***
## wigMidCurv -134.980     13.588  -9.933 2.24e-05 ***
## wigHighCurv -156.696     13.588 -11.532 8.30e-06 ***
## ---
## Signif. codes:  0 '***' 0.001 '**' 0.01 '*' 0.05 '.' 0.1 ' ' 1
##
## Residual standard error: 16.64 on 7 degrees of freedom
## Multiple R-squared:  0.9612, Adjusted R-squared:  0.9391
## F-statistic:  43.4 on 4 and 7 DF,  p-value: 5.003e-05
```

This is also confirmed with an ANOVA.

```
##              Df Sum Sq Mean Sq F value    Pr(>F)
## wind           1  4754    4754    17.16 0.00433 **
## wig            3 43327   14442    52.15 3.72e-05 ***
## Residuals      7  1939     277
## ---
## Signif. codes:  0 '***' 0.001 '**' 0.01 '*' 0.05 '.' 0.1 ' ' 1
```

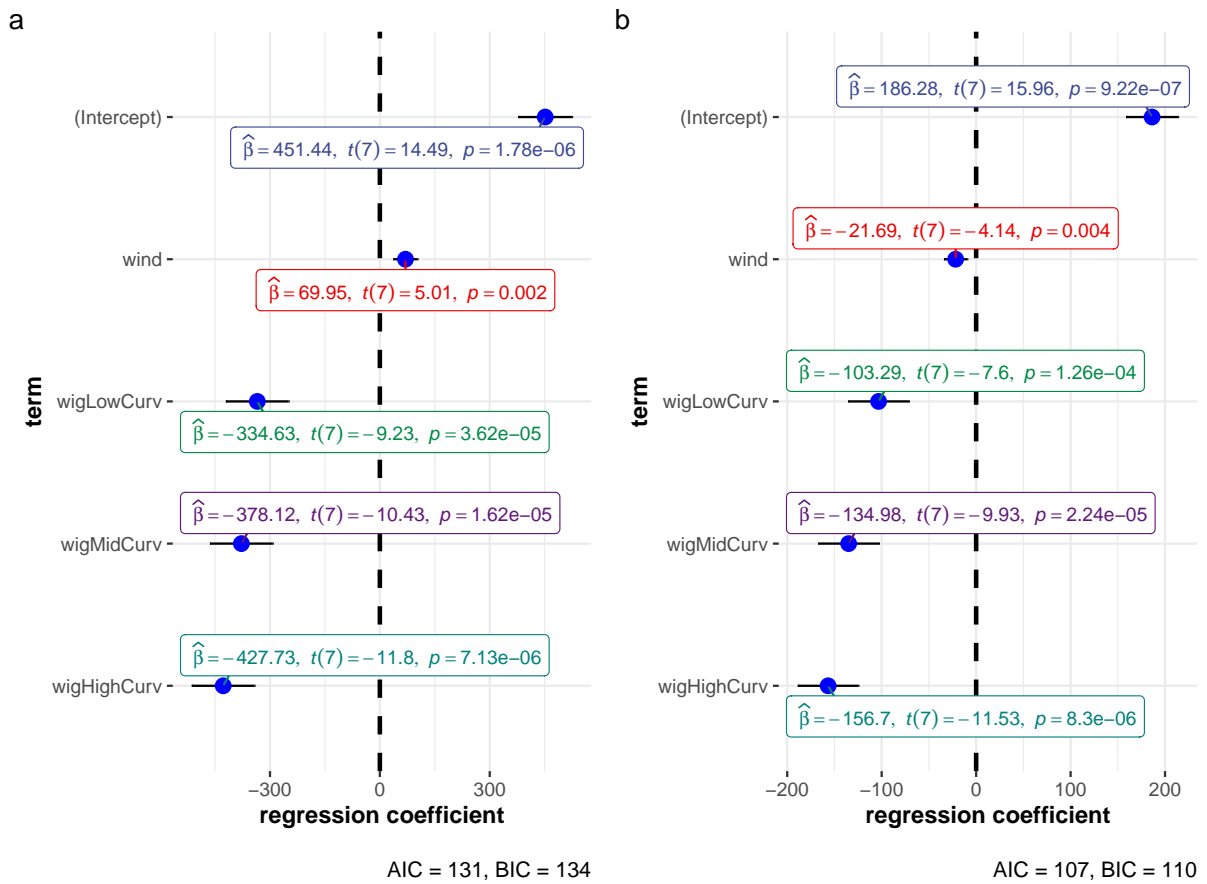


**Figure G.15. Dot-and-whisker plots for linear regression of sweat evaporation potential and requirement.** Only significant terms are plotted and separate plots show regression for (a) maximum sweat potential and (b) sweat required for zero heat gain

## References

- Abdel-Malek, Z., Swope, V. B., Suzuki, I., Akcali, C., Harriger, M. D., Boyce, S. T., ... Hearing, V. J. (1995, February). Mitogenic and melanogenic stimulation of normal human melanocytes by melanotropic peptides. *Proceedings of the National Academy of Sciences of the United States of America*, *92*(5), 1789–1793.
- Adeola, H. A., Khumalo, N. P., Arowolo, A. T., & Mehlala, N. (2020, August). No difference in the proteome of racially and geometrically classified scalp hair sample from a south african cohort: Preliminary findings. *Journal of proteomics*, *226*, 103892.
- Adhikari, K., Fontanil, T., Cal, S., Mendoza-Revilla, J., Fuentes-Guajardo, M., Chacón-Duque, J.-C., ... Ruiz-Linares, A. (2016, March). A genome-wide association scan in admixed latin americans identifies loci influencing facial and scalp hair features. *Nature communications*, *7*(1), 10815.
- Adhikari, K., Mendoza-Revilla, J., Sohail, A., Fuentes-Guajardo, M., Lampert, J., Chacón-Duque, J. C., ... Ruiz-Linares, A. (2019, January). A GWAS in latin americans highlights the convergent evolution of lighter skin pigmentation in eurasia. *Nature communications*, *10*(1), 358.
- Ahmed, S. (2012). *On being included: Racism and diversity in institutional life*. Duke University Press.
- Alexander, D. H., Novembre, J., & Lange, K. (2009, September). Fast model-based estimation of ancestry in unrelated individuals. *Genome research*, *19*(9), 1655–1664.
- American Society for Testing and Materials. (2004). *Measuring the thermal insulation of clothing using a heated manikin1* (Tech. Rep. Nos. F 1291 – 04).
- Andreae, M. O., & Gelencsér, A. (2006, May). Black carbon or brown carbon? the nature of light-absorbing carbonaceous aerosols. *Atmospheric chemistry and physics discussions: ACPD*, *6*(3), 3419–3463.
- Aoki, K. (2002). Sexual selection as a cause of human skin colour variation: Darwin’s hypothesis revisited. *Annals of human biology*, *29*(6), 589–608.
- Armstrong, E. A., Gleckman-Krut, M., & Johnson, L. (2018, July). Silence, power, and inequality: An intersectional approach to sexual violence. *Annual review of sociology*, *44*(1), 99–122.
- Athreya, S. (2019, June). “but you’re not a real minority”: The marginalization of asian voices in paleoanthropology. *American anthropologist*, *121*(2), 472–474.
- Azizi, E., Lusky, A., Kushelevsky, A. P., & Schewach-Millet, M. (1988, July). Skin type, hair color, and freckles are predictors of decreased minimal erythema ultraviolet radiation dose. *Journal of the American Academy of Dermatology*, *19*(1 Pt 1), 32–38.
- Bailey, J. G., & Schliebe, S. A. (1986). Precision of the average curvature measurement in human head hairs. In *Journal of the forensic science society* (Vol. 26, pp. 225–225).
- Balanovska, E., Lukianova, E., Kagazezheva, J., Maurer, A., Leybova, N., Agdzhoyan, A., ... Balanovsky, O. (2020, September). Optimizing the genetic prediction of

- the eye and hair color for north eurasian populations. *BMC genomics*, 21(Suppl 7), 527.
- Ball, P. (2017, November). The trouble with scientists. *Nautilus*.
- Bayer, R., & Spitzer, R. L. (1982, January). Edited correspondence on the status of homosexuality in DSM-III. *Journal of the history of the behavioral sciences*, 18(1), 32–52.
- Beleza, S., Johnson, N. A., Candille, S. I., Absher, D. M., Coram, M. A., Lopes, J., ... Tang, H. (2013, March). Genetic architecture of skin and eye color in an African-European admixed population. *PLoS genetics*, 9(3), e1003372.
- Beleza, S., Santos, A. M., McEvoy, B., Alves, I., Martinho, C., Cameron, E., ... Rocha, J. (2013, January). The timing of pigmentation lightening in europeans. *Molecular biology and evolution*, 30(1), 24–35.
- Benn Torres, J. (2014, January). Prospecting the past: genetic perspectives on the extinction and survival of indigenous peoples of the caribbean. *New genetics and society*, 33(1), 21–41.
- Benn Torres, J. (2019, April). Race, rare genetic variants, and the science of human difference in the post-genomic age. *Transforming anthropology*, 27(1), 37–49.
- Betti, L., Balloux, F., Hanihara, T., & Manica, A. (2009, January). The relative role of drift and selection in shaping the human skull. *American journal of physical anthropology*, 141(1), NA–NA.
- Biasutti, R. (1953). *Le razze ei popoli della terra*. Torino: Unione Tipografico Editrice Torinese.
- Blischak, J. D., Carbonetto, P., & Stephens, M. (2019, October). Creating and sharing reproducible research code the workflow way. *F1000Research*, 8, 1749.
- Bliss, C. (2011, October). Racial taxonomy in genomics. *Social science & medicine*, 73(7), 1019–1027.
- Bliss, C. (2012). *Race decoded: The genomic fight for social justice*. Stanford University Press.
- Blum, H. F. (1945, July). The physiological effects of sunlight on man. *Physiological reviews*, 25(3), 483–530.
- Bolnick, D. A., Smith, R. W. A., & Fuentes, A. (2019, June). How academic diversity is transforming scientific knowledge in biological anthropology. *American anthropologist*, 121(2), 464–464.
- Bonilla, C., Parra, E. J., Pfaff, C. L., Dios, S., Marshall, J. A., Hamman, R. F., ... Shriver, M. D. (2004, March). Admixture in the hispanics of the san luis valley, colorado, and its implications for complex trait gene mapping. *Annals of human genetics*, 68(Pt 2), 139–153.
- Branda, R. F., & Eaton, J. W. (1978, August). Skin color and nutrient photolysis: an evolutionary hypothesis. *Science*, 201(4356), 625–626.
- Branicki, W., Liu, F., van Duijn, K., Draus-Barini, J., Pośpiech, E., Walsh, S., ... Kayser, M. (2011, April). Model-based prediction of human hair color using DNA variants. *Human genetics*, 129(4), 443–454.
- Brenner, M., & Hearing, V. J. (2008, May). The protective role of melanin against UV

- damage in human skin. *Photochemistry and photobiology*, *84*(3), 539–549.
- Brown, M. E. L., & Dueñas, A. N. (2020, March). A medical science educator’s guide to selecting a research paradigm: Building a basis for better research. *Medical Science Educator*, *30*(1), 545–553.
- Brucato, N., Cassar, O., Tonasso, L., Tortevoeye, P., Migot-Nabias, F., Plancoulaine, S., . . . Dugoujon, J.-M. (2010, October). The imprint of the slave trade in an african american population: mitochondrial DNA, Y chromosome and HTLV-1 analysis in the noir marron of french guiana. *BMC evolutionary biology*, *10*, 314.
- Cabanac, M., & Brinnet, H. (1988). Beards, baldness, and sweat secretion. *European journal of applied physiology and occupational physiology*, *58*(1-2), 39–46.
- Cadiou, E., Neff, M. W., Quignon, P., Walsh, K., Chase, K., Parker, H. G., . . . Ostrander, E. A. (2009, October). Coat variation in the domestic dog is governed by variants in three genes. *Science*, *326*(5949), 150–153.
- Caldararo, N. (2005, August). Hair, human evolution, and the idea of human uniqueness. *Evolutionary Anthropology: Issues, News, and Reviews*, *14*(4), 132–133.
- Calderon, P., Otberg, N., & Shapiro, J. (2009, September). Uncombable hair syndrome. *Journal of the American Academy of Dermatology*, *61*(3), 512–515.
- Carpenter, M. (2018, December). Intersex variations, human rights, and the international classification of diseases. *Health and human rights*, *20*(2), 205–214.
- Chaitanya, L., Breslin, K., Zuñiga, S., Wirken, L., Pośpiech, E., Kukla-Bartoszek, M., . . . Walsh, S. (2018, July). The HIrisPlex-S system for eye, hair and skin colour prediction from DNA: Introduction and forensic developmental validation. *Forensic science international. Genetics*, *35*, 123–135.
- Chang, C. C., Chow, C. C., Tellier, L. C., Vattikuti, S., Purcell, S. M., & Lee, J. J. (2015, February). Second-generation PLINK: rising to the challenge of larger and richer datasets. *GigaScience*, *4*, 7.
- Chen, C., LeBoit, P. E., & Price, V. H. (2006, January). Woolly hair in 4 members of a chinese family. *Journal of the American Academy of Dermatology*, *54*(1), 165–166.
- Chen, C.-T., Chuang, C., Cao, J., Ball, V., Ruch, D., & Buehler, M. J. (2014, May). Excitonic effects from geometric order and disorder explain broadband optical absorption in eumelanin. *Nature communications*, *5*, 3859.
- Chen, X. (1997, December). Thomas kuhn’s latest notion of incommensurability. *Journal for General Philosophy of Science. Zeitschrift fur Allgemeine Wissenschaftstheorie*, *28*(2), 257–273.
- Cho, H., Hall, J. G., Kosmoski, C., Fox, R. L., & Mastin, T. (2010, January). Tanning, skin cancer risk, and prevention: A content analysis of eight popular magazines that target female readers, 1997–2006. *Health Communication*, *25*(1), 1–10.
- Claes, P., Liberton, D. K., Daniels, K., Rosana, K. M., Quillen, E. E., Pearson, L. N., . . . Shriver, M. D. (2014). Modeling 3D facial shape from DNA. *PLoS genetics*, *10*(3).
- Claw, K. G., Anderson, M. Z., Begay, R. L., Tsosie, K. S., Fox, K., Garrison, N. A., & Summer internship for INdigenous peoples in Genomics (SING) Consortium. (2018, July). A framework for enhancing ethical genomic research with indigenous communities. *Nature communications*, *9*(1), 2957.

- Clemens, T. L., Adams, J. S., Henderson, S. L., & Holick, M. F. (1982, January). Increased skin pigment reduces the capacity of skin to synthesise vitamin D3. *The Lancet*, 1(8263), 74–76.
- Coelho, L. G. M., Ferreira-Junior, J. B., Martini, A. R. P., Borba, D. A., Coelho, D. B., Passos, R. L. F., . . . Rodrigues, L. O. C. (2010, November). Head hair reduces sweat rate during exercise under the sun. *International journal of sports medicine*, 31(11), 779–783.
- Cole, S. A. (2020, September). Individual and collective identification in contemporary forensics. *BioSocieties*, 15(3), 350–375.
- Collins, P. H. (2002). *Black feminist thought: Knowledge, consciousness, and the politics of empowerment*. Routledge.
- Collins, P. H. (2015, March). Science, critical race theory and colour-blindness. *The British journal of sociology*, 66(1), 46–52.
- Consortium, The 1000 Genomes Project. (2010, October). A map of human genome variation from population-scale sequencing. *Nature*, 467(7319), 1061–1073.
- Crawford, N. G., Kelly, D. E., Hansen, M. E. B., Beltrame, M. H., Fan, S., Bowman, S. L., . . . Tishkoff, S. (2017). Loci associated with skin pigmentation identified in african populations. *Science*, eaan8433–eaaan8433.
- Crawshaw, L. I., Moffitt, B. P., Lemons, D. E., & Downey, J. A. (1981). The evolutionary development of vertebrate thermoregulation: The vertebrates, from fish to humans, have evolved a wide variety of systems to deal with variations in the environmental temperature. *American scientist*, 69(5), 543–550.
- Croyle, R. T. (2008, August). The national cancer institute’s transdisciplinary centers initiatives and the need for building a science of team science. *American journal of preventive medicine*, 35(2 Suppl), S90–3.
- Cruz, C. F., Costa, C., Gomes, A. C., Matamá, T., & Cavaco-Paulo, A. (2016, July). Human hair and the impact of cosmetic procedures: A review on cleansing and Shape-Modulating cosmetics. *Cosmetics and Toiletries*, 3(3), 26.
- Cruz, C. F., Fernandes, M. M., Gomes, A. C., Coderch, L., Martí, M., Méndez, S., . . . Cavaco-Paulo, A. (2013, June). Keratins and lipids in ethnic hair. *International journal of cosmetic science*, 35(3), 244–249.
- Darwin, C. (1871). *The descent of man and selection in relation to sex* (2008th ed.). London: The Folio Society.
- Davenport, G. C., & Davenport, C. B. (1907, November). Heredity of eye-color in man. *Science*, 26(670), 589–592.
- Davies, I., & Corbett, G. (1997). Colour categories in african languages: a test of the berlin and kay theory of colour universals. In R. K. Herbert (Ed.), *African linguistics at the crossroads: Papers from kwaluseni, 1st world congress of african linguistics*. Cologne: Rüdiger Köppe.
- Davies, I., Davies, C., & Corbett, G. (1994, January). The basic colour terms of ndebele. *Africa: journal of the International Institute of African Languages and Cultures*, 7(1), 36–48.
- Davis, G. (2014, January). The power in a name: diagnostic terminology and diverse

- experiences. *Psychology & Sexuality*, 5(1), 15–27.
- Davis, G., Dewey, J. M., & Murphy, E. L. (2016, June). Giving sex: Deconstructing intersex and trans medicalization practices. *Gender & society: official publication of Sociologists for Women in Society*, 30(3), 490–514.
- Dawson, T. J., & Maloney, S. K. (2017, April). Thermal implications of interactions between insulation, solar reflectance, and fur structure in the summer coats of diverse species of kangaroo. *Journal of comparative physiology. B, Biochemical, systemic, and environmental physiology*, 187(3), 517–528.
- Dawson, T. J., Webster, K. N., & Maloney, S. K. (2014, February). The fur of mammals in exposed environments; do crypsis and thermal needs necessarily conflict? the polar bear and marsupial koala compared. *Journal of Comparative Physiology B Biochemical, Systems, and Environmental Physiology*, 184(2), 273–284.
- De La Mettrie, R., Saint-Léger, D., Loussouarn, G., Garcel, A.-L., Porter, C., & Langaney, A. (2007). Shape variability and classification of human hair: A worldwide approach. *Human biology*, 79(3), 265–281.
- DiGangi, E. A., & Bethard, J. D. (2021, January). Uncloaking a lost cause: Decolonizing ancestry estimation in the united states. *American journal of physical anthropology*.
- Down, J. L. H. (1867, April). Observations on an ethnic classification of idiots. *The Journal of mental science*, 13(61), 121–123.
- Du Bois, W. E. B. (1903). *The souls of black folk*. Oxford University Press.
- Du Bois, W. E. B. (1939). The negro scientist. *The American scholar*, 8(3), 309–320.
- Eriksson, N., Macpherson, J. M., Tung, J. Y., Hon, L. S., Naughton, B., Saxonov, S., ... Mountain, J. (2010, June). Web-Based, Participant-Driven studies yield novel genetic associations for common traits. *PLoS genetics*, 6(6), e1000993–e1000993.
- Falk, D. (1990, June). Evolution of a venous “radiator” for cooling cortex: “prime releaser” of brain evolution in homo. *The Behavioral and brain sciences*, 13(2), 368–381.
- Fischer, E., & Saller, K. (1928). Eine neue haarfarbentafel. *Anthropologischer Anzeiger; Bericht über die biologisch-anthropologische Literatur*, 5(3), 238–244.
- Fitzpatrick, T. B. (1975). Soleil et peau. *Journal de Médecine Esthétique*, 2, 33–34.
- Fitzpatrick, T. B. (1988, June). The validity and practicality of Sun-Reactive skin types I through VI. *Archives of dermatology*, 124(6), 869–871.
- Fogel, J., & Krausz, F. (2013). Watching reality television beauty shows is associated with tanning lamp use and outdoor tanning among college students. *Journal of the American Academy of Dermatology*, 68(5), 784–789.
- Franbourg, A., Hallegot, P., Baltenneck, F., Toutain, C., & Leroy, F. (2003, June). Current research on ethnic hair. *Journal of the American Academy of Dermatology*, 48(6 Suppl), S115–9.
- Fujimoto, A., Kimura, R., Ohashi, J., Omi, K., Yuliwulandari, R., Batubara, L., ... Tokunaga, K. (2008a, March). A scan for genetic determinants of human hair morphology: EDAR is associated with asian hair thickness. *Human molecular genetics*, 17(6), 835–843.
- Fujimoto, A., Kimura, R., Ohashi, J., Omi, K., Yuliwulandari, R., Batubara, L., ...

- Tokunaga, K. (2008b, March). A scan for genetic determinants of human hair morphology: EDAR is associated with asian hair thickness. *Human molecular genetics*, *17*(6), 835–843.
- Fujimoto, A., Nishida, N., Kimura, R., Miyagawa, T., Yuliwulandari, R., Batubara, L., ... Ohashi, J. (2009, August). FGFR2 is associated with hair thickness in asian populations. *Journal of human genetics*, *54*(8), 461–465.
- Gandolfi, B., Outerbridge, C. A., Beresford, L. G., Myers, J. A., Pimentel, M., Alhaddad, H., ... Lyons, L. A. (2010, October). The naked truth: Sphynx and devon rex cat breed mutations in KRT71. *Mammalian genome: official journal of the International Mammalian Genome Society*, *21*(9-10), 509–515.
- Garn, S. M. (1950, December). Hair texture: its definition, evaluation and measurement. *American journal of physical anthropology*, *8*(4), 453–465.
- Garn, S. M. (1951, March). Types and distribution of the hair in man. *Annals of the New York Academy of Sciences*, *53*(3), 498–507.
- Garone, M., Howard, J., & Fabrikant, J. (2015, February). A review of common tanning methods. *The Journal of clinical and aesthetic dermatology*, *8*(2), 43–47.
- Gates, R. R. (1925). Mendelian heredity and racial differences. *The Journal of the Royal Anthropological Institute of Great Britain and Ireland*, *55*, 468–482.
- Gatschet, A. S. (1879, August). Adjectives of color in indian languages. *The American naturalist*, *13*(8), 475–485.
- Getreuer, P. (2012, August). Chan-veese segmentation. *Image Processing On Line*, *2*, 214–224.
- Gieryn, T. F. (1983). Boundary-Work and the demarcation of science from Non-Science: Strains and interests in professional ideologies of scientists. *American sociological review*, *48*(6), 781–795.
- Goldstein, J., Davidoff, J., & Roberson, D. (2009, February). Knowing color terms enhances recognition: further evidence from english and himba. *Journal of experimental child psychology*, *102*(2), 219–238.
- Granstein, R. D., Cornelius, L., & Shinkai, K. (2017, June). Diversity in Dermatology-A call for action. *JAMA dermatology*, *153*(6), 499–500.
- Grinde, K. E., Brown, L. A., Reiner, A. P., Thornton, T. A., & Browning, S. R. (2019, March). Genome-wide significance thresholds for admixture mapping studies. *American journal of human genetics*, *104*(3), 454–465.
- Guenther, C. A., Tasic, B., Luo, L., Bedell, M. A., & Kingsley, D. M. (2014, July). A molecular basis for classic blond hair color in europeans. *Nature genetics*, *46*(7), 748–752.
- Guerrero, A. I., & Rogers, T. L. (2019, July). From low to high latitudes: changes in fatty acid desaturation in mammalian fat tissue suggest a thermoregulatory role. *BMC evolutionary biology*, *19*(1), 155.
- Guinot, C., Malvy, D. J.-M., Latreille, J., Ezzedine, K., Galan, P., Tenenhaus, M., ... Tschachler, E. (2005, July). Sun-reactive skin type in 4912 french adults participating in the SU.VI.MAX study. *Photochemistry and photobiology*, *81*(4), 934–940.

- Gupta, V., & Sharma, V. K. (2019, September). Skin typing: Fitzpatrick grading and others. *Clinics in dermatology*, *37*(5), 430–436.
- Halder, I., & Shriver, M. D. (2003, November). Measuring and using admixture to study the genetics of complex diseases. *Human genomics*, *1*(1), 52–62.
- Hansson, S. O. (2009, October). Cutting the gordian knot of demarcation. *International Studies in the Philosophy of Science*, *23*(3), 237–243.
- Hansson, S. O. (2017). Science and Pseudo-Science. In E. N. Zalta (Ed.), *The Stanford encyclopedia of philosophy* (Summer 2017 ed.). Metaphysics Research Lab, Stanford University.
- Haraway, D. (1988). Situated knowledges: The science question in feminism and the privilege of partial perspective. *Feminist studies: FS*, *14*(3), 575–599.
- Harding, S. (2004, March). A socially relevant philosophy of science? resources from standpoint theory’s controversiality. *Hypatia*, *19*(1), 25–47.
- Hasler, G., Drevets, W. C., Manji, H. K., & Charney, D. S. (2004, October). Discovering endophenotypes for major depression. *Neuropsychopharmacology: official publication of the American College of Neuropsychopharmacology*, *29*(10), 1765–1781.
- Hayashi, R., Inoue, A., Suga, Y., Aoki, J., & Shimomura, Y. (2015, June). Analysis of unique mutations in the LPAR6 gene identified in a japanese family with autosomal recessive woolly hair/hypotrichosis: Establishment of a useful assay system for LPA6. *Journal of dermatological science*, *78*(3), 197–205.
- He, A., & Okoye, G. A. (2017). Chemical and physical properties of hair: Comparisons between asian, black, and caucasian hair. In C. Aguh & G. A. Okoye (Eds.), *Fundamentals of ethnic hair: The dermatologist’s perspective* (pp. 3–13). Cham: Springer International Publishing.
- Ho, Y. Y. W., Brims, M., Mcnevin, D., Spector, T. D., Martin, N. G., & Medland, S. E. (2016, August). Variation and heritability in hair diameter and curvature in an australian twin sample. *Twin research and human genetics: the official journal of the International Society for Twin Studies*, *19*(4), 351–358.
- Ho, Y. Y. W., Mina-Vargas, A., Zhu, G., Brims, M., McNevin, D., Montgomery, G. W., ... Painter, J. N. (2020, October). Comparison of Genome-Wide association scans for quantitative and observational measures of human hair curvature. *Twin research and human genetics: the official journal of the International Society for Twin Studies*, *23*(5), 271–277.
- Hong, L., & Page, S. E. (2004, November). Groups of diverse problem solvers can outperform groups of high-ability problem solvers. *Proceedings of the National Academy of Sciences of the United States of America*, *101*(46), 16385–16389.
- Hora, M., Pontzer, H., Wall-Scheffler, C. M., & Sládek, V. (2020, January). Dehydration and persistence hunting in homo erectus. *Journal of Human Evolution*, *138*, 102682.
- Horev, L., Tosti, A., Rosen, I., Hershko, K., Vincenzi, C., Nanova, K., ... Zlotogorski, A. (2009, November). Mutations in lipase H cause autosomal recessive hypotrichosis simplex with woolly hair. *Journal of the American Academy of Dermatology*, *61*(5), 813–818.

- Hrdy, D. B. (1973, July). Quantitative hair form variation in seven populations. *American journal of physical anthropology*, 39(1), 7–17.
- Hrdy, D. B. (1978, August). Analysis of hair samples of mummies from semma south (sudanese nubia). *American journal of physical anthropology*, 49(2), 277–282.
- Hugenberg, K., Young, S. G., Bernstein, M. J., & Sacco, D. F. (2010, October). The categorization-individuation model: An integrative account of the other-race recognition deficit. *Psychological review*, 117(4), 1168–1187.
- Hughes, B. L., Camp, N. P., Gomez, J., Natu, V. S., Grill-Spector, K., & Eberhardt, J. L. (2019, July). Neural adaptation to faces reveals racial outgroup homogeneity effects in early perception. *Proceedings of the National Academy of Sciences of the United States of America*, 116(29), 14532–14537.
- Hurles, M. E., Irlen, C., Nicholson, J., Taylor, P. G., Santos, F. R., Loughlin, J., ... Sykes, B. C. (1998, December). European y-chromosomal lineages in polynesians: a contrast to the population structure revealed by mtDNA. *American journal of human genetics*, 63(6), 1793–1806.
- Hysi, P. G., Valdes, A. M., Liu, F., Furlotte, N. A., Evans, D. M., Bataille, V., ... International Visible Trait Genetics Consortium (2018, May). Genome-wide association meta-analysis of individuals of european ancestry identifies new loci explaining a substantial fraction of hair color variation and heritability. *Nature genetics*, 50(5), 652–656.
- Iliescu, F. M., Chaplin, G., Rai, N., Jacobs, G. S., Basu Mallick, C., Mishra, A., ... Jablonski, N. G. (2018, September). The influences of genes, the environment, and social factors on the evolution of skin color diversity in india. *American journal of human biology: the official journal of the Human Biology Council*, 30(5), e23170.
- Ingber, S. (1984). The marketplace of ideas: A legitimizing myth. *Duke law journal*, 1984(1), 1–91.
- Insel, T. R., & Cuthbert, B. N. (2009, December). Endophenotypes: bridging genomic complexity and disorder heterogeneity. *Biological psychiatry*, 66(11), 988–989.
- International Organization for Standardization. (2015). *Ergonomics of the thermal environment – estimation of thermal insulation and water vapour resistance of a clothing ensemble* (Tech. Rep. No. ISO 9920:2007).
- Ito, S., Nakanishi, Y., Valenzuela, R. K., Brilliant, M. H., Kolbe, L., & Wakamatsu, K. (2011, August). Usefulness of alkaline hydrogen peroxide oxidation to analyze eumelanin and pheomelanin in various tissue samples: application to chemical analysis of human hair melanins. *Pigment cell & melanoma research*, 24(4), 605–613.
- Ito, S., & Wakamatsu, K. (2011, December). Diversity of human hair pigmentation as studied by chemical analysis of eumelanin and pheomelanin. *Journal of the European Academy of Dermatology and Venereology: JEADV*, 25(12), 1369–1380.
- Jablonski, N. G. (2006). *Skin: A natural history*. Berkeley: University of California Press.
- Jablonski, N. G. (2012). *Living color: The biological and social meaning of skin color*. University of California Press.

- Jablonski, N. G. (2020, December). Skin color and race. *American journal of physical anthropology*.
- Jablonski, N. G., & Chaplin, G. (2000, July). The evolution of human skin coloration. *Journal of human evolution*, *39*(1), 57–106.
- Jablonski, N. G., & Chaplin, G. (2010, May). Colloquium paper: human skin pigmentation as an adaptation to UV radiation. *Proceedings of the National Academy of Sciences of the United States of America*, *107* Suppl 2(Supplement\_2), 8962–8968.
- Jablonski, N. G., & Chaplin, G. (2014, April). The evolution of skin pigmentation and hair texture in people of african ancestry. *Dermatologic clinics*, *32*(2), 113–121.
- Jones, P., Lucock, M., Veysey, M., & Beckett, E. (2018, April). The vitamin d–folate hypothesis as an evolutionary model for skin pigmentation: An update and integration of current ideas. *Nutrients*, *10*(5), 554.
- Kamberov, Y. G., Wang, S., Tan, J., Gerbault, P., Wark, A., Tan, L., ... Sabeti, P. C. (2013, February). Modeling recent human evolution in mice by expression of a selected EDAR variant. *Cell*, *152*(4), 691–702.
- Kayser, M., Brauer, S., Schädlich, H., Prinz, M., Batzer, M. A., Zimmerman, P. A., ... Stoneking, M. (2003). Y chromosome STR haplotypes and the genetic structure of US populations of african, european, and hispanic ancestry. *Genome research*, *13*(4), 624–634.
- Kenny, E. E., Timpson, N. J., Sikora, M., Yee, M.-C., Moreno-Estrada, A., Eng, C., ... Myles, S. (2012, May). Melanesian blond hair is caused by an amino acid change in TYRP1. *Science*, *336*(6081), 554–554.
- Khumalo, N. P. (2007, April). Yes, let’s abandon race—it does not accurately correlate with hair form. *Journal of the American Academy of Dermatology*, *56*(4), 709–710.
- Kimura, R., Watanabe, C., Kawaguchi, A., Kim, Y.-I., Park, S.-B., Maki, K., ... Yamaguchi, T. (2015, May). Common polymorphisms in WNT10A affect tooth morphology as well as hair shape. *Human molecular genetics*, *24*(9), 2673–2680.
- Kneberg, M. (1935, April). Improved technique for hair examination. *American journal of physical anthropology*, *20*(1), 51–67.
- Koch, S. L., Shriver, M. D., & Jablonski, N. G. (2019, January). Variation in human hair ultrastructure among three biogeographic populations. *Journal of structural biology*, *205*(1), 60–66.
- Koch, S. L., Tridico, S. R., Bernard, B. A., Shriver, M. D., & Jablonski, N. G. (2020, March). The biology of human hair: A multidisciplinary review. *American journal of human biology: the official journal of the Human Biology Council*, *32*(2), e23316.
- Kollias, N., & Baqer, A. H. (1987). Absorption mechanisms of human melanin in the visible, 400–720 nm. *The Journal of investigative dermatology*, *89*(4), 384–388.
- Krol, E. S., & Liebler, D. C. (1998, December). Photoprotective actions of natural and synthetic melanins. *Chemical research in toxicology*, *11*(12), 1434–1440.
- Kumar, M., Suliburk, J. W., Veeraraghavan, A., & Sabharwal, A. (2020, March). PulseCam: a camera-based, motion-robust and highly sensitive blood perfusion imaging modality. *Scientific reports*, *10*(1), 4825.
- Kuppenheim, H. F., & Heer, R. R. (1952). *Spectral reflectance of white and negro skin*

- between 440 and 1000  $m\mu$  (Vol. 4) (No. 10).
- Lasisi, T. (2020a, November). *Real and simulated cross-sectional and longitudinal images of hair*.
- Lasisi, T. (2020b, November). Sample preparation protocol for cross-sectional microscopy of hair fibers. *protocols.io*.
- Lasisi, T. (2020c, November). Sample preparation protocol for hair fiber curvature analysis. *protocols.io*.
- Lasisi, T. (2021, January). *Phenotyping & evolutionary genomics: what we can learn from studying hair morphology*. Spring Colloquium Series.
- Lasisi, T., Ito, S., Wakamatsu, K., & Shaw, C. N. (2016, June). Quantifying variation in human scalp hair fiber shape and pigmentation. *American journal of physical anthropology*, 160(2), 341–352.
- Lasisi, T., Zaidi, A. A., Webster, T. H., Stephens, N. B., Rutch, K., Jablonski, N. G., & Shriver, M. D. (2020, November). *High-throughput phenotyping methods for quantifying hair fiber morphology*.
- Lee, K. E., Ko, J., Shin, T. J., Hyun, H. K., Lee, S. H., & Kim, J. W. (2014). Oligodontia and curly hair occur with ectodysplasin-a mutations. *Journal of dental research*, 93(4), 371–375.
- Leshner, A. I. (2004, February). Science at the leading edge. *Science*, 303(5659), 729.
- Lima, C. R. R. d. C., de Almeida, M. M., Velasco, M. V. R., & Matos, J. d. R. (2016, March). Thermoanalytical characterization study of hair from different ethnicities. *Journal of thermal analysis and calorimetry*, 123(3), 2321–2328.
- Lindelöf, B., Forslind, B., & Hedblad, M. A. (1988, September). Human hair form: Morphology revealed by light and scanning electron microscopy and computer aided Three-Dimensional reconstruction. *Archives of dermatology*, 124(9), 1359–1363.
- Linnaeus, C. (1758). *Systema naturae* (Vol. 1). Stockholm Laurentii Salvii.
- Liu, F., Chen, Y., Zhu, G., Hysi, P. G., Wu, S., Adhikari, K., ... Kayser, M. (2018, February). Meta-analysis of genome-wide association studies identifies 8 novel loci involved in shape variation of human head hair. *Human molecular genetics*, 27(3), 559–575.
- Lopez, M., Choin, J., Sikora, M., Siddle, K., Harmant, C., Costa, H. A., ... Quintana-Murci, L. (2019, September). Genomic evidence for local adaptation of Hunter-Gatherers to the african rainforest. *Current biology: CB*, 29(17), 2926–2935.e4.
- Loussouarn, G., Garcel, A.-L. A. L., Lozano, I., Collaudin, C., Porter, C., Panhard, S., ... De La Mettrie, R. (2007, October). Worldwide diversity of hair curliness: a new method of assessment. *International journal of dermatology*, 46 Suppl 1(i), 2–6.
- Lu, C. P., Polak, L., Keyes, B. E., & Fuchs, E. (2016). Spatiotemporal antagonism in mesenchymal-epithelial signaling in sweat versus hair fate decision. *Science*, 354(6319).
- Luke, D. A., Carothers, B. J., Dhand, A., Bell, R. A., Moreland-Russell, S., Sarli, C. C., & Evanoff, B. A. (2015, April). Breaking down silos: mapping growth of cross-disciplinary collaboration in a translational science initiative: BreakingDownSilos.

- Clinical and translational science*, 8(2), 143–149.
- Madrigal, L., & Kelly, W. (2007, March). Human skin-color sexual dimorphism: a test of the sexual selection hypothesis. *American journal of physical anthropology*, 132(3), 470–482.
- Mahner, M. (2013). Science and pseudoscience how to demarcate after the (alleged) demise. *Philosophy of pseudoscience: Reconsidering the demarcation problem*, 29–43.
- Manlove, K. R., Walker, J. G., Craft, M. E., Huyvaert, K. P., Joseph, M. B., Miller, R. S., ... Cross, P. C. (2016, April). “one health” or three? publication silos among the one health disciplines. *PLoS biology*, 14(4), e1002448.
- Maples, B. K., Gravel, S., Kenny, E. E., & Bustamante, C. D. (2013, August). RFMix: A discriminative modeling approach for rapid and robust Local-Ancestry inference. *American journal of human genetics*, 93(2), 278–288.
- Martin, A. R., Lin, M., Granka, J. M., Myrick, J. W., Liu, X., Sockell, A., ... Henn, B. M. (2017, November). An unexpectedly complex architecture for skin pigmentation in africans. *Cell*, 171(6), 1340–1353.e14.
- McCrea, F. B. (1983). The politics of menopause: The “discovery” of a deficiency disease. *Social problems*.
- M'charek, A. (2020, June). Tentacular faces: Race and the return of the phenotype in forensic identification. *American anthropologist*, 122(2), 369–380.
- M'charek, A., Toom, V., & Jong, L. (2020, September). The trouble with race in forensic identification. *Science, technology & human values*, 45(5), 804–828.
- McLean, S. (2019, June). Social problems, structural issues, and unsettling science. *American anthropologist*, 121(2), 480–481.
- Medland, S. E., Nyholt, D. R., Painter, J. N., McEvoy, B. P., McRae, A. F., Zhu, G., ... Martin, N. G. (2009, November). Common variants in the trichohyalin gene are associated with straight hair in europeans. *American journal of human genetics*, 85(5), 750–755.
- Mieczkowski, T., & Newel, R. (2020). *An analysis of the racial bias controversy in the use of hair assays*.
- Mkentane, K., Van Wyk, J. C., Sishi, N., Gumedze, F., Ngoepe, M., Davids, L. M., & Khumalo, N. P. (2017, June). Geometric classification of scalp hair for valid drug testing, 6 more reliable than 8 hair curl groups. *PloS one*, 12(6), e0172834–e0172834.
- Moreton-Robinson, A. (2013, December). Towards an australian indigenous women's standpoint theory. *Australian Feminist Studies*, 28(78), 331–347.
- Morgan, M. D., Pairo-Castineira, E., Rawlik, K., Canela-Xandri, O., Rees, J., Sims, D., ... Jackson, I. J. (2018, December). Genome-wide study of hair colour in UK biobank explains most of the SNP heritability. *Nature communications*, 9(1), 5271.
- Morris, D. (1967). *The naked ape: A zoologist's study of the human animal*. Random House.
- Morton, J., Carolan, V. A., & Gardiner, P. H. E. (2002, March). Removal of exogenously bound elements from human hair by various washing procedures and determination

- by inductively coupled plasma mass spectrometry. *Analytica chimica acta*, 455(1), 23–34.
- Mou, C., Thomason, H. A., Willan, P. M., Clowes, C., Edwin Harris, W., Drew, C. F., ... Headon, D. J. (2008, December). Enhanced ectodysplasin-a receptor (EDAR) signaling alters multiple fiber characteristics to produce the east asian hair form. *Human mutation*, 29(12), 1405–1411.
- Nelson, B. (2020). How dermatology is failing melanoma patients with skin of color: Unanswered questions on risk and eye-opening disparities in outcomes are weighing heavily on melanoma patients with darker skin. in this article, part 1 of a 2-part series, we explore the deadly consequences of racism and inequality in cancer care. *Cancer cytopathology*, 128(1), 7–8.
- Nelson, R. G. (2019a, June). Hypervisible and human. *American anthropologist*, 121(2), 469–470.
- Nelson, R. G. (2019b). Methods without meaning: Moving beyond body counts in research on behavior and health. *Evaluating evidence in biological anthropology: The strange and the familiar*, 86–100.
- Nelson, R. G. (2020). Beyond the household: Caribbean families and biocultural models of alloparenting. *Annual review of anthropology*.
- Neufeld, A. H., & Conroy, G. C. (2004, June). Human head hair is not fur. *Evolutionary anthropology*, 13(3), 89–89.
- Norton, H. L., Edwards, M., Krithika, S., Johnson, M., Werren, E. A., & Parra, E. J. (2016, September). Quantitative assessment of skin, hair, and iris variation in a diverse sample of individuals and associated genetic variation. *American journal of physical anthropology*, 160(4), 570–581.
- Norton, H. L., Friedlaender, J. S., Merriwether, D. A., Koki, G., Mgone, C. S., & Shriver, M. D. (2006, June). Skin and hair pigmentation variation in island melanesia. *American journal of physical anthropology*, 130(2), 254–268.
- Norton, H. L. H. L., Kittles, R. A. R. A., Parra, E., McKeigue, P., Mao, X., Cheng, K., ... Shriver, M. D. (2007). Genetic evidence for the convergent evolution of light skin in europeans and east asians. *Molecular biology and evolution*, 24(3), 710–720.
- Ogle, R. R., & Fox, M. J. (1998). Atlas of human hair microscopic characteristic variates. *Science and Justice*, 38, 55.
- Ozeki, H., Ito, S., Wakamatsu, K., & Thody, A. J. (1996, October). Spectrophotometric characterization of eumelanin and pheomelanin in hair. *Pigment cell research / sponsored by the European Society for Pigment Cell Research and the International Pigment Cell Society*, 9(5), 265–270.
- Page, S. E. (2008). *The difference: How the power of diversity creates better groups, firms, schools, and societies - new edition*. Princeton University Press.
- Pandya, A. G., Alexis, A. F., Berger, T. G., & Wintroub, B. U. (2016, March). Increasing racial and ethnic diversity in dermatology: A call to action. *Journal of the American Academy of Dermatology*, 74(3), 584–587.
- Panofsky, A., & Bliss, C. (2017, February). Ambiguity and scientific authority: Population

- classification in genomic science. *American sociological review*, 82(1), 59–87.
- Park, S. B., Suh, D. H., & Youn, J. I. (1998, October). Reliability of self-assessment in determining skin phototype for korean brown skin. *Photodermatology, photoimmunology & photomedicine*, 14(5-6), 160–163.
- Parker, H. G., Chase, K., Cadieu, E., Lark, K. G., & Ostrander, E. A. (2010). An insertion in the RSPO2 gene correlates with improper coat in the portuguese water dog. *The Journal of heredity*, 101(5), 612–617.
- Parra, E. J., Kittles, R. a., & Shriver, M. D. (2004, October). Implications of correlations between skin color and genetic ancestry for biomedical research. *Nature genetics*, 36(11 Suppl), S54–S60.
- Pavone, P., Falsaperla, R., Barbagallo, M., Polizzi, A., Praticò, A. D., & Ruggieri, M. (2017, November). Clinical spectrum of woolly hair: indications for cerebral involvement. *Italian journal of pediatrics*, 43(1), 99.
- Perry, G. H., Foll, M., Grenier, J.-C., Patin, E., Nédélec, Y., Pacis, A., . . . Barreiro, L. B. (2014, September). Adaptive, convergent origins of the pygmy phenotype in african rainforest hunter-gatherers. *Proceedings of the National Academy of Sciences of the United States of America*, 111(35), E3596–603.
- Peters, T., Sedlmeier, R., Büsow, H., Runkel, F., Lüers, G. H., Korthaus, D., . . . Franz, T. (2003, October). Alopecia in a novel mouse model RCO3 is caused by mk6irs1 deficiency. *The Journal of investigative dermatology*, 121(4), 674–680.
- Pichon, L. C., Landrine, H., Corral, I., Hao, Y., Mayer, J. A., & Hoerster, K. D. (2010). Measuring skin cancer risk in african americans: is the fitzpatrick skin type classification scale culturally sensitive? *Ethnicity & disease*, 20(2), 174–179.
- Piil, J. F., Christiansen, L., Morris, N. B., Mikkelsen, C. J., Ioannou, L. G., Flouris, A. D., . . . Nybo, L. (2020, May). Direct exposure of the head to solar heat radiation impairs motor-cognitive performance. *Scientific reports*, 10(1), 7812.
- Porter, A. M. W. (1993, November). Sweat and thermoregulation in hominids. comments prompted by the publications of p. e. wheeler 1984-1993. *Journal of human evolution*, 25(5), 417–423.
- Pozebon, D., Scheffler, G. L., & Dressler, V. L. (2017, November). Elemental hair analysis: A review of procedures and applications. *Analytica chimica acta*, 992, 1–23.
- Premi, S., Wallisch, S., Mano, C. M., Weiner, A. B., Bacchiocchi, A., Wakamatsu, K., . . . Brash, D. E. (2015, February). Photochemistry. chemiexcitation of melanin derivatives induces DNA photoproducts long after UV exposure. *Science*, 347(6224), 842–847.
- Pruner-Bey, F. I. (1864, February). On human hair as a race-character, examined by the aid of the microscope. *Anthropological review*, 2(4), 1.
- Pruner-Bey, F. I. (1877). On human hair as a race character. *The journal of the Anthropological Institute of Great Britain and Ireland*, 6, 71.
- Quillen, E. E., Norton, H. L., Parra, E. J., Lona-Durazo, F., Ang, K. C., Illiescu, F. M., . . . Jablonski, N. G. (2019, January). Shades of complexity: New perspectives on the evolution and genetic architecture of human skin. *American journal of physical*

- anthropology*, 168 Suppl 67, 4–26.
- Raffaelli, I., Katunar, D., & Kerovec, B. (2019). *Lexicalization patterns in color naming: A cross-linguistic perspective*. John Benjamins Publishing Company.
- Ramot, Y., & Zlotogorski, A. (2015, April). The twisting tale of woolly hair: a trait with many causes. *Journal of medical genetics*, 52(4), 217–223.
- Rampen, F. H., Fleuren, B. A., de Boo, T. M., & Lemmens, W. A. (1988, June). Unreliability of self-reported burning tendency and tanning ability. *Archives of dermatology*, 124(6), 885–888.
- Reardon, J., & TallBear, K. (2012, April). “your DNA is our history”: Genomics, anthropology, and the construction of whiteness as property. *Current anthropology*, 53(S5), S233–S245.
- Reis, J., Brandão, J. R., Rodrigues, A., Coelho, A., & Machado, S. (2020, July). Hair cross-sectioning in uncombable hair syndrome: An epoxy embedding technique. *Journal of cutaneous pathology*.
- Relethford, J. H. (2000). Human skin color diversity is highest in sub-saharan african populations. *Human biology*, 72(5), 773–780.
- Relethford, J. H. (2002, August). Apportionment of global human genetic diversity based on craniometrics and skin color. *American journal of physical anthropology*, 118(4), 393–398.
- Rose, H. (1983, October). Hand, brain, and heart: A feminist epistemology for the natural sciences. *Signs: Journal of Women in Culture and Society*, 9(1), 73–90.
- Ruff, C. B., Trinkaus, E., & Holliday, T. W. (1997). Body mass and encephalization in pleistocene homo. *Nature*.
- Ruxton, G. D., & Wilkinson, D. M. (2011, August). Thermoregulation and endurance running in extinct hominins: Wheeler’s models revisited. *Journal of human evolution*, 61(2), 169–175.
- Saini, A. (2019). *Superior: The return of race science*. Beacon Press.
- Scott, W. J. (1990, August). PTSD in DSM-III: A case in the politics of diagnosis and disease. *Social problems*, 37(3), 294–310.
- Scully, J. L. (2004, July). What is a disease? *EMBO reports*, 5(7), 650–653.
- Seta, S., Sato, H., & Miyake, B. (1988). Forensic hair investigation. In (Vol. 2, pp. 47–166). Springer, Berlin, Heidelberg.
- Shimomura, Y., Wajid, M., Zlotogorski, A., Lee, Y.-J., Rice, R. H., & Christiano, A. M. (2009, August). Founder mutations in the lipase h gene in families with autosomal recessive woolly hair/hypotrichosis. *The Journal of investigative dermatology*, 129(8), 1927–1934.
- Shin, S., Park, J., & Lee, J.-Y. (2015, July). Does the hair influence heat extraction from the head during head cooling under heat stress? *Industrial health*, 53(6), 533–541.
- Shriver, M. D., Parra, E. J., Dios, S., Bonilla, C., Norton, H., Jovel, C., . . . Kittles, R. a. (2003, April). Skin pigmentation, biogeographical ancestry and admixture mapping. *Human genetics*, 112(4), 387–399.
- Siemens, J., & Kamm, G. B. (2018, May). Cellular populations and thermosensing mechanisms of the hypothalamic thermoregulatory center. *Pflugers Archiv: European*

- journal of physiology*, 470(5), 809–822.
- Skinner, D. (2020, September). Forensic genetics and the prediction of race: What is the problem? *BioSocieties*, 15(3), 329–349.
- Smit, A. L., Sprangers, J. F. C. M., Sablik, P. W., & Groenwold, J. (1994, January). Automated measurement of root length with a three-dimensional high-resolution scanner and image analysis. *Plant and soil*, 158(1), 145–149.
- Smith, L. T. (2011). *Decolonising methodologies: Research and indigenous peoples*. W. Ross MacDonald School Resource Services Library.
- Smith, R. W. A., & Bolnick, D. A. (2019, June). Situating science: Doing biological anthropology as a view from somewhere: Situating science. *American anthropologist*, 121(2), 465–467.
- Sporer, S. L. (2001, March). The cross-race effect: Beyond recognition of faces in the laboratory. *Psychology, public policy, and law: an official law review of the University of Arizona College of Law and the University of Miami School of Law*, 7(1), 170–200.
- Stecksén-Blicks, C., Falk Kieri, C., Hägg, D., & Schmitt-Egenolf, M. (2015). *Hair shaft structures in EDAR induced ectodermal dysplasia* (Vol. 16) (No. 1).
- Strutt, J. W. (1871, January). Some experiments on colour. *Nature*, 3(64), 234–236.
- Sturm, R. A. R. A., & Larsson, M. (2009, October). Genetics of human iris colour and patterns. *Pigment cell & melanoma research*, 22(5), 544–562.
- Sun, H., Biedermann, L., & Bond, T. C. (2007, September). Color of brown carbon: A model for ultraviolet and visible light absorption by organic carbon aerosol. *Geophysical research letters*, 34(17), 3131.
- Tan, J., Yang, Y., Tang, K., Sabeti, P. C., Jin, L., & Wang, S. (2013, October). The adaptive variant EDARV370A is associated with straight hair in east asians. *Human genetics*, 132(10), 1187–1191.
- Tarlo, E. (2017). *Entanglement: The secret lives of hair*. Oneworld Publications.
- Taubin, G. (1991, November). Estimation of planar curves, surfaces, and nonplanar space curves defined by implicit equations with applications to edge and range image segmentation. *IEEE transactions on pattern analysis and machine intelligence*, 13(11), 1115–1138.
- Thibaut, S., Gaillard, O., Bouhanna, P., Cannell, D. W., & Bernard, B. A. (2005, April). Human hair shape is programmed from the bulb. *The British journal of dermatology*, 152(4), 632–638.
- Thierry, B. (2005, January). Hair grows to be cut. *Evolutionary anthropology*, 14(1), 5–5.
- Thompson, C. (2009, October). Black women, beauty, and hair as a matter of being. *Women's studies*, 38(8), 831–856.
- Thomson, M. L. (1955, February). Relative efficiency of pigment and horny layer thickness in protecting the skin of europeans and africans against solar ultraviolet radiation. *The Journal of physiology*, 127(2), 236–246.
- Torres, J. B. (2019). A parrot among john crows: Diversity as risk and reward. *American anthropologist*.

- Tracy, R. P. (2008, April). 'deep phenotyping': characterizing populations in the era of genomics and systems biology. *Current opinion in lipidology*, 19(2), 151–157.
- Trotter, M. (1930, July). The form, size, and color of head hair in american whites. *American journal of physical anthropology*, 14(3), 433–445.
- Trotter, M. (1938, July). A review of the classifications of hair. *American journal of physical anthropology*, 24(1), 105–126.
- Tsosie, K. S., Begay, R. L., Fox, K., & Garrison, N. A. (2020, June). Generations of genomes: advances in paleogenomics technology and engagement for indigenous people of the americas. *Current opinion in genetics & development*, 62, 91–96.
- Tzur, S., Rosset, S., Shemer, R., Yudkovsky, G., Selig, S., Tarekegn, A., . . . Skorecki, K. (2010, September). Missense mutations in the APOL1 gene are highly associated with end stage kidney disease risk previously attributed to the MYH9 gene. *Human genetics*, 128(3), 345–350.
- Ü Basmanav, F. B., Cau, L., Tafazzoli, A., Méchin, M.-C., Wolf, S., Romano, M. T., . . . Betz, R. C. (2016, December). Mutations in three genes encoding proteins involved in hair shaft formation cause uncombable hair syndrome. *American journal of human genetics*, 99(6), 1292–1304.
- van den Berghe, P. L., & Frost, P. (1986, January). Skin color preference, sexual dimorphism and sexual selection: A case of gene culture co-evolution? *Ethnic and racial studies*, 9(1), 87–113.
- van der Walt, S., Schönberger, J. L., Nunez-Iglesias, J., Boulogne, F., Warner, J. D., Yager, N., . . . scikit-image contributors (2014, June). scikit-image: image processing in python. *PeerJ*, 2, e453.
- Vernall, D. G. (1961, December). A study of the size and shape of cross sections of hair from four races of men. *American journal of physical anthropology*, 19(4), 345–350.
- Vidal, V. P. I., Chaboissier, M. C., Lützkendorf, S., Cotsarelis, G., Mill, P., Hui, C. C., . . . Schedl, A. (2005). Sox9 is essential for outer root sheath differentiation and the formation of the hair stem cell compartment. *Current biology: CB*, 15(15), 1340–1351.
- Wacker, C. B., McAllan, B. M., Körtner, G., & Geiser, F. (2016, August). The functional requirements of mammalian hair: a compromise between crypsis and thermoregulation? *Die Naturwissenschaften*, 103(7-8), 53.
- Wagner, G., Heine, M., & Sachse, M. M. (2015, January). The heat shrink tube technology—a simple method for making hair cross sections. *Journal der Deutschen Dermatologischen Gesellschaft = Journal of the German Society of Dermatology: JDDG*, 13(1), 55–57.
- Wagner, H. R. (1962, May). Mongolism in orientals. *American journal of diseases of children*, 103, 706–714.
- Wakamatsu, K., Hu, D.-N., McCormick, S. A., & Ito, S. (2008, February). Characterization of melanin in human iridal and choroidal melanocytes from eyes with various colored irides. *Pigment cell & melanoma research*, 21(1), 97–105.
- Walsberg, G. E. (1990, September). Convergence of solar heat gain in two squirrel species with contrasting coat colors. *Physiological zoology*, 63(5), 1025–1042.

- Walsh, S., Pagani, L., Xue, Y., Laayouni, H., Tyler-Smith, C., & Bertranpetit, J. (2020, October). Positive selection in admixed populations from ethiopia. *BMC genetics*, *21*(Suppl 1), 108.
- Walters, J. T. R., & Owen, M. J. (2007, October). Endophenotypes in psychiatric genetics. *Molecular psychiatry*, *12*(10), 886–890.
- Wang, F., Gao, C., Kuklane, K., & Holmér, I. (2011, August). Determination of clothing evaporative resistance on a sweating thermal manikin in an isothermal condition: heat loss method or mass loss method? *The Annals of occupational hygiene*, *55*(7), 775–783.
- Ware, O. R., Dawson, J. E., Shinohara, M. M., & Taylor, S. C. (2020, February). Racial limitations of fitzpatrick skin type. *Cutis; cutaneous medicine for the practitioner*, *105*(2), 77–80.
- Watkins, R. J. (2020, December). “[this] system was not made for [you]:” a case for decolonial scientia. *American journal of physical anthropology*.
- Weng, C., Shah, N. H., & Hripcsak, G. (2020, May). Deep phenotyping: Embracing complexity and temporality-towards scalability, portability, and interoperability. *Journal of biomedical informatics*, *105*, 103433.
- Wheeler, M. E., & Fiske, S. T. (2005, January). Controlling racial prejudice: Social-Cognitive goals affect amygdala and stereotype activation. *Psychological science*, *16*(1), 56–63.
- Wheeler, P. E. (1984, January). The evolution of bipedality and loss of functional body hair in hominids. *Journal of human evolution*, *13*(1), 91–98.
- Wheeler, P. E. (1985, January). The loss of functional body hair in man: the influence of thermal environment, body form and bipedality. *Journal of human evolution*, *14*(1), 23–28.
- Wheeler, P. E. (1990, May). The significance of selective brain cooling in hominids. *Journal of human evolution*, *19*(3), 321–322.
- White, J. D., Ortega-Castrillón, A., Matthews, H., Zaidi, A. A., Ekrami, O., Snyders, J., . . . Claes, P. (2019, April). MeshMonk: Open-source large-scale intensive 3D phenotyping. *Scientific reports*, *9*(1), 6085.
- Wickham, H., & Others. (2017). Tidyverse: Easily install and load the ‘tidyverse’. *R package version*, *1*(1), 2017.
- Wilke, C. O. (2016). cowplot: streamlined plot theme and plot annotations for ‘ggplot2’. *CRAN Repos*, *2*, R2.
- Willis, I., & Earles, R. M. (2005, March). A new skin classification system relevant to people of african descent. *Cosmetic Dermatology*, *18*(3), 209–216.
- Winawer, J., Witthoft, N., Frank, M. C., Wu, L., Wade, A. R., & Boroditsky, L. (2007, May). Russian blues reveal effects of language on color discrimination. *Proceedings of the National Academy of Sciences of the United States of America*, *104*(19), 7780–7785.
- Winkler, C. A., Nelson, G. W., & Smith, M. W. (2010). Admixture mapping comes of age. *Annual review of genomics and human genetics*, *11*, 65–89.
- Wolf, S. T., Jablonski, N. G., & Kenney, W. L. (2020, December). Examining “race”

- in physiology. *American Journal of Physiology-Heart and Circulatory Physiology*, 319(6), H1409–H1413.
- Wolfram, L. J. (2003, June). Human hair: a unique physicochemical composite. *Journal of the American Academy of Dermatology*, 48(6 Suppl), S106–14.
- Wortmann, F. J., Wortmann, G., & Sripho, T. (2019). Why is hair curly?-deductions from the structure and the biomechanics of the mature hair shaft. *Experimental dermatology*.
- Wylie, A. (2003). *Why standpoint Matters.'Science and other cultures: Issues in philosophies of science and technology*, eds. r. figueroa, s. harding. New York: Routledge.
- Xie, Y. (2020). knitr: A General-Purpose package for dynamic report generation in R [Computer software manual].
- Yarmolenko, P. S., Moon, E. J., Landon, C., Manzoor, A., Hochman, D. W., Viglianti, B. L., & Dewhirst, M. W. (2011). Thresholds for thermal damage to normal tissues: an update. *International journal of hyperthermia: the official journal of European Society for Hyperthermic Oncology, North American Hyperthermia Group*, 27(4), 320–343.
- Yehia, L., & Eng, C. (2019, March). Largescale population genomics versus deep phenotyping: Brute force or elegant pragmatism towards precision medicine. *NPJ genomic medicine*, 4, 6.
- Zaidi, A. A., Mattern, B. C., Claes, P., McEcoy, B., Hughes, C., & Shriver, M. D. (2017, March). Investigating the case of human nose shape and climate adaptation. *PLoS genetics*, 13(3), e1006616–e1006616.
- Zuberi, T., & Bonilla-Silva, E. (2008). *White logic, white methods: Racism and methodology*. Rowman & Littlefield Publishers.

## Vita

Tina Lasisi

### EDUCATION

<b><i>Doctor of Philosophy in Biological Anthropology</i></b>	2021
The Pennsylvania State University	
<b><i>Master of Arts in Biological Anthropology</i></b>	2017
The Pennsylvania State University	
<b><i>Bachelor of Arts in Archaeology &amp; Anthropology</i></b>	2014
University of Cambridge	

### SELECTED & AWARDS

Wenner-Gren Foundation Dissertation Fieldwork Grant (Gr. 9911)	2019
Africana Research Center Grant, Penn State	2019
Hill Post-Comprehensive Fellowship, Department of Anthropology, Penn State	2019
William T. Sanders Graduate Award, Department of Anthropology, Penn State	2019
National Science Foundation Dissertation Improvement Grant (No.1847845)	2019
Juan Comas Prize, American Association of Physical Anthropologists	2018

### SELECTED PUBLICATIONS

**Lasisi, T.** (2021). The constraints of racialization: How classification and valuation hinder scientific research on human variation. *American Journal of Physical Anthropology*.

**Lasisi, T.**, Zaidi, A. A., Webster, T. H., Stephens, N. B., Rouch, K., Jablonski, N. G., & Shriver, M. D. (in review). High-throughput phenotyping methods for quantifying hair fiber morphology. *Scientific Reports*.

Quillen, E. E., Norton, H. L., Parra, E. J., Lona-Durazo, F., Ang, K. C., Illiescu, F. M., Pearson, L. N., Shriver, M. D., **Lasisi, T.**, Gokcumen, O., Starr, I., Lin, Y.-L., Martin, A. R., & Jablonski, N. G. (2019). Shades of complexity: New perspectives on the evolution and genetic architecture of human skin. *American Journal of Physical Anthropology*, 168 Suppl 67(S66), 4–26.

**Lasisi, T.**, & Shriver, M. D. (2018). Focus on African diversity confirms complexity of skin pigmentation genetics. *Genome Biology*, 19(1), 13.